Available on the CMS information server **CMS AN-13-346**

CMS Draft Analysis Note

The content of this note is intended for CMS internal use and distribution only

2015/03/04
Head Id:
Archive Id: 279404M
Archive Date:

Measurement of prompt and non-prompt J/ψ production in pPb collisions at $\sqrt{s_{\mathrm{NN}}} = 5.02\,\mathrm{TeV}$

Lamia Benhabib, Mihee Jo, Hyunchul Kim, Yongsun Kim, Kisoo Lee, Songkyo Lee
(The CMS heavy ion dilepton group)

Abstract

The note describes a J/ψ measurement in proton-lead collisions at a center-of-mass energy per nucleon pair of 5.02 TeV with an integrated luminosity of 34.6 nb^{-1} recorded by the CMS experiment at the LHC in 2013. Prompt J/ψ and non-prompt J/ψ from B hadron decays are separately measured via their $\mu^+\mu^-$ decay mode. The differential cross sections are presented with the center-of-mass rapidity of $-2.87 < y_{CM} < 1.93$ and transverse momentum of $p_{\mathrm{T}} < 30$ GeV/c. The forward to backward yield ratio is also measured as a function of the event-activity as measured by the sum of transverse energy deposited at forward pseudorapidity, $4.0 < |\eta| < 5.2$. Below $p_{\mathrm{T}} = 10$ GeV/c, the prompt and non-prompt J/ψ yields at forward rapidities are relatively suppressed compared to backward rapidities. The forward-backward asymmetry is larger for increasingly forward rapidity and for smaller event-activity. Such an observation confirms the presence of "cold nuclear matter" effects in the production of J/ψ in p-Pb collisions at the LHC.

Version notices

V1

- Skeleton is created on Nov. 27th 2013.

V2

- frozen for pre-approval meeting on Mar. 19th 2014.

V3

- frozen to be reviewed by ARC on April. 3rd 2014.

V4

- filled with technical comments from ARC on April. 26th 2014.

V5

- filled with technical comments from ARC on May. 5th 2014.

Contents

1 Introduction

In this document, we report the measurement of J/ψ meson produced from pPb collisions at $\sqrt{s_{\mathrm{NN}}} = 5.02\,\mathrm{TeV}$, with the recorded integrated luminosity of 34.6 nb^{-1}. J/ψ mesons are reconstructed via their decays into $\mu^+\mu^-$ pairs. For this analysis, *non-prompt* J/ψ from B hadron decays have been separated from *prompt* J/ψ utilizing the reconstructed decay vertex of the $\mu^+\mu^-$ pair. Directly produced J/ψ as well as those from decays of higher charmonium states (e.g. ψ' and χ_c) are considered *prompt* as their decay length is unmeasurably small compared to those from B decays and are not distinguished in this analysis.

The differential cross sections of prompt and non-prompt J/ψ production are reported in center of mass rapidity domains $-2.87 < y_{CM} < 1.93$ and the transverse moementum $p_{\mathrm{T}} < 30$ GeV/c, where ”forward” regions (positive rapidity) are defined by the proton-going direction. Then The asymmetry of yields in forward and backward rapidities, in the center-of-mass frame has been measured within $|y_{CM}| < 1.93$ to probe the cold nuclear matter effects. In addition, the correlation between forward-to-backward ratio and the event-activity is evaluated to study the dependence on impact parameter of collision.

The note starts with a description of the data selection in Section 2 and Section 3. The signal extraction of J/ψ are detailed in Section 4. In Sections 5 and 6 the acceptance correction and the measurement of the efficiencies to reconstruction, identification and triggering on single muons are described. The full correction factor and systematic uncertainties are summarized in Section 7. Section 8 shows the results.

2 Event selection

2.1 Datasets

The prompt reco datasets of proton lead collisions (pARun2013) namely /PAMuon/HIRun2013-PromptReco-v1/RECO have been used in the analysis. The data have been reconstructed in the CMSSW version CMSSW_5_3_8_HI_patch2 with global tag GR_P_V43D::All. Since the 1st 7 runs (run numbers 210498-210658) are mis-aligned, the reprocessed reco datasets have been used with global tag GR_P_V43F::All. All events in this dataset were selected by the muon trigger HLT_PAL1DoubleMuOpen_v1 trigger, an online hardware-based trigger system requiring two muon candidates in the muon detectors with no explicit momentum or rapidity thresholds. The trigger condition was kept unprescaled during the whole run. The data were then skimmed for events with two tracker muons with an invariant mass of more than 2 GeV/c^2. All charge combinations have been considered in the pairing. The skimming and the root tuples were created using the BPH onia software for these tasks.

The proton lead sample comprises two subsets: one corresponding to Pb going to +z direction(run numbers 210498 to 211256 and integrated luminosity 20.7 $(\mathrm{nb})^{-1}$) and one corresponding to Pb going to the -z direction (run number 211313 to 211631 and integrated luminosity is 14.0 $(\mathrm{nb})^{-1}$). In the analysis, "forward" regions (positive rapidity) are defined by the proton-going direction. Data from two different directions are fitted separately for the signal extraction and then merged after respective acceptance and efficiency corrections. Bookkeeping of the files is done at
https://twiki.cern.ch/twiki/bin/view/CMS/HIOnia2MuMuSkimProcessingDetails2013.

3 Muon selection

The analysis starts with producing the Onia2MuMu skim, which contains all pairs of tracker muons with an invariant mass larger than 2 GeV/c^2. All charge combinations are considered and all possible combinations within an event are kept. The package that was used for the skimming can be found in CVS under CMSSW/tdahms/Onia2MuMu and is the same used in the BPH group for similar analyses. Starting from this skim, a TTree is filled with single muons within a defined acceptance, and muon pairs that pass quality criteria to reject the background of fake muons while keeping the efficiency of selecting real muons high.

3.1 Muon reconstruction

Muon candidates used in this analysis are accepted only if they belong to the following kinematic regions which will be revisited in sections 5 :

$$|\eta^{\mu}| < 1.3 \quad \rightarrow \quad p_{\mathrm{T}}^{\mu} > 3.3\ GeV/c \tag{1}$$

$$1.3 < |\eta^{\mu}| < 2.2 \quad \rightarrow \quad p^{\mu} > 2.9\ GeV/c \tag{2}$$

$$2.2 < |\eta^{\mu}| < 2.4 \quad \rightarrow \quad p_{\mathrm{T}}^{\mu} > 0.8\ GeV/c \tag{3}$$

The muon candidates are further selected if reconstructed as *tracker muons*, and pass the 'soft muon ID' selection, as defined by the Muon POG
https://twiki.cern.ch/twiki/bin/view/CMSPublic/SWGuideMuonId.
The complete list of all the cuts applied on muons and dimuons is the following :

- the number of valid tracker layers > 5, indicating how good the inner track part of the track is;

- the number of pixel layers with valid hits > 0;
- the track high purity flag to rejects bad quality tracks, basically just few outliers;
- the distance between the event vertex and the muon track in the transverse plane, $D_{xy} < 0.3$ cm, and the longitudinal plane, $D_z < 20.0$ cm;
- the probability of two tracks to belong to the same decay vertex $> 1\%$;
- Tracker muon arbitration is done (resolves ambiguity of sharing segments, picks best based on matching based on position and pull cuts);
- TMOneStationTight (requires one well matched segment in the muon stations for the track);
- opposite sign muons.

3.2 Muon quality cuts and single muon kinematic variables

3.2.1 Distribution of muon quality variables in MC and data

In this section we compare data and MC distributions for single muon quality cut variables as shown in 1, 2 . Muons coming from the MC prompt J/ψ sample produced in the first run configuration are shown in green histograms while muons from data (first run period) falling in the mass range [2.95,3.25] are shown with red points. It is important to note that in the following we are comparing a pure MC prompt J/ψ signal to a contaminated J/ψ signal form data where a cut on $c\tau < 50\ \mu$m is applied in order to remove the non-prompt contribution form data. For each variable plotted all other cuts were applied, as given in Table 1, except for the cut on the variable shown. All of the variable distributions are normalized to have area of unity. For most of the muon Identification variables, within the cut region, the muons from the J/ψ signal region (red points) match the distributions from MC J/ψ (green histogram) except for the number of the tracker layers. The discrepancy between Data and MC for the number of tracker layers and for the number of pixel hits cannot be explained only by the background present in Data and absent in MC.

Table 1 summarizes the values of the cuts for the analysis and the percentile of signal in simulation removed independently by each cut in the third column and after all the other cuts are applied.

Table 1: Quality cuts applied to tracker muons

Cut variable	Cut value	Only this cut	All except this cut
#tracker layers	> 5	98.21%	88.43%
#pixel hits	> 1	92.46%	93.76%
$\chi^2_{InnerTrack}/ndof$	< 1.8	98.00%	88.72 %
$\lvert d_{xy}\rvert$	< 3	99.99 %	87.04 %
$\lvert d_z\rvert$	< 30	99.99 %	87.04 %
vertex probability	> 0.01	97.27 %	89.15 %
All cuts applied			87.03 % %

3.2.2 single muon kinematic variable distributions

Although the background contamination is present in the data sample we compare the kinematic distributions of single muons from Data and MC as shown in 3.

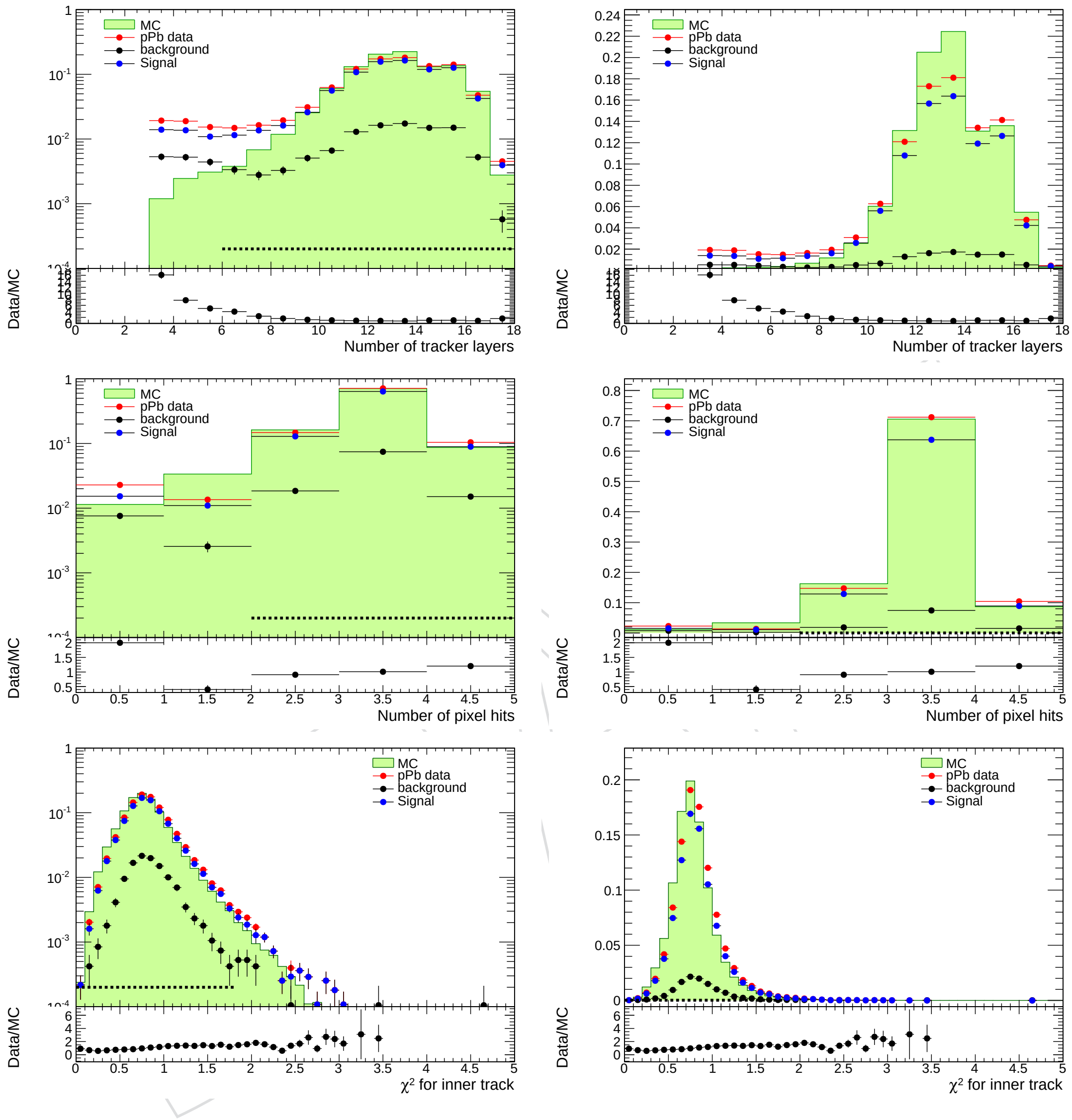

Figure 1: Single tracker muon quality distributions, from MC J/ψ signal events (green histogram) and from the data (red points). All other cuts are applied to the muons but the one displayed. The histograms are normalized to unity. The horizontal dashed lines indicate the cuts region considered (Linear scale on the right and Log scale on the left). Here are shown the number of tracker layers, number of pixel hits and the ^{2} for inner tracks distributions.

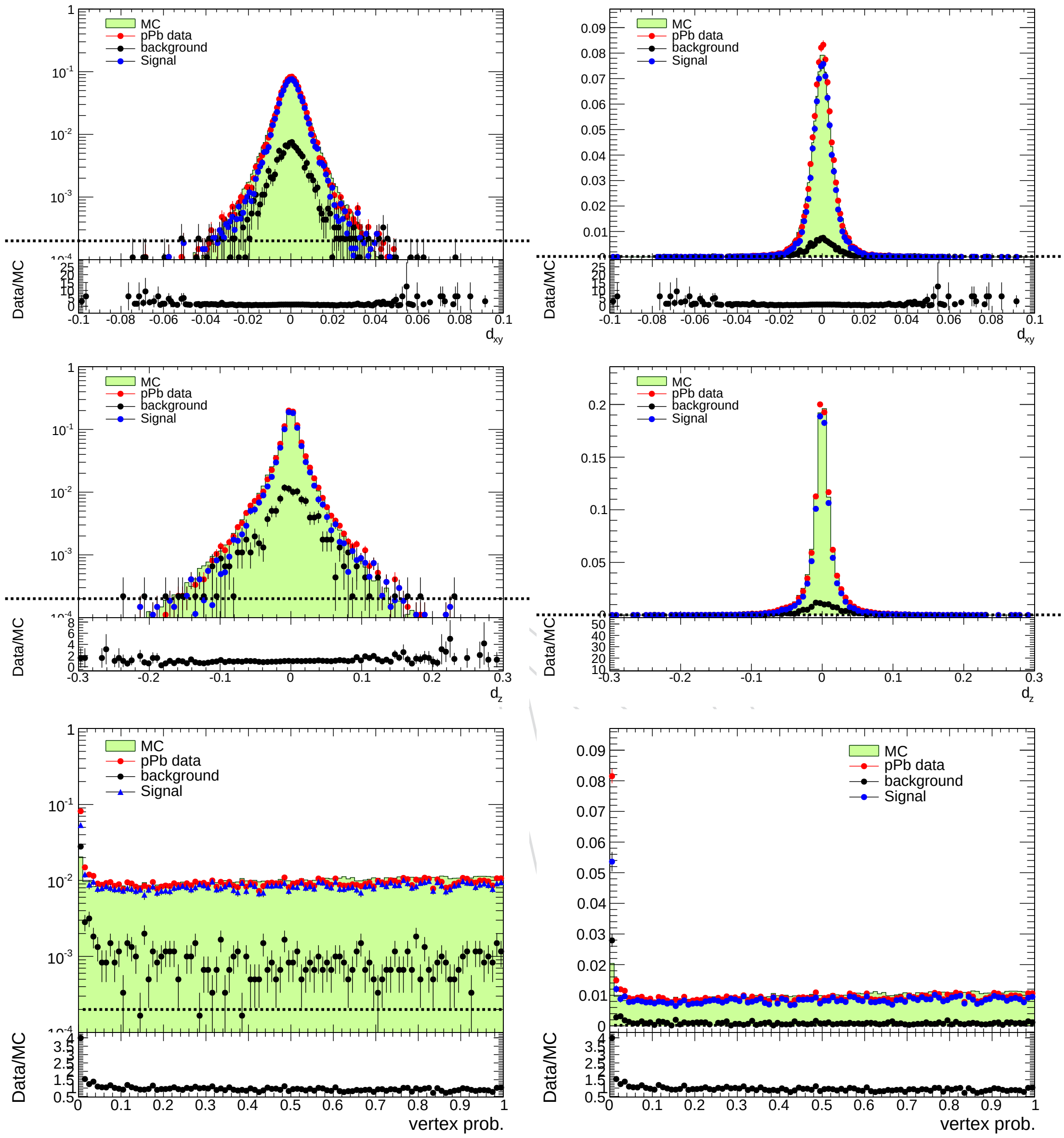

Figure 2: Single tracker muon quality distributions, from MC J/ψ signal events (green histogram) and from the data (red points). All other cuts are applied to the muons but the one displayed. The histograms are normalized to unity. The horizontal dashed lines indicate the cuts region considered (Linear scale on the right and Log scale on the left). Here are shown d_{xy}, d_z and the z vertex probability distributions

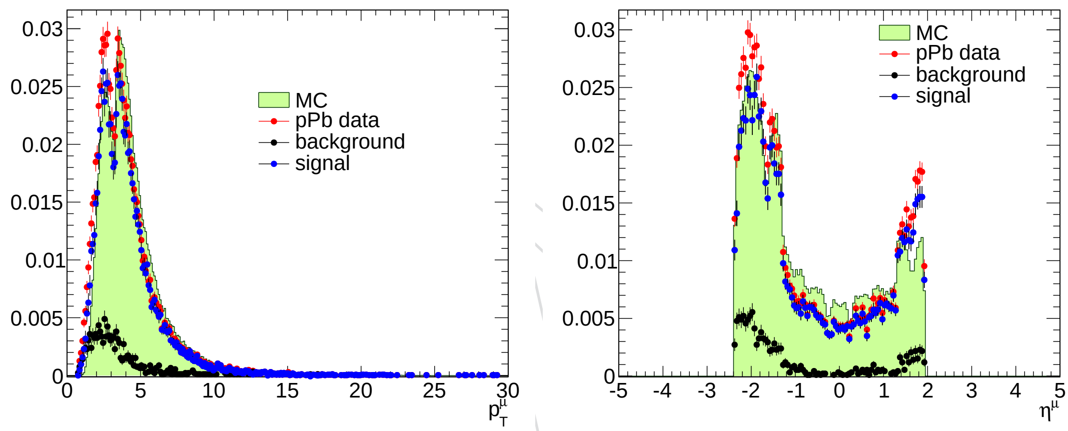

Figure 3: single muon η and p_T distributions

4 Signal extraction

4.1 Inclusive J/ψ

The invariant mass spectrum of $\mu^+\mu^-$ pairs is shown in fiqure 4 in the region of $2.6 < m_{\mu\mu} < 3.5$ GeV/c^2 with the transverse momentum $p_{\mathrm{T}} < 30$ GeV/c and center-of-mass rapidity $-2.87 < y_{CM} < 1.93$, which corresponds to $-2.4 < y_{lab} < 2.4$ in the detector frame, after applying the single muon quality requirements. No minimum pair-p_{T} requirement has been applied explicitly in this plot. In this integrated kinematic regions, 123114 ± 444 dimuon pairs are selected for the 1st run, and 84014 ± 370 pairs for the 2nd run. In the actual anaylsis with binning in p_{T} and rapidity, we have applied the lower limit of $p_{\mathrm{T}} > 6.5$ GeV/c for the mid-rapidity regions because of the detector coverage. More details can be found in the acceptance section 5.

The black curve is an extended (the number of signal and background are directly calculated) unbinned maximum likelihood fit to the $\mu^+\mu^-$ pair spectrum with the sum of a Crystal Ball and a Gaussian functions for the signal, with common mean, m_0, and independent widths, σ_{CB} and σ_{Gaus}, and an exponential for the background. The Crystal Ball function combines a Gaussian core with a power-law tail, described by exponent the n, to account for energy loss due to final-state photon radiation:

$$f_{CB}(m) = \begin{cases} \frac{N}{\sqrt{2\pi}\sigma_{CB}} \exp\left(-\frac{(m-m_0)^2}{2\sigma_{CB}^2}\right), & \text{for } \frac{m-m_0}{\sigma_{CB}} > -\alpha; \\ \frac{N}{\sqrt{2\pi}\sigma_{CB}} \left(\frac{n}{|\alpha|}\right)^n \exp\left(-\frac{|\alpha|^2}{2}\right) \left(\frac{n}{|\alpha|} - |\alpha| - \frac{m-m_0}{\sigma_{CB}}\right)^{-n}, & \text{for } \frac{m-m_0}{\sigma_{CB}} \leq -\alpha. \end{cases} \tag{4}$$

The parameter α defines the threshold, in units of σ_{CB}, between the Gaussian and the power-law functions.

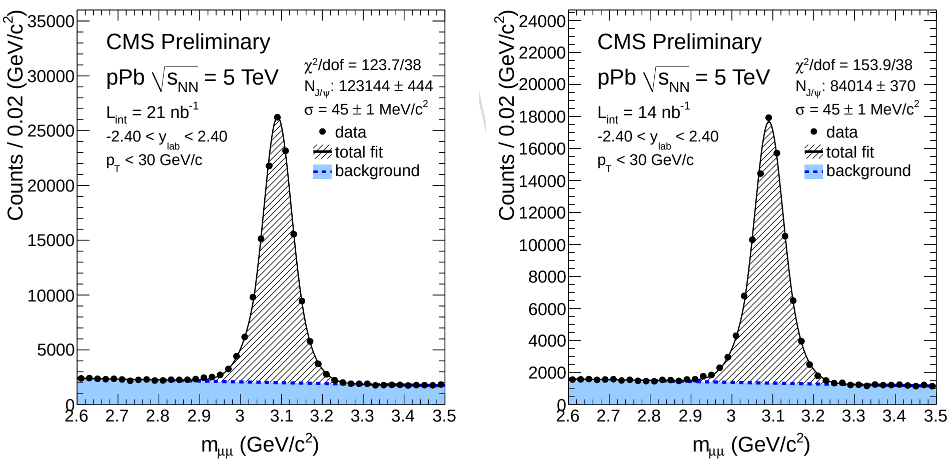

Figure 4: Invariant mass spectrum of $\mu^+\mu^-$ pairs (black circles) in the region of $-2.87 < y_{CM} < 1.93$ and $p_{\mathrm{T}} < 30$ GeV/c for the 1st run(Left) and the 2nd run period(RIGHT).

In order to study the p_{T} and y dependence of cross-section and R_{FB} measurement, the results were split in several bins of the J/ψ p_{T} and rapidity. For each measurement, bins are selected according to statistics.

Rapidity binning is as following :

$$y_{CM} = [-2.87, -2.4, -1.93, -1.5, -0.9, 0, 0.9, 1.5, 1.93]$$

Considering the rapidity shift due to the energy asymmetry between proton and Pb ion, y_{CM} corresponds to

$$y^{1st}_{lab} = [-2.4, -1.97, -1.37, -0.47, 0.43, 1.03, 1.46, 1.93, 2.4]$$

$$y^{2nd}_{lab} = [2.4, 1.97, 1.37, , 0.47, -0.43, -1.03, -1.46, -1.93, -2.4]$$

in the lab frame for the 1st run and 2nd run respectively, ordering from the forward to backward rapidity.

For the forward and backward rapidity, the CMS acceptance extends to lower p_{T}, so p_{T} binning is as following :

$$\text{For } 1.5 < y_{CM} < 1.93 \text{ and } -2.87 < y_{CM} < -2.4,\ p_{\mathrm{T}} = [0, 3, 4, 5, 6.5, 7.5, 8.5, 10, 14, 30]\ \mathrm{GeV}/c.$$

$$\text{For } 0.9 < y_{CM} < 1.5 \text{ and } -2.4 < y_{CM} < -1.93,\ p_{\mathrm{T}} = [3, 4, 5, 6.5, 7.5, 8.5, 10, 14, 30]\ \mathrm{GeV}/c.$$

$$\text{For } -1.93 < y_{CM} < -1.5,\ p_{\mathrm{T}} = [5, 6.5, 7.5, 8.5, 10, 14, 30]\ \mathrm{GeV}/c.$$

$$\text{For } -1.5 < y_{CM} < 0.9,\ p_{\mathrm{T}} = [6.5, 7.5, 8.5, 10, 14, 30]\ \mathrm{GeV}/c.$$

These values allow a better comparison with the low-p_{T} measurements of the ALICE experiment, which has acceptance for J/ψ with $p_{\mathrm{T}} > 0\,\mathrm{GeV}/c$ for the rapidity intervals $|y_{CM}| < 0.9$ and $2.4 < |y_{CM}| < 4.0$, in the electron and muon decay channels, respectively [1].

For the R_{FB} measurement, y_{CM} ranges are restricted to be symmetric as $|y_{CM}| < 1.93$. p_{T} binning is

$$\text{For } 1.5 < |y_{CM}| < 1.93,\ p_{\mathrm{T}} = [5, 6.5, 10, 30]\ \mathrm{GeV}/c.$$

$$\text{For } |y_{CM}| < 1.5,\ p_{\mathrm{T}} = [6.5, 10, 30]\ \mathrm{GeV}/c.$$

The dependency of R_{FB} with respect to event-activity variable $E_T^{HF|\eta|>4}$, the transverse energy deposited in forward hadronic calorimeter in $4 < |\eta| < 5.2$, also has been measured. Three bins of $E_T^{HF|\eta|>4}$ has been determined so that bin boundaries are consistent with other pPb analysis.

$$E_T^{HF|\eta|>4} = [0, 20, 30, 120]\,\mathrm{GeV}$$

We give two reasons for the choice of the upper bound of the p_{T} value at 30 GeV/c. First, it will allow us the direct and unambiguous comparison with PbPb analysis by using exactly the same cut. Second, the number of dimuons lost by this cut is not large, as it is illustrated in Fig. 5, where the raw counts of **all dimuons** versus their p_{T}, and 2-dimensional plots for the invariant mass vs p_{T} are shown. For the fitting, not only the yields in the mass regions [2.95-3.25] GeV/c^2, but also the yields in the side-band regions are needed to get the $\ell_{J/\psi}$ distributions of the background. Therefore, in order to get a stable statistics also for the background, we have selected the wider range for the highest p_{T} bins.

The extended unbinned maximum likelihood fit with the sum of Crystal Ball and Gaussian functions has been performed in each bins. For all the p_{T}, y and event activity binning, all parameters of the fit are left free except for the resolution model for the lifetime distribution of prompt J/ψ which are extracted from prompt MC sample. More details on fitting procedure will be elevated in the following section.

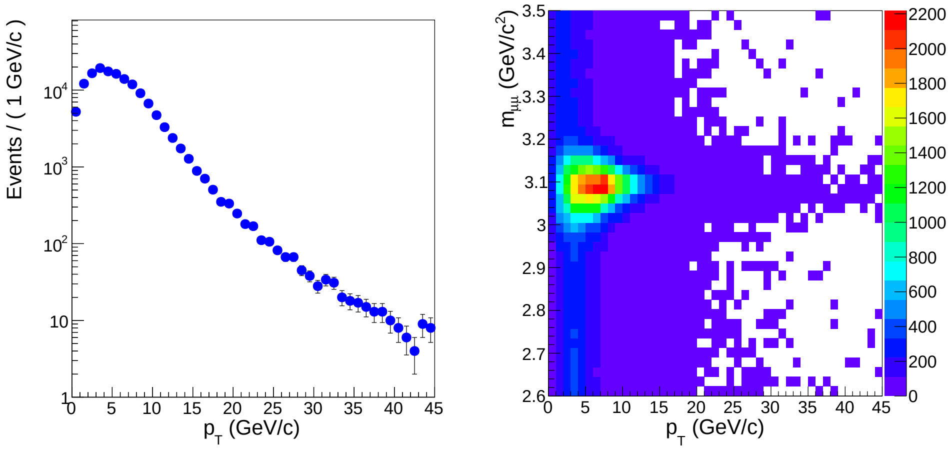

Figure 5: $\mu^+\mu^-$ pairs raw counts versus p_T (Left) and invariant mass vs p_T (Right) in $-2.87 < y_C M < 1.93$ for the 2nd run. before separating signal J/ψ dimuons from the background.

4.2 Prompt and Non-prompt J/ψ

4.2.1 Yield extraction

The identification of J/ψ mesons coming from b-hadron decays relies on the measurement of a secondary $\mu^+\mu^-$ vertex displaced from the primary collision vertex. The displacement between the $\mu^+\mu^-$ vertex and the primary vertex $\vec{r}$ is measured in the plane transverse to the beam direction. The most probable transverse b-hadron decay length in the laboratory frame [2, 3] is calculated as

$$L_{xy} = \frac{\hat{u}^T S^{-1} \vec{r}}{\hat{u}^T S^{-1} \hat{u}}, \tag{5}$$

where $\hat{u}$ is the unit vector in the direction of the J/ψ meson p_T and S is the sum of the primary and secondary vertex covariance matrices. From this quantity (which is the projected decay length of the J/ψ on transverse plane), the pseudo-proper decay length $\ell_{J/\psi} = L_{xy}\, m_{J/\psi}/p_T$ is computed as an estimate of the b-hadron decay length.

To measure the fraction of non-prompt J/ψ (the so called *b-fraction*), the invariant-mass spectrum of $\mu^+\mu^-$ pairs and their $\ell_{J/\psi}$ distribution are fitted in a two-dimensional, extended unbinned maximum likelihood fit, in bins of p_T, rapidity and event activities. In this fit, the fraction of non-prompt J/ψ is a free fit parameter. The 2D fit is a simultaneous way to take correlated probability between dimuon mass and pseudo-proper decay length into account properly [4]. For example, a event lying on the sideband region will not have high probability to be a prompt or non-prompt J/ψ. This probability calculation cannot be performed on each event without considering dimuon mass and pseudo-proper decay length at the same time.

The fitting procedure is similar to the one used in the pp analysis at $\sqrt{s}$ = 7 TeV [5] and PbPb analysis at $\sqrt{s}$ = 2.76 TeV [6]. Prompt J/ψ are produced at the primary vertex; therefore their observed displacement is described only by the resolution function. This resolution is described by a function that depends on the "per-event error" of the measured $\ell_{J/\psi}$, i.e. the uncertainty on the $\ell_{J/\psi}$ reconstructed each event, as determined from the covariance matrices of the primary and secondary vertex. These errors affect on the width of resolution function more precisely, hence the parameterization is quite improved with this technique.

The expression for the total PDF (probability density function) $F(\ell_{J/\psi}, m_{\mu\mu})$, the functional form used for the 2D fit including per-event-uncertainties, are defined as :

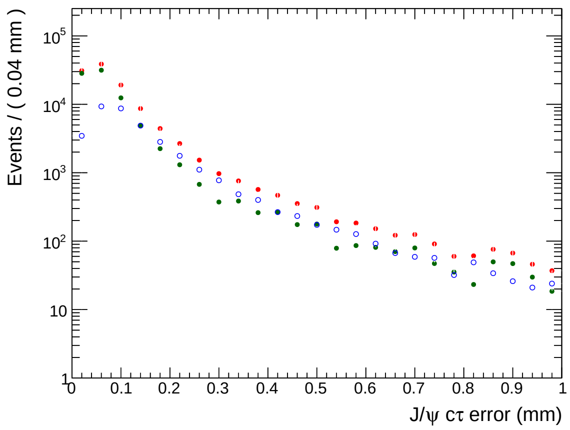

Figure 6: The distributions of lifetime errors in kinematic ranges $-2.87 < y_{CM} < 1.93$ and $p_T < 30$ GeV/c for the 2nd run period. Blue open points represent the distributions for backgrounds $D_{Bkg}(\sigma_\ell)$. Red closed points represent the distributions in mass range $[2.9-3.2]$ GeV/c^2. and green closed points indicate $D_{Sig}(\sigma_\ell)$, that is used in fitting procedure, after subtracting scaled $D_{Bkg}(\sigma_\ell)$.

$$F(\ell_{J/\psi}, m_{\mu\mu}) = \int [f_{Sig} \cdot D_{Sig}(\sigma_\ell) F_{Sig}(\ell_{J/\psi}, \sigma_\ell) \cdot M_{Sig}(m_{\mu\mu}) + (1 - f_{Sig}) \cdot D_{Bkg}(\sigma_\ell) F_{Bkg}(\ell_{J/\psi}, \sigma_\ell) \cdot M_{Bkg}(m_{\mu\mu})] d\sigma_\ell, \quad (6)$$

where:

$$F_{Sig,Bkg}(\ell_{J/\psi}, \sigma_\ell) = \sum_i F^{true}_{Sig,Bkg}(\ell_{J/\psi}) \otimes R_i(\ell_{J/\psi} - \ell'_{J/\psi} | \mu, s_i \sigma_\ell), \quad (7)$$

with

1. s_i the weighting (uncertainty) of each point in the resolution distribution, due to the consideration of the per-event-uncertainties. It modifies the shape of the resolution function (its width), but not its mean.

2. $D_{Bkg,Sig}(\sigma_\ell)$ are the distributions of the errors (as they are calculated event-by-event), separately for signal and background. $D_{Bkg}(\sigma_\ell)$ is assumed uniform over the whole mass region, [2.6-3.5] GeV/c^2. $D_{Sig}(\sigma_\ell)$ is obtained from $\ell_{J/\psi}$ distribution within the mass signal region [2.9-3.2] GeV/c^2, after subtracting scaled $D_{Bkg}(\sigma_\ell)$.

No fit is performed to $D_{Bkg,Sig}(\sigma_\ell)$ distributions; instead, they are multiplied with the prompt, non-prompt and background $\ell_{J/\psi}$ distributions, and then converted to PDFs with a suitable binning in the $\ell_{J/\psi}$ variable. The binning of $D_{Bkg,Sig}(\sigma_\ell)$ should not be too fine, otherwise there would be empty bins in the PDFs due to the lack of statistics and it cause a failure of the fit. Binning should not be too coarse either, as it affects the quality of the fit. There is no general recipe for deciding on the binning. Figure fig:cterr shows the distributions of life time errors $D_{Bkg,Sig}(\sigma_\ell)$.

With the complete formula, the 2D unbinned maximum likelihood fit is performed in 5 steps as listed below.

1. From dimuon mass distribution (the projection of the 2D PDF), get the yield of signal (inclusive, prompt and non-prompt J/ψ) and background. For the whole p_T, rapidity and event-activity bins, all the parameters related to mass distributions (parameters for the sum of Gaussian and Crystal Ball functions for signal, and an exponential function for backgrounds) are free and determined in this step.

2. Non-prompt J/ψ MC template is used to constrain the $\ell_{J/\psi}$ of B to J/ψ. Lifetime of B hadron can be ideally described by one exponential function but there is an additional resolutions when it decays into J/ψ. Therefore, for lifetime distribution of non-prompt J/ψ, we use the convolution of one resolution function and one Gaussian. Slope of the exponential function is estimated but this value is only used as a initial value and determined in the last step. Parameters related to the resolution functions are fixed to MC templates.

3. The prompt J/ψ $\ell_{J/\psi}$ function parameters are initialized based on the prompt J/ψ MC template. Since the per-event-error method is used for this analysis, prompt J/ψ pseudo-proper decay length can be described with sum of 2 Gaussian functions. One of them describes most of the parts and the other Gaussian takes the tail components. Fraction of the two Gaussian and narrower width of one Gaussian are fixed by MC, and wider width of another Gaussian will be left free and determined in the last step of fitting.

4. The background parameters of $\ell_{J/\psi}$ are determined with the mass sideband regions: [2.6-2.9] and [3.2-3.5] GeV/c^2. Combination of exponential decay functions with 3 different slopes are used for $\ell_{J/\psi}$ background function. Their slopes are determined in this step.

5. With the pre-fitted setting of the parameters, the total PDF is fit over all dimuons, to get the B-fraction. In summary, B-fraction, the slope of non-prompt J/ψ lifetime, and wider width of resolution model is determined at this last step. Non-prompt J/ψ yields are calculated by multiplying the B-fraction with the inclusive yields.

Example of 2D fits are given in Fig. 7, for the 1st run period. For the 2nd run period, Example of 2D fits are given in Fig. 8. Plots for the whole bins can be found in appendix A.

Also, information of all the fit parameters for each bins is reported in more details in appendix D.

4.2.2 Systematic Uncertainties

To estimate the systematic uncertainty due to fitting procedure, alternative fit functions have been considered for the mass and lifetime distributions [6]. The differences compared to the nominal method are taken as the systematic uncertainties. The detailed sources of the systematic uncertainty include the followings:

- Variation of the signal lineshape in the dimuon mass distribution: single Crystal Ball function is considered and compared to the nominal model that uses the sum of a Crystal Ball and a Gaussian function.
- Variation of the background fit function in the dimuon mass distribution: the straight line is tested and compare to the nominal one exponential function.
- Resolution model for the lifetime of prompt J/ψ: the nominal double-Gaussian shape for the pseudo proper decay length per-event resolution is compared to single Gaussian shape to estimate the effect of the tail components.

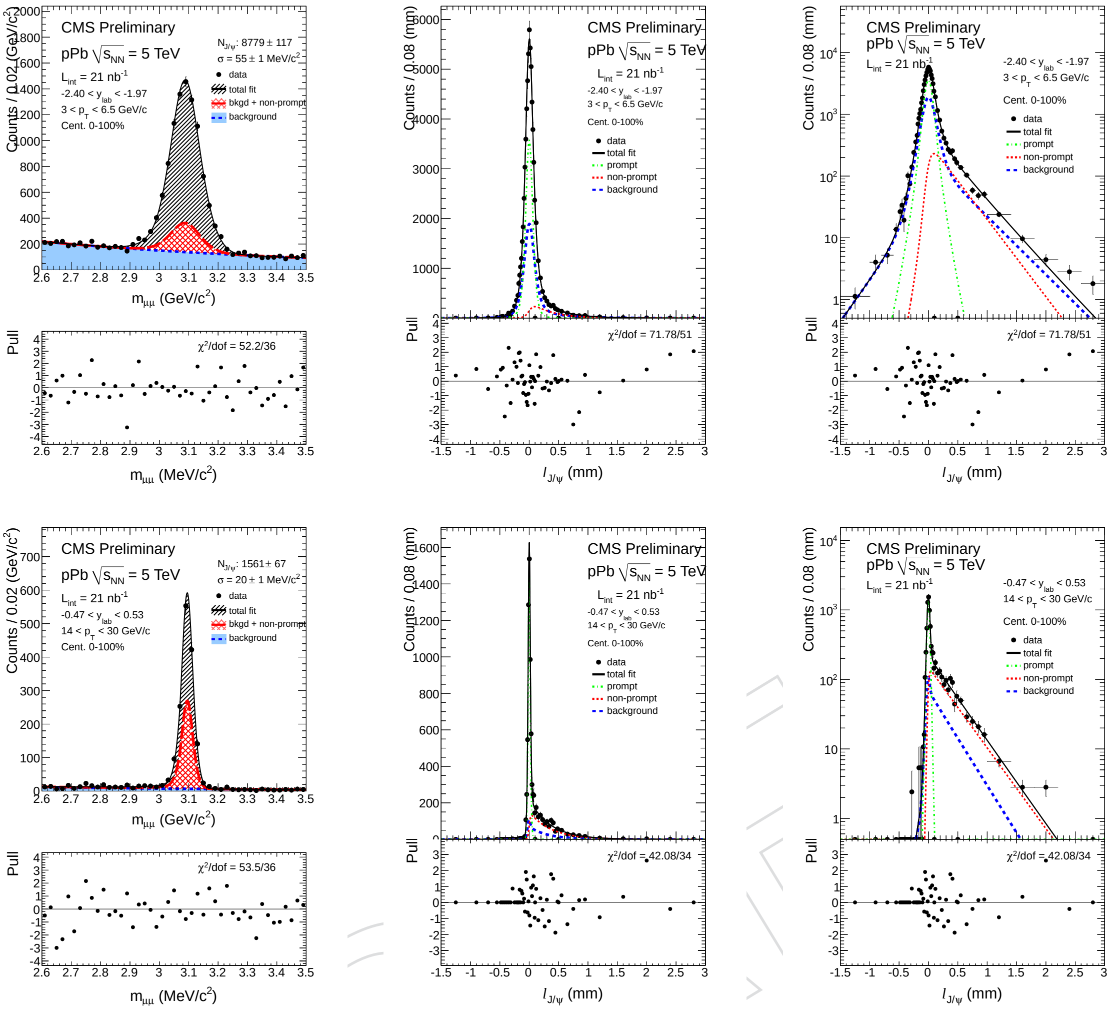

Figure 7: Invariant-mass spectra (left) and pseudo-proper decay length distributions (center, right) of $\mu^{+}\mu^{-}$ pairs for the most forward rapidity $-2.4 < y_{lab} < -1.97$ with $3 < p_{\mathrm{T}} < 6.5$ GeV/c (top) and the mid-rapidity bin $-0.47 < y_{lab} < 1.97$ with $14 < p_{\mathrm{T}} < 30$ GeV/c (bottom) from the 1st run period. The projections of the two-dimensional fit onto the respective axes are overlaid as solid black lines. The dashed red lines show the fitted contribution of non-prompt J/ψ. The fitted background contributions are shown as dotted blue lines.

- B lifetime model: alternative B lifetime model used in Ref. [7], based on MC templates is tested and the difference in the fitted non-prompt fraction is taken as the systematic uncertainty.

All the case are summed in quadrature to estimate systematic uncertainties of the J/ψ yields and they vary from 0.6% to 3.5% for prompt J/ψ component and up to 5.9% for non-prompt component. Table 2 and table 3 show the raw yields of prompt J/ψ extracted from the nominal fitting and 4 other options, and consequent values of the systematic uncertainties with the binning of cross-section measurement.

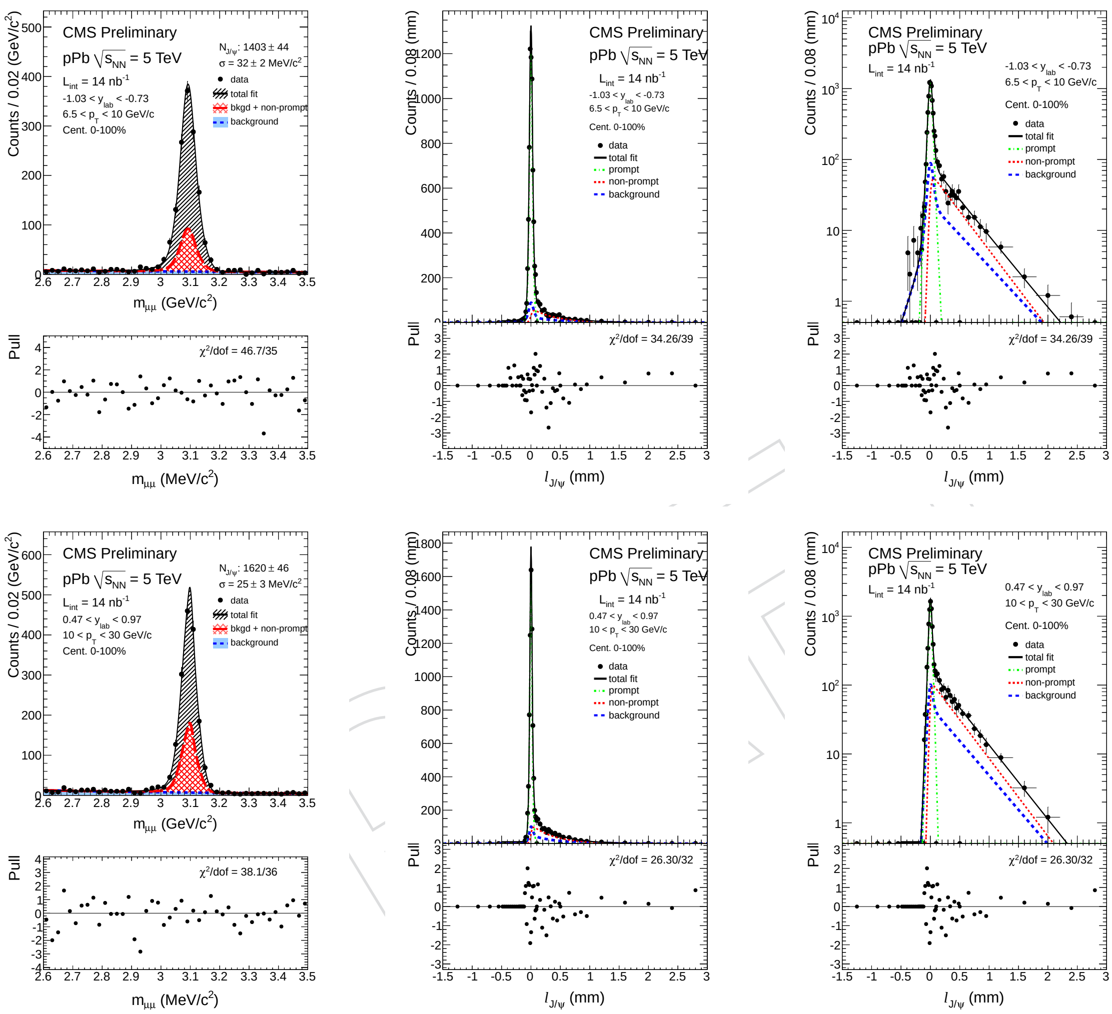

Figure 8: Invariant-mass spectra (left) and pseudo-proper decay length distributions (center, right) of $\mu^+\mu^-$ pairs for the rapidity bin $-1.03 < y_{lab} < 0.73$ with $6.5 < p_T < 10$ GeV/c(top) and the rapidity bin $0.47 < y_{lab} < 0.97$ with $10 < p_T < 30$ GeV/c(bottom) from the 2nd run period. The projections of the two-dimensional fit onto the respective axes are overlaid as solid black lines. The dashed red lines show the fitted contribution of non-prompt J/ψ. The fitted background contributions are shown as dotted blue lines.

Table 2: Systematic uncertainties of prompt J/ψ from signal extraction. ″mass sig.″ refers to the variation of the lineshape in the dimuon mass distribution, ″mass bkg.″ refers to the variation of the background fit function in the dimuon mass distribution, ″lifetime PR″ refers to the resolution model for the lifetime of prompt J/ψ, and ″lifetime NP″ refers to the B lifetime model described in the text.

y_{CM}(J/ψ)	p_T(J/ψ) [GeV/c]	nominal	mass sig.	mass bkg.	lifetime PR	lifetime NP	rel.err[%]
$1.5 < y_{CM} < 1.93$	$0.0 \leq p_T < 3.0$	8932.7	8953.06	8807.53	8828.53	8736.62	2.86
	$3.0 \leq p_T < 4.0$	4685.47	4712.65	4599.49	4662.3	4641.93	2.19
	$4.0 \leq p_T < 5.0$	3866.25	3844.93	3760.31	3856.84	3906.9	3.00
	$5.0 \leq p_T < 6.5$	4039.35	4166.55	4003.93	4046.44	4082.62	2.37
	$6.5 \leq p_T < 7.5$	1871.931	1887.7	1850.697	1866.856	1866.827	1.75
	$7.5 \leq p_T < 8.5$	1306.929	1307.923	1294.191	1320.098	1317.63	1.63
	$8.5 \leq p_T < 10.0$	1024.946	1045.074	1019.823	1028.802	1048.039	3.05
	$10.0 \leq p_T < 14.0$	1035.018	1039.28	1026.131	1069.727	1045.724	3.64
	$14.0 \leq p_T < 30.0$	344.863	352.462	343.405	345.116	359.68	4.85
$0.9 < y_{CM} < 1.5$	$3.0 \leq p_T < 4.0$	4058.85	4051.7	4017.69	4048.43	4038.07	1.18
	$4.0 \leq p_T < 5.0$	5891.42	5735.96	5864.44	5909.73	5925.41	2.76
	$5.0 \leq p_T < 6.5$	9667.06	9713.44	9608.75	9749.12	9630.33	1.21
	$6.5 \leq p_T < 7.5$	5049.04	5050.19	5040.55	5022.93	5071.47	0.70
	$7.5 \leq p_T < 8.5$	3357.58	3362.81	3334.37	3353.21	3364.52	0.75
	$8.5 \leq p_T < 10.0$	3023.64	3049.33	3301.21	3046.67	3364.52	1.39
	$10.0 \leq p_T < 14.0$	2640.11	2653.98	2631.65	2675.28	2634.11	1.48
	$14.0 \leq p_T < 30.0$	847.574	847.111	843.956	836.541	835.101	2.01
$0.0 < y_{CM} < 0.9$	$6.5 \leq p_T < 7.5$	2844.63	2849.41	2843.51	2851.7	2829.76	0.60
	$7.5 \leq p_T < 8.5$	2831.81	2825.93	2827.64	2790.04	2849.76	1.63
	$8.5 \leq p_T < 10.0$	3121.5	3119.59	3108.92	3166.16	3117.96	1.49
	$10.0 \leq p_T < 14.0$	3569.01	3562.04	3559.57	3535.57	3562.6	1.01
	$14.0 \leq p_T < 30.0$	1346.237	1349.229	1342.377	1311.205	1340.373	2.66
$-0.9 < y_{CM} < 0.0$	$6.5 \leq p_T < 7.5$	896.83	898.993	897.278	894.499	896.105	0.37
	$7.5 \leq p_T < 8.5$	1697.993	1694.513	1695.888	1687.697	1694.16	0.69
	$8.5 \leq p_T < 10.0$	2430.902	2429.409	2427.952	2409.694	2414.415	1.11
	$10.0 \leq p_T < 14.0$	3127.94	3126.57	3121.72	3116.3	3138.15	0.54
	$14.0 \leq p_T < 30.0$	1302.543	1300.443	1298.618	1285.706	1301.198	1.34

Table 3: Systematic uncertainties of prompt J/ψ from signal extraction ,continued from table 2.

y_{CM}(J/ψ)	p_{T}(J/ψ) [GeV/c]	nominal	mass sig.	mass bkg.	lifetime PR	lifetime NP	rel.err[%]
$-1.5 < y_{CM} < -0.9$	$6.5 \leq p_{\mathrm{T}} < 7.5$	1152.02	1151.281	1151.893	1148.427	1161.793	0.91
	$7.5 \leq p_{\mathrm{T}} < 8.5$	1494.142	1490.047	1497.268	1481.068	1492.454	0.95
	$8.5 \leq p_{\mathrm{T}} < 10.0$	1816.908	1830.611	1825.883	1803.911	1823.232	1.20
	$10.0 \leq p_{\mathrm{T}} < 14.0$	2183.251	2176.103	2173.579	2181.169	2173.394	0.72
	$14.0 \leq p_{\mathrm{T}} < 30.0$	802.378	798.946	794.322	802.576	793.544	1.55
$-1.93 < y_{CM} < -1.5$	$5.0 \leq p_{\mathrm{T}} < 6.5$	2717.85	2705.59	2711.51	2717.82	2738.18	0.90
	$6.5 \leq p_{\mathrm{T}} < 7.5$	2150.914	2173.281	2159.24	2128.726	2158.171	1.55
	$7.5 \leq p_{\mathrm{T}} < 8.5$	1717.211	1720.342	1711.173	1730.888	1715.922	0.89
	$8.5 \leq p_{\mathrm{T}} < 10.0$	1758.656	1753.602	1754.027	1719.87	1753.02	2.26
	$10.0 \leq p_{\mathrm{T}} < 14.0$	1642.792	1648.573	1635.128	1627.051	1634.542	1.23
	$14.0 \leq p_{\mathrm{T}} < 30.0$	468.969	475.062	466.31	472.737	469.811	1.64
$-2.4 < y_{CM} < -1.93$	$3.0 \leq p_{\mathrm{T}} < 4.0$	3664.91	3652.58	3635.64	3669.34	3648.52	0.98
	$4.0 \leq p_{\mathrm{T}} < 5.0$	5302.43	5160.8	5139.12	5268.3	5357.5	4.26
	$5.0 \leq p_{\mathrm{T}} < 6.5$	8022.13	7984.93	7941.18	7939.76	7999.48	1.54
	$6.5 \leq p_{\mathrm{T}} < 7.5$	3584.72	3618.41	3577.28	3576.8	3602.1	1.10
	$7.5 \leq p_{\mathrm{T}} < 8.5$	2422.534	2459.48	2416.355	2420.409	2418.678	1.56
	$8.5 \leq p_{\mathrm{T}} < 10.0$	2051.496	2035.532	2024.754	2071.799	2041.911	1.87
	$10.0 \leq p_{\mathrm{T}} < 14.0$	1614.691	1612.199	1608.408	1608.908	1622.787	0.74
	$14.0 \leq p_{\mathrm{T}} < 30.0$	472.825	478.694	472.466	474.471	472.941	1.29
$-2.87 < y_{CM} < -2.4$	$0.0 \leq p_{\mathrm{T}} < 3.0$	10815.79	11018.08	10826.62	10772.11	11054.81	2.92
	$3.0 \leq p_{\mathrm{T}} < 4.0$	5534.38	5626.49	5417.99	5544.21	5571.98	2.77
	$4.0 \leq p_{\mathrm{T}} < 5.0$	4512.36	4597.84	4435.82	4543.12	4502.22	2.64
	$5.0 \leq p_{\mathrm{T}} < 6.5$	4406.48	4496.34	4346.63	4366.15	4413.08	2.62
	$6.5 \leq p_{\mathrm{T}} < 7.5$	1797.776	1780.905	1783.01	1810.386	1810.32	1.59
	$7.5 \leq p_{\mathrm{T}} < 8.5$	1195.763	1193.49	1177.81	1177.071	1187.959	2.27
	$8.5 \leq p_{\mathrm{T}} < 10.0$	1038.421	1045.595	1021.3	1031.026	1030.985	2.05
	$10.0 \leq p_{\mathrm{T}} < 14.0$	916.741	904.895	909.26	922.1	933.303	2.44
	$14.0 \leq p_{\mathrm{T}} < 30.0$	224.4437	232.4449	223.7684	229.0889	231.5863	5.22

Table 4: Systematic uncertainties of non-prompt J/ψ from signal extraction. "mass sig." refers to the variation of the lineshape in the dimuon mass distribution, "mass bkg." refers to the variation of the background fit function in the dimuon mass distribution, "lifetime PR" refers to the resolution model for the lifetime of prompt J/ψ, and "lifetime NP" refers to the B lifetime model described in the text.

$y_{CM}(J/\psi)$	$p_T(J/\psi)$ [GeV/c]	nominal	mass sig.	mass bkg.	lifetime PR	lifetime NP	rel.err[%]
$1.5 < y_{CM} < 1.93$	$0.0 \le p_T < 3.0$	1326.22	1326.17	1305.752	1430.393	1522.299	16.81
	$3.0 \le p_T < 4.0$	718.542	721.966	704.785	741.709	762.087	7.14
	$4.0 \le p_T < 5.0$	807.897	805.276	783.63	817.313	767.25	5.98
	$5.0 \le p_T < 6.5$	1003.352	1031.983	989.485	996.268	960.084	5.40
	$6.5 \le p_T < 7.5$	450.868	454.158	439.413	461.944	461.976	4.37
	$7.5 \le p_T < 8.5$	369.578	370.389	358.34	356.409	358.877	5.51
	$8.5 \le p_T < 10.0$	393.865	407.617	388.432	390.01	370.772	7.03
	$10.0 \le p_T < 14.0$	517.51	522.416	509.008	482.801	506.804	7.27
	$14.0 \le p_T < 30.0$	268.634	278.09	266.533	268.381	253.817	6.59
$0.9 < y_{CM} < 1.5$	$3.0 \le p_T < 4.0$	762.514	759.246	755.765	772.934	783.286	3.20
	$4.0 \le p_T < 5.0$	1192.304	1167.086	1113.729	1173.99	1158.317	7.64
	$5.0 \le p_T < 6.5$	2237.047	2254.146	2214.686	2154.983	2273.787	4.21
	$6.5 \le p_T < 7.5$	1397.461	1400.639	1390.451	1423.56	1375.02	2.52
	$7.5 \le p_T < 8.5$	1037.314	1036.204	1024.347	1041.684	1030.379	1.48
	$8.5 \le p_T < 10.0$	1070.405	1089.468	1052.093	1047.384	1079.581	3.39
	$10.0 \le p_T < 14.0$	1346.296	1360.949	1333.506	1311.129	1352.302	3.02
	$14.0 \le p_T < 30.0$	661.413	661.884	650.393	672.447	673.887	3.02
$0.0 < y_{CM} < 0.9$	$6.5 \le p_T < 7.5$	771.408	771.879	770.647	764.334	786.288	2.14
	$7.5 \le p_T < 8.5$	893.116	890.027	889.835	934.887	875.163	5.12
	$8.5 \le p_T < 10.0$	1289.022	1288.329	1275.783	1244.363	1292.552	3.62
	$10.0 \le p_T < 14.0$	1626.986	1615.827	1613.052	1660.428	1633.393	2.36
	$14.0 \le p_T < 30.0$	1112.933	1115.148	1105.446	1147.965	1118.797	3.27
$-0.9 < y_{CM} < 0.0$	$6.5 \le p_T < 7.5$	287.681	288.654	286.964	290.011	288.406	0.95
	$7.5 \le p_T < 8.5$	601.176	599.798	598.987	611.474	605.009	1.88
	$8.5 \le p_T < 10.0$	802.236	801.261	798.45	823.446	818.728	3.38
	$10.0 \le p_T < 14.0$	1500.194	1495.259	1492.2	1511.834	1489.989	1.21
	$14.0 \le p_T < 30.0$	933.462	929.975	924.589	950.3	934.807	2.08

Table 5: Systematic uncertainties of non-prompt J/ψ from signal extraction ,continued from table 4.

y_{CM}(J/ψ)	p_T(J/ψ) [GeV/c]	nominal	mass sig.	mass bkg.	lifetime PR	lifetime NP	rel.err[%]
$-1.5 < y_{CM} < -0.9$	$6.5 \leq p_T < 7.5$	1307.222	304.19	307.093	310.815	297.449	3.53
	$7.5 \leq p_T < 8.5$	483.884	483.724	485.677	496.958	485.572	2.75
	$8.5 \leq p_T < 10.0$	601.585	614.781	606.358	614.585	595.26	3.35
	$10.0 \leq p_T < 14.0$	1041.078	1032.184	1027.496	1043.157	1050.931	1.84
	$14.0 \leq p_T < 30.0$	636.419	632.447	620.758	636.221	645.252	2.89
$-1.93 < y_{CM} < -1.5$	$5.0 \leq p_T < 6.5$	606.938	607.182	605.353	606.966	586.609	3.36
	$6.5 \leq p_T < 7.5$	603.16	608.972	604.658	625.348	595.904	4.00
	$7.5 \leq p_T < 8.5$	475.837	476.909	470.336	462.165	477.128	3.12
	$8.5 \leq p_T < 10.0$	503.632	502.732	500.709	542.417	509.268	7.81
	$10.0 \leq p_T < 14.0$	671.807	676.858	664.081	687.547	680.056	2.98
	$14.0 \leq p_T < 30.0$	368.359	379.309	361.906	364.59	367.517	3.61
$-2.4 < y_{CM} < -1.93$	$3.0 \leq p_T < 4.0$	557.543	553.387	553.186	553.105	573.925	3.23
	$4.0 \leq p_T < 5.0$	938.231	910.81	907.247	972.371	883.17	8.19
	$5.0 \leq p_T < 6.5$	1502.96	1495.256	1483.663	1585.319	1525.607	5.85
	$6.5 \leq p_T < 7.5$	868.59	879.589	866.02	876.509	851.211	2.55
	$7.5 \leq p_T < 8.5$	596.915	606.48	594.172	599.034	600.765	1.82
	$8.5 \leq p_T < 10.0$	617.953	611.953	602.233	597.645	627.536	4.54
	$10.0 \leq p_T < 14.0$	710.75	713.192	703.23	716.533	702.654	1.79
	$14.0 \leq p_T < 30.0$	291.753	298.723	291.321	290.107	291.637	2.46
$-2.87 < y_{CM} < -2.4$	$0.0 \leq p_T < 3.0$	1129.365	1147.869	1127.838	1301.164	1018.464	18.18
	$3.0 \leq p_T < 4.0$	871.431	884.125	849.533	861.593	833.829	5.32
	$4.0 \leq p_T < 5.0$	767.994	784.31	752.083	737.24	778.15	5.16
	$5.0 \leq p_T < 6.5$	788.876	811.272	774.454	829.211	782.277	6.18
	$6.5 \leq p_T < 7.5$	470.148	465.316	463.94	457.532	457.604	4.14
	$7.5 \leq p_T < 8.5$	308.483	306.44	300.644	327.174	316.285	7.07
	$8.5 \leq p_T < 10.0$	321.22	324.838	312.878	328.615	328.656	4.32
	$10.0 \leq p_T < 14.0$	371.091	360.568	362.867	380.294	369.091	4.40
	$14.0 \leq p_T < 30.0$	151.536	159.7017	150.6509	146.8912	144.3938	7.81

Table 6: Systematic uncertainties of prompt J/ψ from signal extraction. "mass sig." refers to the variation of the lineshape in the dimuon mass distribution, "mass bkg." refers to the variation of the background fit function in the dimuon mass distribution, "lifetime PR" refers to the resolution model for the lifetime of prompt J/ψ, and "lifetime NP" refers to the B lifetime model described in the text. Bins are tuned for R_{FB} measurement with $E_T^{HF|\eta|>4}$ dependence

y_{CM}(J/ψ)	p_T(J/ψ) [GeV/c]	$E_T^{HF\|\eta\|>4}$ [GeV]	nominal	mass sig.	mass bkg.	lifetime PR	lifetime NP	rel.err[%]
$1.5 < y_{CM} < 1.93$	$5.0 \le p_T < 6.5$	0-20	1833.83	1846.506	1812.184	1842.606	1856.22	1.89
	$5.0 \le p_T < 6.5$	20-30	1265.182	1284.425	1269.627	1260.078	1266.44	1.62
	$5.0 \le p_T < 6.5$	30 $\le$	957.205	972.861	941.577	956.036	972.94	2.84
	$6.5 \le p_T < 10.0$	0-20	1862.403	1888.996	1845.713	1871.198	1864.529	1.75
	$6.5 \le p_T < 10.0$	20-30	1298.578	1311.539	1284.058	1302.746	1309.368	1.74
	$6.5 \le p_T < 10.0$	30 $\le$	1057.264	1063.212	1046.964	1054.07	1053.266	1.22
	$10.0 \le p_T < 30.0$	0-20	624.12	627.663	620.087	636.727	637.079	3.02
	$10.0 \le p_T < 30.0$	20-30	432.845	442.475	430.914	440.761	436.624	3.04
	$10.0 \le p_T < 30.0$	30 $\le$	328.658	332.39	326.224	338.472	335.853	3.94
$0.9 < y_{CM} < 1.5$	$6.5 \le p_T < 10.0$	0-20	4988.19	4989.1	4952.37	4991.79	4988	0.72
	$6.5 \le p_T < 10.0$	20-30	3655.37	3664.18	3624.45	3656.97	3675.83	1.04
	$6.5 \le p_T < 10.0$	30 $\le$	2763.07	2780.95	2753.84	2764.47	2761.95	0.73
	$10.0 \le p_T < 30.0$	0-20	1521.555	1516.425	1514.939	1543.592	1509.061	1.75
	$10.0 \le p_T < 30.0$	20-30	1122.981	1125.45	1116.457	1125.916	1107.178	1.56
	$10.0 \le p_T < 30.0$	30 $\le$	849.562	850.412	848.478	848.106	863.937	1.71
$0.0 < y_{CM} < 0.9$	$6.5 \le p_T < 10.0$	0-20	3737.76	3730.52	3732.21	3750.5	3734.45	0.43
	$6.5 \le p_T < 10.0$	20-30	2875.36	2868.41	2868.84	2884.9	2887.5	0.63
	$6.5 \le p_T < 10.0$	30 $\le$	2163.796	2158.983	2148.453	2175.669	2157.223	0.97
	$10.0 \le p_T < 30.0$	0-20	2082.92	2084.342	2076.291	2065.489	2078.273	0.93
	$10.0 \le p_T < 30.0$	20-30	1594.895	1590.896	1585.585	1584.704	1597.095	0.91
	$10.0 \le p_T < 30.0$	30 $\le$	1197.559	1191.972	1193.82	1191.483	1191.835	0.89

Table 7: Systematic uncertainties of prompt J/ψ from signal extraction ,continued from table 6.

y_{CM}(J/ψ)	p_T(J/ψ) [GeV/c]	$E_T^{HF\|\eta\|>4}$ [GeV]	nominal	mass sig.	mass bkg.	lifetime PR	lifetime NP	rel.err[%]
$-0.9 < y_{CM} < 0.0$	$6.5 \leq p_T < 10.0$	0-20	2063.17	2062.946	2060.842	2044.489	2054.425	1.01
	$6.5 \leq p_T < 10.0$	20-30	1633.163	1634.019	1633.486	1616.761	1617.31	1.40
	$6.5 \leq p_T < 10.0$	$30 \leq$	1367.821	1356.552	1365.12	1348.514	1365.123	1.66
	$10.0 \leq p_T < 30.0$	0-20	1869.308	1868.251	1860.778	1850.516	1873.525	1.13
	$10.0 \leq p_T < 30.0$	20-30	1480.037	1466.695	1465.161	1471.476	1482.929	1.48
	$10.0 \leq p_T < 30.0$	$30 \leq$	1092.244	1094.728	1090.211	1084.862	1092.85	074
$-1.5 < y_{CM} < -0.9$	$6.5 \leq p_T < 10.0$	0-20	1827.36	1812.979	1823.171	1813.985	1821.424	1.15
	$6.5 \leq p_T < 10.0$	20-30	1477.311	1493.423	1489.849	1478.569	1478.156	1.39
	$6.5 \leq p_T < 10.0$	$30 \leq$	1156.392	1154.927	1152.297	1144.935	1172.471	1.75
	$10.0 \leq p_T < 30.0$	0-20	1263.806	1261.601	1259.292	1253.229	1259.403	0.99
	$10.0 \leq p_T < 30.0$	20-30	953.962	953.734	950.946	944.839	942.076	0.60
	$10.0 \leq p_T < 30.0$	$30 \leq$	766.307	771.163	764	765.726	756.082	1.51
$-1.93 < y_{CM} < -1.5$	$5.0 \leq p_T < 6.5$	0-20	1039.869	1030.329	1039.425	1037.4	1039.279	0.95
	$5.0 \leq p_T < 6.5$	20-30	916.871	916.235	912.675	914.394	929.199	1.45
	$5.0 \leq p_T < 6.5$	$30 \leq$	759.06	755.463	757.89	762.405	766.857	1.22
	$6.5 \leq p_T < 10.0$	0-20	2228.353	2240.095	2232.806	2219.799	2223.671	0.71
	$6.5 \leq p_T < 10.0$	20-30	1857.555	1859.05	1853.983	1846.449	1848.742	0.79
	$6.5 \leq p_T < 10.0$	$30 \leq$	1540.581	1538.286	1538.02	1530.636	1541.803	0.69
	$10.0 \leq p_T < 30.0$	0-20	834.44	833.428	830.162	830.956	830.049	0.85
	$10.0 \leq p_T < 30.0$	20-30	706.806	712.087	705.045	710.593	701.64	1.20
	$10.0 \leq p_T < 30.0$	$30 \leq$	565.056	562.498	557.477	557.177	566.752	2.01

Table 8: Systematic uncertainties of non-prompt J/ψ from signal extraction. "mass sig." refers to the variation of the lineshape in the dimuon mass distribution, "mass bkg." refers to the variation of the background fit function in the dimuon mass distribution, "lifetime PR" refers to the resolution model for the lifetime of prompt J/ψ, and "lifetime NP" refers to the B lifetime model described in the text. Bins are tuned for R_{FB} measurement with $E_T^{HF|\eta|>4}$ dependence

y_{CM}(J/ψ)	p_T(J/ψ) [GeV/c]	$E_T^{HF\|\eta\|>4}$ [GeV]	nominal	mass sig.	mass bkg.	lifetime PR	lifetime NP	rel.err[%]
$1.5 < y_{CM} < 1.93$	$5.0 \leq p_T < 6.5$	0-20	462.514	468.897	452.977	453.737	440.126	5.76
	$5.0 \leq p_T < 6.5$	20-30	336.189	341.965	337.199	341.292	334.932	2.34
	$5.0 \leq p_T < 6.5$	$30 \leq$	227.0126	233.1408	221.0744	228.182	211.2772	7.90
	$6.5 \leq p_T < 10.0$	0-20	572.635	585.416	560.048	563.846	570.51	3.51
	$6.5 \leq p_T < 10.0$	0-20	377.699	383.891	369.206	373.531	366.908	4.14
	$6.5 \leq p_T < 10.0$	0-20	238.699	240.373	233.602	241.893	242.697	3.11
	$10.0 \leq p_T < 30.0$	0-20	364.44	370.578	358.226	351.833	351.48	5.51
	$10.0 \leq p_T < 30.0$	0-20	242.372	250.772	239.982	234.455	238.593	5.11
	$10.0 \leq p_T < 30.0$	0-20	185.4467	187.8651	183.8101	175.6326	178.2518	6.75
$0.9 < y_{CM} < 1.5$	$6.5 \leq p_T < 10.0$	0-20	1598.351	1601.751	1573.414	1594.743	1598.538	1.59
	$6.5 \leq p_T < 10.0$	20-30	1147.034	1154.066	1129.887	1145.432	1126.58	2.41
	$6.5 \leq p_T < 10.0$	$30 \leq$	789.059	796.114	784.136	787.676	790.191	1.11
	$10.0 \leq p_T < 30.0$	0-20	970.197	965.559	957.141	948.16	982.691	2.98
	$10.0 \leq p_T < 30.0$	20-30	577.932	580.449	568.535	574.996	593.734	3.25
	$10.0 \leq p_T < 30.0$	$30 \leq$	486.905	485.406	485.308	488.361	472.53	3.00
$0.0 < y_{CM} < 9.0$	$6.5 \leq p_T < 10.0$	0-20	1368.293	1362.768	1363.066	1355.557	1371.608	1.11
	$6.5 \leq p_T < 10.0$	20-30	916.762	911.9	912.108	907.218	904.618	1.84
	$6.5 \leq p_T < 10.0$	$30 \leq$	710.963	709.018	702.58	699.091	717.542	2.26
	$10.0 \leq p_T < 30.0$	0-20	1268.221	1265.856	1254.668	1285.645	1272.866	1.79
	$10.0 \leq p_T < 30.0$	20-30	910.567	904.233	897.719	920.759	908.369	1.95
	$10.0 \leq p_T < 30.0$	$30 \leq$	612.541	603.812	606.69	618.617	618.266	2.19

Table 9: Systematic uncertainties of non-prompt J/ψ from signal extraction ,continued from table 8.

y_{CM}(J/ψ)	p_T(J/ψ) [GeV/c]	$E_T^{HF\|\eta\|>4}$ [GeV]	nominal	mass sig.	mass bkg.	lifetime PR	lifetime NP	rel.err[%]
$-0.9 < y_{CM} < 0.0$	$6.5 \leq p_T < 10.0$	0-20	703.266	703.546	700.589	721.944	712.01	2.96
	$6.5 \leq p_T < 10.0$	20-30	552.143	551.826	551.333	568.548	567.997	4.13
	$6.5 \leq p_T < 10.0$	30 ≤	408.044	403.836	406.126	427.351	410.742	4.91
	$10.0 \leq p_T < 30.0$	0-20	1031.729	1029.328	1022.45	1050.516	1027.511	2.08
	$10.0 \leq p_T < 30.0$	20-30	761.936	749.575	745.061	770.499	759.044	2.99
	$10.0 \leq p_T < 30.0$	30 ≤	646.025	643.102	643.059	653.407	645.419	1.32
$-1.5 < y_{CM} < -0.9$	$6.5 \leq p_T < 10.0$	0-20	629.031	621.309	625.337	642.413	634.973	2.70
	$6.5 \leq p_T < 10.0$	20-30	404.937	415.397	411.837	403.681	404.093	3.12
	$6.5 \leq p_T < 10.0$	30 ≤	370.931	370.15	368.131	382.388	354.852	5.38
	$10.0 \leq p_T < 30.0$	0-20	711.394	706.536	701.264	721.971	715.797	2.26
	$10.0 \leq p_T < 30.0$	20-30	525.693	527.206	517.863	534.817	537.58	3.23
	$10.0 \leq p_T < 30.0$	30 ≤	417.676	417.481	413.511	418.256	427.901	2.65
$-1.93 < y_{CM} < -1.5$	$5.0 \leq p_T < 6.5$	0-20	250.1595	246.4091	250.0079	252.6288	250.7498	1.81
	$5.0 \leq p_T < 6.5$	20-30	214.5905	216.618	213.4172	217.0674	202.2619	5.96
	$5.0 \leq p_T < 6.5$	30 ≤	146.8327	148.0078	146.6114	143.4875	139.0352	5.84
	$6.5 \leq p_T < 10.0$	0-20	695.217	699.013	695.223	703.77	699.899	1.51
	$6.5 \leq p_T < 10.0$	20-30	477.588	480.444	475.544	488.701	486.407	3.06
	$6.5 \leq p_T < 10.0$	30 ≤	417.765	416.44	416.71	427.71	416.543	2.43
	$10.0 \leq p_T < 30.0$	0-20	487.039	485.734	479.795	490.524	491.431	1.90
	$10.0 \leq p_T < 30.0$	20-30	328.977	333.246	326.345	325.19	334.144	2.47
	$10.0 \leq p_T < 30.0$	30 ≤	250.8379	249.6105	245.1381	258.7167	249.1419	3.97

5 Acceptance

For the calculation of the acceptance, same acceptable range of single muon as pp collision is used [????] because pp reconstruction algorithm is applied for pPb data reconstruction. For the J/ψ analysis at pPb collision, Monte Carlo samples with boosting at $\sqrt{s_{\mathrm{NN}}} = 5.02$ TeV are generated for prompt and non-prompt J/ψ using PYTHIA6 ver. 6.424 [7]. Samples for prompt and non-prompt J/ψ are independently produced applying D6Ttune and Z2StarTune respectively. The rapidity boosting in MC samples is -0.465 and this is equivalent to the 1st run period in which proton bunch is going to the negative η_{lab} region. ($\eta_{CM} = -(\eta_{lab} + 0.465)$) Since the acceptance is not affected by detector performance, we have estimated the acceptance values using samples equivalent to the 1st run period, and flipped the rapidity sign for the 2nd run period. The Prompt J/ψ sample is generated assuming no decay polarization, and the non-prompt J/ψ sample includes the polarization determined by the sum of the exclusive states from EVTGEN[8]. In addition during the generation of the event, any filter which can limit the eta or p_{T} range of muons is not used because filtered event can distort the denominator of the acceptance value.

5.1 Method

We call *dimuon signal acceptance* α, the fraction of dimuon signal, within a restricted mass interval $M1$ that is considered detectable and reconstructible in the CMS detector, but as stated above, with rapidity domain $-2.87 < |y_{CM}| < 1.93$.

$$\alpha = \frac{N^{dimuon}_{reconstructible,M1}(p_{\mathrm{T}}, y)}{N^{dimuon}_{generated}(p_{\mathrm{T}}, y)} \tag{8}$$

where $\mathrm{N}^{dimuon}_{reconstructible,M1}$ is the number of generated events in the Monte Carlo simulation, declared detectable in a given (p_{T}, y) bin and within a mass interval $M1$ ($[2.6, 3.5]$ GeV/c^2 for J/ψ) expressed in terms of the dimuon variables, and $\mathrm{N}^{dimuon}_{generated}$ represents all dimuons generated within the muon stations coverage of the CMS detector.

We declare a muon to be *detectable/reconstructible* if its reconstruction efficiency is higher than 10%. This definition is founded as the standard kinematic limit for tracker muons by pp reconstruction. The cuts in single muon p_{T} and η defined like below.

$$|\eta^{\mu}| < 1.3 \rightarrow p^{\mu}_{\mathrm{T}} > 3.3\ GeV/c \tag{9}$$

$$1.3 < |\eta^{\mu}| < 2.2 \rightarrow p^{\mu} > 2.9\ GeV/c \tag{10}$$

$$2.2 < |\eta^{\mu}| < 2.4 \rightarrow p^{\mu}_{\mathrm{T}} > 0.8\ GeV/c \tag{11}$$

5.2 Results

Figure **??** presents the generated prompt and non-prompt J/ψ in Monte-Carlo simulation, which are used as the denominator of the acceptance calculation, as a function of p_{T} and rapidity of J/ψ in the laboratory frame of the 1st run period. Figure 10 shows J/ψ that pass the single muon acceptance cut, and therefore correspond to the numerator of the acceptance. The acceptance of prompt and non-prompt J/ψ as a function of dimuon p_{T} and rapidity are shown in figure 11 with fine-grained binning, and in figure 11 with the binning for the analysis. Dashed line indicates the actual kinematic ranges actually considered in the analsysis.

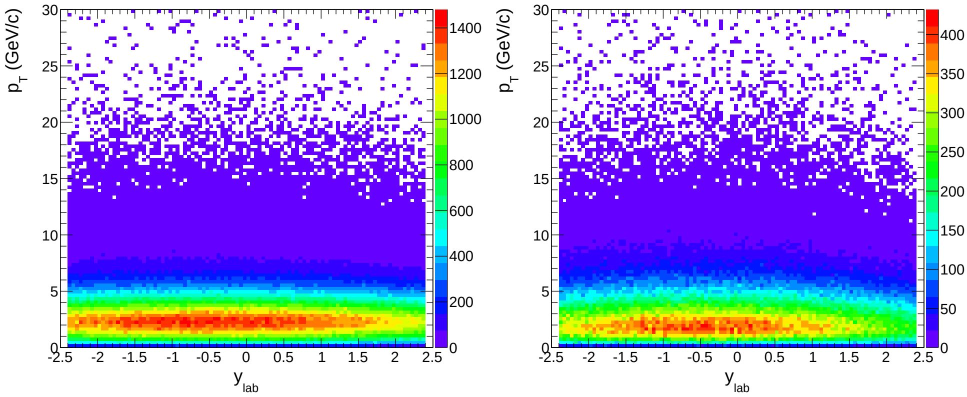

Figure 9: Generated prompt(left) and non-prompt(right) J/ψ which correspond to the denominator of the acceptance, as a function of $p_{\rm T}$ and y^{1st}_{lab} of J/ψ.

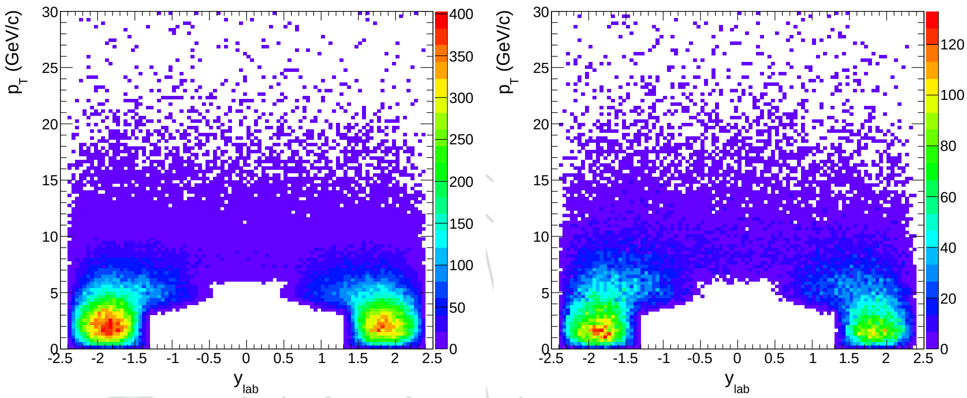

Figure 10: Generated prompt(left) and non-prompt(right) J/ψ after single muons kinematic cut is applied, as a function of $p_{\rm T}$ and y^{1st}_{lab} of J/ψ.

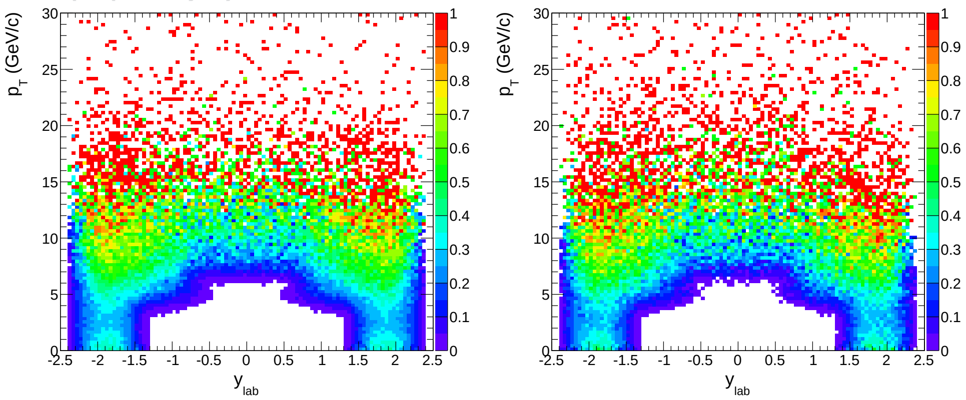

Figure 11: Acceptance of prompt(left) and non-prompt(right) J/ψ in fined-grained $p_{\rm T}$ and y_{lab}.

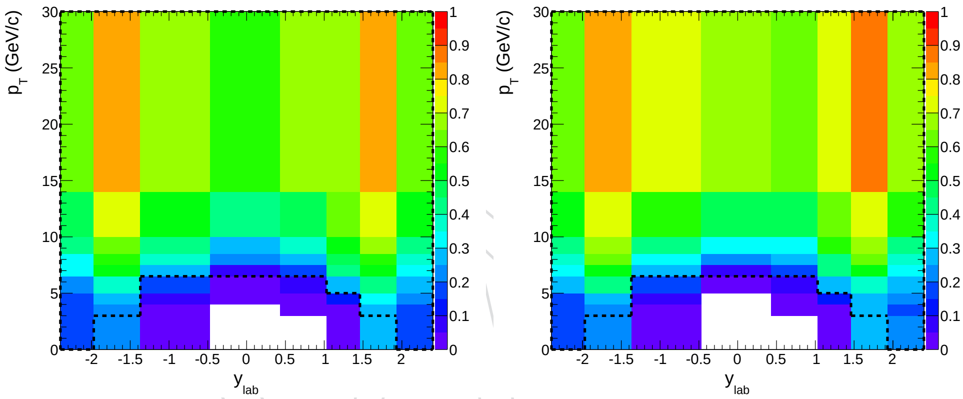

Figure 12: Acceptance of prompt(left) and non-prompt(right) J/ψ in p_{T} and y_{lab} bining used in the analysis. Dashed line indicates the actual kinematic ranges actually considered in the analsysis.

The differential acceptances as a function of rapidity y_{CM} for different p_T ranges, and as a function of p_T for different y_{CM} ranges, are shown in fig 13 for prompt J/ψ and fig 14 for non-prompt J/ψ.

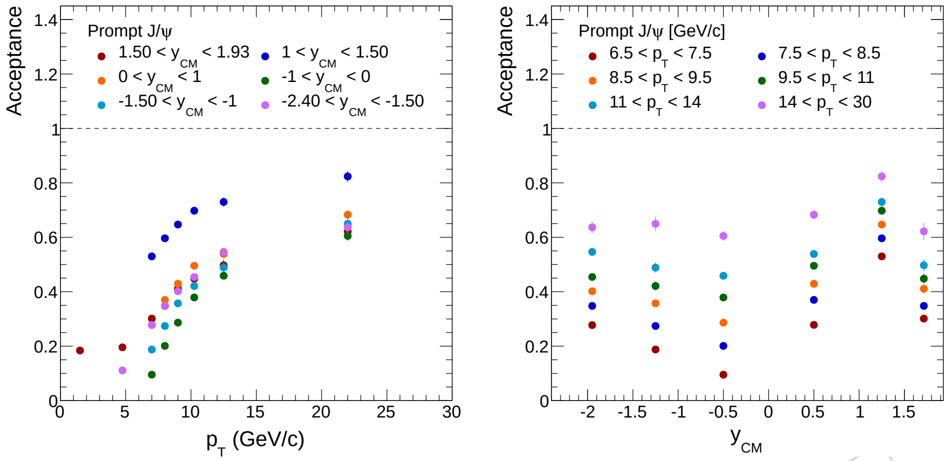

Figure 13: Binned acceptance of prompt J/ψ. Left: as the function of p_T; as the function of rapidity (Right)

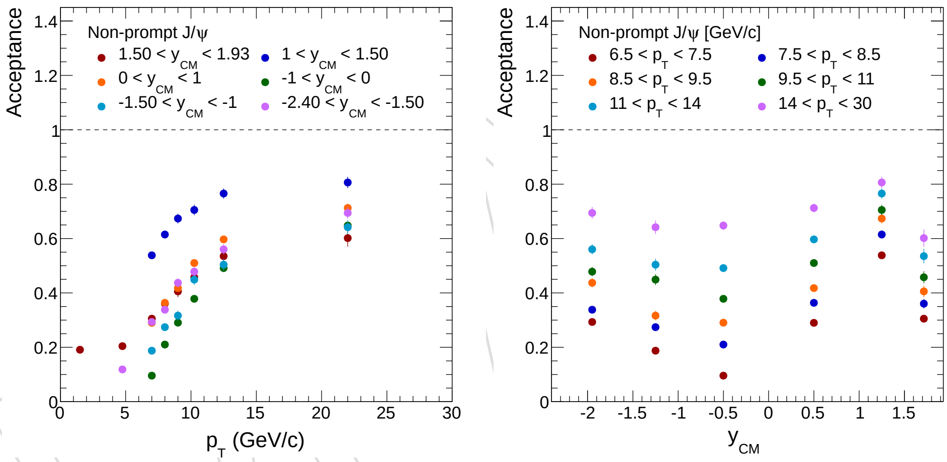

Figure 14: Binned acceptance of non-prompt J/ψ. Left: as the function of p_T; as the function of rapidity (Right)

5.3 Systematic uncertainties

Since the acceptance correction factors are fully obtained from MC, possible differences between MC and data are considered to estimate the systematic uncertainty. First, the distribution shape of p_T and rapidity in MC and data was different as shown in Section 9.3. The toy MC test has been performed to apply this discrepancy in order to inspect the propagated variance of acceptance values. With different generator tuning, initial and final state effects could be considered as one of the sources of discrepancy. But in this study we assume all the effects from various sources are mixed and reflected with the discrepancy, so we don't consider the contribution of each source.

The study is performed with following steps.

- Get ratios of normalized and uncorrected yield between data and MC with p_T and y binning for prompt J/ψ and non-prompt J/ψ. And then fit them with appropriate functions as shown in Figure 15 and Figure 16.
- Divide each p_T bin in 5 small bins to get fine binning than the current analysis binning and set the content as ratio from the fit function.
- Generate toy ratio by gaussian distribution in order that mean and sigma of the gaussian is above ratio from fit function and its relative statistical error, respectively. Those randomly generated ratios could be weighted to the Monte-Carlo and we can get the toy acceptance. Repeat that process 5k and then 5k acceptance distributions would be generated. Plots for the acceptance distributions for prompt J/ψ in each p_T and rapidity bins, and that of non-prompt can be found in appendix D.
- From the set of acceptance in each p_T and y bin, the largest differences in acceptance values between the nominal one and distribution are quoted as the systematic uncertainty. The results are shown in table 10-11 for prompt J/ψ and table 12-13 for non-prompt J/ψ with binning for cross section measurement.

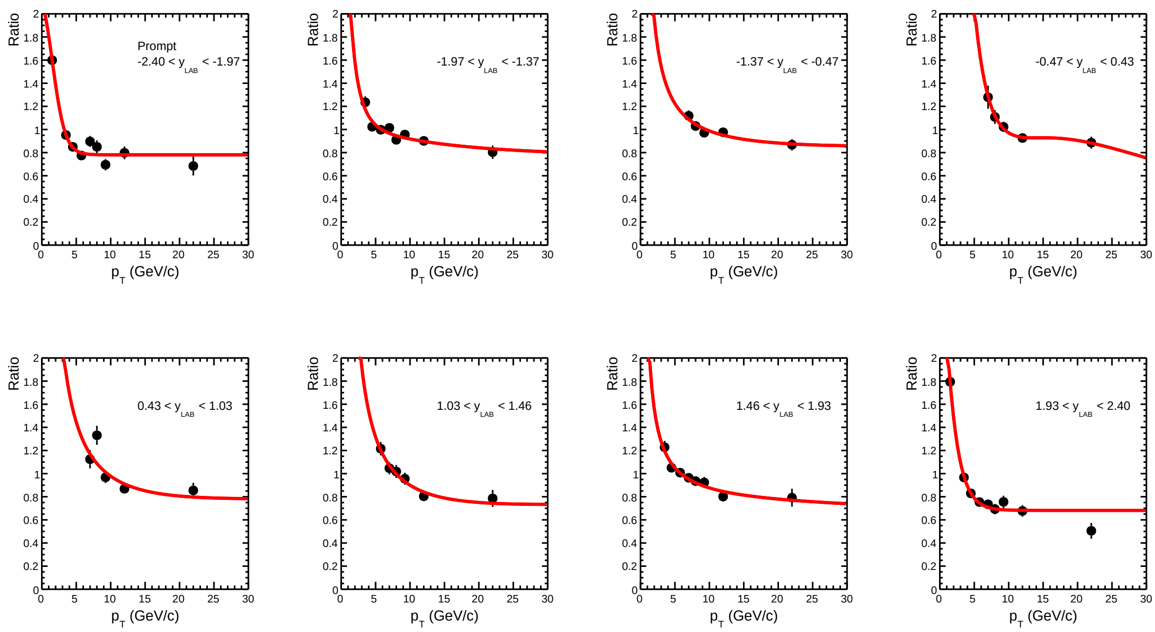

Figure 15: Ratio (DATA/MC) distributions for prompt J/ψ of the 1st run period as a function of p_T in different rapidity ranges

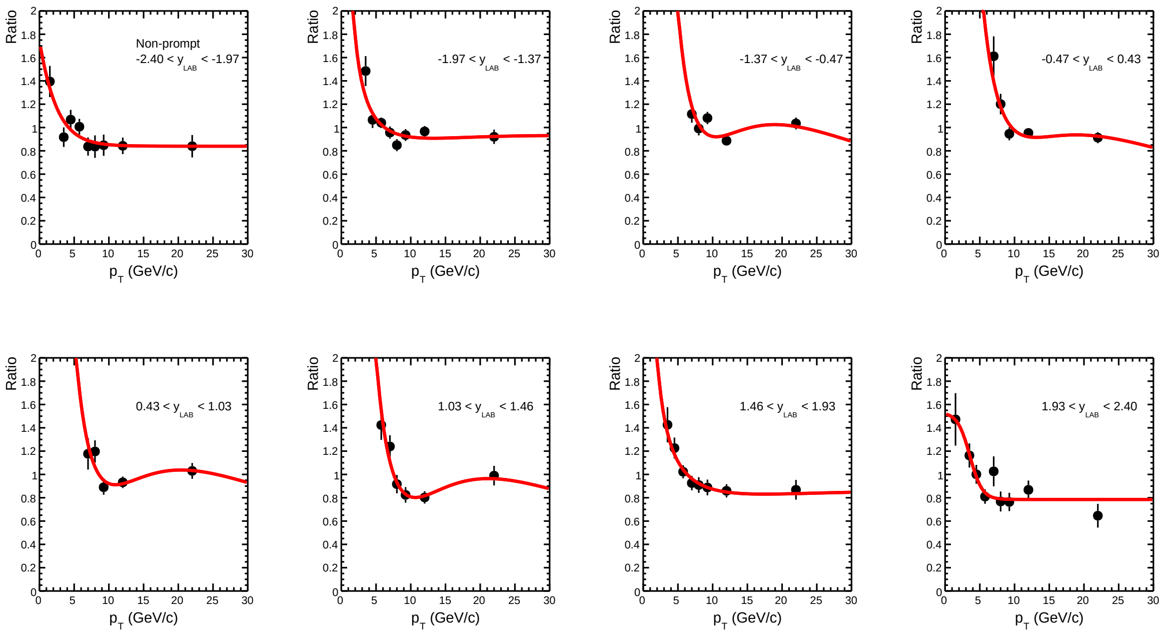

Figure 16: Ratio (DATA/MC) distributions for non-prompt J/ψ of the 1st run period as a function of p_{T} in different rapidity ranges

Table 10: The acceptance systematic values which make largest difference between nominal value and distribution and its relative errors [%] are shown as a function of p_{T} and rapidity for the prompt J/ψ.

$y_{CM}(\mathrm{J}/\psi)\|$	$p_{\mathrm{T}}(\mathrm{J}/\psi)$ [GeV/c]	Default	Max Dist. Val	rel.err [%]
	$0.0 \leq p_{\mathrm{T}} < 3.0$	0.184	0.186	0.012
$1.5 < y_{CM} < 1.93$	$3.0 \leq p_{\mathrm{T}} < 4.0$	0.178	0.177	0.337
	$4.0 \leq p_{\mathrm{T}} < 5.0$	0.197	0.196	0.406
	$5.0 \leq p_{\mathrm{T}} < 6.5$	0.236	0.235	0.339
	$6.5 \leq p_{\mathrm{T}} < 7.5$	0.301	0.304	0.796
	$7.5 \leq p_{\mathrm{T}} < 8.5$	0.348	0.344	1.265
	$8.5 \leq p_{\mathrm{T}} < 10.0$	0.427	0.423	1.030
	$10.0 \leq p_{\mathrm{T}} < 14.0$	0.466	0.460	1.286
	$14.0 \leq p_{\mathrm{T}} < 30.0$	0.622	0.639	2.799
	$3.0 \leq p_{\mathrm{T}} < 4.0$	0.236	0.235	0.297
$0.9 < y_{CM} < 1.5$	$4.0 \leq p_{\mathrm{T}} < 5.0$	0.293	0.293	0.273
	$5.0 \leq p_{\mathrm{T}} < 6.5$	0.395	0.393	0.279
	$6.5 \leq p_{\mathrm{T}} < 7.5$	0.522	0.521	0.249
	$7.5 \leq p_{\mathrm{T}} < 8.5$	0.591	0.590	0.271
	$8.5 \leq p_{\mathrm{T}} < 10.0$	0.646	0.644	0.340
	$10.0 \leq p_{\mathrm{T}} < 14.0$	0.700	0.698	0.328
	$14.0 \leq p_{\mathrm{T}} < 30.0$	0.820	0.826	0.744
	$6.5 \leq p_{\mathrm{T}} < 7.5$	0.257	0.255	0.429
$0.0 < y_{CM} < 0.9$	$7.5 \leq p_{\mathrm{T}} < 8.5$	0.351	0.349	0.342
	$8.5 \leq p_{\mathrm{T}} < 10.0$	0.423	0.421	0.378
	$10.0 \leq p_{\mathrm{T}} < 14.0$	0.517	0.515	0.329
	$14.0 \leq p_{\mathrm{T}} < 30.0$	0.669	0.664	0.762

Table 11: The acceptance systematic values, continued with table 10

y_{CM}(J/ψ)|	p_T(J/ψ) [GeV/c]	Default	Max Dist. Val	rel.err [%]
$-0.9 < y_{CM} < 0.0$	$6.5 \leq p_T < 7.5$	0.094	0.092	2.654
	$7.5 \leq p_T < 8.5$	0.204	0.202	1.079
	$8.5 \leq p_T < 10.0$	0.297	0.295	0.639
	$10.0 \leq p_T < 14.0$	0.436	0.434	0.413
	$14.0 \leq p_T < 30.0$	0.593	0.587	1.079
$-1.5 < y_{CM} < -0.9$	$6.5 \leq p_T < 7.5$	0.176	0.174	1.024
	$7.5 \leq p_T < 8.5$	0.258	0.256	0.929
	$8.5 \leq p_T < 10.0$	0.360	0.358	0.584
	$10.0 \leq p_T < 14.0$	0.460	0.456	0.739
	$14.0 \leq p_T < 30.0$	0.662	0.672	1.495
$-1.93 < y_{CM} < -1.5$	$5.0 \leq p_T < 6.5$	0.275	0.273	0.835
	$6.5 \leq p_T < 7.5$	0.406	0.404	0.443
	$7.5 \leq p_T < 8.5$	0.476	0.473	0.609
	$8.5 \leq p_T < 10.0$	0.527	0.523	0.777
	$10.0 \leq p_T < 14.0$	0.618	0.613	0.809
	$14.0 \leq p_T < 30.0$	0.691	0.677	2.084
$-2.4 < y_{CM} < -1.93$	$3.0 \leq p_T < 4.0$	0.259	0.259	0.270
	$4.0 \leq p_T < 5.0$	0.307	0.306	0.261
	$5.0 \leq p_T < 6.5$	0.422	0.420	0.356
	$6.5 \leq p_T < 7.5$	0.518	0.516	0.290
	$7.5 \leq p_T < 8.5$	0.582	0.585	0.447
	$8.5 \leq p_T < 10.0$	0.658	0.654	0.517
	$10.0 \leq p_T < 14.0$	0.747	0.743	0.496
	$14.0 \leq p_T < 30.0$	0.835	0.822	1.545
$-2.87 < y_{CM} < -2.4$	$0.0 \leq p_T < 3.0$	0.196	0.199	1.786
	$3.0 \leq p_T < 4.0$	0.188	0.187	0.426
	$4.0 \leq p_T < 5.0$	0.216	0.215	0.509
	$5.0 \leq p_T < 6.5$	0.258	0.257	0.464
	$6.5 \leq p_T < 7.5$	0.324	0.320	1.205
	$7.5 \leq p_T < 8.5$	0.391	0.395	1.177
	$8.5 \leq p_T < 10.0$	0.447	0.454	1.522
	$10.0 \leq p_T < 14.0$	0.532	0.523	1.674
	$14.0 \leq p_T < 30.0$	0.640	0.618	3.375

Table 12: The acceptance systematic values which make largest difference between nominal value and distribution and its relative errors [%] are shown as a function of p_T and rapidity for the non-prompt J/ψ.

y_{CM}(J/ψ)|	p_T(J/ψ) [GeV/c]	Default	Max Dist. Val	rel.err [%]
$1.5 < y_{CM} < 1.93$	$0.0 \leq p_T < 3.0$	0.191	0.193	1.047
	$3.0 \leq p_T < 4.0$	0.180	0.178	0.944
	$4.0 \leq p_T < 5.0$	0.195	0.193	1.181
	$5.0 \leq p_T < 6.5$	0.260	0.258	1.037
	$6.5 \leq p_T < 7.5$	0.305	0.300	1.867
	$7.5 \leq p_T < 8.5$	0.360	0.352	2.303
	$8.5 \leq p_T < 10.0$	0.409	0.417	2.129
	$10.0 \leq p_T < 14.0$	0.512	0.505	1.444
	$14.0 \leq p_T < 30.0$	0.602	0.618	2.759
$0.9 < y_{CM} < 1.5$	$3.0 \leq p_T < 4.0$	0.241	0.239	0.872
	$4.0 \leq p_T < 5.0$	0.295	0.294	0.643
	$5.0 \leq p_T < 6.5$	0.411	0.409	0.462
	$6.5 \leq p_T < 7.5$	0.530	0.527	0.453
	$7.5 \leq p_T < 8.5$	0.601	0.597	0.549
	$8.5 \leq p_T < 10.0$	0.673	0.676	0.535
	$10.0 \leq p_T < 14.0$	0.735	0.732	0.395
	$14.0 \leq p_T < 30.0$	0.808	0.813	0.681
$0.0 < y_{CM} < 0.9$	$6.5 \leq p_T < 7.5$	0.269	0.266	1.117
	$7.5 \leq p_T < 8.5$	0.346	0.343	0.838
	$8.5 \leq p_T < 10.0$	0.416	0.413	0.697
	$10.0 \leq p_T < 14.0$	0.553	0.556	0.542
	$14.0 \leq p_T < 30.0$	0.701	0.697	0.514
$-0.9 < y_{CM} < 0.0$	$6.5 \leq p_T < 7.5$	0.096	0.093	3.439
	$7.5 \leq p_T < 8.5$	0.212	0.208	1.891
	$8.5 \leq p_T < 10.0$	0.301	0.298	0.963
	$10.0 \leq p_T < 14.0$	0.461	0.458	0.607
	$14.0 \leq p_T < 30.0$	0.654	0.650	0.703

Table 13: The acceptance systematic values, continued with table 12.

$y_{CM}(J/\psi)\|$	$p_T(J/\psi)$ [GeV/c]	Default	Max Dist. Val	rel.err [%]
$-1.5 < y_{CM} < -0.9$	$6.5 \leq p_T < 7.5$	0.175	0.170	2.692
	$7.5 \leq p_T < 8.5$	0.261	0.256	1.727
	$8.5 \leq p_T < 10.0$	0.349	0.344	1.459
	$10.0 \leq p_T < 14.0$	0.465	0.469	0.816
	$14.0 \leq p_T < 30.0$	0.631	0.624	1.030
$-1.93 < y_{CM} < -1.5$	$5.0 \leq p_T < 6.5$	0.292	0.284	2.706
	$6.5 \leq p_T < 7.5$	0.408	0.401	1.740
	$7.5 \leq p_T < 8.5$	0.447	0.440	1.455
	$8.5 \leq p_T < 10.0$	0.561	0.569	1.391
	$10.0 \leq p_T < 14.0$	0.649	0.655	1.048
	$14.0 \leq p_T < 30.0$	0.743	0.732	1.494
$-2.4 < y_{CM} < -1.93$	$3.0 \leq p_T < 4.0$	0.252	0.249	1.033
	$4.0 \leq p_T < 5.0$	0.298	0.295	0.941
	$5.0 \leq p_T < 6.5$	0.394	0.390	0.863
	$6.5 \leq p_T < 7.5$	0.528	0.523	0.965
	$7.5 \leq p_T < 8.5$	0.609	0.603	0.952
	$8.5 \leq p_T < 10.0$	0.652	0.659	1.027
	$10.0 \leq p_T < 14.0$	0.735	0.729	0.830
	$14.0 \leq p_T < 30.0$	0.850	0.838	1.424
$-2.87 < y_{CM} < -2.4$	$0.0 \leq p_T < 3.0$	0.203	0.206	1.032
	$3.0 \leq p_T < 4.0$	0.195	0.193	1.026
	$4.0 \leq p_T < 5.0$	0.210	0.213	1.425
	$5.0 \leq p_T < 6.5$	0.275	0.271	1.310
	$6.5 \leq p_T < 7.5$	0.327	0.313	4.342
	$7.5 \leq p_T < 8.5$	0.396	0.408	3.084
	$8.5 \leq p_T < 10.0$	0.444	0.433	2.412
	$10.0 \leq p_T < 14.0$	0.581	0.569	2.099
	$14.0 \leq p_T < 30.0$	0.678	0.701	3.423

Since the acceptance correction factors are fully obtained from MC, possible differences between MC and data are considered to estimate the systematic uncertainty. First, the distribution shape of p_{T} and rapidity in MC and data was different by 18% and 14% respectively as shown in Section 9.3. The p_{T} and rapidity shapes of the generated MC distributions are varied linearly by $\pm$18% and $\pm$14% over the range $-2.87|y_{CM}| < 1.93$ and $0 < p_{\mathrm{T}} < 30\,\mathrm{GeV}/c$ and illustrated in figure 17 and figure 18 for prompt J/ψ. The largest differences in acceptance values between the nominal one and each cases are quoted as the systematic uncertainty.

Furthermore, the effect of the decay polarization was studied. In the nominal prompt MC sample, there is no polarization in the decay angle, while previous experimental results indicated reported non-zero values [9]. The toy MC test has been performed to include polarization by the previously measured amount [9] in order to inspect the propagated variance of acceptance value. We varied $\lambda_\theta = -0.03$ and $+0.23$ in Helicity frame based on pp analysis results as shown in figure 19. Variation of the raw distributions is 7.5%, so we concluded the effect of the polarization can be covered by the artificial variation above and didn't include into the systematic uncertainties explicitly.

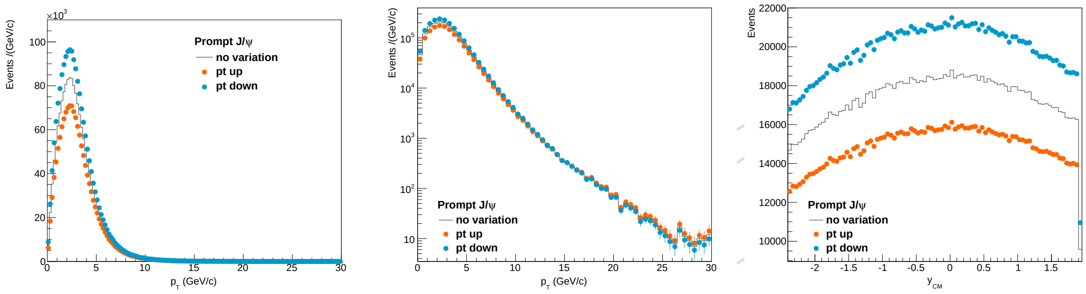

Figure 17: Raw distribution of prompt J/ψ Monte-Carlo sample with variation of p_{T} shape by $\pm$18%. p_{T} distributions with linear scale(left), log scale(middle) and rapidity distribution(right).

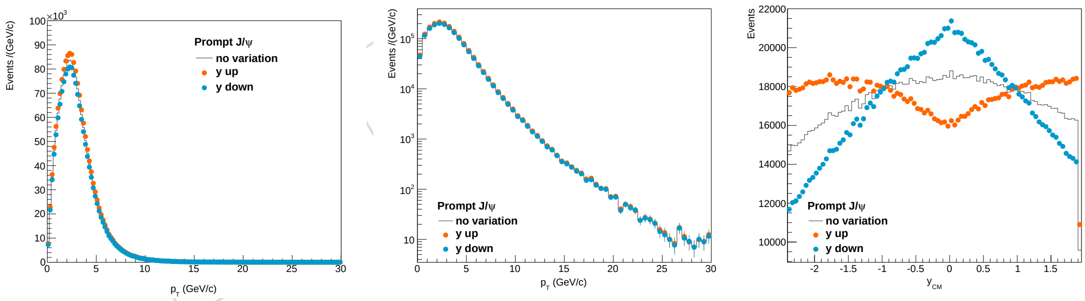

Figure 18: Raw distribution of prompt J/ψ Monte-Carlo sample with variation of y shape by $\pm$14%. p_{T} distributions with linear scale(left), log scale(middle) and rapidity distribution(right).

The results for each y_{CM} and p_{T} bins are shown in table **??** and **??** with binning for cross-section measurement, in table **??** and **??** with binning for R_{FB} measurement, and in table **??** and **??**with binning for R_{FB} measurement with event-activity dependence.

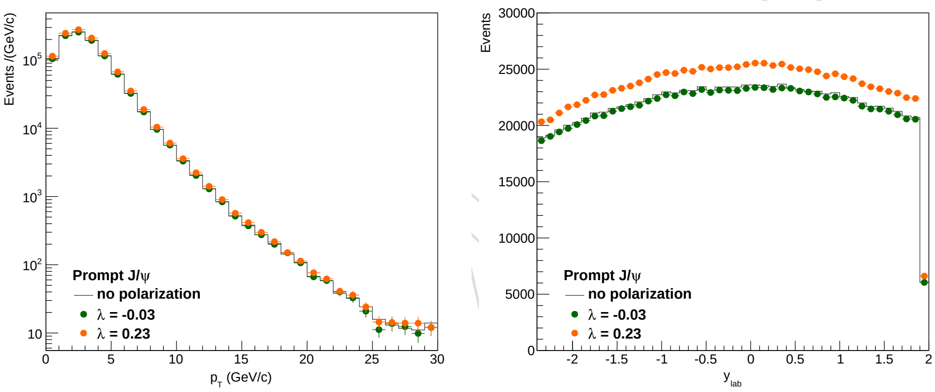

Figure 19: Raw distribution of prompt J/ψ Monte-Carlo test with variation of polarization $\lambda_\theta = -0.03$ and $+0.23$.

6 Efficiency

This chapter discusses the calculation of the efficiency correction factors introduced by trigger, tracking and muon ID cuts. The primodial effcieincy was computed by dividing the number of reconstructed di-muon pairs by generated ones in MC samples (Section 6.1). Then the secondary correction based on data-driven single muon reconstruction efficiency was applied to account the discrepancy of detector response in MC and real data (6.2).

6.1 Dimuon efficiency from Monte Carlo sample

6.1.1 Method

Dimuons generated with realistic PYTHIA are reconstructed with the pp reconstruction algorithm in CMSSW_5_3_8_HI environment using the global tag STARTHI53_V27::All. The Monte-Carlo samples were produced centrally and the location is `/PYTHIA6_JPsiWithFSR_tuneD6T_5TeV02/tdahms-Onia2MuMu_Jpsi_HiWinter13-pa_STARTHI53_V25-v1-68bf48a49e3ccdbf9aa4b3fd783a356e/USER` for the prompt J/ψ and `/PYTHIA6_inclBtoPsiMuMu_5TeV02/tdahms-Onia2MuMu_InclB2Psi_HiWinter13-pa_STARTHI53_V25-v1-68bf48a49e3ccdbf9aa4b3fd783a356e/USER` for the non prompt J/ψ. Generated MC samples are boosted in negative rapidity direction by 0.47 rapidity units as expected in the 1st run period of the p+Pb collsion system. The samples for the 2nd run are boosted in the oppsite directions.

In order to get enough statistics, single muon kinematic filters are applied when we generte the official Monte-Carlo samples. This pre-filter is looser than the single muon kinematic cuts that is actually used in the analysis and illustrated in figure 20.

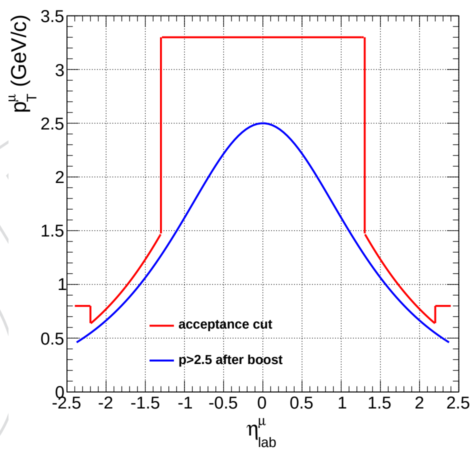

Figure 20: $p_T - \eta$ phase space of the single muons kinematic cut actually used in the analysis (red) and pre-filter cut for the Monte-Carlon sample generation (blue).

The peak counting method consists of estimating the reconstruction efficiency making the ratio of the number of signal that is reconstructed and passes the quality cuts, and the number of signal that was generated.

$$\varepsilon = \frac{N^{dimuons\ reconstructed,M2,muIDcut,triggerselection}_{detectable}(p_T, y)}{N^{dimuon\ generated,M1}_{detectable}(p_T, y)} \quad (12)$$

where the denominator is the number of generated events declared detectable within the mass range M1=[2.6-3.5] GeV/c^2, which is same as the numerator of the acceptance definition in given (p_T,y). The numerator represents the number of reconstructed event within the mass range M2 = [2.95 - 3.25] GeV/c ^{2}, with the muon ID cut described in Section 3, and trigger selection ($HLT\_PAL1DoubleMuOpen\_v1$).

This would be done as if the MC was data, that is applying closely the signal extraction method developed for the data. The reconstructed numbers include all efficiency corrections: trigger, identification (cuts) and tracking.

Figure **??** presents the efficiency plots in p_T vs y_{CM} for prompt and non-prompt J/ψ which are obtained from MC_truth with the peak counting method. In real analysis, we weighted this efficiency MC{truth using the TNP scale factor which will be described in the next chapter in detail. Also, we studied bin migration effects in efficiency estimation and decide not to perform unfolding since p_T of the generated and reconstructed particles show a strong correlation between 0.92-0.98 More detailed explanation can be found on Appendix B.

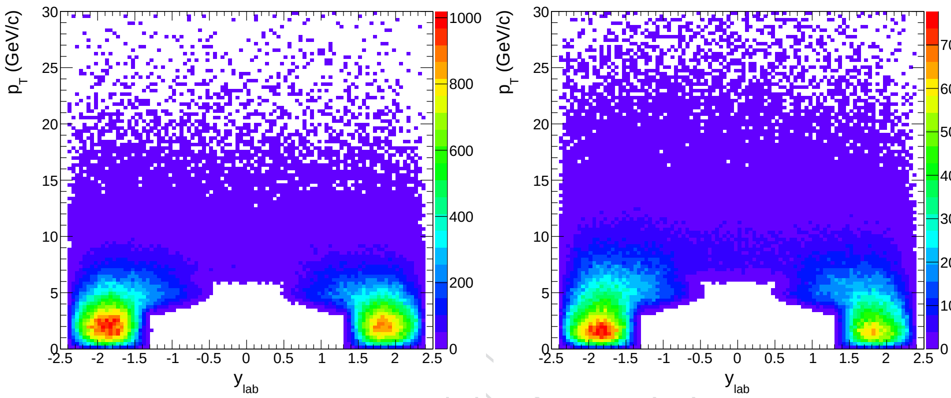

Figure 21: Generated prompt(left) and non-prompt(right) J/ψ after single muons kinematic cut is applied, as a function of p_T and y^{1st}_{lab} of J/ψ.

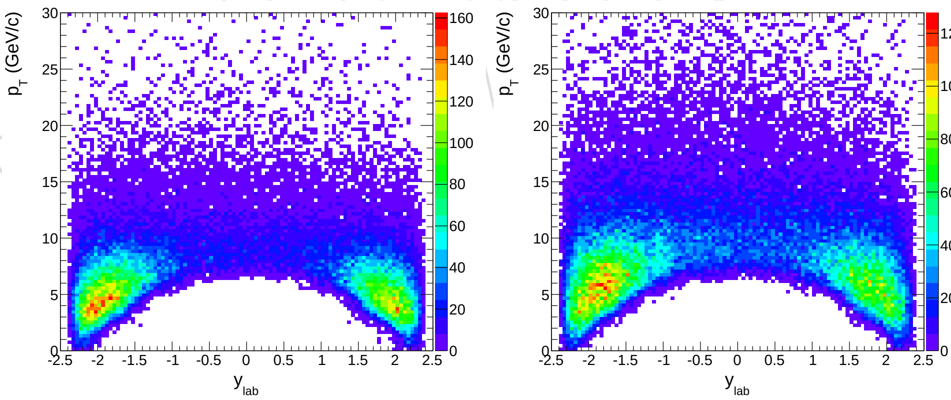

Figure 22: Reconstructed prompt(left) and non-prompt(right) J/ψ with muon quality cuts and trigger matching as a function of p_T and y^{1st}_{lab} of J/ψ, which corresponds to the numerator of the efficiency.

6.1.2 Reweighting of primary vertex position distribution

Figure 25 shows the longitudinal position of the reconstructed primary vertex in Monte carlo simulation and real data for the 1st run. The Monte-Carlo has a broader distribution and this could cause a bias in the acceptance and efficiency corrections.

In order to correct the difference, a weighting is applied to the Monte-Carlo events. Both distributions are fitted with one Gaussian function independently and shown on the left plot of

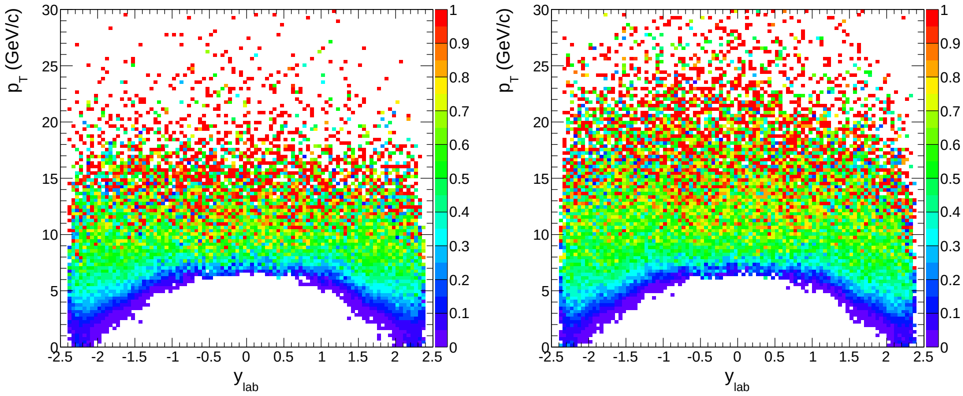

Figure 23: Efficiency of prompt(left) and non-prompt(right) J/ψ in fined-grained p_{T} and y_{lab}.

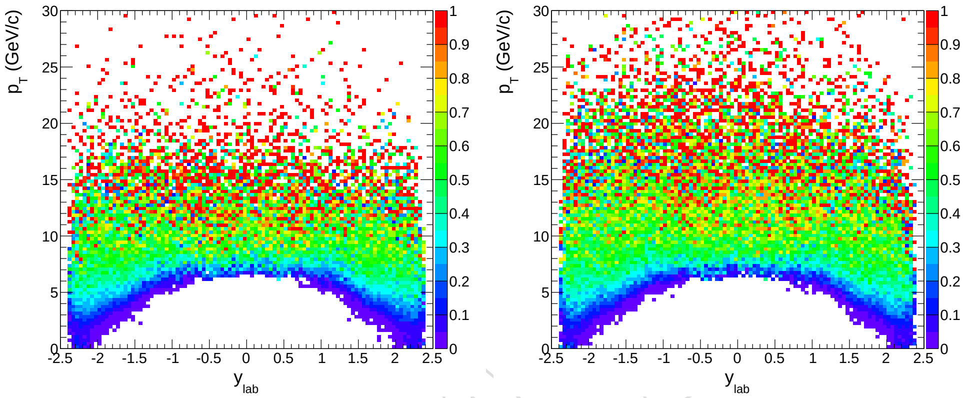

Figure 24: Efficiency of prompt(left) and non-prompt(right) J/ψ in p_{T} and y_{lab} binning used in the analysis. Dashed line indicates the actual kinematic ranges actually considered in the analysis.

figure 25. The ratio of the two fitted function and the ratio of distributions themselves are shown on the right side of figure 25. The ratio of the fits is used to reweight the Monte-Carlo.

We also applied the cut on the primary vertex z : $|zVtx| < 10$ cm to exclude poor quality events, and select where 1st run and 2nd run distributions matches well. By this cut, about 6% of events are rejected both in Monte-Carlo and Data.

The relative effect of the vertex weighting and cut is smaller than 3% as it can be seen in figure 26 and figure 27 for the prompt J/ψ. For the non-prompt J/ψ whose vertex could be further from the primary vertex, the efficiency values become higher over the whole range about 10% at maximum as it can be seen in figure 28 and figure 29.

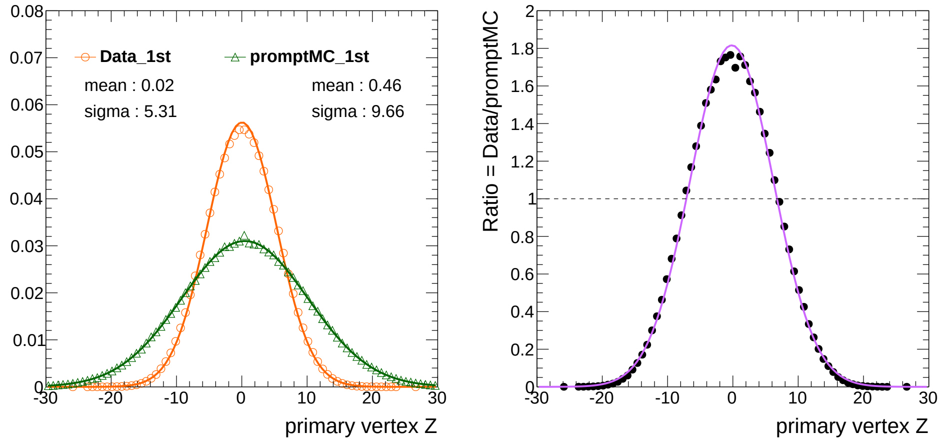

Figure 25: Left : Comparison of the primary vertex longitudinal position of J/ψ candidates in real data and in Monte Carlo simulations. Each distributions are fitted with a gaussian function with the shown parameters. Right : violet line shows the ratio of the fitted functions that is used to reweight the MC. black points are the ratio of real data and MC distributions.

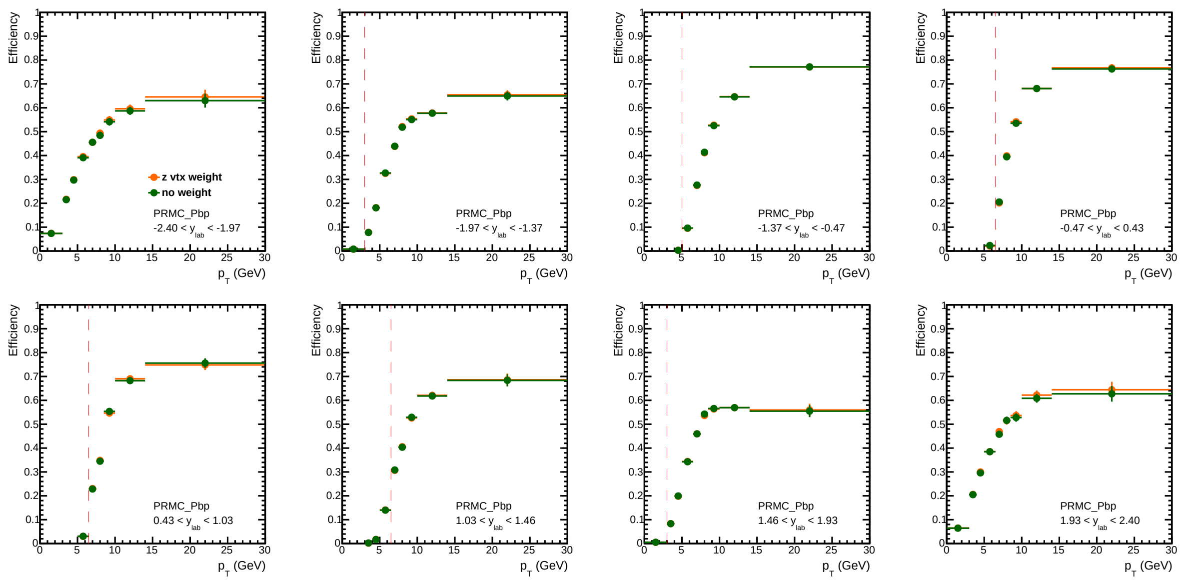

Figure 26: The efficiency values with(orange) and without(green) the z vertex weighting as a function of p_T for different rapidity ranges in prompt MC. Red dashed lines indicate the minimum p_T bin boundaries actually used in the analysis.

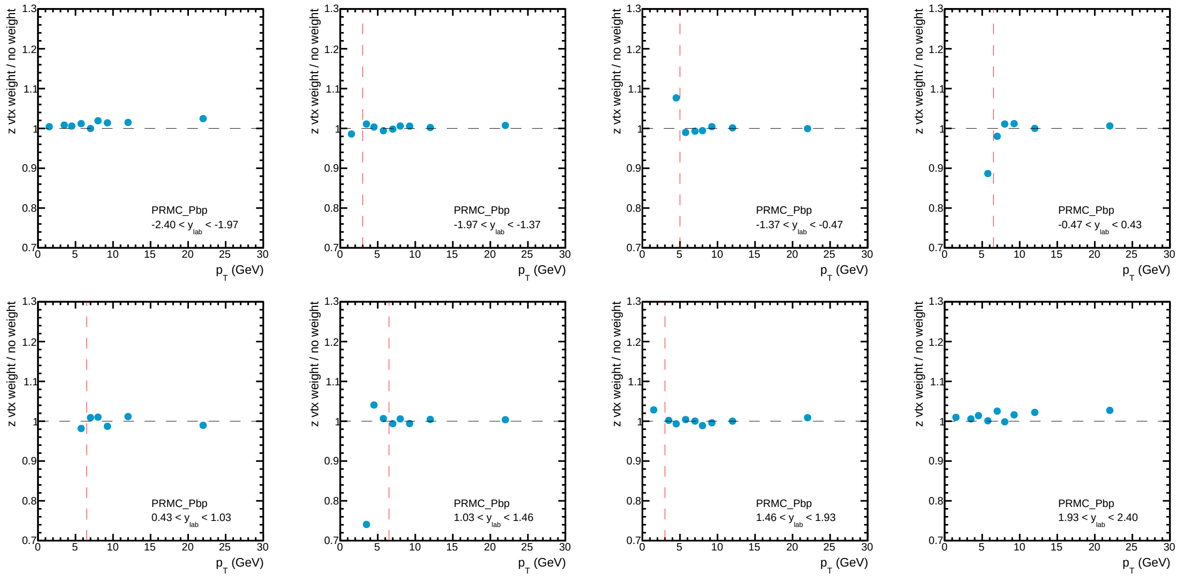

Figure 27: The ratio of efficiency values with(orange) and without(green) the z vertex weighting as a function of p_T for different rapidity ranges in prompt MC. Red dashed lines indicate the minimum p_T bin boundaries actually used in the analysis.

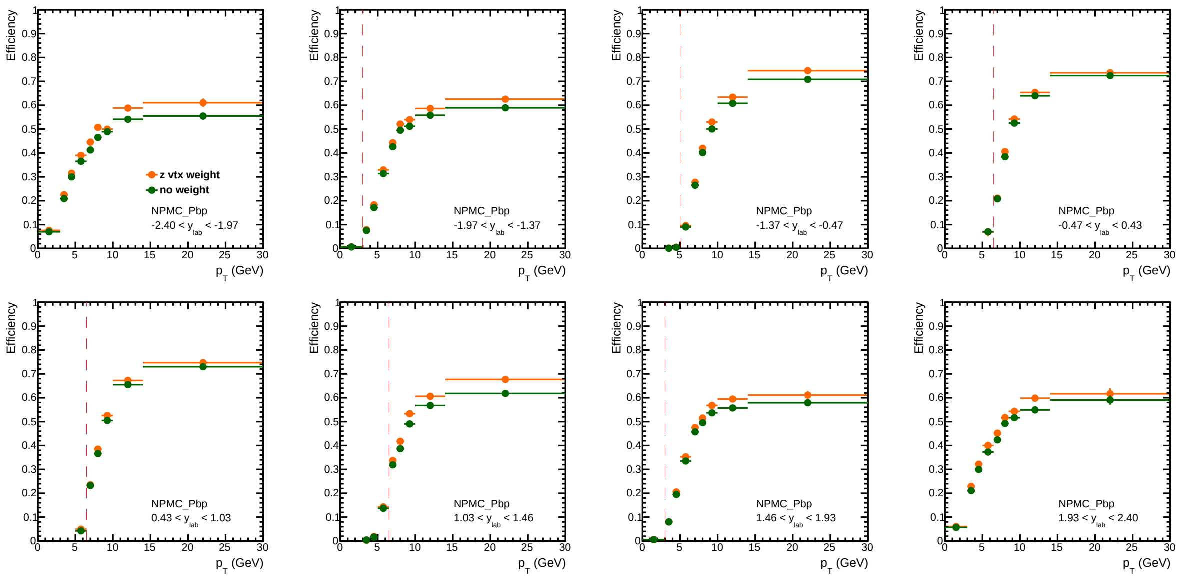

Figure 28: The efficiency values with(orange) and without(green) the z vertex weighting as a function of p_T for different rapidity ranges in non-prompt MC. Red dashed lines indicate the minimum p_T bin boundaries actually used in the analysis.

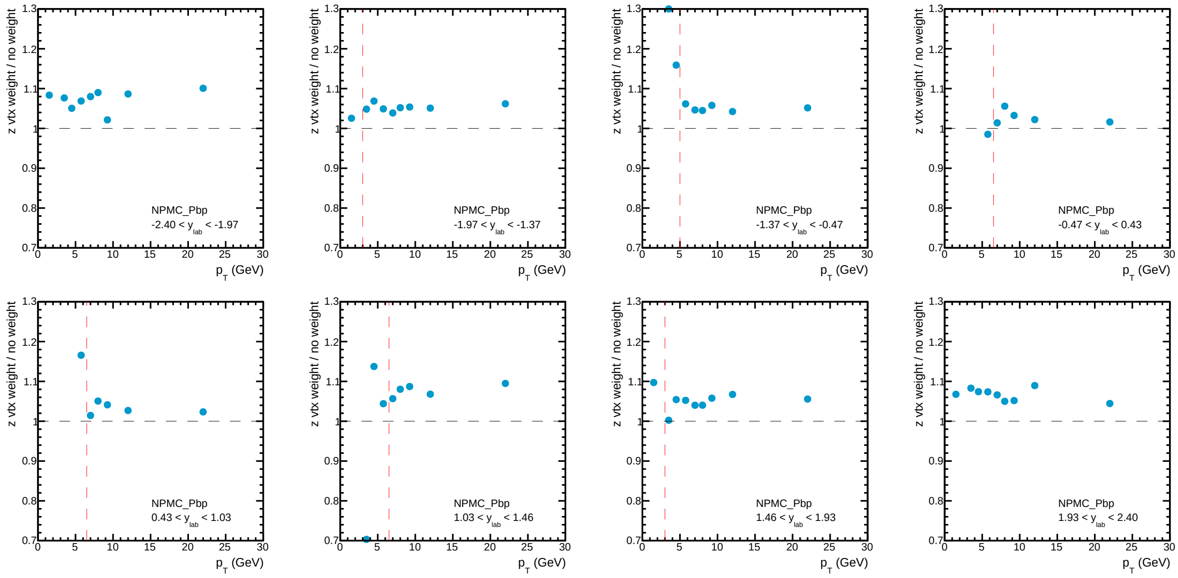

Figure 29: The ratio of efficiency values with(orange) and without(green) the z vertex weighting as a function of p_T for different rapidity ranges in non-prompt MC. Red dashed lines indicate the minimum p_T bin boundaries actually used in the analysis.

6.1.3 Unfolding

6.2 Secondary correction for efficiency - Tag And Probe

The primitive efficiency correction factors in the previous section was computed based on the assumption that the MC sample reproduced perfectly the exact detector condition, which is not possible. In order to account the discrepancy of MC and reality, an additional correction step - called Tag and Probe method - was carried out. A detailed description of T&P method is explained in [10]. Briefly, this procedure provides the data-driven single muon efficiency in terms of triggering, Muon ID and tracking cut. The efficiency ratio of real data to MC is computed is called the efficiency T&P scale factor for single muon. The scale factors are calcuclated in several p_{T} and bins and interpolated to cover the entire muon acceptance range. Those scale factors ($SF(p_T^{\mu}, \eta^{\mu})$) are used to correct the counted number of reconstructed Dimuon pairs (Sec. 6.1) in the event-by-event manner. In terms of technics, the Eq. 13 is modified into

$$\varepsilon_{\mathrm{T\&Pcorrected}} = \frac{N_{detectable}^{dimuons\, reconstructed}(p_T, y) \otimes (SF(p_T^{\mu-}, \eta^{\mu-}) \times SF(p_T^{\mu+}, \eta^{\mu+}))}{N_{detectable}^{dimuon\, generated, M1}(p_T, y)}$$

(13)

, or

$$\varepsilon_{\mathrm{T\&Pcorrected}} = \varepsilon_{\mathrm{T\&Pcorrected}} \otimes \frac{\text{TNP efficiency of } \mu^+}{\text{MC efficiency of } \mu^+} \frac{\text{TNP efficiency of } \mu^-}{\text{MC efficiency of } \mu^-} \quad (14)$$

The tag muons are selected by a strict criteria including track quality cut and HLT_PAMu3 trigger matching in order to suppress the background level. In case of probes, two sets are used for obtain two efficiencies. The stand alone muons are used to measure the tracking efficiency and the track muons to measure the Muon ID $\times triggeringefficiency$.

- Muon ID & trigger efficiency:
  - tag: tracker muon with quality cut & matching to single muon trigger (HLT_PAMu3)
  - probe: calorimeter muons with inner track quality cuts, without trigger matching.
  - passing criteria : probes that is one leg of HLT_PAL1DoubleMuOPen trigger path and passes track quality cuts.
- Tracking efficiency:
  - tag: tracker muon with quality cut & matching to single muon trigger (HLT_PAMu3)
  - probe: stand-alone muons with at least 12 valid hits
  - passing criteria : probes matched to a tracker muon when it is extrapolated to the inner tracker.

In all cases, identical selection criteria are applied to both data and simulation.

In the following are presented the muon ID $\times triggereffiicncy(Fig. \textbf{??})andtrackingefficiency(Fig. 31)asafunct$ ¡ —$\eta| < 1.2$, $1.2 < |\eta| < 1.6$, $1.6 < |\eta| < 2.4$ - are chosen where the efficiency is radically changed due to the detector geometry. And the p_{T} bins are determined in order to distribute enough statistics for invariant mass fitting in every bin.

6.2.1 Trigger and Muon ID efficiency

The trigger efficiency, more spectifically the probability of being one of legs that contributed in HLT_PAL1DoubleMuOpen firing, and the muon ID efficiency was combined in a procedure because they shares the same basic probe criteria. The signal shape is described by a Crystal Ball plus a Gaussian. The addition of the Gaussian is motivated to describe varying detector resolution. The parameters in the Crystal Ball as well as the width of the Gaussian are free parameters of the fit. The background is described by fourth order polynomial functions. The summary of efficiencies and the scale factors are in Fig 30.

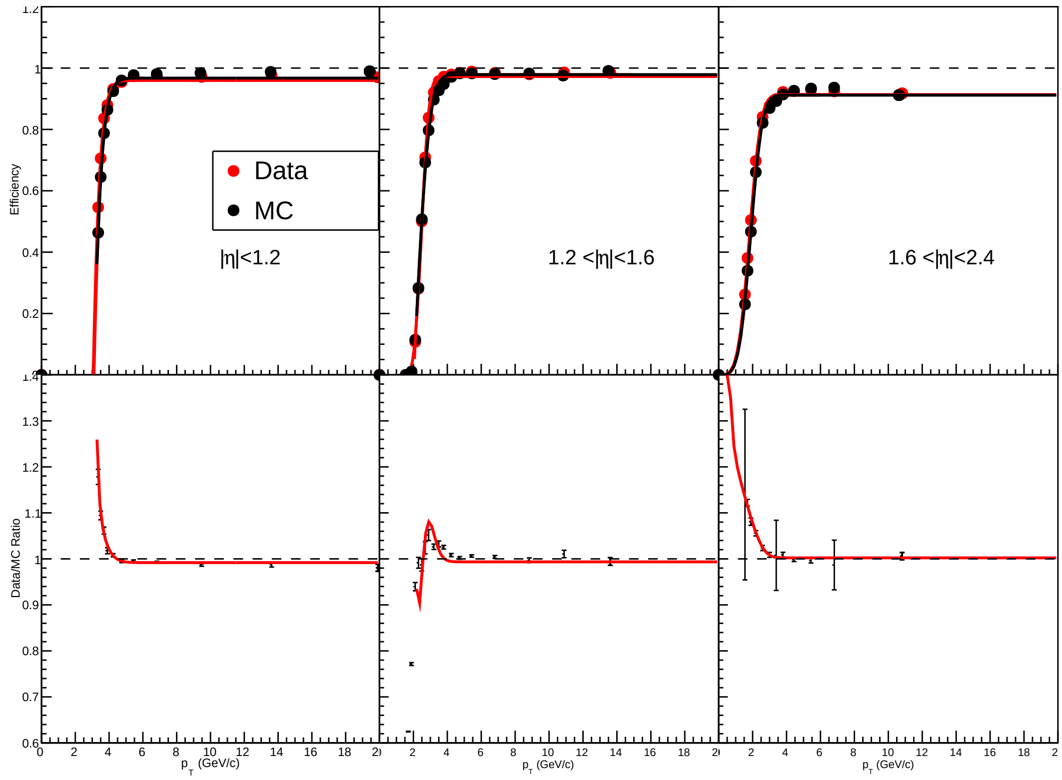

Figure 30: Efficiency of trigger object matching (HLT_PAL1DoubleMuOpen) and Muon ID cuts in PYTHIA and real data (Top), and data-to-MC ratio(Bottom).

6.2.2 Tracking efficiency

The fits for the tracking efficiency are challenging due to the poor resolution of the standalone muons used as probes. For the same reason, an enlarged fitting range is used. A double Gaussian is chosen to describe the signal shape with all its parameters left to float. The background is described by a exponential function. As shown in Fig 31, the tracking efficiency of muons is higher than 95% for the entire acceptance range, and the data-to-MC ratio is consistent to the unity in 2% level which is very small. Therefore, we decided to use the MC tracking efficiency in raw rather than applying this small correction factor. Instead, the upper limit, 2%, was used to estimate the systematic uncertainty by computing the error propagation to Dimuon pair efficiency.

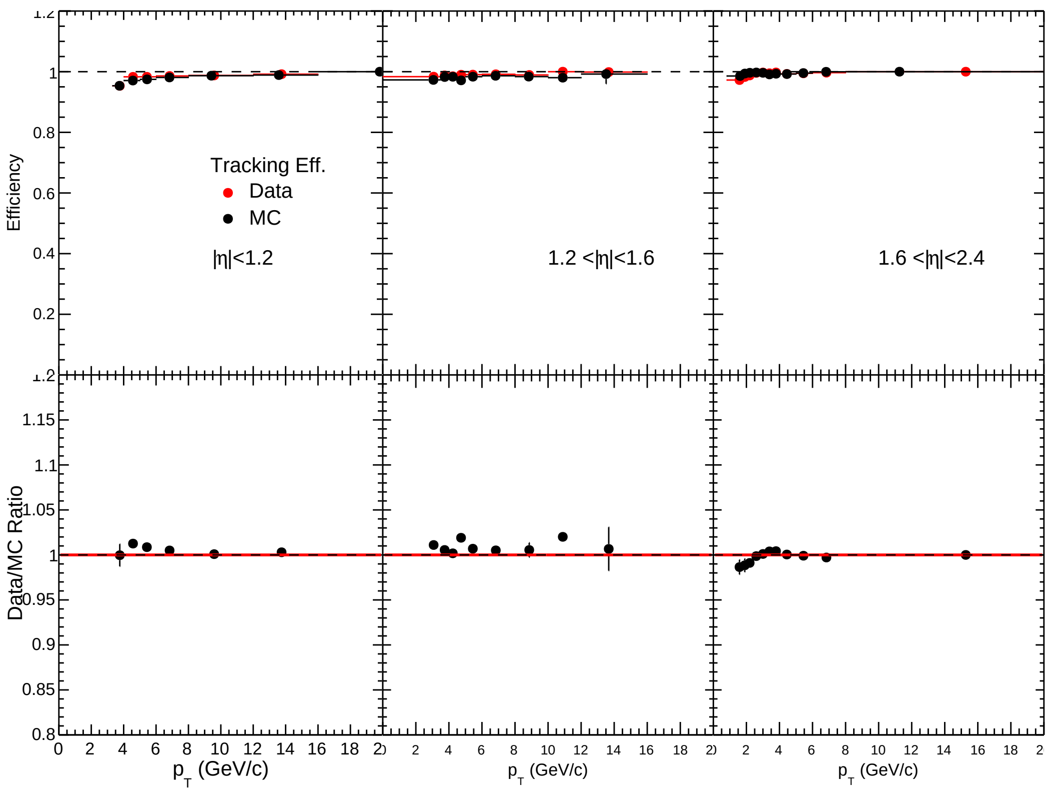

Figure 31: Efficiency of tracking in PYTHIA and real data (Top), and the data-to-MC ratio (Bottom).

6.2.3 Dimuon efficiency factors corrected by Tag and Probe

The J/ψ reconstruction efficiency derived from MC sample was modified by covoluting the scale factors in event-by-event manner as described in the previous section. The Fig. 38 – Fig. **??** shows how much the efficiency was modifed by this procedure. The T&P corrected efficiency correction factor is used for the rest of this note.

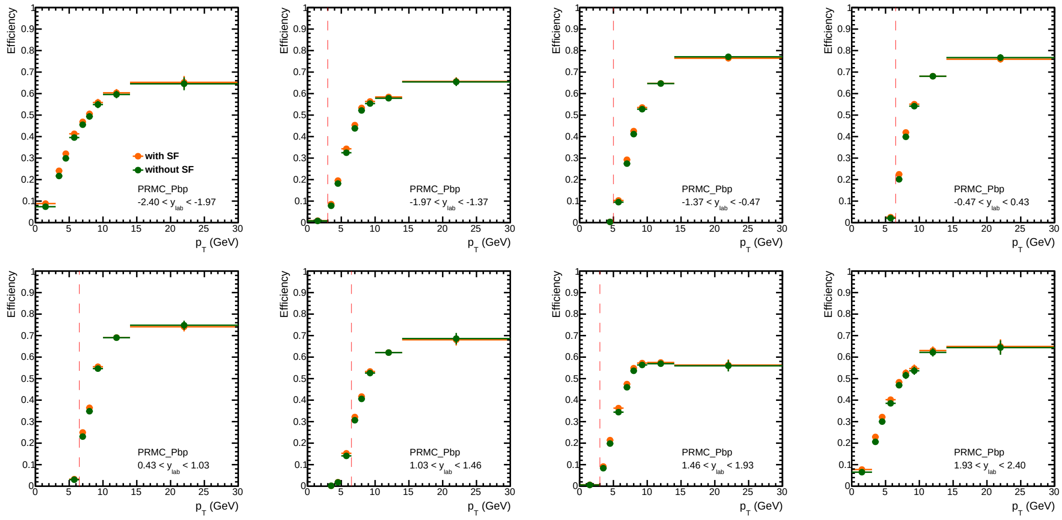

Figure 32: Dimuon efficiencies before and after T&P corrections in prompt J/ψ in Pb-p direction collision

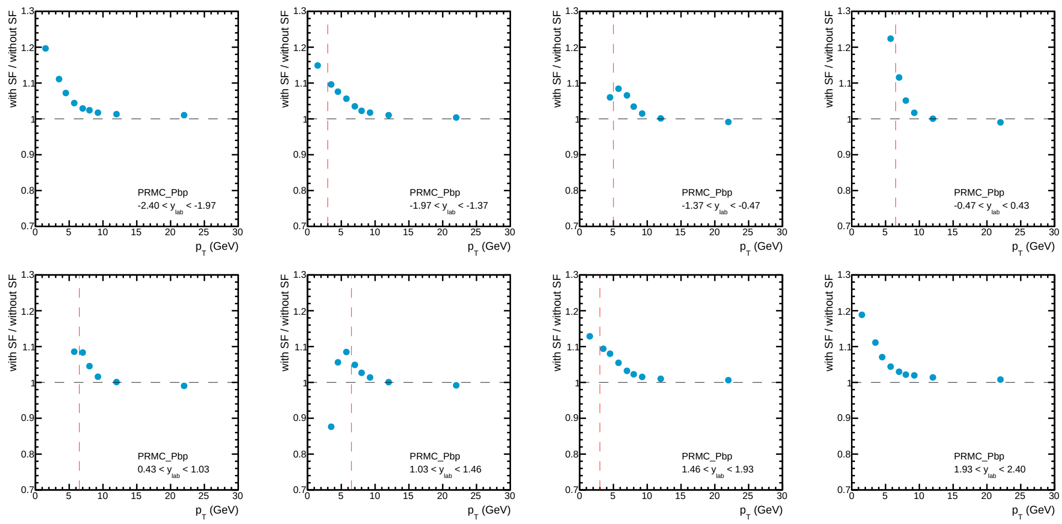

Figure 33: Ratio of efficiencies before and after T&P corrections in prompt J/ψ in Pb-p direction collision

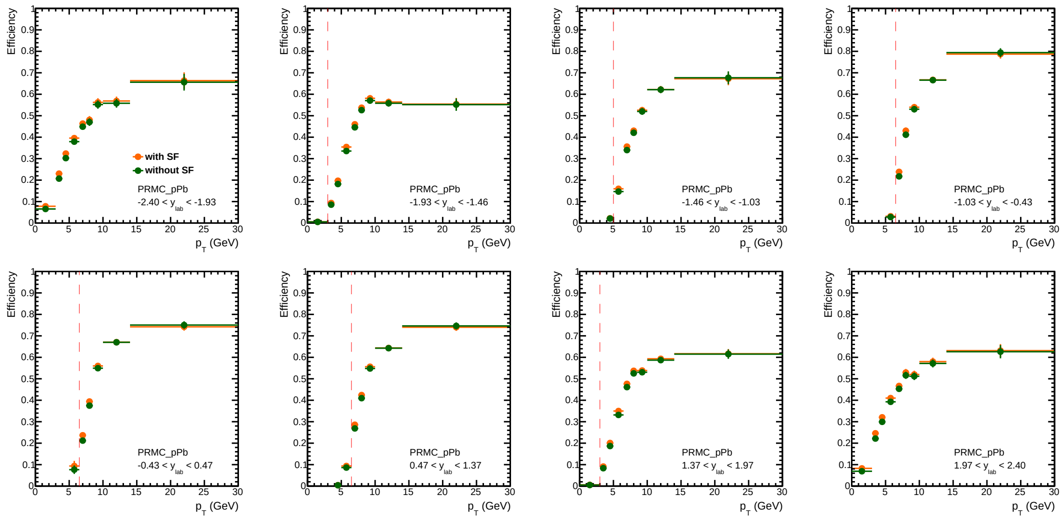

Figure 34: Dimuon efficiencies before and after T&P corrections in prompt J/ψ in p-Pb direction collision

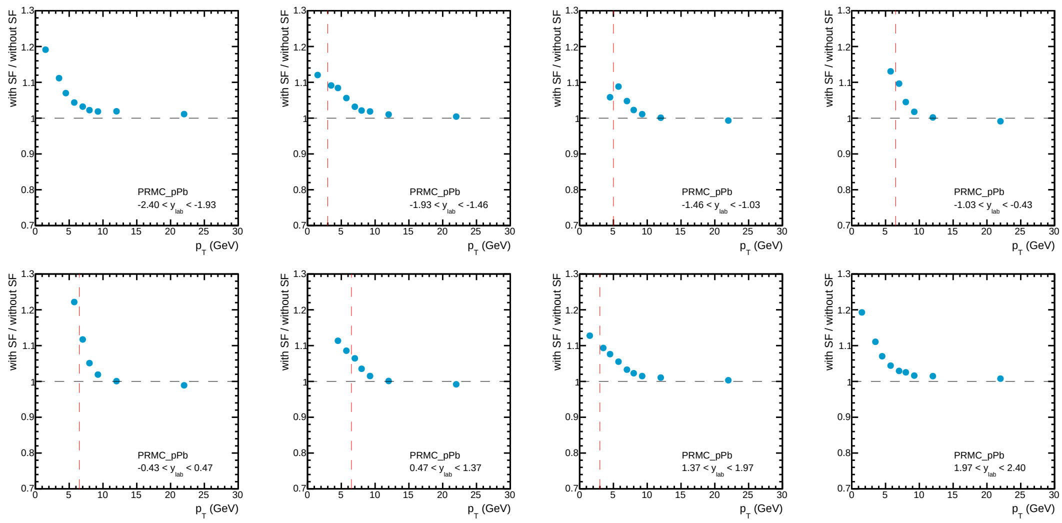

Figure 35: Ratio of efficiencies before and after T&P corrections in prompt J/ψ in p-Pb direction collision

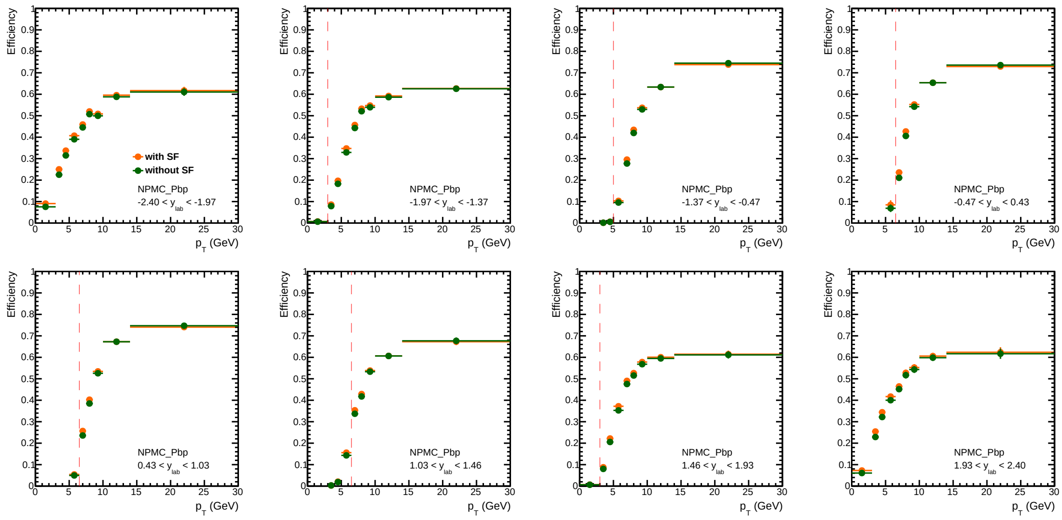

Figure 36: Dimuon efficiencies before and after T&P corrections in non-prompt J/ψ in Pb-p direction collision

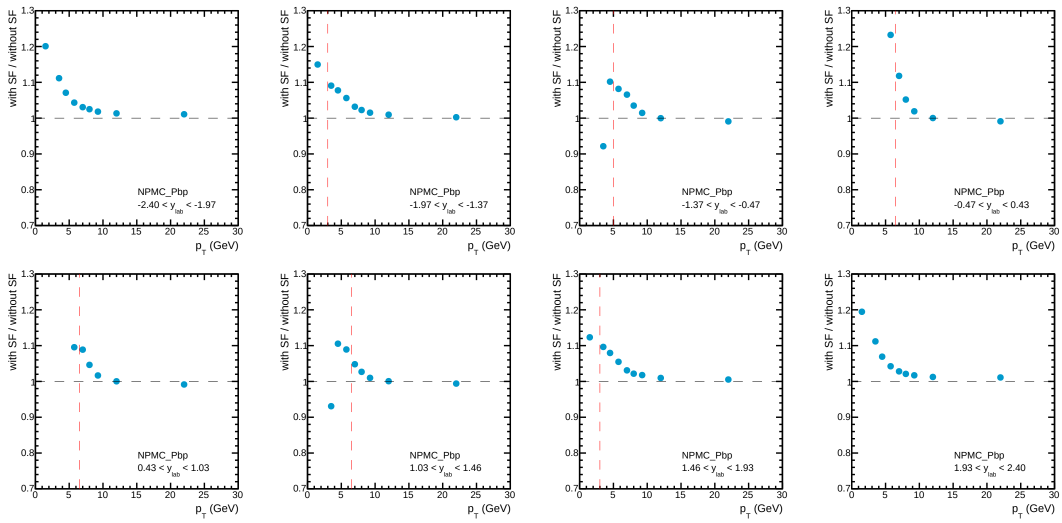

Figure 37: Ratio of efficiencies before and after T&P corrections in non-prompt J/ψ in Pb-p direction collision

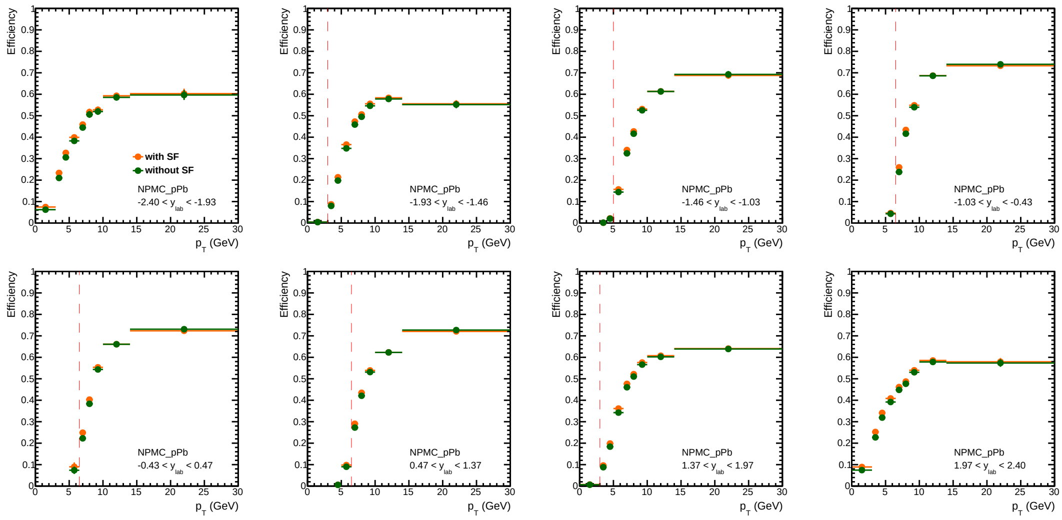

Figure 38: Dimuon efficiencies before and after T&P corrections in non-prompt J/ψ in p-Pb direction collision

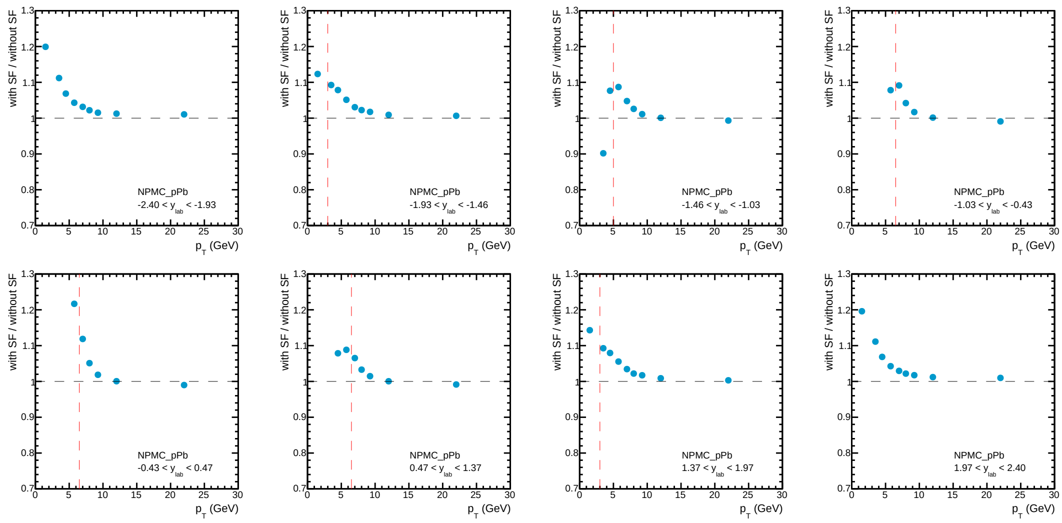

Figure 39: Ratio of efficiencies before and after T&P corrections in non-prompt J/ψ in p-Pb direction collision

6.3 Systematic uncertainties

The bin-to-bin systematic uncertainties are taken from the differences between the efficiency values after applying weight from T&P and those from MC samples before weighting. Overall systematic uncertainties from efficiency are 0.2 - 8.5% for prompt J/ψ and 0.5-8.7% for non-prompt J/ψ for $p_{\mathrm{T}} > 6.5$ GeV/c. The systematic uncertainties are up to 25% for $0 < p_{\mathrm{T}} < 3\,\mathrm{GeV}/c$.

Table 14: p_{T} T&P efficiencies for pPb, for data and MC for $-2.4 < \eta^{\mu}_{Lab} < -0.8$ for Cross Section.

	Trigger				Muon ID				Inner tracking			
	Data	MC	Data-MC	Data/MC	Data	MC	Data-MC	Data/MC	Data	MC	Data-MC	Data/MC
0-1.5	0.100	0.098	0.002	1.020	0.668	0.533	0.135	1.253	0.952	0.822	0.130	1.158
1.5-2.5	0.517	0.500	0.017	1.034	0.851	0.798	0.053	1.066	0.936	0.924	0.012	1.013
2.5-3.5	0.841	0.824	0.017	1.021	0.936	0.919	0.017	1.018	0.948	0.947	0.001	1.001
3.5-4.5	0.918	0.908	0.010	1.011	0.961	0.949	0.012	1.013	0.953	0.950	0.003	1.003
4.5-5.5	0.940	0.936	0.004	1.004	0.981	0.977	0.004	1.004	0.961	0.964	-0.003	0.997
5.5-6.5	0.916	0.910	0.006	1.007	0.982	0.976	0.006	1.006	0.949	0.946	0.003	1.003
6.5-7.5	0.914	0.907	0.007	1.008	0.990	0.987	0.003	1.003	0.963	0.965	-0.002	0.998
7.5-8.5	0.910	0.907	0.003	1.003	0.984	0.976	0.008	1.008	0.976	0.981	-0.005	0.995
8.5-9.5	0.919	0.915	0.004	1.004	0.983	0.983	0.000	1.000	0.946	0.947	-0.001	0.999
9.5-11	0.906	0.912	-0.006	0.993	0.992	0.989	0.003	1.003	0.957	0.969	-0.012	0.988
11-14	0.916	0.904	0.012	1.013	0.988	0.985	0.003	1.003	0.962	0.999	-0.037	0.963
14-30	0.917	0.912	0.05	1.005	0.981	0.975	0.006	1.006	0.944	0.976	-0.032	0.967
MAX	0.017				0.135				0.130			

Table 15: p_{T} T&P efficiencies for pPb, for data and MC for $-0.8 < \eta^{\mu}_{Lab} < 0.8$ for Cross Section.

	Trigger				Muon ID				Inner tracking			
	Data	MC	Data-MC	Data/MC	Data	MC	Data-MC	Data/MC	Data	MC	Data-MC	Data/MC
0-1.5	0.000	0.000	0.000	1.000	0.000	0.000	0.000	1.000	0.000	0.000	0.000	1.000
1.5-2.5	0.000	0.000	0.000	1.000	0.000	0.000	0.000	1.000	0.000	0.000	0.000	1.000
2.5-3.5	0.560	0.541	0.019	1.035	0.659	0.571	0.088	1.154	0.000	0.000	0.000	1.000
3.5-4.5	0.847	0.839	0.008	1.010	0.901	0.869	0.032	1.037	0.932	0.946	-0.014	0.985
4.5-5.5	0.956	0.953	0.003	1.003	0.973	0.965	0.008	1.008	0.966	0.973	-0.007	0.993
5.5-6.5	0.983	0.983	0.000	1.000	0.984	0.975	0.009	1.009	0.963	0.975	-0.012	0.988
6.5-7.5	0.984	0.986	-0.002	0.998	0.984	0.980	0.004	1.004	0.973	0.981	-0.008	0.992
7.5-8.5	0.983	0.984	-0.001	0.999	0.986	0.981	0.005	1.005	0.961	0.972	-0.011	0.989
8.5-9.5	0.982	0.988	- 0.006	0.994	0.982	0.977	0.005	1.005	0.966	0.967	-0.001	0.999
9.5-11	0.977	0.975	0.002	1.002	0.980	0.973	0.007	1.007	0.976	0.977	-0.001	0.999
11-14	0.977	0.975	0.002	1.002	0.988	0.983	0.005	1.005	0.972	0.980	-0.008	0.992
14-30	0.978	0.986	-0.008	0.992	0.992	0.987	0.005	1.005	0.952	0.978	-0.026	0.973
MAX	0.019				0.088				0.026			

Table 16: p_{T} T&P efficiencies for pPb, for data and MC for $0.8 < \eta^{\mu}_{CM} < 1.93$ for Cross Section.

	Trigger				Muon ID				Inner tracking			
	Data	MC	Data-MC	Data/MC	Data	MC	Data-MC	Data/MC	Data	MC	Data-MC	Data/MC
0-1.5	0.003	0.002	0.001	1.500	0.499	0.378	0.121	1.320	1.000	1.000	0.000	1.000
1.5-2.5	0.234	0.225	0.009	1.040	0.758	0.682	0.076	1.111	0.954	0.956	-0.002	0.998
2.5-3.5	0.774	0.751	0.023	1.031	0.929	0.911	0.018	1.020	0.954	0.957	-0.003	0.997
3.5-4.5	0.866	0.851	0.015	1.018	0.955	0.940	0.015	1.016	0.963	0.958	0.005	1.005
4.5-5.5	0.909	0.901	0.008	1.009	0.977	0.972	0.005	1.005	0.957	0.962	-0.005	0.995
5.5-6.5	0.920	0.914	0.006	1.007	0.983	0.978	0.005	1.005	0.957	0.963	-0.006	0.994
6.5-7.5	0.930	0.926	0.004	1.004	0.985	0.975	0.010	1.010	0.966	0.964	0.002	1.002
7.5-8.5	0.928	0.920	0.008	1.009	0.986	0.976	0.010	1.010	0.959	0.956	0.003	1.003
8.5-9.5	0.927	0.934	-0.007	0.993	0.987	0.985	0.002	1.002	0.962	0.967	-0.005	0.995
9.5-11	0.932	0.921	0.011	1.012	0.996	0.990	0.006	1.006	0.969	0.988	-0.019	0.981
11-14	0.925	0.901	0.024	1.027	0.991	0.985	0.006	1.006	0.969	0.983	-0.014	0.986
14-30	0.932	0.918	0.014	1.015	0.990	0.984	0.006	1.006	0.965	0.985	-0.020	0.980
MAX	0.024				0.121				0.020			

Table 17: p_{T} T&P efficiencies for pPb, for data and MC for $-2.4 < \eta^{\mu}_{Lab} < -0.8$ for R_{FB}.

	Trigger				Muon ID				Inner tracking			
	Data	MC	Data-MC	Data/MC	Data	MC	Data-MC	Data/MC	Data	MC	Data-MC	Data/MC
0-1.5	0.106	0.102	0.004	1.039	0.673	0.542	0.131	1.242	0.952	0.822	0.130	1.158
1.5-2.5	0.517	0.501	0.016	1.032	0.852	0.798	0.054	1.068	0.936	0.924	0.012	1.013
2.5-3.5	0.841	0.824	0.017	1.021	0.936	0.919	0.017	1.018	0.948	0.947	0.001	1.001
3.5-4.5	0.918	0.908	0.010	1.011	0.961	0.949	0.012	1.013	0.953	0.950	0.003	1.003
4.5-5.5	0.940	0.936	0.004	1.004	0.981	0.978	0.003	1.003	0.961	0.964	-0.003	0.997
5.5-6.5	0.916	0.910	0.006	1.007	0.982	0.976	0.006	1.006	0.949	0.946	0.003	1.003
6.5-7.5	0.914	0.907	0.007	1.008	0.990	0.987	0.003	1.003	0.963	0.965	-0.002	0.998
7.5-8.5	0.910	0.907	0.003	1.003	0.985	0.976	0.009	1.009	0.976	0.981	-0.005	0.995
8.5-9.5	0.919	0.915	0.004	1.004	0.983	0.983	0.000	1.000	0.946	0.947	-0.001	0.999
9.5-11	0.906	0.912	-0.006	0.993	0.992	0.989	0.003	1.003	0.957	0.969	-0.012	0.988
11-14	0.916	0.904	0.012	1.013	0.988	0.985	0.003	1.003	0.962	0.999	-0.037	0.963
14-30	0.917	0.912	0.005	1.005	0.981	0.975	0.006	1.006	0.944	0.976	-0.032	0.967
MAX	0.017				0.131				0.130			

Table 18: p_{T} T&P efficiencies for pPb, for data and MC for $-0.8 < \eta^{\mu}_{Lab} < 0.8$ for R_{FB}.

	Trigger				Muon ID				Inner tracking			
	Data	MC	Data-MC	Data/MC	Data	MC	Data-MC	Data/MC	Data	MC	Data-MC	Data/MC
0-1.5	0.000	0.000	0.000	1.000	0.000	0.000	0.000	1.000	0.000	0.000	0.000	1.000
1.5-2.5	0.000	0.000	0.000	1.000	0.000	0.000	0.000	1.000	0.000	0.000	0.000	1.000
2.5-3.5	0.560	0.541	0.019	1.035	0.659	0.571	0.088	1.154	0.000	0.000	0.000	1.000
3.5-4.5	0.847	0.839	0.008	1.010	0.901	0.869	0.032	1.037	0.932	0.946	-0.014	0.985
4.5-5.5	0.956	0.953	0.003	1.003	0.973	0.965	0.008	1.008	0.966	0.973	-0.007	0.993
5.5-6.5	0.983	0.983	0.000	1.000	0.984	0.975	0.009	1.009	0.963	0.975	-0.012	0.988
6.5-7.5	0.984	0.986	-0.002	0.998	0.984	0.980	0.004	1.004	0.973	0.981	-0.008	0.992
7.5-8.5	0.983	0.984	-0.001	0.999	0.986	0.981	0.005	1.005	0.961	0.972	-0.011	0.989
8.5-9.5	0.982	0.988	-0.006	0.994	0.982	0.977	0.005	1.005	0.966	0.967	-0.001	0.999
9.5-11	0.977	0.975	0.002	1.002	0.980	0.973	0.007	1.007	0.976	0.977	-0.001	0.999
11-14	0.977	0.975	0.002	1.002	0.988	0.983	0.005	1.005	0.972	0.980	-0.008	0.992
14-30	0.978	0.986	-0.008	0.992	0.992	0.987	0.005	1.005	0.952	0.978	-0.026	0.973
MAX	0.019				0.088				0.026			

Table 19: p_{T} T&P efficiencies for pPb, for data and MC for $0.8 < \eta^{\mu}_{Lab} < 1.93$ for R_{FB}.

	Trigger				Muon ID				Inner tracking			
	Data	MC	Data-MC	Data/MC	Data	MC	Data-MC	Data/MC	Data	MC	Data-MC	Data/MC
0-1.5	0.001	0.001	0.000	1.000	0.499	0.369	0.130	1.352	1.000	1.000	0.000	1.000
1.5-2.5	0.213	0.204	0.009	1.044	0.734	0.651	0.083	1.127	0.954	0.956	-0.002	0.998
2.5-3.5	0.784	0.766	0.018	1.023	0.900	0.878	0.022	1.025	0.954	0.957	-0.003	0.007
3.5-4.5	0.929	0.917	0.012	1.013	0.937	0.916	0.021	1.023	0.963	0.958	0.005	1.005
4.5-5.5	0.983	0.984	-0.001	0.999	0.975	0.968	0.007	1.007	0.957	0.962	-0.005	0.995
5.5-6.5	0.985	0.985	0.000	1.000	0.979	0.974	0.005	1.005	0.957	0.963	-0.006	0.994
6.5-7.5	0.987	0.987	0.000	1.000	0.983	0.970	0.013	1.013	0.966	0.964	0.002	1.002
7.5-8.5	0.993	0.995	-0.002	0.998	0.985	0.974	0.011	1.011	0.959	0.956	0.003	1.003
8.5-9.5	0.973	0.978	-0.005	0.995	0.980	0.977	0.003	1.003	0.962	0.967	-0.005	0.995
9.5-11	0.988	0.997	-0.009	0.991	0.995	0.990	0.005	1.005	0.969	0.988	-0.019	0.981
11-14	0.982	0.978	0.004	1.004	0.992	0.988	0.004	1.004	0.969	0.983	-0.014	0.986
14-30	0.978	0.977	0.001	1.001	0.983	0.976	0.007	1.007	0.965	0.985	-0.02	0.980
MAX	0.018				0.130				0.019			

Table 20: p_{T} T&P total scale factor for pPb, for Cross Section.

	$-2.4 < \eta^{\mu}_{Lab} < -0.8$			$-0.8 < \eta^{\mu}_{Lab} < 0.8$			$0.8 < \eta^{\mu}_{Lab} < 1.93$		
	SF	Error	Error/SF	SF	Error	Error/SF	SF	Error	Error/SF
0-1.5	1.481	0.185	0.125	1.000	0.000	0.000	2.751	1.642	0.597
1.5-2.5	1.116	0.019	0.017	1.000	0.000	0.000	1.151	0.035	0.030
2.5-3.5	1.041	0.009	0.009	1.193	0.040	0.034	1.045	0.176	0.169
3.5-4.5	1.028	0.007	0.007	1.031	0.013	0.012	1.039	0.009	0.009
4.5-5.5	1.005	0.007	0.007	1.004	0.007	0.007	1.010	0.009	0.009
5.5-6.5	1.016	0.010	0.010	0.997	0.007	0.007	1.006	0.011	0.011
6.5-7.5	1.008	0.014	0.014	0.995	0.012	0.013	1.017	0.015	0.014
7.5-8.5	1.007	0.016	0.016	0.993	0.010	0.010	1.024	0.020	0.020
8.5-9.5	1.002	0.021	0.021	0.997	0.015	0.015	0.992	0.022	0.022
9.5-11	0.984	0.024	0.025	1.008	0.016	0.016	0.999	0.024	0.024
11-14	0.978	0.023	0.024	1.000	0.014	0.014	1.018	0.047	0.046
14-30	0.979	0.039	0.040	0.971	0.017	0.018	1.001	0.040	0.040

Table 21: p_{T} T&P total scale factor for pPb, for R_{FB}

	$-2.4 < \eta^{\mu}_{Lab} < -0.8$			$-0.8 < \eta^{\mu}_{Lab} < 0.8$			$0.8 < \eta^{\mu}_{Lab} < 1.93$		
	SF	Error	Error/SF	SF	Error	Error/SF	SF	Error	Error/SF
0-1.5	1.498	0.186	0.124	1.000	0.000	0.000	1.269	2.186	1.722
1.5-2.5	1.117	0.019	0.017	1.000	0.000	0.000	1.179	0.083	0.070
2.5-3.5	1.042	0.009	0.009	1.193	0.040	0.034	1.045	0.164	0.157
3.5-4.5	1.028	0.007	0.007	1.031	0.013	0.012	1.041	0.010	0.010
4.5-5.5	1.005	0.014	0.014	1.004	0.072	0.072	1.003	0.010	0.010
5.5-6.5	1.016	0.010	0.010	0.997	0.007	0.007	1.000	0.010	0.010
6.5-7.5	1.009	0.014	0.014	0.995	0.012	0.013	1.016	0.014	0.013
7.5-8.5	1.007	0.016	0.016	0.993	0.007	0.007	1.014	0.017	0.017
8.5-9.5	1.002	0.021	0.021	0.997	0.015	0.015	0.993	0.020	0.021
9.5-11	0.984	0.023	0.024	1.008	0.016	0.016	0.977	0.020	0.021
11-14	0.978	0.023	0.024	1.000	0.014	0.014	0.994	0.043	0.043
14-30	0.979	0.038	0.039	0.971	0.017	0.018	0.988	0.037	0.037

Table 22: Prompt R_{FB} efficiency systametic uncertainty.

Range			Efficiency		Error	
y_{CM}	p_{T}	E_T	Before	After	Abs.	Rel. (%)
1.5 - 1.93	3-6.5	0.0-120.0	0.259	0.301	0.042	13.97
	6.5-10.0		0.391	0.421	0.030	7.12
	10.0-30.0		0.458	0.473	0.015	3.26
1.2 - 1.5	6.5-10.0		0.451	0.482	0.031	6.52
	10.0-30.0		0.459	0.511	0.016	3.13
0.9 - 1.2	6.5-10.0		0.453	0.486	0.033	6.71
	10.0-30.0		0.586	0.604	0.019	3.08
0.5 - 0.9	6.5-10.0		0.377	0.399	0.022	5.52
	10.0-30.0		0.626	0.640	0.014	2.12
0.0 - 0.5	6.5-10.0		0.386	0.408	0.022	5.39
	10.0-30.0		0.668	0.668	0.009	1.33
-0.5 - 0.0	6.5-10.0		0.375	0.396	0.021	5.30
	10.0-3.0		0.660	0.665	0.005	0.75
-0.9 - -0.5	6.5-10.0		0.379	0.401	0.022	5.49
	10.0-30.0		0.663	0.670	0.007	1.04
-1.2 - -0.9	6.5-10.0		0.376	0.398	0.022	5.53
	10.0-30.0		0.668	0.677	0.008	1.24
-1.5 - -1.2	6.5-10.0		0.342	0.366	0.024	6.55
	10.0-30.0		0.613	0.624	0.012	1.86
-1.93 - -1.5	3-6.5		0.079	0.091	0.012	13.19
	6.5-10.0		0.396	0.425	0.029	6.83
	10.0-30.0		0.582	0.598	0.016	2.61

Table 23: Non-Prompt R_{FB} efficiency systematic uncertainty.

Range			Efficiency		Error	
y_{CM}	p_{T}	E_T	Before	After	Abs.	Rel. (%)
1.5 - 1.93	3-6.5	0.0-120.0	0.273	0.315	0.041	13.17
	6.5-10.0		0.401	0.429	0.028	6.46
	10.0-30.0		0.456	0.467	0.011	2.46
1.2 - 1.5	6.5-10.0		0.448	0.477	0.029	6.10
	10.0-30.0		0.524	0.537	0.013	2.49
0.9 - 1.2	6.5-10.0		0.460	0.490	0.030	6.13
	10.0-30.0		0.585	0.598	0.013	2.20
0.5 - 0.9	6.5-10.0		0.387	0.409	0.021	5.23
	10.0-30.0		0.610	0.619	0.009	1.46
0.0 - 0.5	6.5-10.0		0.402	0.421	0.019	4.59
	10.0-30.0		0.658	0.663	0.004	0.64
-0.5 - 0.0	6.5-10.0		0.390	0.410	0.020	4.96
	10.0-3.0		0.648	0.650	0.002	0.35
-0.9 - -0.5	6.5-10.0		0.396	0.415	0.019	4.65
	10.0-30.0		0.653	0.655	0.002	0.43
-1.2 - -0.9	6.5-10.0		0.396	0.416	0.020	4.89
	10.0-30.0		0.664	0.668	0.003	0.48
-1.5 - -1.2	6.5-10.0		0.353	0.374	0.021	5.49
	10.0-30.0		0.619	0.625	0.006	1.02
-1.93 - -1.5	3-6.5		0.089	0.103	0.014	13.23
	6.5-10.0		0.399	0.424	0.025	5.97
	10.0-30.0		0.598	0.586	0.012	1.93

Table 24: Prompt R_{FB} efficiency E_T dependent systematic uncertainty.

Range			Efficiency		Error	
y_{CM}	p_T	E_T	Before	After	Abs.	Rel. (%)
1.5 - 1.93	3-6.5	0.0-20.0	0.258	0.299	0.042	13.89
		20.0-30.0	0.253	0.293	0.041	13.91
		30.0 <	0.253	0.294	0.041	13.82
	6.5-10.0	0.0-20.0	0.389	0.419	0.030	7.15
		20.0-30.0	0.389	0.418	0.029	7.03
		30.0 <	0.388	0.417	0.029	6.95
	10.0-30.0	0.0-20.0	0.451	0.466	0.016	3.34
		20.0-30.0	0.455	0.470	0.015	3.19
		30.0 <	0.452	0.468	0.016	3.33
0.9 - 1.5	6.5-10.0	0.0-20.0	0.451	0.483	0.032	6.67
		20.0-30.0	0.449	0.481	0.032	6.69
		30.0 <	0.451	0.483	0.032	6.63
	10.0-30.0	0.0-20.0	0.526	0.542	0.016	2.99
		20.0-30.0	0.534	0.550	0.016	2.91
		30.0 <	0.528	0.543	0.016	2.87
0.0 - 0.9	6.5-10.0	0.0-20.0	0.380	0.402	0.023	5.62
		20.0-30.0	0.378	0.400	0.022	5.49
		30.0 <	0.379	0.402	0.022	5.58
	10.0-30.0	0.0-20.0	0.650	0.662	0.012	1.75
		20.0-30.0	0.649	0.660	0.011	1.73
		30.0 <	0.636	0.647	0.010	1.61
-0.9 - 0.0	6.5-10.0	0.0-20.0	0.375	0.396	0.021	5.30
		20.0-30.0	0.375	0.396	0.021	5.30
		30.0 <	0.375	0.396	0.021	5.30
	10.0-30.0	0.0-20.0	0.653	0.658	0.006	0.85
		20.0-30.0	0.662	0.669	0.007	0.99
		30.0 <	0.659	0.665	0.006	0.90
-1.5 - -0.9	6.5-10.0	0.0-20.0	0.350	0.371	0.022	5.82
		20.0-30.0	0.350	0.371	0.022	5.82
		30.0 <	0.356	0.379	0.022	5.91
	10.0-30.0	0.0-20.0	0.632	0.641	0.009	1.47
		20.0-30.0	0.636	0.646	0.010	1.55
		30.0 <	0.626	0.635	0.009	1.42
-1.93 - -1.5	3-6.5	0.0-20.0	0.075	0.087	0.011	12.93
		20.0-30.0	0.077	0.088	0.011	12.53
		30.0 <	0.075	0.085	0.011	12.65
	6.5-10.0	0.0-20.0	0.396	0.425	0.029	6.83
		20.0-30.0	0.394	0.423	0.029	6.86
		30.0 <	0.396	0.425	0.029	6.83
	10.0-30.0	0.0-20.0	0.562	0.575	0.014	2.36
		20.0-30.0	0.561	0.575	0.014	2.37
		30.0 <	0.574	0.590	0.016	2.71

Table 25: Non-Prompt R_{FB} efficiency E_T dependent systematic uncertainty.

Range			Efficiency		Error	
y_{CM}	p_{T}	E_T	Before	After	Abs.	Rel. (%)
1.5 - 1.93	3-6.5	0.0-20.0	0.272	0.314	0.042	13.39
		20.0-30.0	0.269	0.312	0.042	13.61
		30.0 <	0.270	0.312	0.042	13.47
	6.5-10.0	0.0-20.0	0.398	0.427	0.029	6.79
		20.0-30.0	0.398	0.427	0.029	6.80
		30.0 <	0.397	0.426	0.029	6.81
	10.0-30.0	0.0-20.0	0.449	0.462	0.013	2.81
		20.0-30.0	0.453	0.466	0.013	2.79
		30.0 <	0.451	0.464	0.014	2.93
0.9 - 1.5	6.5-10.0	0.0-20.0	0.451	0.483	0.031	6.46
		20.0-30.0	0.450	0.481	0.031	6.44
		30.0 <	0.451	0.482	0.031	6.43
	10.0-30.0	0.0-20.0	0.546	0.560	0.014	2.54
		20.0-30.0	0.549	0.563	0.015	2.59
		30.0 <	0.545	0.559	0.014	2.51
0.0 - 0.9	6.5-10.0	0.0-20.0	0.391	0.413	0.022	5.33
		20.0-30.0	0.390	0.412	0.022	5.44
		30.0 <	0.390	0.412	0.022	5.33
	10.0-30.0	0.0-20.0	0.633	0.642	0.009	1.40
		20.0-30.0	0.633	0.642	0.009	1.40
		30.0 <	0.627	0.636	0.009	1.42
-0.9 - 0.0	6.5-10.0	0.0-20.0	0.391	0.412	0.021	5.10
		20.0-30.0	0.391	0.412	0.021	5.10
		30.0 <	0.391	0.412	0.021	5.10
	10.0-30.0	0.0-20.0	0.644	0.649	0.004	0.68
		20.0-30.0	0.648	0.652	0.005	0.70
		30.0 <	0.647	0.651	0.004	0.61
-1.5 - -0.9	6.5-10.0	0.0-20.0	0.367	0.389	0.022	5.66
		20.0-30.0	0.367	0.389	0.022	5.66
		30.0 <	0.368	0.391	0.022	5.73
	10.0-30.0	0.0-20.0	0.636	0.643	0.007	1.15
		20.0-30.0	0.638	0.645	0.007	1.15
		30.0 <	0.633	0.641	0.007	1.16
-1.93 - -1.5	3-6.5	0.0-20.0	0.087	0.100	0.013	12.97
		20.0-30.0	0.088	0.101	0.013	12.92
		30.0 <	0.087	0.100	0.013	13.03
	6.5-10.0	0.0-20.0	0.397	0.424	0.027	6.36
		20.0-30.0	0.396	0.424	0.028	6.51
		30.0 <	0.397	0.424	0.027	6.36
	10.0-30.0	0.0-20.0	0.575	0.587	0.013	2.14
		20.0-30.0	0.572	0.585	0.013	2.16
		30.0 <	0.564	0.578	0.014	2.42

Table 26: Prompt R_{FB} efficiency N_{trk} dependent systematic uncertainty.

Range			Efficiency		Error	
y_{CM}	p_{T}	N_{trk}	Before	After	Abs.	Rel. (%)
1.5 - 1.93	3-6.5	0-55	0.258	0.300	0.042	13.99
		56-85	0.258	0.299	0.042	13.89
		86 <	0.256	0.297	0.041	13.94
	6.5-10.0	0-55	0.389	0.418	0.029	7.03
		56-85	0.380	0.409	0.029	7.00
		86 <	0.390	0.420	0.029	7.00
	10.0-30.0	0-55	0.451	0.466	0.016	3.34
		55-85	0.454	0.469	0.016	3.32
		86 <	0.450	0.465	0.015	3.23
0.9 - 1.5	6.5-10.0	0-55	0.443	0.474	0.031	6.54
		56-85	0.446	0.477	0.031	6.50
		86 <	0.452	0.484	0.032	6.61
	10.0-30.0	0-55	0.539	0.556	0.017	2.99
		56-85	0.528	0.544	0.016	2.97
		86 <	0.534	0.550	0.016	2.91
0.0 - 0.9	6.5-10.0	0-55	0.378	0.400	0.022	5.50
		56-85	0.381	0.404	0.023	5.69
		86 <	0.382	0.405	0.023	5.68
	10.0-30.0	0-55	0.650	0.662	0.012	1.75
		55-85	0.649	0.660	0.011	1.73
		86 <	0.636	0.647	0.010	1.61
-0.9 - 0.0	6.5-10.0	0-55	0.375	0.396	0.021	5.30
		56-85	0.375	0.396	0.021	5.30
		86 <	0.375	0.396	0.021	5.30
	10.0-30.0	0-55	0.656	0.662	0.006	0.94
		56-85	0.653	0.658	0.006	0.85
		86 <	0.662	0.669	0.007	0.99
-1.5 - -0.9	6.5-10.0	0-55	0.347	0.369	0.021	5.80
		56-85	0.346	0.368	0.022	5.88
		86 <	0.356	0.379	0.022	5.91
	10.0-30.0	0-55	0.632	0.641	0.009	1.47
		56-85	0.641	0.651	0.010	1.54
		86 <	0.626	0.635	0.009	1.42
-1.93 - -1.5	3-6.5	0-55	0.075	0.087	0.011	12.93
		56-85	0.075	0.086	0.011	12.79
		86 <	0.075	0.085	0.011	12.65
	6.5-10.0	0-55	0.391	0.419	0.028	6.77
		56-85	0.391	0.420	0.029	6.90
		86 <	0.396	0.425	0.029	6.83
	10.0-30.0	0-55	0.554	0.567	0.014	2.40
		56-85	0.562	0.575	0.014	2.36
		86 <	0.577	0.593	0.016	2.70

Table 27: Non-Prompt R_{FB} efficiency N_{trk} dependent systematic uncertainty.

Range			Efficiency		Error	
y_{CM}	p_{T}		Before	After	Abs.	Rel. (%)
1.5 - 1.93	3-6.5	0-55	0.272	0.314	0.042	13.39
		56-85	0.272	0.314	0.042	13.39
		86 $<$	0.270	0.313	0.042	13.56
	6.5-10.0	0-55	0.398	0.427	0.029	6.80
		56-85	0.391	0.420	0.029	6.90
		86 $<$	0.398	0.427	0.029	6.79
	10.0-30.0	0-55	0.449	0.462	0.013	2.81
		56-85	0.452	0.465	0.013	2.80
		86 $<$	0.449	0.462	0.013	2.81
0.9 - 1.5	6.5-10.0	0-55	0.446	0.476	0.030	6.39
		56-85	0.448	0.478	0.030	6.27
		86 $<$	0.452	0.483	0.032	6.54
	10.0-30.0	0-55	0.552	0.567	0.015	2.64
		56-85	0.538	0.553	0.015	2.75
		86 $<$	0.549	0.563	0.015	2.59
0.0 - 0.9	6.5-10.0	0-55	0.390	0.412	0.022	5.34
		56-85	0.391	0.413	0.022	5.33
		86 $<$	0.391	0.413	0.022	5.32
	10.0-30.0	0-55	0.633	0.642	0.009	1.40
		56-85	0.633	0.642	0.009	1.40
		86 $<$	0.627	0.636	0.009	1.41
-0.9 - 0.0	6.5-10.0	0-55	0.391	0.412	0.021	5.10
		56-85	0.391	0.412	0.021	5.10
		86 $<$	0.391	0.412	0.021	5.10
	10.0-30.0	0-55	0.645	0.650	0.005	0.77
		56-85	0.644	0.649	0.004	0.68
		86 $<$	0.648	0.652	0.005	0.70
-1.5 - -0.9	6.5-10.0	0-55	0.366	0.388	0.022	5.67
		56-85	0.358	0.380	0.021	5.63
		86 $<$	0.368	0.391	0.022	5.73
	10.0-30.0	0-55	0.635	0.643	0.008	1.24
		56-85	0.639	0.647	0.008	1.24
		86 $<$	0.634	0.641	0.007	1.09
-1.93 - -1.5	3-6.5	0-55	0.087	0.100	0.013	12.97
		56-85	0.087	0.100	0.013	13.00
		86 $<$	0.087	0.100	0.013	13.03
	6.5-10.0	0-55	0.393	0.420	0.027	6.43
		56-85	0.395	0.422	0.027	6.40
		86 $<$	0.397	0.424	0.027	6.36
	10.0-30.0	0-55	0.653	0.566	0.013	2.33
		56-85	0.575	0.587	0.013	2.14
		86 $<$	0.572	0.586	0.014	2.32

Table 28: Prompt Cross Section efficiency systametic uncertainty.

Range			Efficiency		Error	
y_{CM}	p_{T}	E_T	Before	After	Abs.	Rel. (%)
1.5 - 1.93	0.0-3.0	0.0-120.0	0.070	0.093	0.024	25.32
	3.0-6.5		0.259	0.300	0.042	13.86
	6.5-7.5		0.362	0.392	0.031	7.80
	7.5-8.5		0.387	0.417	0.030	7.10
	8.5-9.5		0.441	0.468	0.027	5.77
	9.5-11.0		0.438	0.460	0.022	4.78
	11.0-14.0		0.463	0.481	0.018	3.66
	14.0-30.0		0.443	0.447	0.004	0.89
1.0 - 1.5	6.5-7.5		0.424	0.459	0.035	7.63
	7.5-8.5		0.470	0.501	0.031	6.27
	8.5-9.5		0.493	0.520	0.027	5.27
	9.5-11.0		0.505	0.530	0.025	4.79
	11.0-14.0		0.535	0.553	0.018	3.25
	14.0-30.0		0.552	0.555	0.004	0.65
0.0 - 1.0	6.5-7.5		0.286	0.309	0.024	7.63
	7.5-8.5		0.412	0.436	0.024	5.51
	8.5-9.5		0.500	0.522	0.022	4.21
	9.5-11.0		0.571	0.590	0.019	3.22
	11.0-14.0		0.628	0.642	0.014	2.18
	14.0-30.0		0.710	0.711	0.001	0.14
-1.0 - 0.0	6.5-7.5		0.206	0.229	0.023	10.04
	7.5-8.5		0.373	0.397	0.024	6.05
	8.5-9.5		0.492	0.512	0.020	3.91
	9.5-11.0		0.575	0.587	0.012	2.05
	11.0-14.0		0.657	0.663	0.006	0.97
	14.0-30.0		0.731	0.732	0.001	0.14
-1.5 - -1.0	6.5-7.5		0.212	0.233	0.021	9.01
	7.5-8.5		0.365	0.390	0.025	6.46
	8.5-9.5		0.488	0.510	0.023	4.43
	9.5-11.0		0.543	0.561	0.019	3.31
	11.0-14.0		0.638	0.652	0.014	2.21
	14.0-30.0		0.720	0.729	0.009	1.23
-2.4 - 1.5	3.0-6.5		0.106	0.123	0.016	13.36
	6.5-7.5		0.336	0.367	0.032	8.60
	7.5-8.5		0.424	0.454	0.030	6.52
	8.5-9.5		0.487	0.514	0.027	5.18
	9.5-11.0		0.502	0.526	0.024	4.56
	11.0-14.0		0.569	0.590	0.021	3.56
	14.0-30.0		0.625	0.642	0.017	2.65

Table 29: Non-Prompt Cross Section efficiency systametic uncertainty.

Range			Efficiency		Error	
y_{CM}	p_{T}	E_T	Before	After	Abs.	Rel. (%)
1.5 - 1.93	0.0-3.0	0.0-120.0	0.068	0.092	0.023	25.55
	3.0-6.5		0.272	0.314	0.042	13.38
	6.5-7.5		0.372	0.403	0.032	7.83
	7.5-8.5		0.399	0.428	0.029	6.78
	8.5-9.5		0.422	0.448	0.026	5.80
	9.5-11.0		0.448	0.471	0.023	4.89
	11.0-14.0		0.446	0.462	0.016	3.38
	14.0-30.0		0.454	0.457	0.003	0.66
1.0 - 1.5	6.5-7.5		0.422	0.457	0.035	7.67
	7.5-8.5		0.463	0.494	0.031	6.72
	8.5-9.5		0.488	0.516	0.028	5.43
	9.5-11.0		0.514	0.539	0.025	4.64
	11.0-14.0		0.545	0.565	0.020	3.57
	14.0-30.0		0.558	0.558	0.000	0.00
0.0 - 1.0	6.5-7.5		0.290	0.314	0.024	7.65
	7.5-8.5		0.406	0.429	0.024	5.50
	8.5-9.5		0.487	0.508	0.021	4.14
	9.5-11.0		0.550	0.568	0.018	3.17
	11.0-14.0		0.619	0.632	0.013	2.06
	14.0-30.0		0.682	0.681	0.000	0.06
-1.0 - 0.0	6.5-7.5		0.209	0.233	0.024	10.30
	7.5-8.5		0.374	0.399	0.025	6.27
	8.5-9.5		0.490	0.509	0.019	3.74
	9.5-11.0		0.571	0.584	0.013	2.16
	11.0-14.0		0.638	0.643	0.006	0.87
	14.0-30.0		0.700	0.700	0.000	0.00
-1.5 - -1.0	6.5-7.5		0.220	0.242	0.022	9.11
	7.5-8.5		0.366	0.390	0.024	6.15
	8.5-9.5		0.473	0.494	0.021	4.25
	9.5-11.0		0.548	0.565	0.017	3.01
	11.0-14.0		0.618	0.631	0.013	2.06
	14.0-30.0		0.695	0.701	0.006	0.86
-2.4 - 1.5	3.0-6.5		0.121	0.139	0.018	13.20
	6.5-7.5		0.333	0.363	0.030	8.26
	7.5-8.5		0.419	0.449	0.030	6.68
	8.5-9.5		0.467	0.494	0.027	5.39
	9.5-11.0		0.519	0.544	0.024	4.49
	11.0-14.0		0.562	0.583	0.021	3.60
	14.0-30.0		0.617	0.634	0.017	2.62

7 Correction factor and total systematic uncertainties

7.1 Full correction factor (Acceptance*Efficiency)

The full correction factor for the raw yields, which is the product of efficiency and acceptance, is shown on figure 40(1st run) and figure 41 (2nd run) for prompt J/ψ. Plots for non-prompt J/ψ is shown in figure 42 (1st run) and figure 43 (2nd run).

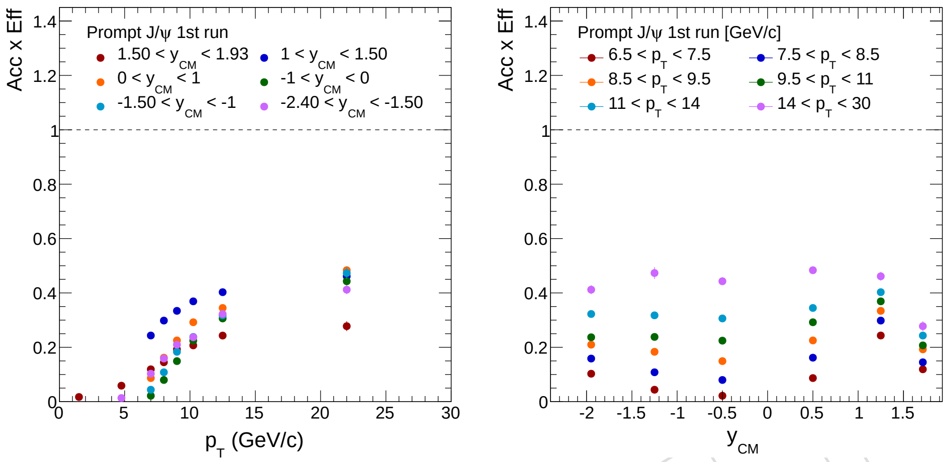

Figure 40: correction factor(=$\alpha * \varepsilon$) for prompt J/ψ as a function of p_{T} (Left) and y_{lab}(Right) in case of 1st run period.

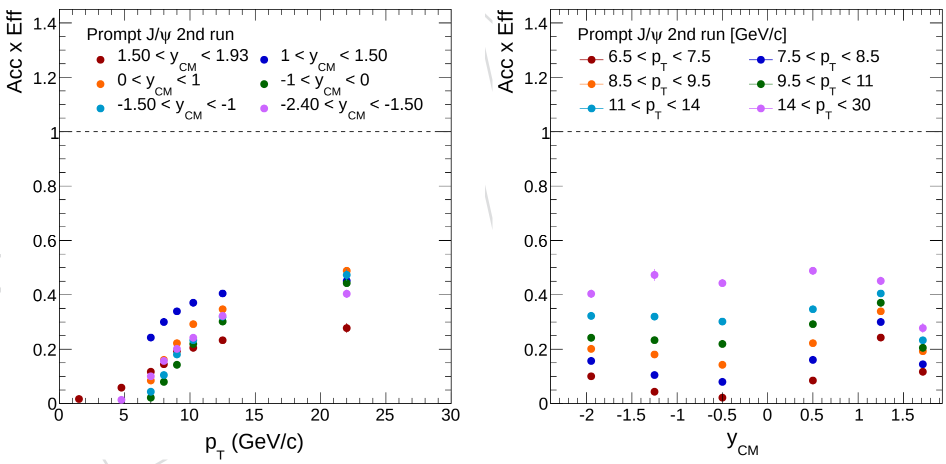

Figure 41: correction factor(=$\alpha * \varepsilon$) for prompt J/ψ as a function of p_{T} (Left) and y_{lab}(Right) in case of 2nd run period.

The event-activity dependency of correction factor is not considered, but from Tag and Probe study using pp and pPb data, it would be expected smaller than 0.5%.

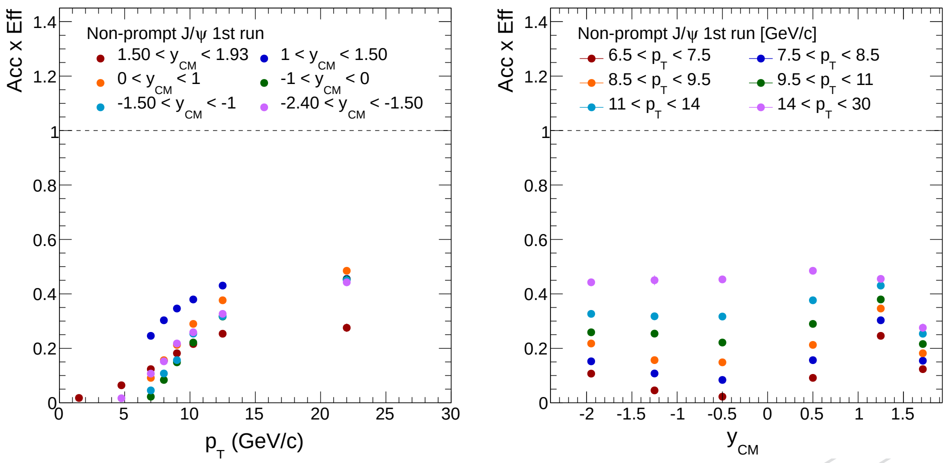

Figure 42: correction factor(=$\alpha * \varepsilon$) for non-prompt J/ψ as a function of p_{T} (Left) and y_{lab}(Right) in case of 1st run period.

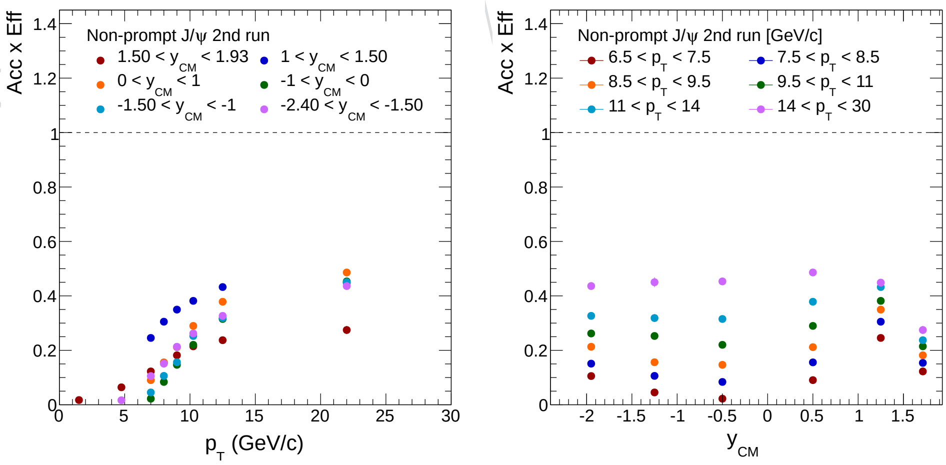

Figure 43: correction factor(=$\alpha * \varepsilon$) for non-prompt J/ψ as a function of p_{T} (Left) and y_{lab}(Right) in case of 2nd run period.

7.2 Summary for total systematic uncertainties

The total systematic uncertainty is estimated by summing in quadrature the contributions from the investigated sources that are acceptance, efficiency and signal extraction. Also in case of cross section measurements, the uncertainties from luminosity and branching ratio that are global to all points are also considered.

$$\text{Total} = \sqrt{(\text{Yield extraction})^2 + (\text{Acceptance})^2 + (\text{Efficiency})^2}\,, \tag{15}$$

The ranges of the variations are summarized in Table 30. The largest uncertainty comes from the lowest p_T bin 0-3 GeV/c mainly from T&P weighted efficiency. For the bin $3 < p_\mathrm{T} < 6.5$ GeV/c, systematic uncertainties from efficiency are 13.9% and 13.3% for prompt and non-prompt J/ψ repectively. For the region with p_T larger than 6.5 GeV/c, systematic uncertainties from efficiencies are up to 7.2% for prompt J/ψ, and 7.8% for non-prompt J/ψ.

Table 30: Summary of the relative systematic uncertainties on prompt and non-prompt J/ψ. "Luminosity" and "branching" ratio are global uncertainties that is common to all data points, and only for cross section measurement.

	prompt J/ψ	non-prompt J/ψ
luminosity	3.5	3.5
branching ratio	1	1
Yield extraction	0.6-3.5	1.3-5.9
Acceptance	0.0-2.2	0.2-1.7
efficiency	0.1-25.3	0.1-25.5

8 Results

8.1 J/ψ production Cross section

The production cross section of prompt and non-prompt J/ψ are computed by

$$\frac{d^2\sigma}{dp_{\mathrm{T}}dy} = \frac{N_{fit}^{\mathrm{J}/\psi}/(A \cdot \varepsilon)}{L_{int} \times B(\mathrm{J}/\psi \to \mu^+\mu^-) \times \Delta p_{\mathrm{T}} \Delta y}, \tag{16}$$

where variables are defined as follows:

- $N_{fit}^{\mathrm{J}/\psi}$ is the raw yield of J/ψ extracted from the fit procedure in a given (p_{T}, y) bin,
- A is the acceptance,
- ε is the dimuon efficiencies,
- $L_{int} = (34.7 \pm 1.2)\ \mathrm{nb}^{-1}$ is the integrated luminosity,
- $B(\mathrm{J}/\psi \to \mu^+\mu^-) = (5.93 \pm 0.06)\%$ is the branching ratio to the $\mu^+\mu^-$ channel [11],
- Δp_{T} and Δy are the widths of the (p_{T}, y) bin.

In Figs 44 and 45, the double differential cross-sections are plotted as a function of p_{T} in six different rapidity ranges for prompt and non-prompt J/ψ, respectively. The bin abscissae are given by the bin-averaged values, and the uncertainties from luminosity and branching ratio, that are global to all points are $\pm$ 3.6% and not drawn on the plots.

In particular at low p_{T}, the cross section of forward and backward repidities are not identical. This can be further quantified by studying R_{FB}, the forward to backward ratio of the yields.

In Fig 46, differential cross sections are plotted as a function of the center-of-mass rapidity after integrated p_{T} for prompt and non-prompt J/ψ, respectively.

8.2 Forward-backward production ratio R_{FB}

The nuclear parton distribution functions are suppressed, compared to the proton PDFs, increasingly for lower values of $x\ \frac{m_{\mathrm{J}/\psi}}{\sqrt{s}} e^{\pm y}$. The rapidity dependence of the J/ψ yields provides thus important information on the nPDF effects. We study this effect through the forward-backward ratio defined by:

$$R_{FB} = \frac{N_{forward}^{fit}}{N_{backward}^{fit}} \cdot \frac{A_{backward} \cdot \varepsilon_{backward}}{A_{forward} \cdot \varepsilon_{forward}}, \tag{17}$$

where variables are defined as

- $N_{forward/backward}^{fit}$ is the raw yield extracted from the fit procedure in the forward or backward rapidity bins,
- $A_{backward/backward}$ is the acceptance values for the forward or backward rapidity,
- $\varepsilon_{backward/backward}$ is the efficiency for the forward or backward rapidity bins.

Fig 47 displays the ratio R_{FB} as a function of p_{T} in three different rapidity ranges for prompt and non-prompt J/ψ. The bin abscissae are determined by the bin-averaged values. The points are plotted at x values corresponding to the average of the event distribution within the bins.

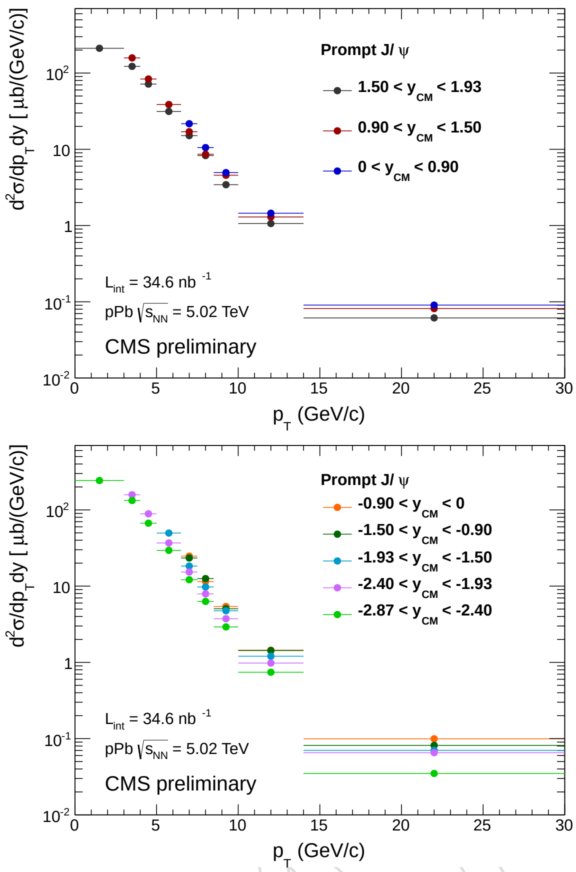

Figure 44: Double differential cross sections for prompt J/ψ. The data points are scaled by 10 for $1 < |y_{CM}| < 1.5$ and by 100 for $1.5 < y_{CM} < 1.93$ and $-2.4 < y_{CM} < -1.5$. The global uncertainties are $\pm$ 3.6%.

Especially, for the most forward or backward regions, the CMS detector covers p_{T} of J/ψ down to 3 GeV/c. It is manifest that the R_{FB} values increase with p_{T}, starting from a relatively suppressed value R_{FB} 0.7 at the most forward and backward rapidity bin corresponding to the smaller Bjorken x values.

Fig 48 displays the ratios R_{FB} as a function of rapidity for two p_{T} bins for prompt and non-prompt J/ψ. No strong rapidity dependence can be observed within uncertainties, which is different from other experiments at LHC. This can be understood by the fact that the CMS covers the mid-rapidity regions and ALICE [12] and LHCb[13] experiments cover more forward rapidities. and the difference of rapidity values between forward and backward are relatively small.

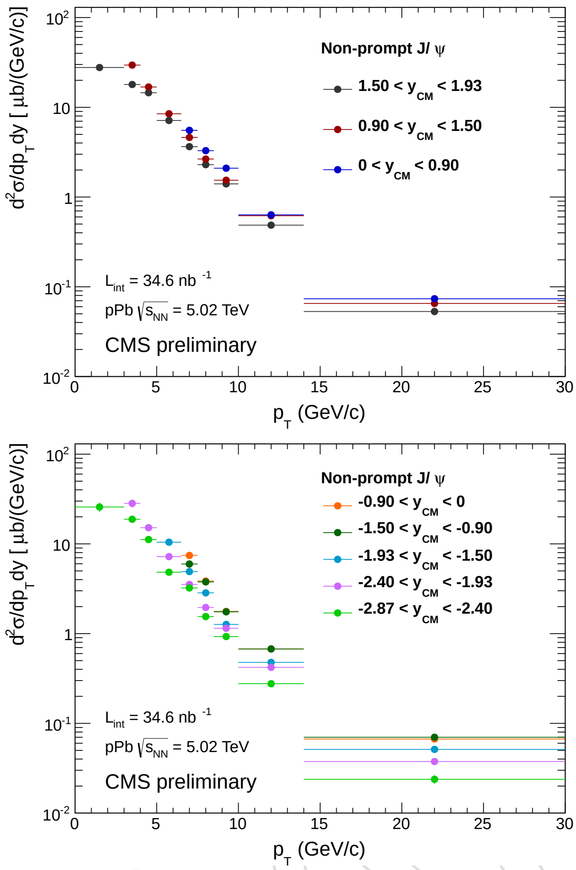

Figure 45: Double differential cross sections for non-prompt J/ψ. The data points are scaled by 10 for $1 < |y_{CM}| < 1.5$ and by 100 for $1.5 < y_{CM} < 1.93$ and $-2.4 < y_{CM} < -1.5$. The global uncertainties are $\pm$ 3.6%.

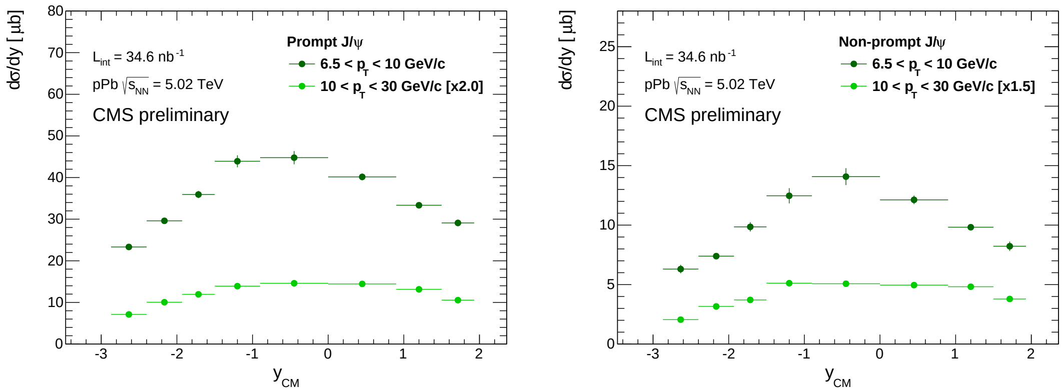

Figure 46: Rapidity dependenc of the cross sections for prompt J/ψ (left) and non-prompt J/ψ (right). For $9.5 < p_T < 30$ GeV/c, the data points are scaled by 2 for prompt and 1.5 for non-prompt J/ψ. The global uncertainties are $\pm$ 3.6%

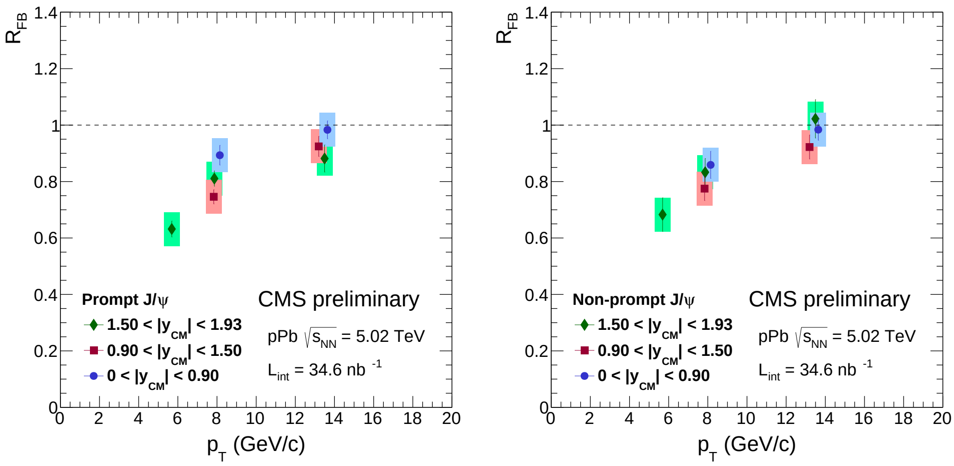

Figure 47: p_{T} dependences of R_{FB} for prompt (left) and non-prompt J/ψ (right) in several rapidity ranges.

Table 31: R_{FB} of prompt J/ψ as function of rapidity, and p_{T}. Quoted uncertainties are statistical and systematic.

$\lvert y_C M(\mathrm{J}/\psi)\rvert$	$p_{\mathrm{T}}(\mathrm{J}/\psi)$ [GeV/c]	$E_T^{HF\lvert\eta\rvert>4}$ [GeV/c]	$\langle p_{\mathrm{T}}(\mathrm{J}/\psi)\rangle$ [GeV/c]	R_{FB}
$1.5 \leq \lvert y\rvert < 1.93$	$3.0 \leq p_{\mathrm{T}} < 6.5$	0–120	4.48	0.69±0.03±0.10
	$6.5 \leq p_{\mathrm{T}} < 10.0$		7.90	0.86±0.03±0.06
	$10.0 \leq p_{\mathrm{T}} < 30.0$		13.22	0.98±0.06±0.03
$0.9 \leq \lvert y\rvert < 1.5$	$6.5 \leq p_{\mathrm{T}} < 10.0$	0–120	7.94	0.83±0.02±0.06
	$10.0 \leq p_{\mathrm{T}} < 30.0$		13.36	0.96±0.04±0.03
$0.0 \leq \lvert y\rvert < 0.9$	$6.5 \leq p_{\mathrm{T}} < 10.0$	0–120	8.23	0.90±0.03±0.05
	$10.0 \leq p_{\mathrm{T}} < 30.0$		13.64	0.95±0.03±0.02

Table 32: R_{FB} of non-prompt J/ψ as function of rapidity, and p_{T}. Quoted uncertainties are statistical and systematic.

$\lvert y_C M(\mathrm{J}/\psi)\rvert$	$p_{\mathrm{T}}(\mathrm{J}/\psi)$ [GeV/c]	$E_T^{HF\lvert\eta\rvert>4}$ [GeV/c]	$\langle p_{\mathrm{T}}(\mathrm{J}/\psi)\rangle$ [GeV/c]	R_{FB}
$1.5 \leq \lvert y\rvert < 1.93$	$3.0 \leq p_{\mathrm{T}} < 6.5$	0–120	4.48	0.72±0.06±0.10
	$6.5 \leq p_{\mathrm{T}} < 10.0$		7.90	0.89±0.05±0.07
	$10.0 \leq p_{\mathrm{T}} < 30.0$		13.22	1.09±0.08±0.03
$0.9 \leq \lvert y\rvert < 1.5$	$6.5 \leq p_{\mathrm{T}} < 10.0$	0–120	7.94	0.82±0.04±0.05
	$10.0 \leq p_{\mathrm{T}} < 30.0$		13.36	0.95±0.04±0.03
$0.0 \leq \lvert y\rvert < 0.9$	$6.5 \leq p_{\mathrm{T}} < 10.0$	0–120	8.23	0.95±0.04±0.05
	$10.0 \leq p_{\mathrm{T}} < 30.0$		13.64	0.99±0.04±0.03

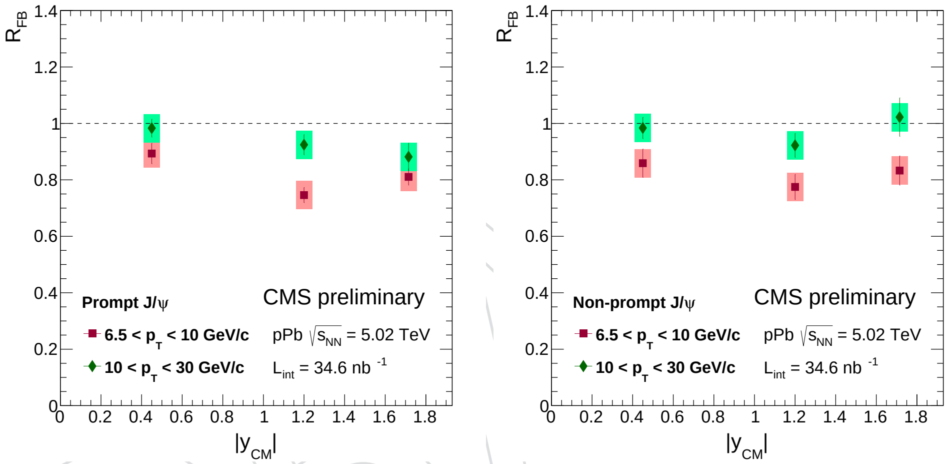

Figure 48: Rapidity distributions of R_{FB} for prompt (left) and non-prompt J/ψ (right) in several rapidity ranges.

8.3 Event activity dependence

The R_{FB} are further analyzed as a function of the multiplicity-related variables, such as the transverse energy deposited in the forward hadronic calorimeters in $4 < |\eta| < 5.2$, $E_T^{HF|\eta|>4}$, or the number of charged tracks reconstructed in central region in $N_{tracks}^{|\eta|<2.4}$.

The bin sizes in Table 33 were chosen according to the statistics in the muon triggered data. The mean value for each bin is computed from minimum bias sample. The table also includes the fraction of the minimum bias events in each bin.

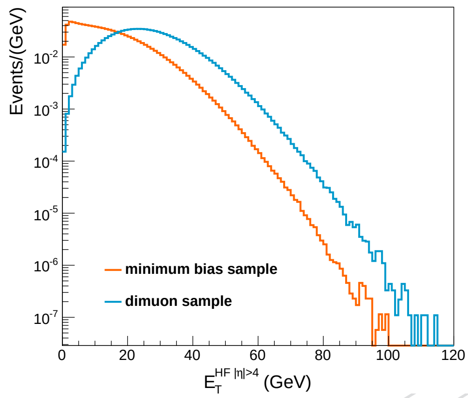

Figure 49: distributions of $E_T^{HF|\eta|>4}$ (left) and $N_{tracks}^{|\eta|<2.4}$ (right) from the minimum bias sample and muon sample used in the analysis.

Table 33: Multiplicity-related bins in $E_T^{HF|\eta|>4}$ and $N_{tracks}^{|\eta|<2.4}$ comprising the bin edges, the mean within the bin, and the fraction of recorded events falling in the bin.

$[E_T^{HF|\eta|>4}$ (GeV)]	$\langle E_T^{HF|\eta|>4} \rangle$	Event fraction	$[N_{tracks}^{|\eta|<2.4}]$	$\langle N_{tracks}^{|\eta|<2.4} \rangle$	Event fraction
0–20.0	9.4	73%	0-55%	25	72%
20.0–30.0	24.3	18%	56-85%	69	18%
30.0≤	37.2	9%	86≤	108	10%

Fig 50 shows the ratio R_{FB} as a function of $E_T^{HF|\eta|>4}$ for prompt and non-prompt J/ψ. Fig **??** shows the same R_{FB} data as a function of $N_{tracks}^{|\eta|<2.4}$ employing the same p_T and y binning as fig 50. The bin abscissae are given by the bin-averaged values. It can be observed that R_{FB} decreases with both event-activity variables, $E_T^{HF|\eta|>4}$ and $N_{tracks}^{|\eta|<2.4}$ in all rapidity bins. The R_{FB} data do not show any rapidity dependence for $6.5 < p_T < 30.0\,\mathrm{GeV}/c$, but the decreasing rate is larger for the lower p_T data. This observation on the p_T dependence of R_{FB} may provide an important constraint on the cold nuclear matter effect.

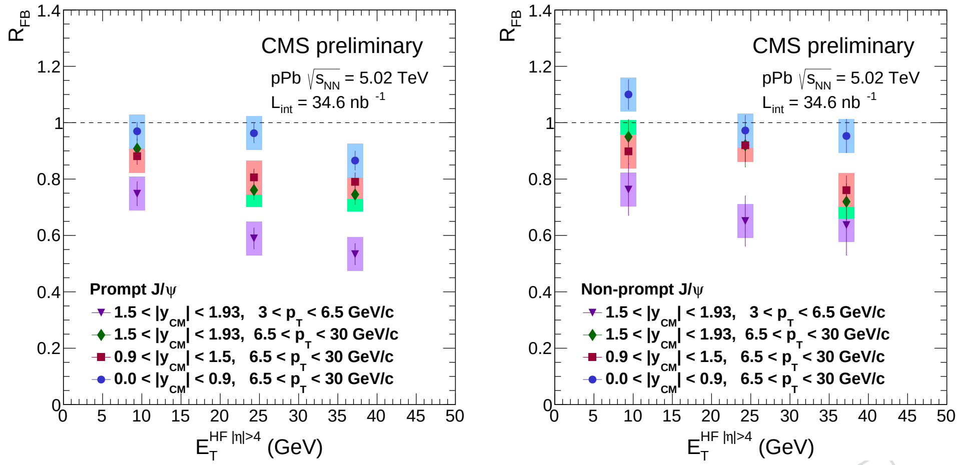

Figure 50: R_{FB} as a function of $E_T^{HF|\eta|>4}$ for prompt (left) and non-prompt J/ψ (right). The data are integrated over $6.5 < p_{\mathrm{T}} < 30\ GeV/c$. For the most forward data in $1.5 < y_{CM}| < 1.93$, the lower p_{T} data $3 < p_{\mathrm{T}} 6.5\ GeV/c$ are given in addition.

Table 34: R_{FB} of prompt J/ψ as function of rapidity, p_{T}, and $E_T^{HF|\eta|>4}$. Quoted uncertainties are statistical and systematic.

$\|y_C M(\mathrm{J}/\psi)\|$	$p_{\mathrm{T}}(\mathrm{J}/\psi)$ [GeV/c]	$E_T^{HF\|\eta\|>4}$ [GeV/c]	R_{FB}
$1.5 \leq \|y\| < 1.93$	$3.0 \leq p_{\mathrm{T}} < 6.5$	0–20	0.80±0.04±0.11
	$6.5 \leq p_{\mathrm{T}} < 30.0$		0.98±0.04±0.07
$1.5 \leq \|y\| < 1.93$	$3.0 \leq p_{\mathrm{T}} < 6.5$	20–30	0.62±0.04±0.09
	$6.5 \leq p_{\mathrm{T}} < 30.0$		0.81±0.04±0.07
$1.5 \leq \|y\| < 1.93$	$3.0 \leq p_{\mathrm{T}} < 6.5$	30–120	0.51±0.03±0.07
	$6.5 \leq p_{\mathrm{T}} < 30.0$		0.83±0.04±0.06
$0.9 \leq \|y\| < 1.5$	$6.5 \leq p_{\mathrm{T}} < 30.0$	0–20	0.91±0.03±0.06
$0.9 \leq \|y\| < 1.5$	$6.5 \leq p_{\mathrm{T}} < 30.0$	20–30	0.81±0.03±0.05
$0.9 \leq \|y\| < 1.5$	$6.5 \leq p_{\mathrm{T}} < 30.0$	30–120	0.83±0.04±0.05
$0.0 \leq \|y\| < 0.9$	$6.5 \leq p_{\mathrm{T}} < 30.0$	0–20	0.94±0.03±0.05
$0.0 \leq \|y\| < 0.9$	$6.5 \leq p_{\mathrm{T}} < 30.0$	20–30	0.92±0.03±0.05
$0.0 \leq \|y\| < 0.9$	$6.5 \leq p_{\mathrm{T}} < 30.0$	30–120	0.85±0.04±0.05

Table 35: R_{FB} of non-prompt J/ψ as function of rapidity, p_{T}, and $E_T^{HF|\eta|>4}$. Quoted uncertainties are statistical and systematic.

$\lvert y_C M(\mathrm{J}/\psi)\rvert$	$p_{\mathrm{T}}(\mathrm{J}/\psi)$ [GeV/c]	$E_T^{HF\lvert\eta\rvert>4}$ [GeV/c]	R_{FB}
$1.5 \leq \lvert y\rvert < 1.93$	$3.0 \leq p_{\mathrm{T}} < 6.5$	0–20	0.83±0.09±0.12
	$6.5 \leq p_{\mathrm{T}} < 30.0$		1.01±0.09±0.07
$1.5 \leq \lvert y\rvert < 1.93$	$3.0 \leq p_{\mathrm{T}} < 6.5$	20–30	0.68±0.09±0.10
	$6.5 \leq p_{\mathrm{T}} < 30.0$		0.97±0.09±0.07
$1.5 \leq \lvert y\rvert < 1.93$	$3.0 \leq p_{\mathrm{T}} < 6.5$	30–120	0.63±0.10±0.09
	$6.5 \leq p_{\mathrm{T}} < 30.0$		0.75±0.08±0.05
$0.9 \leq \lvert y\rvert < 1.5$	$6.5 \leq p_{\mathrm{T}} < 30.0$	0–20	0.87±0.04±0.06
$0.9 \leq \lvert y\rvert < 1.5$	$6.5 \leq p_{\mathrm{T}} < 30.0$	20–30	0.92±0.06±0.06
$0.9 \leq \lvert y\rvert < 1.5$	$6.5 \leq p_{\mathrm{T}} < 30.0$	30–120	0.76±0.05±0.05
$0.0 \leq \lvert y\rvert < 0.9$	$6.5 \leq p_{\mathrm{T}} < 30.0$	0–20	1.04±0.05±0.06
$0.0 \leq \lvert y\rvert < 0.9$	$6.5 \leq p_{\mathrm{T}} < 30.0$	20–30	0.93±0.05±0.05
$0.0 \leq \lvert y\rvert < 0.9$	$6.5 \leq p_{\mathrm{T}} < 30.0$	30–120	0.83±0.05±0.05

Table 36: R_{FB} of prompt J/ψ as function of rapidity, p_{T}, and $N_{tracks}^{|\eta|<2.4}$. Quoted uncertainties are statistical and systematic.

$\lvert y_C M(\mathrm{J}/\psi)\rvert$	$p_{\mathrm{T}}(\mathrm{J}/\psi)$ [GeV/c]	$N_{tracks}^{\lvert\eta\rvert<2.4}$	R_{FB}
$1.5 \leq \lvert y\rvert < 1.93$	$3.0 \leq p_{\mathrm{T}} < 6.5$	0–55	0.81±0.04±0.11
	$6.5 \leq p_{\mathrm{T}} < 30.0$		1.04±0.03±0.08
$1.5 \leq \lvert y\rvert < 1.93$	$3.0 \leq p_{\mathrm{T}} < 6.5$	56–85	0.66±0.03±0.09
	$6.5 \leq p_{\mathrm{T}} < 30.0$		0.83±0.03±0.07
$1.5 \leq \lvert y\rvert < 1.93$	$3.0 \leq p_{\mathrm{T}} < 6.5$	86-350	0.53±0.03±0.07
	$6.5 \leq p_{\mathrm{T}} < 30.0$		0.78±0.03±0.05
$0.9 \leq \lvert y\rvert < 1.5$	$6.5 \leq p_{\mathrm{T}} < 30.0$	0–55	0.98±0.04±0.06
$0.9 \leq \lvert y\rvert < 1.5$	$6.5 \leq p_{\mathrm{T}} < 30.0$	56–85	0.82±0.04±0.05
$0.9 \leq \lvert y\rvert < 1.5$	$6.5 \leq p_{\mathrm{T}} < 30.0$	86-350	0.79±0.03±0.05
$0.0 \leq \lvert y\rvert < 0.9$	$6.5 \leq p_{\mathrm{T}} < 30.0$	0–55	0.95±0.03±0.06
$0.0 \leq \lvert y\rvert < 0.9$	$6.5 \leq p_{\mathrm{T}} < 30.0$	56-85	0.93±0.03±0.05
$0.0 \leq \lvert y\rvert < 0.9$	$6.5 \leq p_{\mathrm{T}} < 30.0$	86-350	0.84±0.03±0.05

Table 37: R_{FB} of non-prompt J/ψ as function of rapidity, p_{T}, and $N_{tracks}^{|\eta|<2.4}$. Quoted uncertainties are statistical and systematic.

$\lvert y_C M(\mathrm{J}/\psi)\rvert$	$p_{\mathrm{T}}(\mathrm{J}/\psi)$ [GeV/c]	$N_{tracks}^{\lvert\eta\rvert<2.4}$	R_{FB}
$1.5 \leq \lvert y\rvert < 1.93$	$3.0 \leq p_{\mathrm{T}} < 6.5$	0–55	0.97±0.12±0.13
	$6.5 \leq p_{\mathrm{T}} < 30.0$		1.00±0.07±0.06
$1.5 \leq \lvert y\rvert < 1.93$	$3.0 \leq p_{\mathrm{T}} < 6.5$	56-85	0.66±0.08±0.09
	$6.5 \leq p_{\mathrm{T}} < 30.0$		0.93±0.07±0.08
$1.5 \leq \lvert y\rvert < 1.93$	$3.0 \leq p_{\mathrm{T}} < 6.5$	86–350	0.56±0.07±0.07
	$6.5 \leq p_{\mathrm{T}} < 30.0$		0.81±0.06±0.06
$0.9 \leq \lvert y\rvert < 1.5$	$6.5 \leq p_{\mathrm{T}} < 30.0$	0–55	0.96±0.05±0.06
$0.9 \leq \lvert y\rvert < 1.5$	$6.5 \leq p_{\mathrm{T}} < 30.0$	56-85	0.89±0.06±0.06
$0.9 \leq \lvert y\rvert < 1.5$	$6.5 \leq p_{\mathrm{T}} < 30.0$	86–350	0.72±0.04±0.05
$0.0 \leq \lvert y\rvert < 0.9$	$6.5 \leq p_{\mathrm{T}} < 30.0$	0–55	1.03±0.05±0.06
$0.0 \leq \lvert y\rvert < 0.9$	$6.5 \leq p_{\mathrm{T}} < 30.0$	56-85	0.97±0.05±0.06
$0.0 \leq \lvert y\rvert < 0.9$	$6.5 \leq p_{\mathrm{T}} < 30.0$	86–350	0.84±0.05±0.05

9 Cross check

9.1 MC closure test

In order to validate our acceptance and efficiency values, we have compared reconstructed candidates corrected by acceptance and efficiency to generated particles in MC. However, this can not be matched 100% since we are using two MC samples for acceptance and efficiency respectively. For efficiency measurement, we are using a official MC sample which will be described in detail in section 6. For acceptance, we use the sample produced with the same configuration setting as the official sample, but in which the kinematic filters for generated muons are removed in section 5. This kinematic filter is applied to the official sample for enough statistics to estimate efficiency, but it will bias the distributions of generated particles and therefore, bias acceptance values. In other words, we compare the reconstructed particle from one sample, to the generated particles from the other sample, and even though their configuration setting is exactly the same, there is a fluctuation when we generate particles randomly in each samples.

Figure **??** and **??** show the closure test result of the prompt J/ψ for $p_{\mathrm{T}} < 30$ GeV/c and $3 < p_{\mathrm{T}} < 30$ GeV/c. They agree well except for the lower $p_{\mathrm{T}} < 3$ GeV/c regions. Figure **??** and **??** show the result of the non-prompt J/ψ and similar disagreement in lower p_{T} has been observed.

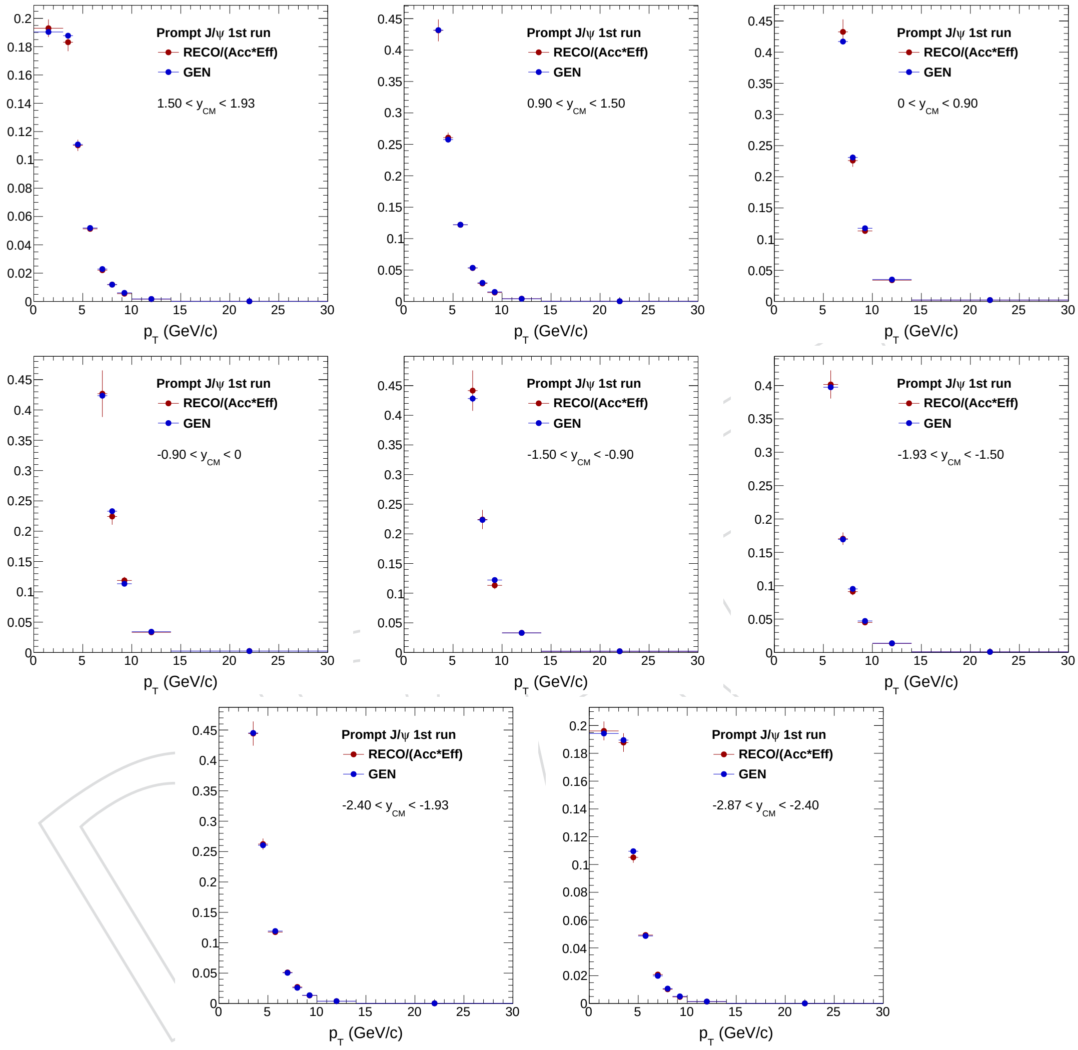

Figure 51: The p_{T} distribution of corrected reconstructed J/ψ $RECO/(Acc*Eff)$ and generated J/ψ GEN in prompt J/ψ Monte-carlo for the 1st run in each rapidity bins.

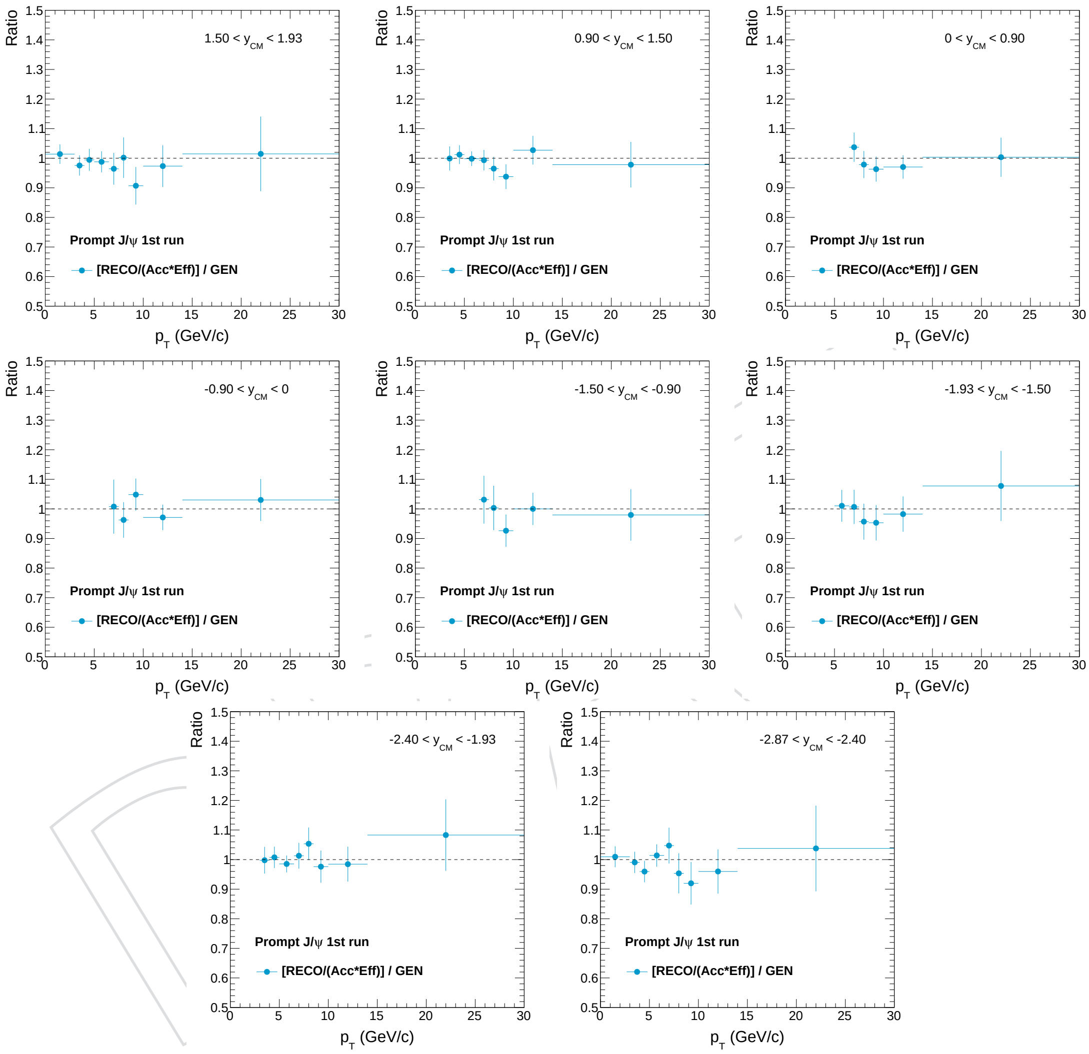

Figure 52: The p_{T} distribution of the ratio of $RECO/(Acc * Eff)$ over GEN in prompt J/ψ Monte-carlo for the 1st run in each rapidity bins.

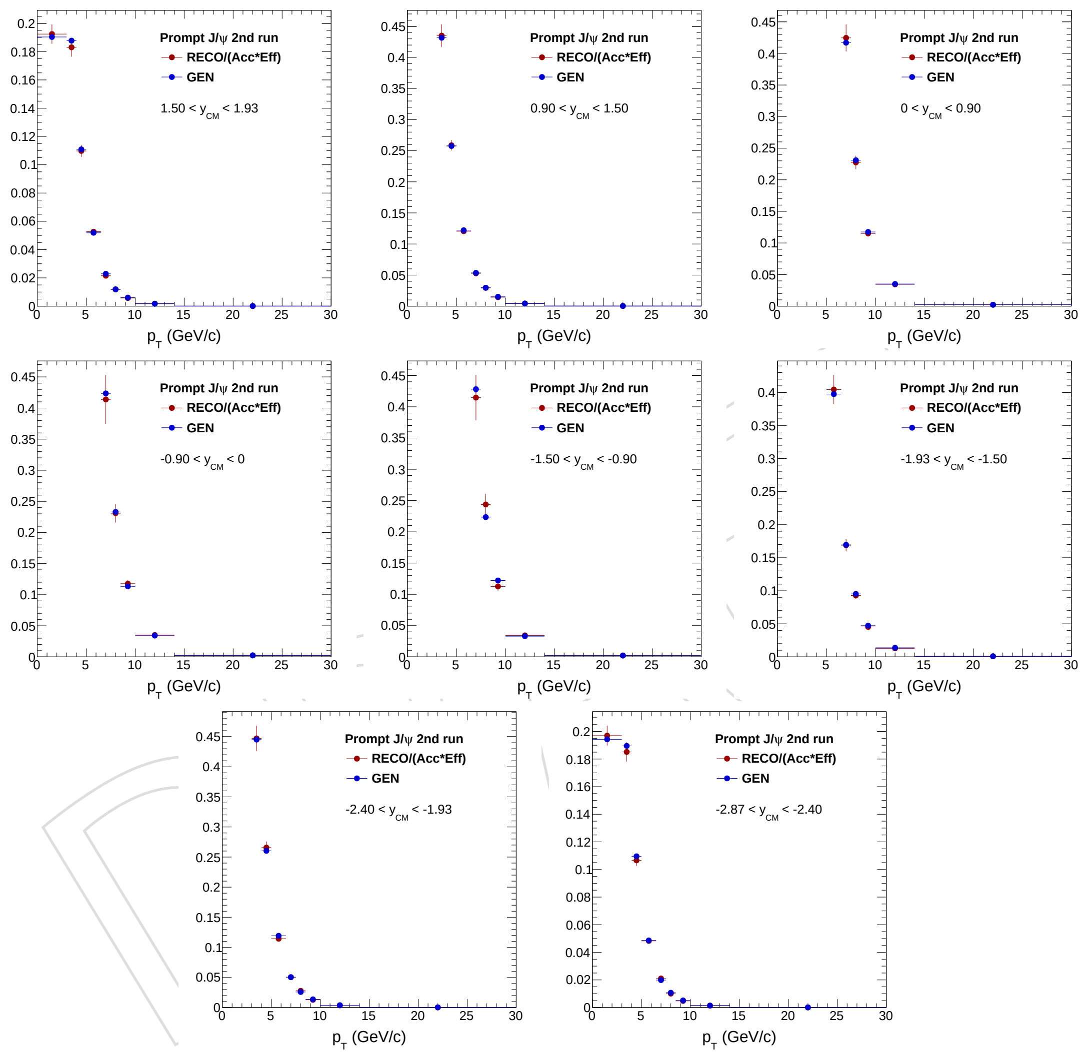

Figure 53: The p_{T} distribution of corrected reconstructed J/ψ $RECO/(Acc*Eff)$ and generated J/ψ GEN in prompt J/ψ Monte-carlo for the 2nd run in each rapidity bins.

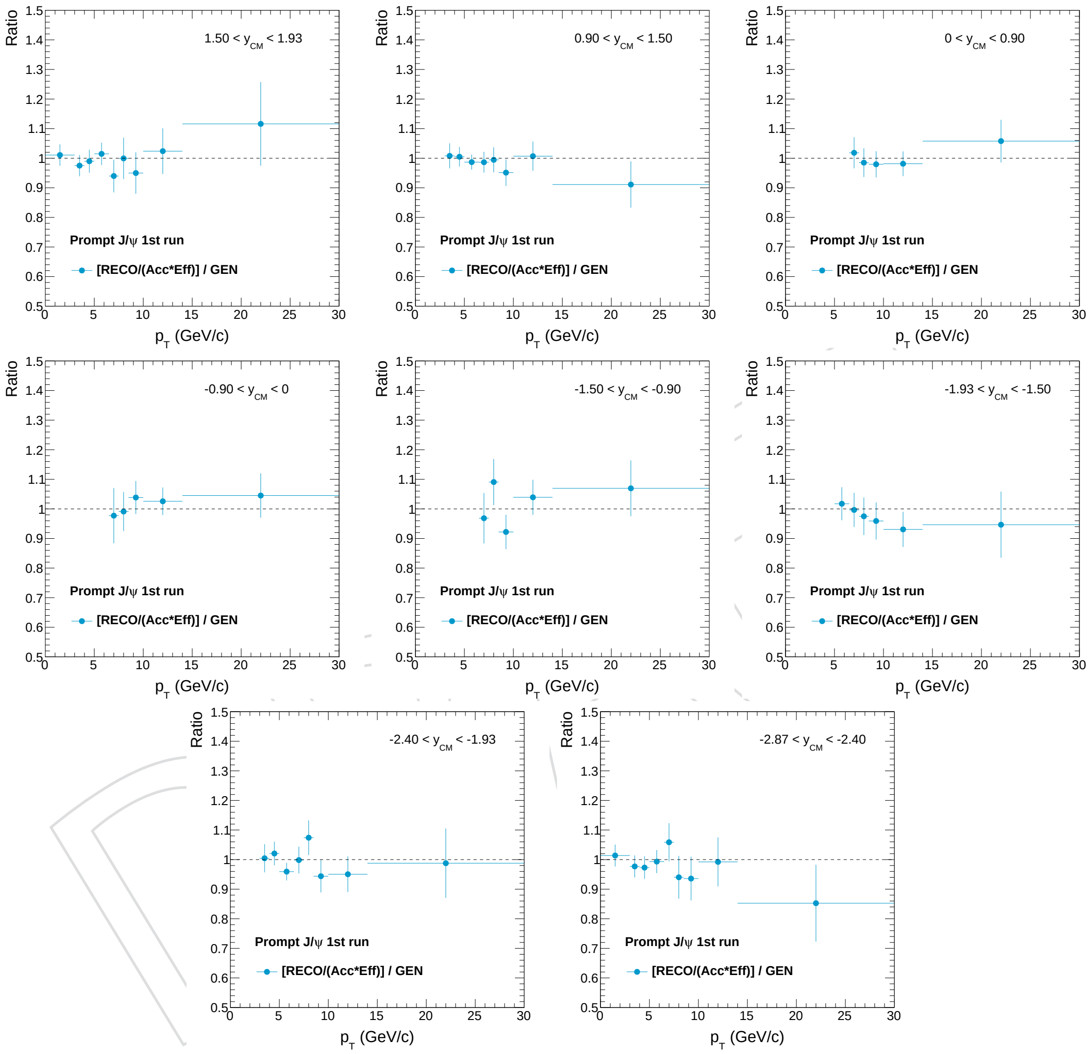

Figure 54: The p_{T} distribution of the ratio of $RECO/(Acc * Eff)$ over GEN in prompt J/ψ Monte-carlo for the 2nf run in each rapidity bins.

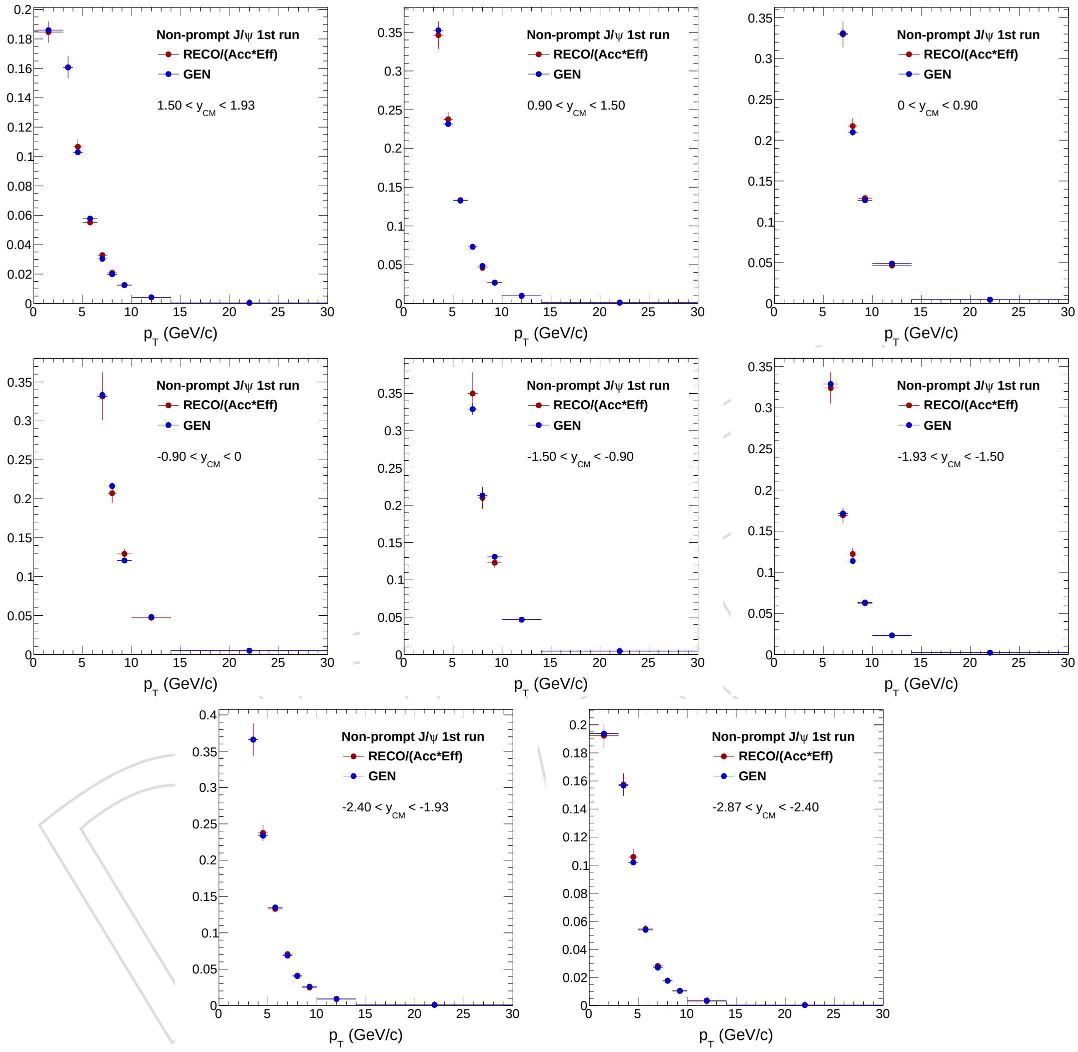

Figure 55: The p_{T} distribution of corrected reconstructed J/ψ $RECO/(Acc * Eff)$ and generated J/ψ GEN in non-prompt J/ψ Monte-carlo for the 1st run in each rapidity bins.

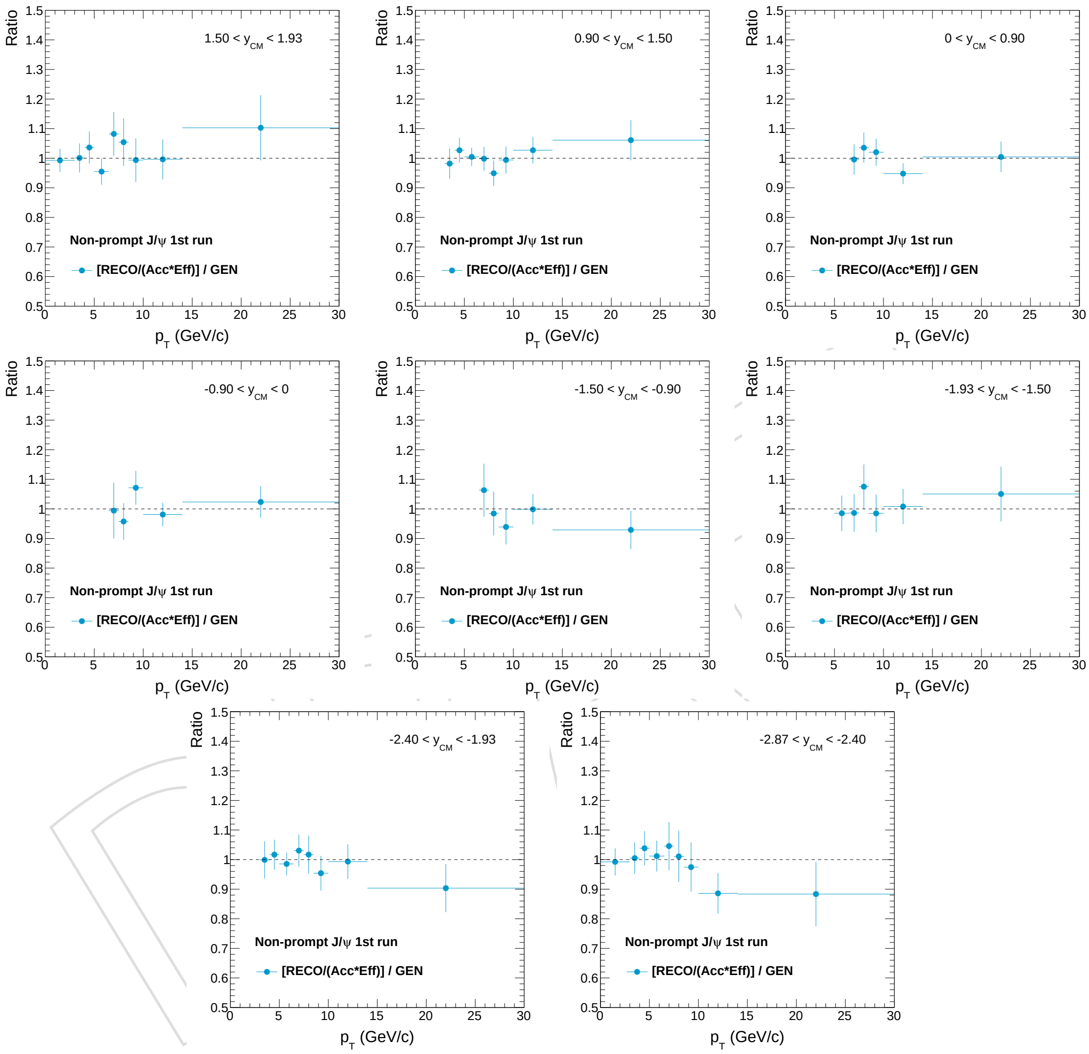

Figure 56: The p_{T} distribution of the ratio of $RECO/(Acc * Eff)$ over GEN in non-prompt J/ψ Monte-carlo for the 1st run in each rapidity bins.

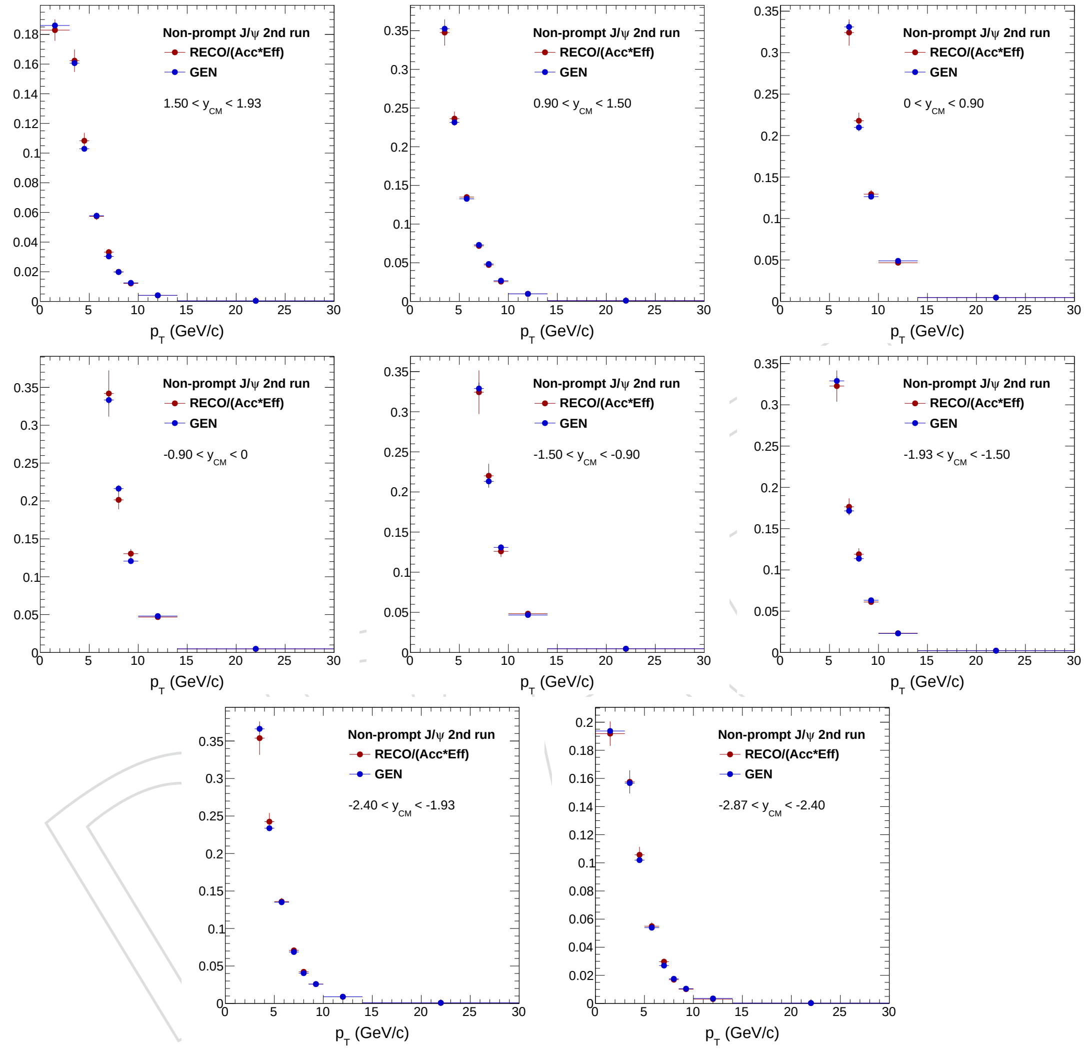

Figure 57: The p_T distribution of corrected reconstructed J/ψ $RECO/(Acc*Eff)$ and generated J/ψ GEN in non-prompt J/ψ Monte-carlo for the 2nd run in each rapidity bins.

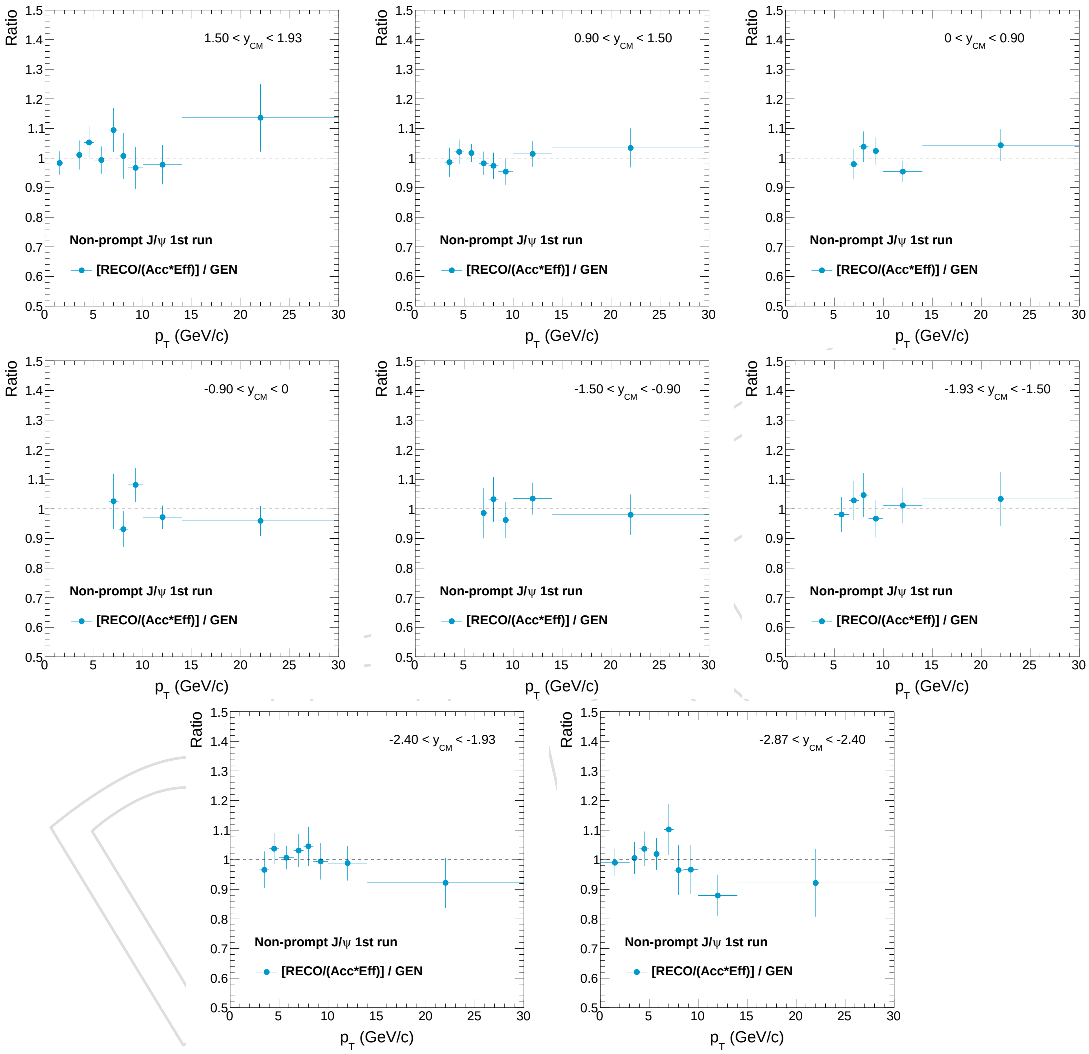

Figure 58: The p_{T} distribution of the ratio of $RECO/(Acc * Eff)$ over GEN in non-prompt J/ψ Monte-carlo for the 2nf run in each rapidity bins.

9.2 comparison with embedded samples

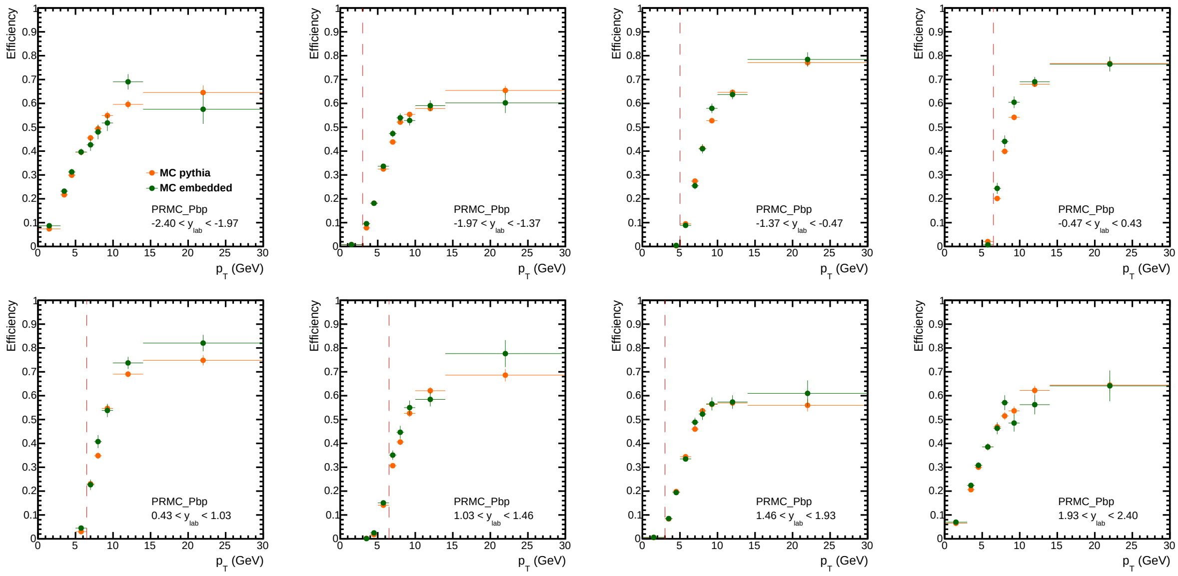

Figure 59: The efficiency values from the pure pythia samples used in the anlaysis (orange) and HIJING embedded samples (green) as a function of p_{T} for different rapidity ranges. Red dashed lines indicate the minimum p_{T} bin boundaries actually used in the analysis. Samples are prompt J/ψ and boosted as the 1st run.

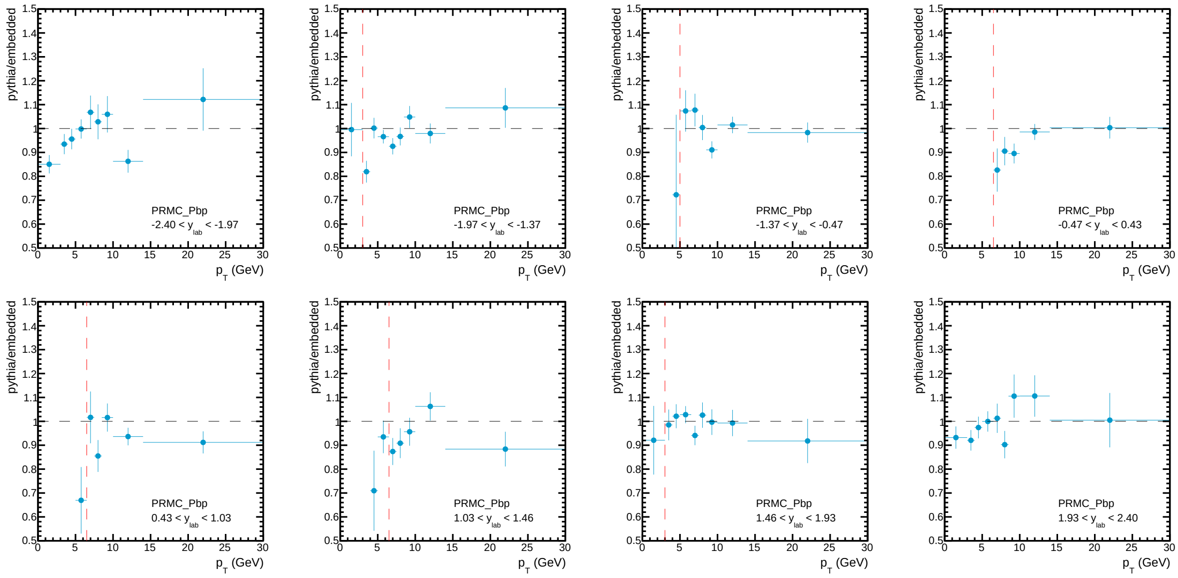

Figure 60: The ratio of the efficiency values from the pure pythia samples used in the anlaysis (orange) and HIJING embedded samples (green) as a function of p_T for different rapidity ranges. Red dashed lines indicate the minimum p_T bin boundaries actually used in the analysis. Samples are prompt J/ψ and boosted as the 1st run.

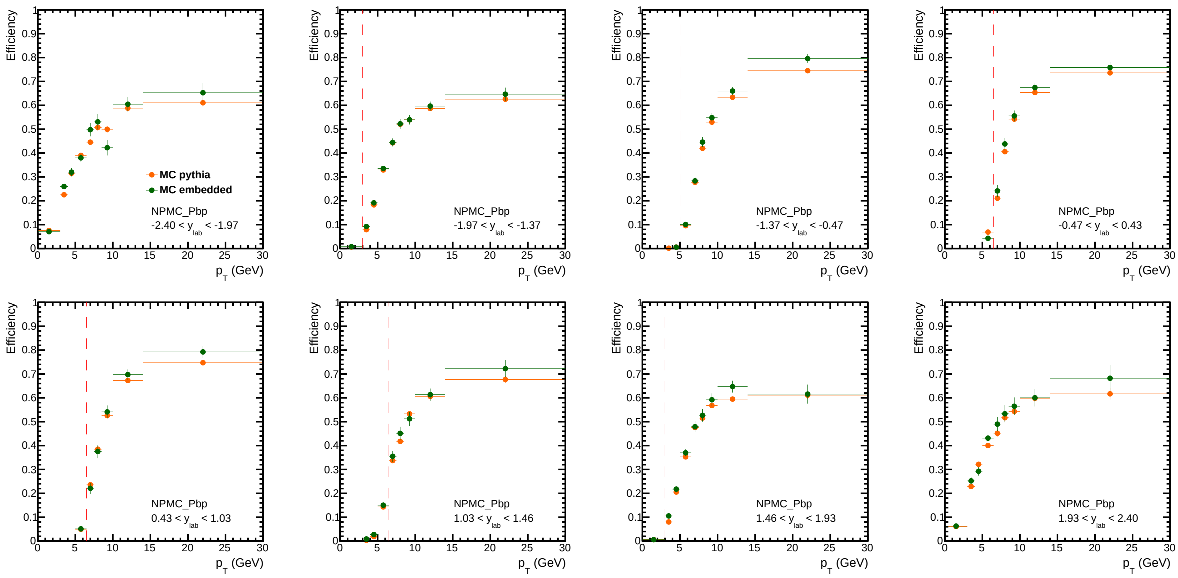

Figure 61: The efficiency values from the pure pythia samples used in the anlaysis (orange) and HIJING embedded samples (green) as a function of p_T for different rapidity ranges. Red dashed lines indicate the minimum p_T bin boundaries actually used in the analysis. Samples are non-prompt J/ψ and boosted as the 1st run.

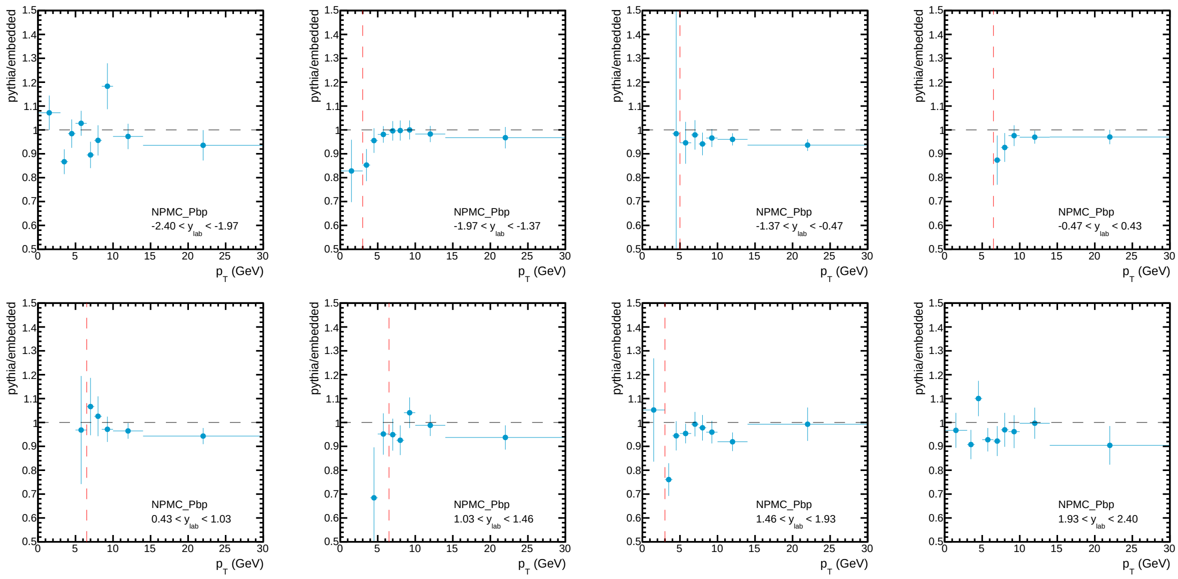

Figure 62: The ratio of the efficiency values from the pure pythia samples used in the anlaysis (orange) and HIJING embedded samples (green) as a function of p_T for different rapidity ranges. Red dashed lines indicate the minimum p_T bin boundaries actually used in the analysis. Samples are non-prompt J/ψ and boosted as the 1st run.

9.3 Data and Monte Carlo comparisons for dimuons

In order to trust the acceptance and efficiency values obtained from Monte Carlo simulations, the basic kinematic distributions for the J/ψ candidates in data and MC are compared.

Figure 63 and figure 64 show the comparison between data (1st run and 2nd run) and simulation (prompt and non-prompt J/ψ)of the invariant mass, rapidity in CM frame, and azimuthal angle distributions.

For the dimuon invariant mass distributions, there are no backgrounds in MC samples because we are using pp boosted samples without embedding procedure. In the rapidity distributions, the overall shapes of DATA, prompt MC, and non-prompt MC are different and this can be understood that actual data is the combination of prompt and non-prompt J/ψ with proper B-fraction. More proper comparison can be done after separating prompt and non-prompt in data as shown in fig 67. Lastly, the ϕ distributions agree well.

Fig 65 shows the p_T distribution of raw data and reconstructed candidates in MC. Here, data includes background, so they show discrepancies especially in lower p_T region, when we compare the distribution in the mass region $2.6 < m_{\mu\mu} < 3.5\,\mathrm{GeV}/c^2$ (left), and signal region $2.95 < m_{\mu\mu} < 3.25\,\mathrm{GeV}/c^2$ (middle), and signal regions in $2.95 < m_{\mu\mu} < 3.25\,\mathrm{GeV}/c^2$ with $p_T > 3$ GeV/c (right).

Fig 66 show the p_T distribution of prompt and non-prompt yields extracted from the fit procedure and reconstructed candidates in MC in $1.5 < y_{CM} < 1.93$. Left plot shows the p_T distributions in $p_T < 30$ GeV/c and right plot shows the distributions in $3 < p_T < 30$ GeV/c. Even after background are subtracted in data, they still show discrepancies in $p_T < 3$ GeV/c, They rather agree in $3 < p_T < 30$ GeV/c. Another comparison can be done after acceptance and efficiency correction as shown in fig 68.

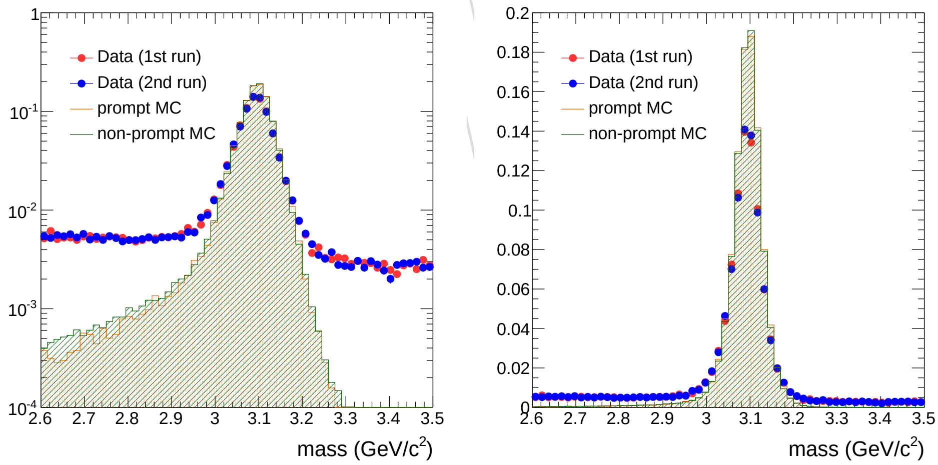

Figure 63: Data and MC comparison for the invariant mass distribution

Fig 67 and Fig 68 show the transverse momentum and rapidity distributions for prompt and non-prompt J/ψ. There yields from data, with acceptance and efficiency fully corrected, are compared to the generated distributions in Monte Carlo simulations. Kinematic ranges of J/ψ used in the analysis are selected which correspond to $-2.4 < y_{CM} < 1.93$ and $0 < p_T < 30\,\mathrm{GeV}/c$ and binning are chosen same as the cross-section measurements. The discrepancies of p_T distributions between DATA and MC are 1-18% for prompt J/ψ and 1-12% for non-prompt J/ψ in p_T. In rapidity distributions, differences are 1-14% for prompt J/ψ and 1-10% for non-prompt J/ψ. The rapidity distributions for the same p_T range $6.5 < p_T < 30\,\mathrm{GeV}/c$ are also

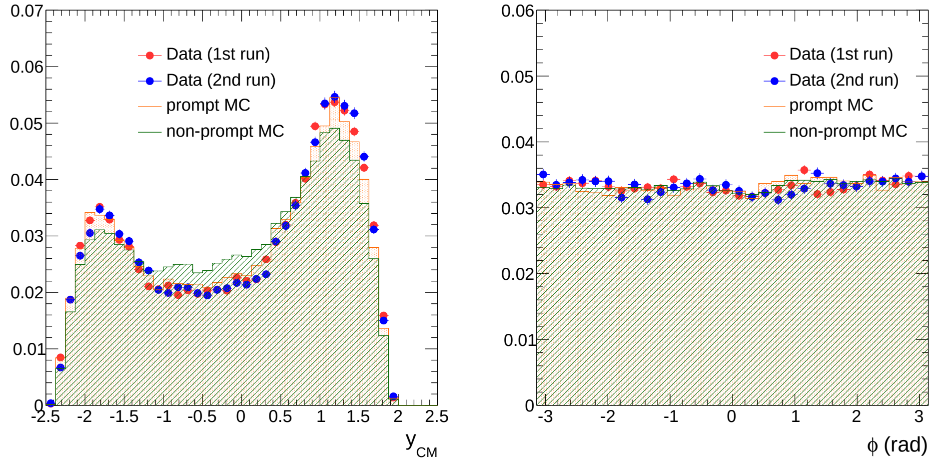

Figure 64: The rapidity(left) and azimuthal angle(right) distributions of J/ψ candidates in real data compared to the reconstructed distributions in Monte Carlo simulations.

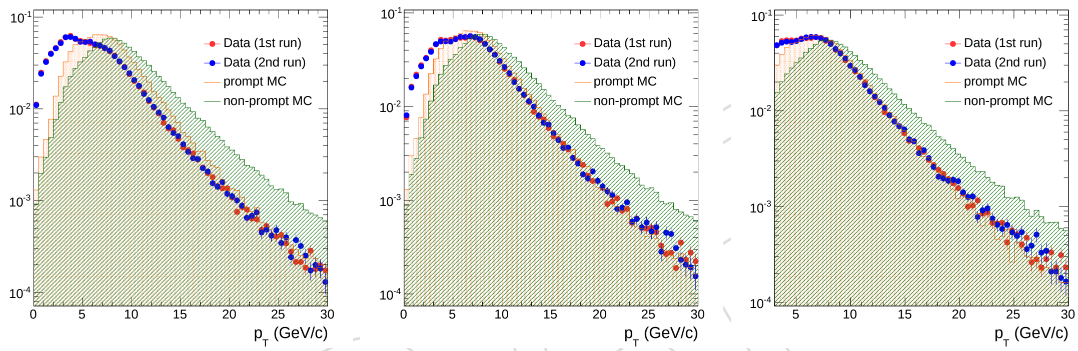

Figure 65: p_T distribution of J/ψ candidates in real data compared to the reconstructed distributions in Monte Carlo simulations. Distributions are for the mass range $2.6 < m_{\mu\mu} < 3.5\,\mathrm{GeV}/c^2$ (left), and signal region $2.95 < m_{\mu\mu} < 3.25\,\mathrm{GeV}/c^2$ (middle), and $2.95 < m_{\mu\mu} < 3.25\,\mathrm{GeV}/c^2$ with $p_T > 3$ GeV/c (right).

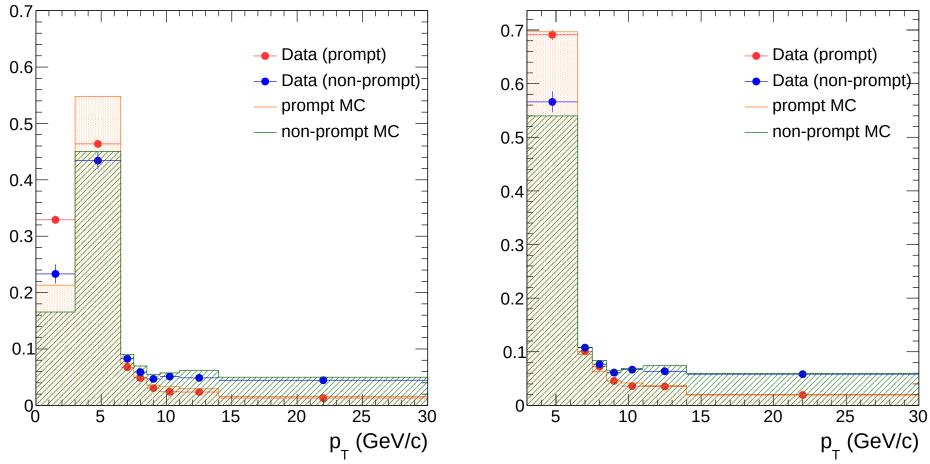

Figure 66: p_T distribution of raw yields of prompt and non-prompt J/ψ extracted from the fit compared to the reconstructed distributions in Monte Carlo simulations. Distributions in $p_T < 30$ GeV/c (left) and $3 < p_T < 30$ GeV/c (right).

checked to investigate the rapidity-dependent shape more clearly and displayed in Fig 69. These discrepancies will be considered as a systematic uncertainties of acceptance estimation.

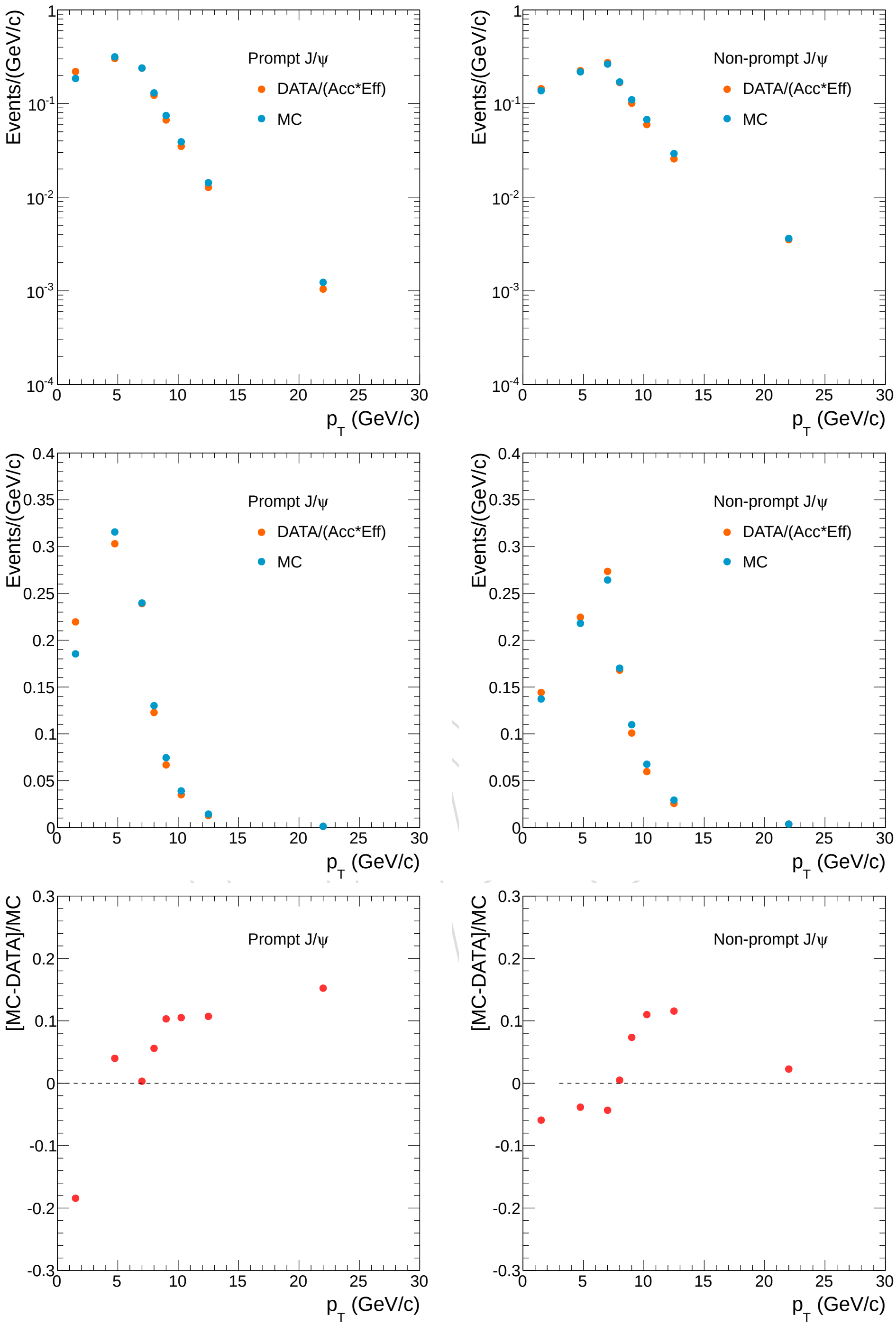

Figure 67: The transverse momentum distributions of prompt(left) and non-prompt(right) J/ψ from data with acceptance and efficiency corrected and the generated particles in Monte Carlo simulations within the kinematic range used in the analysis. Top panels are drawn with log-scale and middle panels are drawn with linear scale. Bottom panels represent their discrepancies.

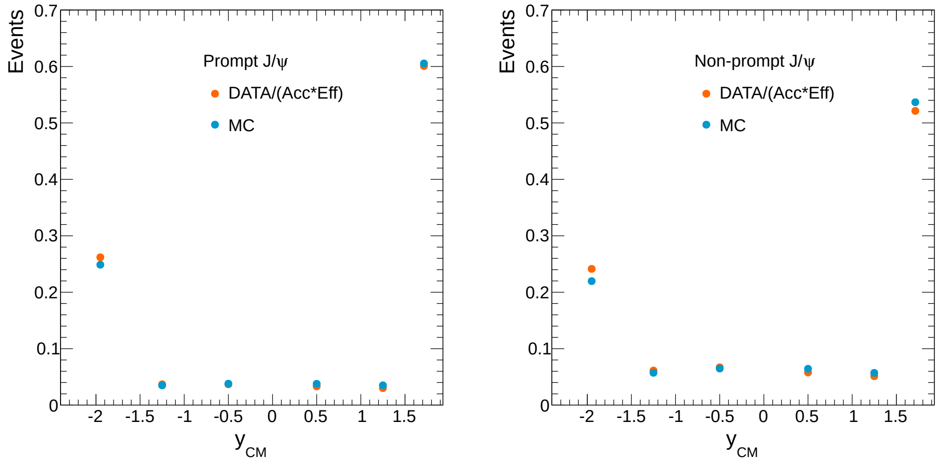

Figure 68: The center-of-mass rapidity distributions of prompt(left) and non-prompt(right) J/ψ from data with acceptance and efficiency corrected and the generated particles in Monte Carlo simulations within the kinematic range used in the analysis.

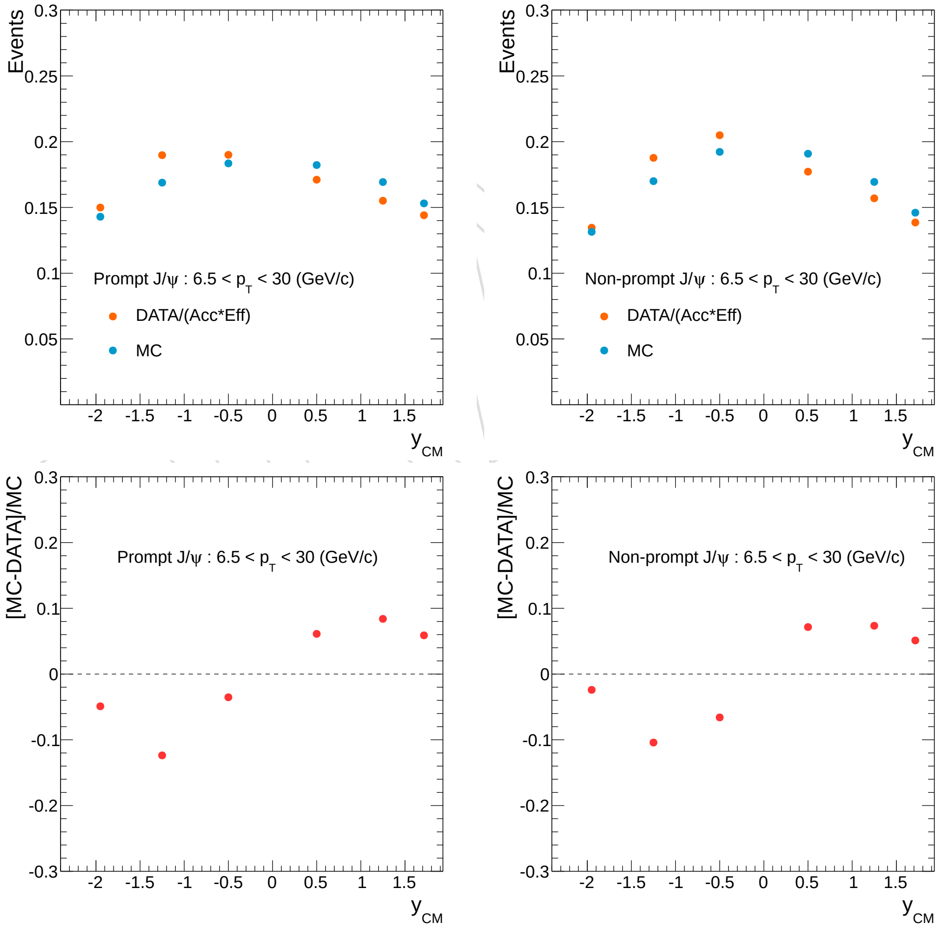

Figure 69: Top panels represent the center-of-mass rapidity distributions of prompt(left) and non-prompt(right) J/ψ from data with acceptance and efficiency corrected and the generated particles in Monte Carlo simulations within $-2.4 < y_{CM} < 1.93$ and $6.5 < p_{\mathrm{T}} < 30$ GeV/c. Bottom panels represent their discrepancies.

References

[1] ALICE Collaboration, "ALICE: Physics performance report, volume II", *J. Phys. G* **32** (2006) 1295, doi:10.1088/0954-3899/32/10/001.

[2] ALEPH Collaboration, "Measurement of the $\overline{B}^0$ and B^- meson lifetimes", *Phys. Lett. B* **307** (1993) 194, doi:10.1016/0370-2693(93)90211-Y.

[3] ALEPH Collaboration, "Errata: Measurement of the $\overline{B}^0$ and B^- meson lifetimes", *Phys. Lett. B* **325** (1994) 537, doi:10.1016/0370-2693(94)90054-X.

[4] CDF Collaboration, "Measurement of the J/ψ meson and b-hadron production cross sections in p$\overline{p}$ collisions at $\sqrt{s}$ = 1960 GeV", *Phys. Rev. D* **71** (2005) 032001, doi:10.1103/PhysRevD.71.032001, arXiv:hep-ex/0412071.

[5] CMS Collaboration Collaboration, "J/ψ and ψ(2S) production in pp collisions at $\sqrt{s}$ = 7 TeV", *JHEP* **02** (2012) arXiv:1111.1557.

[6] CMS Collaboration, "Suppression of non-prompt J/ψ, prompt J/ψ, and Υ(1S) in PbPb collisions at $\sqrt{s_{\mathrm{NN}}}$ = 2.76 TeV", *JHEP* **05** (2012) 063, doi:10.1007/JHEP05(2012)063, arXiv:1201.5069.

[7] T. Sjöstrand, S. Mrenna, and P. Skands, "PYTHIA 6.4 physics and manual", *JHEP* **05** (2006) 026, doi:10.1088/1126-6708/2006/05/026, arXiv:hep-ph/0603175.

[8] D. J. Lange, "The EvtGen particle decay simulation package", *Nucl. Instrum. Meth. A* **462** (2001) 152, doi:10.1016/S0168-9002(01)00089-4.

[9] N. Brambilla et al., "Heavy quarkonium: progress, puzzles, and opportunities", *Eur.Phys.J.* **C71** (2011) 1534, doi:10.1140/epjc/s10052-010-1534-9, arXiv:1010.5827.

[10] L. Z. V. K. P. F. C. L. Hermine K. Wohri, Ilse Kratschmer and G. Abbiendi, "Low pT Muon and Dimuon Efficiencies, TYPE =", technical report.

[11] Particle Data Group Collaboration, "Review of Particle Physics (RPP)", *Phys.Rev.* **D86** (2012) 010001, doi:10.1103/PhysRevD.86.010001.

[12] ALICE Collaboration Collaboration, "J/ψ production and nuclear effects in p-Pb collisions at $\sqrt{S_{NN}}$ = 5.02 TeV", *JHEP* **1402** (2014) 073, doi:10.1007/JHEP02(2014)073, arXiv:1308.6726.

[13] LHCb Collaboration, "Study of J/ψ production and cold nuclear matter effects in pPb collisions at $\sqrt{s_{NN}} = 5$ TeV", *JHEP* **1402** (2014) 072, doi:10.1007/JHEP02(2014)072, arXiv:1308.6729.

A Mass and liftime distibutions

Mass fits and litetime distributions for each rapidity, p_{T}, and $E_T^{HF|\eta|>4}$ bins used for the analysis are plotted here.

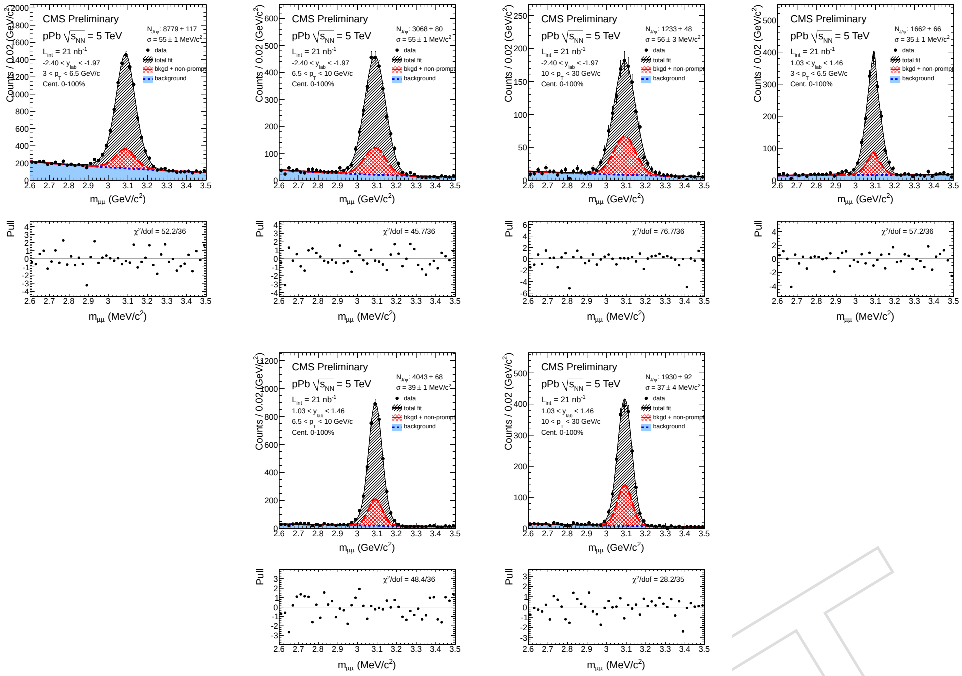

Figure 70: Mass fit for $-2.4 < y_{lab} < -1.97$ and $1.03 < y_{lab} < 1.46$, for the different transverse momentum $3.0 < p_{\mathrm{T}} < 6.5$, $6.5 < p_{\mathrm{T}} < 10$, and $10 < p_{\mathrm{T}} < 30\,\mathrm{GeV}/c$ bins for the 1st run.

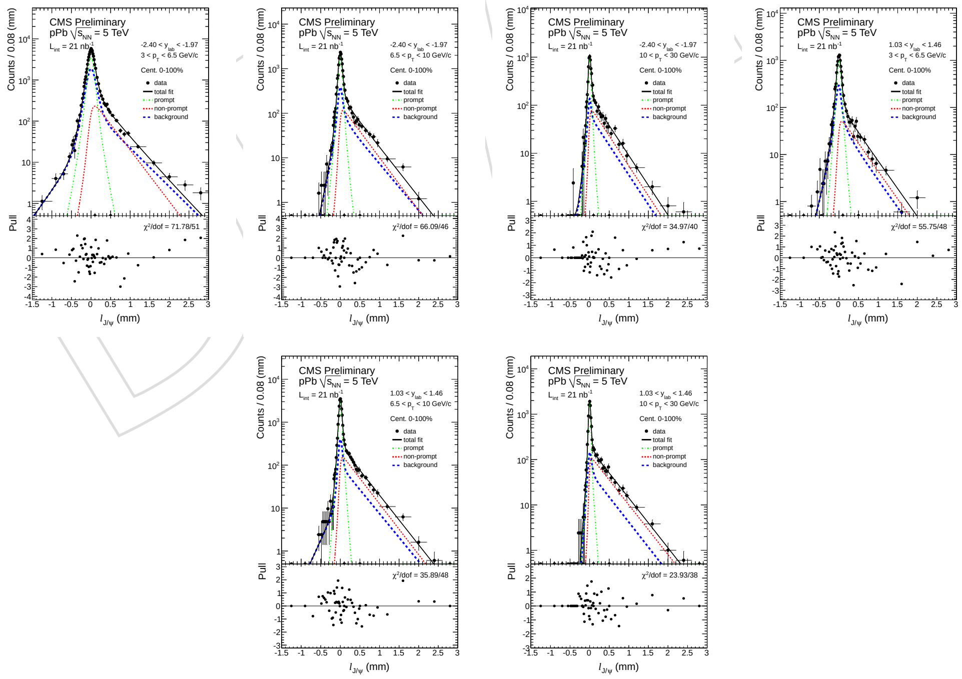

Figure 71: Lifetime fit for $-2.4 < y_{lab} < -1.97$ and $1.03 < y_{lab} < 1.46$, for the different transverse momentum $3.0 < p_{\mathrm{T}} < 6.5$, $6.5 < p_{\mathrm{T}} < 10$, and $10 < p_{\mathrm{T}} < 30\,\mathrm{GeV}/c$ bins for the 1st run.

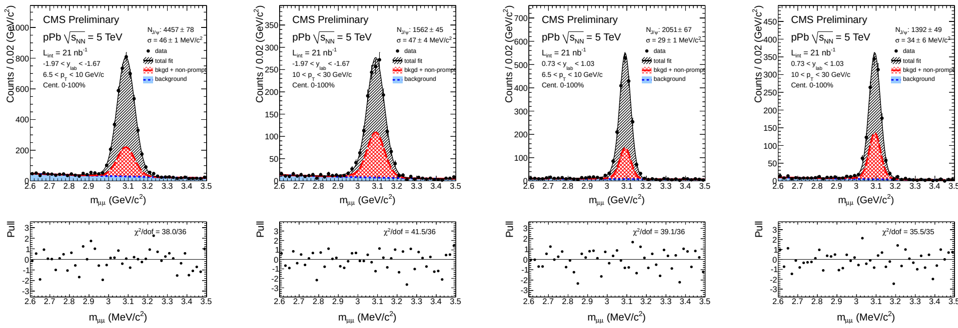

Figure 72: Mass fit for $-1.97 < y_{lab} < -1.67$ and $0.73 < y_{lab} < 1.03$, for the different transverse momentum $6.5 < p_T < 10$, and $10 < p_T < 30\,\text{GeV}/c$ bins for the 1st run.

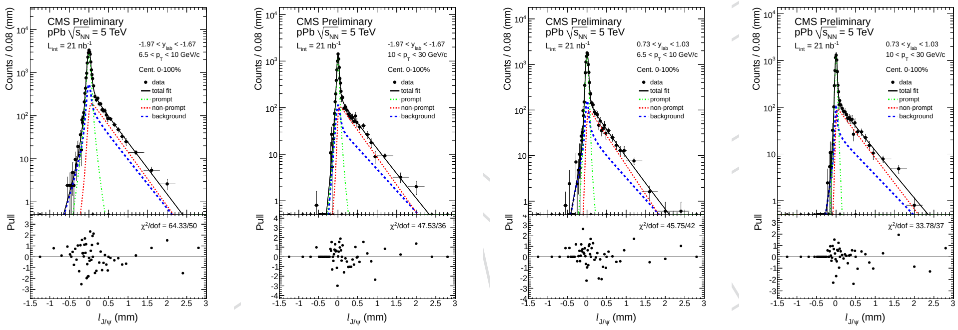

Figure 73: Lifetime fit for $-1.97 < y_{lab} < -1.67$ and $0.73 < y_{lab} < 1.03$, for the different transverse momentum $6.5 < p_T < 10$, and $10 < p_T < 30\,\text{GeV}/c$ bins for the 1st run.

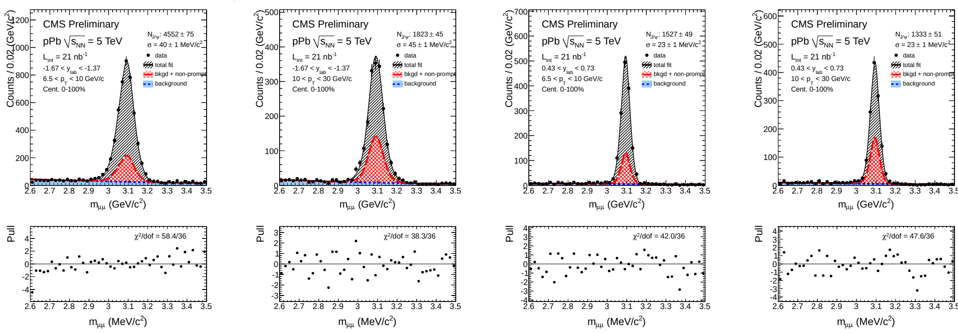

Figure 74: Mass fit for $-1.67 < y_{lab} < -1.37$ and $0.43 < y_{lab} < 0.73$, for the different transverse momentum $6.5 < p_T < 10$, and $10 < p_T < 30\,\text{GeV}/c$ bins for the 1st run.

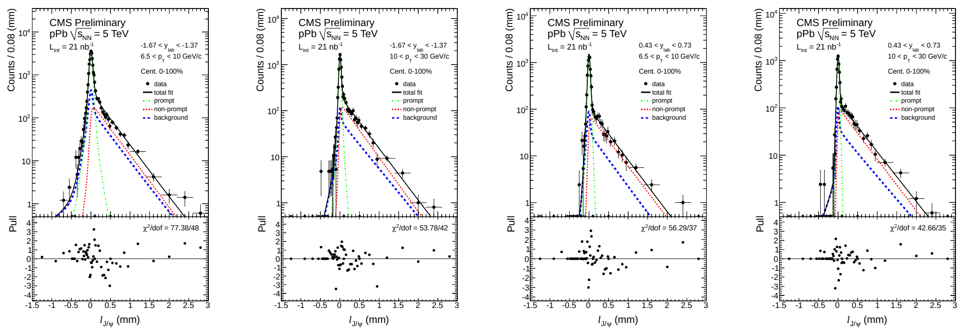

Figure 75: Lifetime fit for $-1.67 < y_{lab} < -1.37$ and $0.43 < y_{lab} < 0.73$, for the different transverse momentum $6.5 < p_{\mathrm{T}} < 10$, and $10 < p_{\mathrm{T}} < 30\,\mathrm{GeV}/c$ bins for the 1st run.

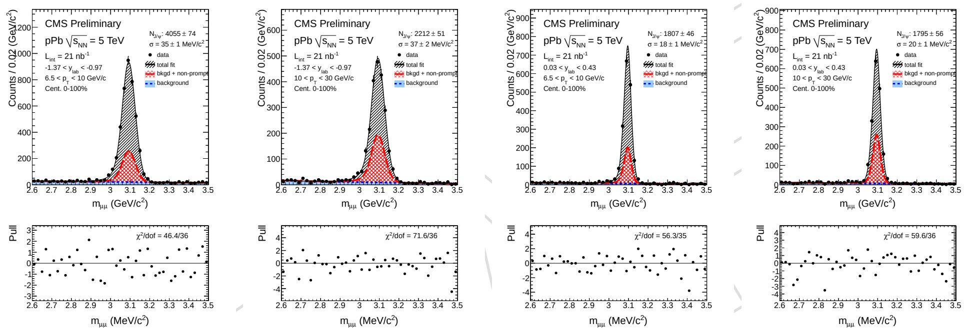

Figure 76: Mass fit for $-1.37 < y_{lab} < -0.97$ and $0.03 < y_{lab} < 0.43$, for the different transverse momentum $6.5 < p_{\mathrm{T}} < 10$, and $10 < p_{\mathrm{T}} < 30\,\mathrm{GeV}/c$ bins for the 1st run.

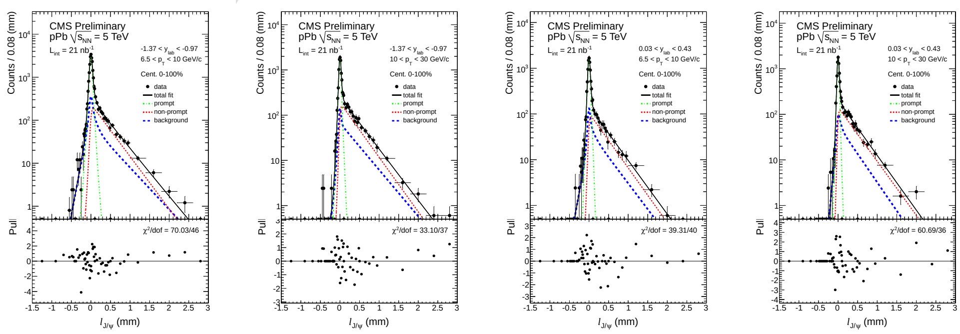

Figure 77: Lifetime fit for $-1.37 < y_{lab} < -0.97$ and $0.03 < y_{lab} < 0.43$, for the different transverse momentum $6.5 < p_{\mathrm{T}} < 10$, and $10 < p_{\mathrm{T}} < 30\,\mathrm{GeV}/c$ bins for the 1st run.

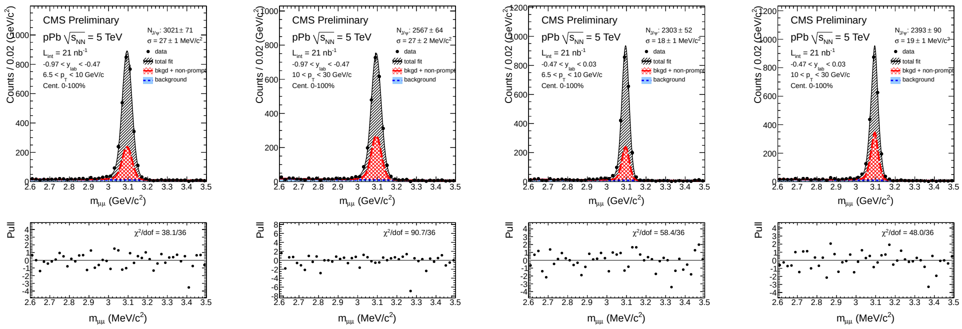

Figure 78: Mass fit for $-0.97 < y_{lab} < -0.47$ and $-0.47 < y_{lab} < 0.03$, for the different transverse momentum $6.5 < p_{\mathrm{T}} < 10$, and $10 < p_{\mathrm{T}} < 30\,\mathrm{GeV}/c$ bins for the 1st run.

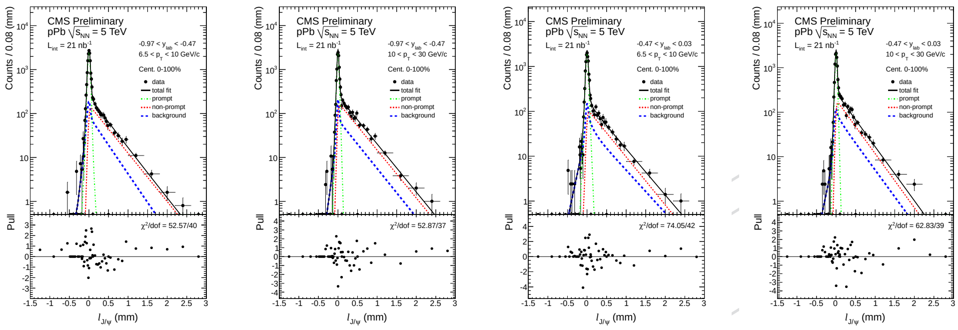

Figure 79: Lifetime fit for $-0.97 < y_{lab} < -0.47$ and $-0.47 < y_{lab} < 0.03$, for the different transverse momentum $6.5 < p_{\mathrm{T}} < 10$, and $10 < p_{\mathrm{T}} < 30\,\mathrm{GeV}/c$ bins for the 1st run.

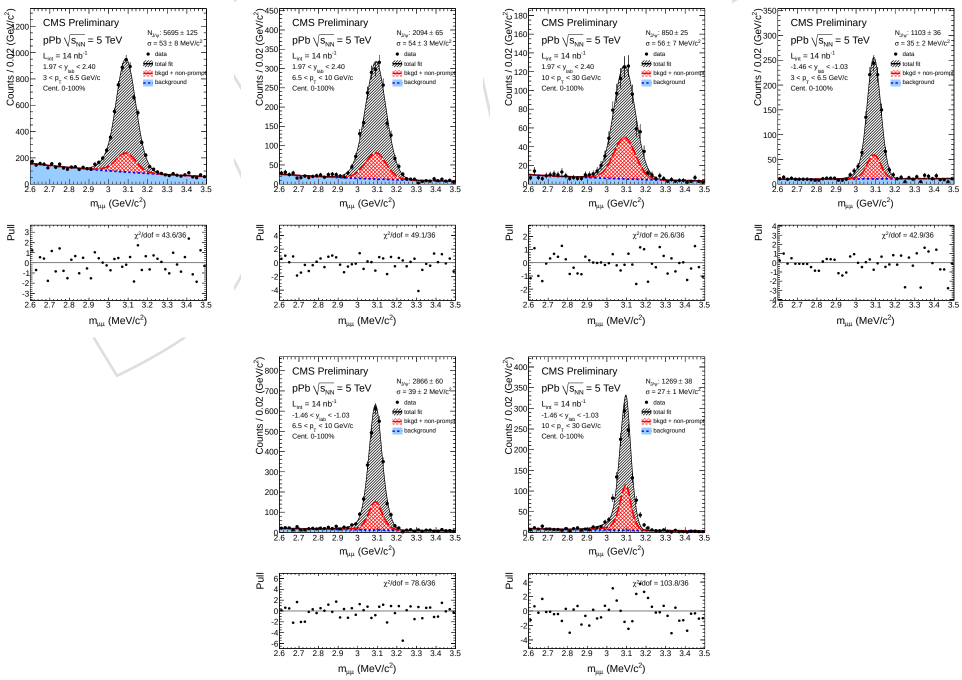

Figure 80: Mass fit for $1.97 < y_{lab} < 2.4$ and $-1.46 < y_{lab} < -1.03$, for the different transverse momentum $3.5 < p_{\mathrm{T}} < 6.5$, $6.5 < p_{\mathrm{T}} < 10$, and $10 < p_{\mathrm{T}} < 30\,\mathrm{GeV}/c$ bins for the 2nd run.

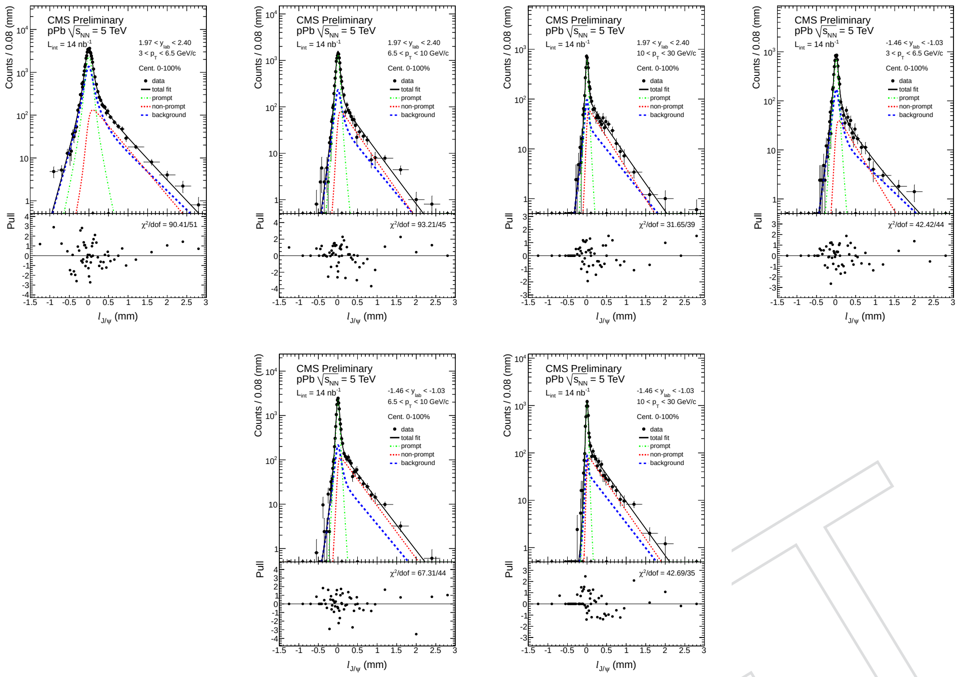

Figure 81: Lifetime fit for $1.97 < y_{lab} < 2.4$ and $-1.46 < y_{lab} < -1.03$, for the different transverse momentum $3.5 < p_{\mathrm{T}} < 6.5$, $6.5 < p_{\mathrm{T}} < 10$, and $10 < p_{\mathrm{T}} < 30\,\mathrm{GeV}/c$ bins for the 2nd run.

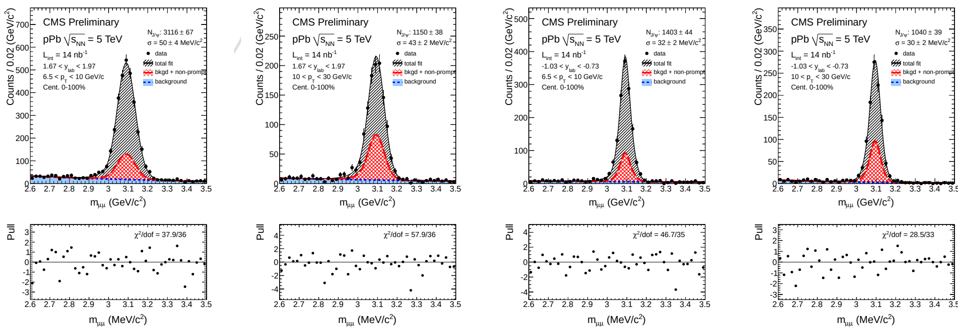

Figure 82: Mass fit for $1.67 < y_{lab} < 1.97$ and $-1.03 < y_{lab} < -0.73$, for the different transverse momentum $6.5 < p_{\mathrm{T}} < 10$, and $10 < p_{\mathrm{T}} < 30\,\mathrm{GeV}/c$ bins for the 2nd run.

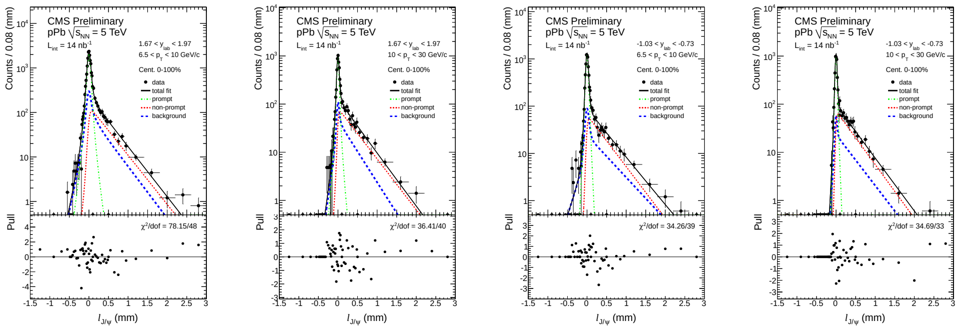

Figure 83: Lifetime fit for $1.67 < y_{lab} < 1.97$ and $-1.03 < y_{lab} < -0.73$, for the different transverse momentum $6.5 < p_{\rm T} < 10$, and $10 < p_{\rm T} < 30\,{\rm GeV}/c$ bins for the 2nd run.

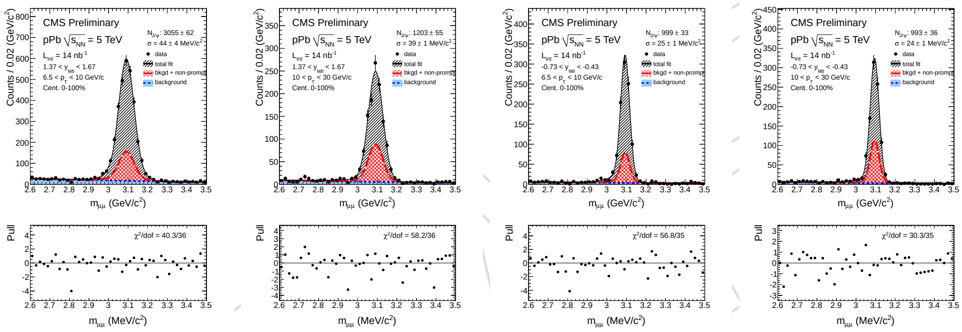

Figure 84: Mass fit for $1.37 < y_{lab} < 1.67$ and $-0.73 < y_{lab} < -0.43$, for the different transverse momentum $6.5 < p_{\rm T} < 10$, and $10 < p_{\rm T} < 30\,{\rm GeV}/c$ bins for the 2nd run.

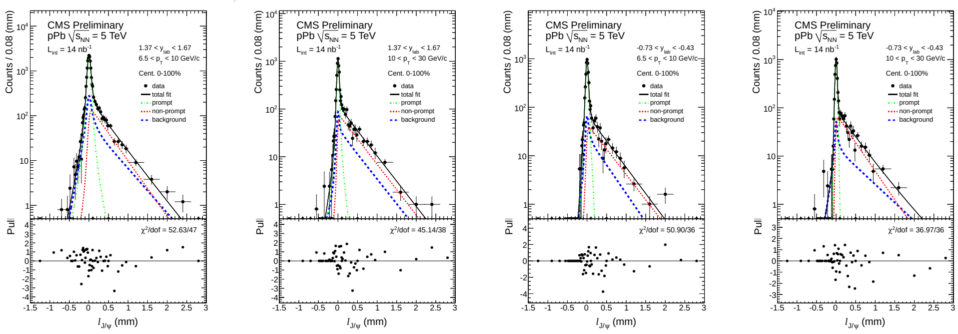

Figure 85: Lifetime fit for $1.37 < y_{lab} < 1.67$ and $-0.73 < y_{lab} < -0.43$, for the different transverse momentum $6.5 < p_{\rm T} < 10$, and $10 < p_{\rm T} < 30\,{\rm GeV}/c$ bins for the 2nd run.

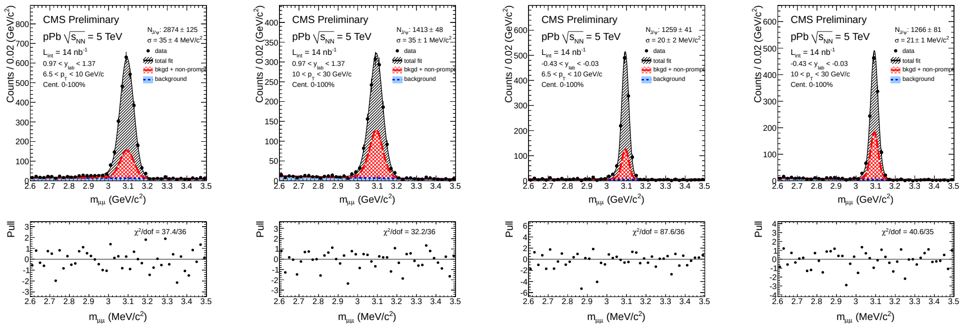

Figure 86: Mass fit for $0.97 < y_{lab} < 1.37$ and $-0.43 < y_{lab} < -0.03$, for the different transverse momentum $6.5 < p_T < 10$, and $10 < p_T < 30$ GeV/c bins for the 2nd run.

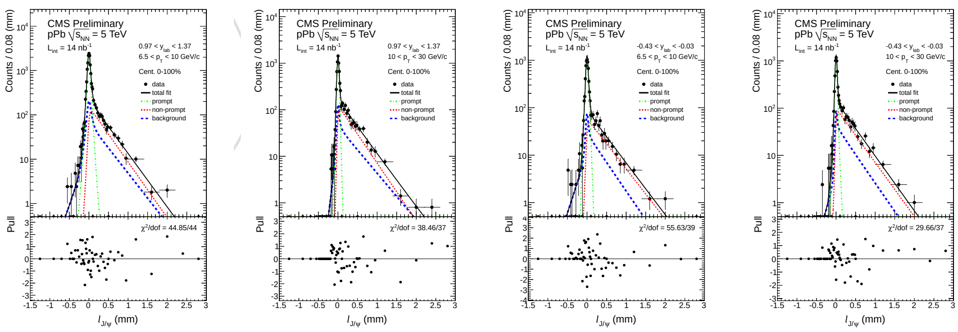

Figure 87: Lifetime fit for $0.97 < y_{lab} < 1.37$ and $-0.43 < y_{lab} < -0.03$, for the different transverse momentum $6.5 < p_T < 10$, and $10 < p_T < 30$ GeV/c bins for the 2nd run.

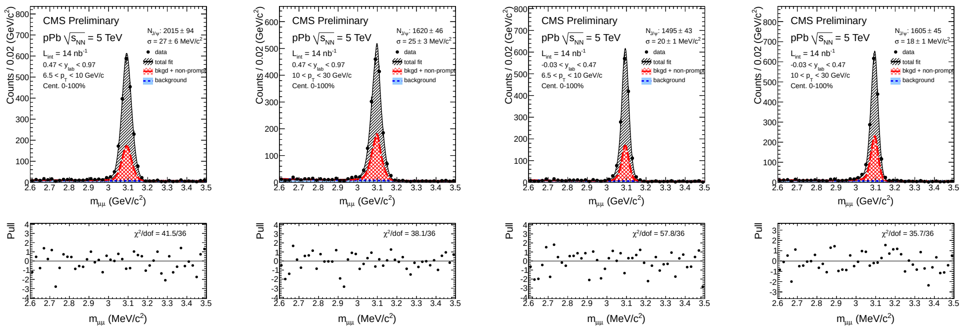

Figure 88: Mass fit for $0.47 < y_{lab} < 0.97$ and $-0.03 < y_{lab} < 0.47$, for the different transverse momentum $6.5 < p_T < 10$, and $10 < p_T < 30\,\mathrm{GeV}/c$ bins for the 2nd run.

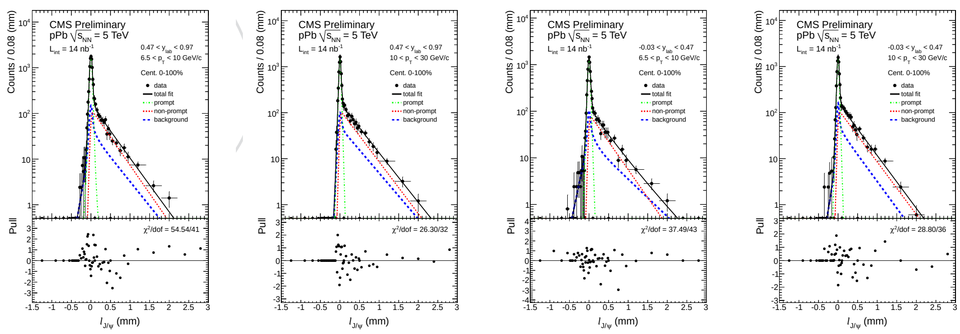

Figure 89: Lifetime fit for $0.47 < y_{lab} < 0.97$ and $-0.03 < y_{lab} < 0.47$, for the different transverse momentum $6.5 < p_T < 10$, and $10 < p_T < 30\,\mathrm{GeV}/c$ bins for the 2nd run.

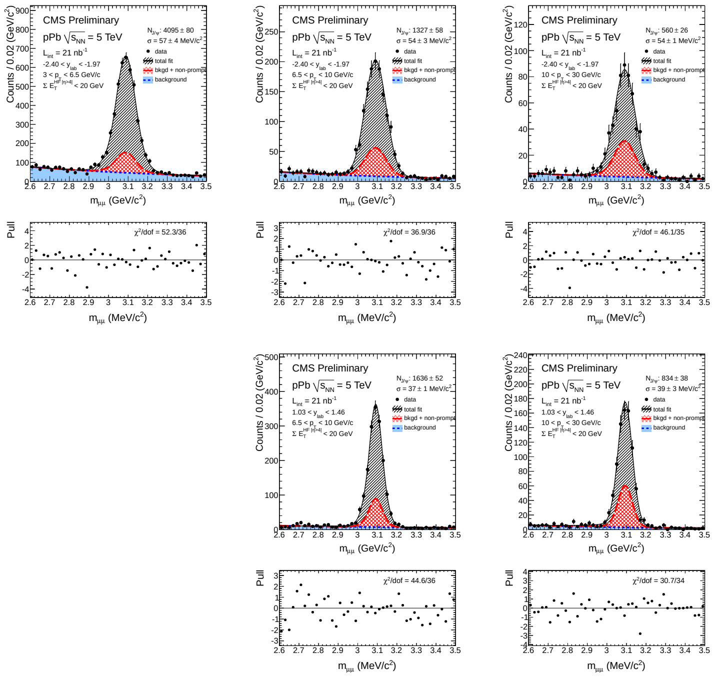

Figure 90: Mass fit for $-2.4 < y_{lab} < -1.97$ and $1.03 < y_{lab} < 1.46$, for the different transverse momentum $3.0 < p_{\mathrm{T}} < 6.5$, $6.5 < p_{\mathrm{T}} < 10$, and $10 < p_{\mathrm{T}} < 30\,\mathrm{GeV}/c$ bins for the 1st run. Transvers energy in HF is $0 < E_T^{HF|\eta|>4} < 20\,\mathrm{GeV}$.

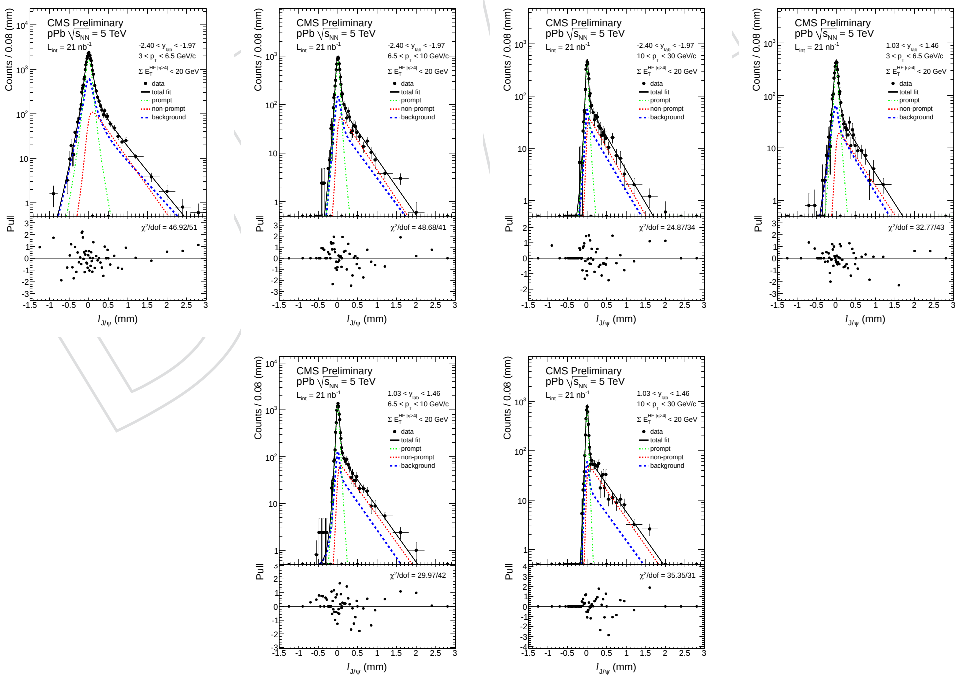

Figure 91: Lifetime fit for $-2.4 < y_{lab} < -1.97$ and $1.03 < y_{lab} < 1.46$, for the different transverse momentum $3.0 < p_{\mathrm{T}} < 6.5$, $6.5 < p_{\mathrm{T}} < 10$, and $10 < p_{\mathrm{T}} < 30\,\mathrm{GeV}/c$ bins for the 1st run. Transvers energy in HF is $0 < E_T^{HF|\eta|>4} < 20\,\mathrm{GeV}$.

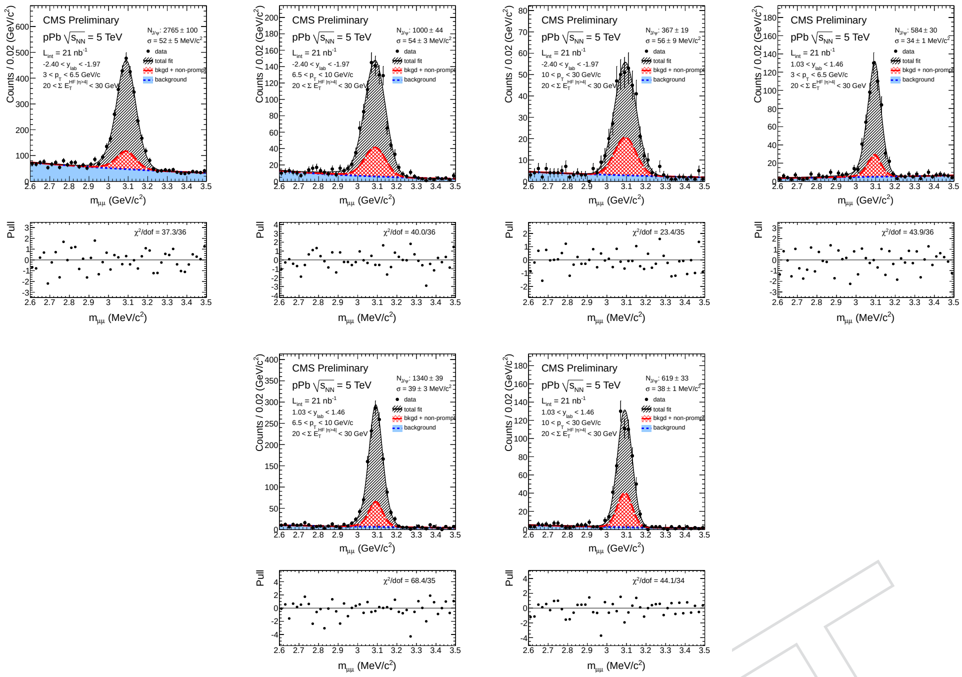

Figure 92: Mass fit for $-2.4 < y_{lab} < -1.97$ and $1.03 < y_{lab} < 1.46$, for the different transverse momentum $3.0 < p_{\mathrm{T}} < 6.5$, $6.5 < p_{\mathrm{T}} < 10$, and $10 < p_{\mathrm{T}} < 30\,\mathrm{GeV}/c$ bins for the 1st run. Transvers energy in HF is $20 < E_T^{HF|\eta|>4} < 30\,\mathrm{GeV}$.

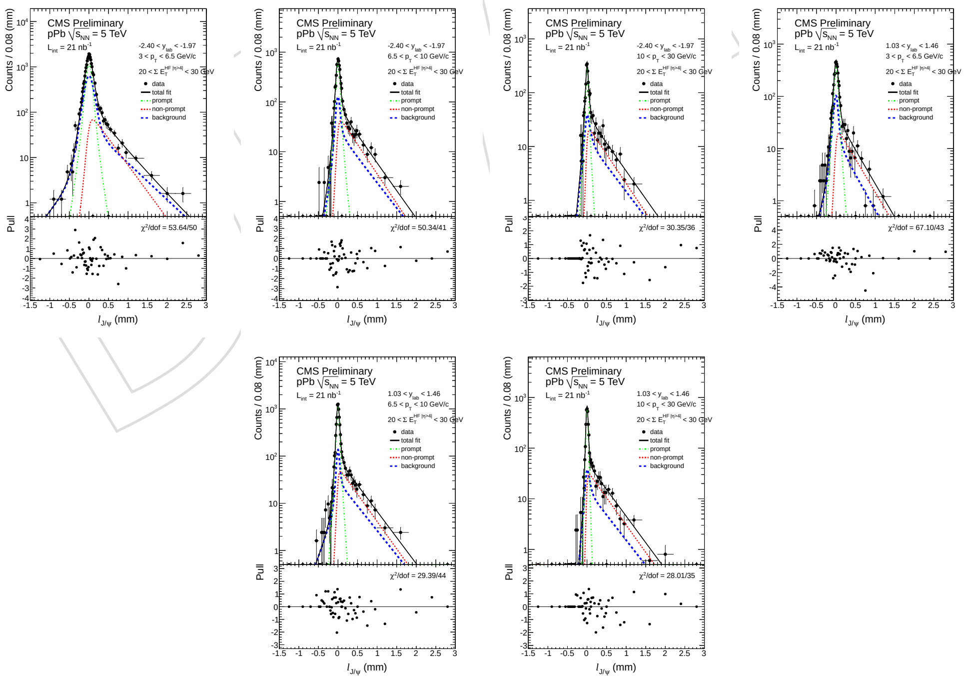

Figure 93: Lifetime fit for $-2.4 < y_{lab} < -1.97$ and $1.03 < y_{lab} < 1.46$, for the different transverse momentum $3.0 < p_{\mathrm{T}} < 6.5$, $6.5 < p_{\mathrm{T}} < 10$, and $10 < p_{\mathrm{T}} < 30\,\mathrm{GeV}/c$ bins for the 1st run. Transvers energy in HF is $20 < E_T^{HF|\eta|>4} < 30\,\mathrm{GeV}$.

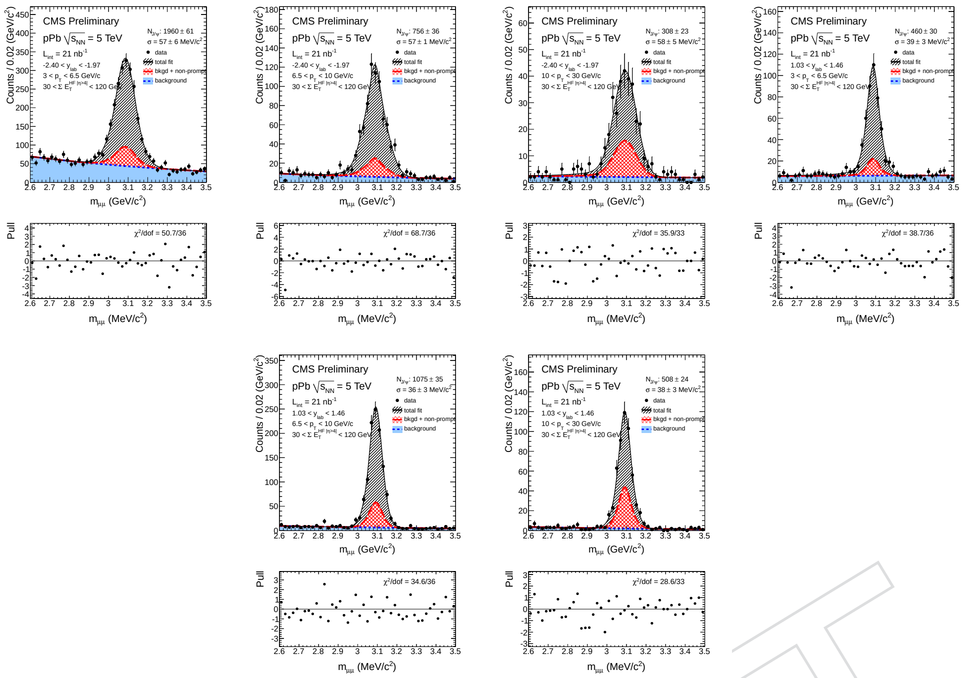

Figure 94: Mass fit for $-2.4 < y_{lab} < -1.97$ and $1.03 < y_{lab} < 1.46$, for the different transverse momentum $3.0 < p_{\mathrm{T}} < 6.5$, $6.5 < p_{\mathrm{T}} < 10$, and $10 < p_{\mathrm{T}} < 30\,\mathrm{GeV}/c$ bins for the 1st run. Transvers energy in HF is $30 < E_T^{HF|\eta|>4} < 120\,\mathrm{GeV}$.

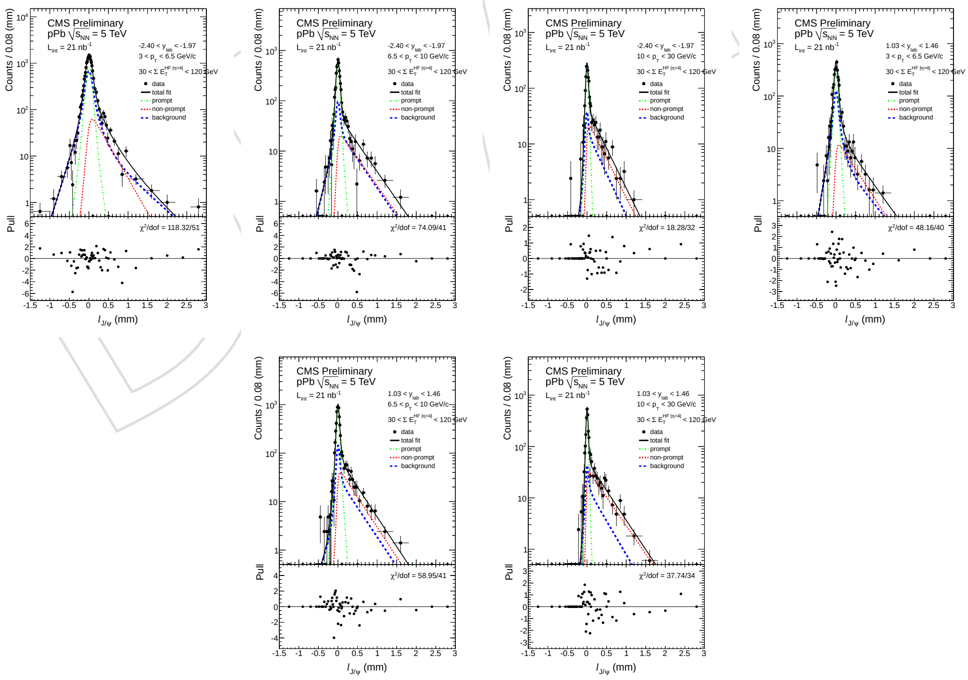

Figure 95: Lifetime fit for $-2.4 < y_{lab} < -1.97$ and $1.03 < y_{lab} < 1.46$, for the different transverse momentum $3.0 < p_{\mathrm{T}} < 6.5$, $6.5 < p_{\mathrm{T}} < 10$, and $10 < p_{\mathrm{T}} < 30\,\mathrm{GeV}/c$ bins for the 1st run. Transvers energy in HF is $30 < E_T^{HF|\eta|>4} < 120\,\mathrm{GeV}$.

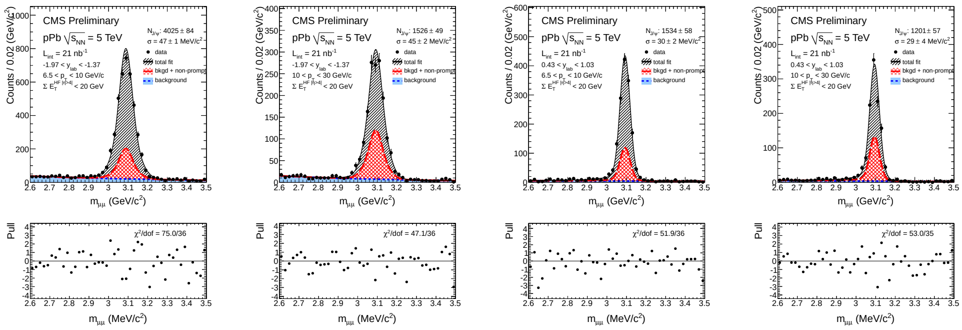

Figure 96: Mass fit for $-1.97 < y_{lab} < -1.37$ and $0.43 < y_{lab} < 1.03$, for the different transverse momentum $6.5 < p_{\mathrm{T}} < 10$, and $10 < p_{\mathrm{T}} < 30\,\mathrm{GeV}/c$ bins for the 1st run. Transvers energy in HF is $0 < E_T^{HF|\eta|>4} < 20\,\mathrm{GeV}$.

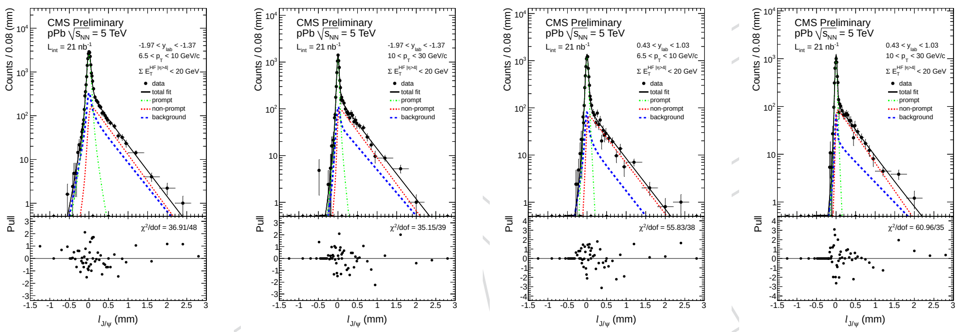

Figure 97: Lifetime fit for $-1.97 < y_{lab} < -1.37$ and $0.43 < y_{lab} < 1.03$, for the different transverse momentum $6.5 < p_{\mathrm{T}} < 10$, and $10 < p_{\mathrm{T}} < 30\,\mathrm{GeV}/c$ bins for the 1st run. Transvers energy in HF is $0 < E_T^{HF|\eta|>4} < 20\,\mathrm{GeV}$.

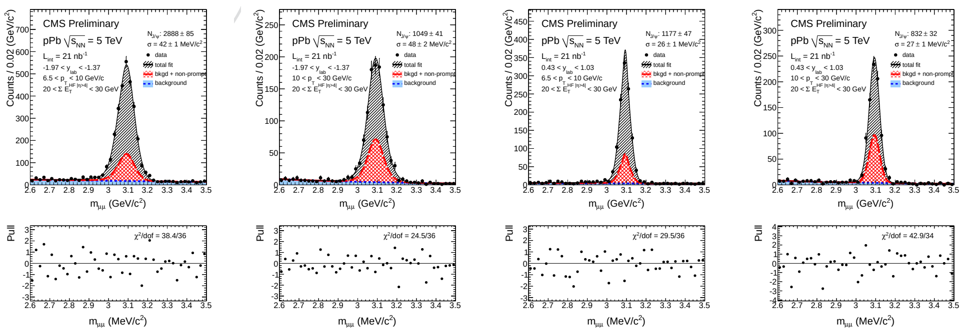

Figure 98: Mass fit for $-1.97 < y_{lab} < -1.37$ and $0.43 < y_{lab} < 1.03$, for the different transverse momentum $6.5 < p_{\mathrm{T}} < 10$, and $10 < p_{\mathrm{T}} < 30\,\mathrm{GeV}/c$ bins for the 1st run. Transvers energy in HF is $20 < E_T^{HF|\eta|>4} < 30\,\mathrm{GeV}$.

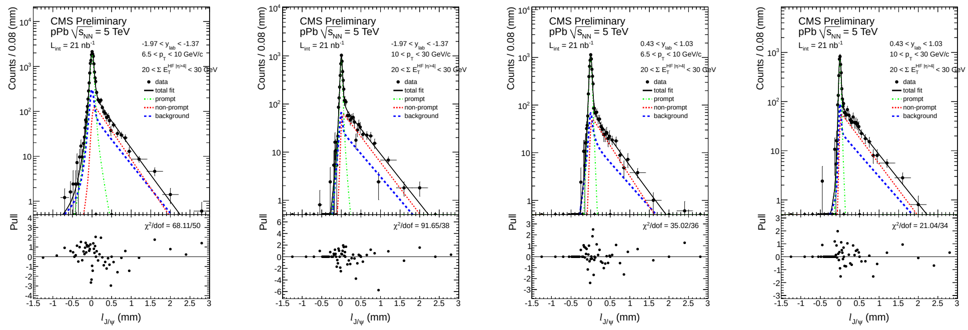

Figure 99: Lifetime fit for $-1.97 < y_{lab} < -1.37$ and $0.43 < y_{lab} < 1.03$, for the different transverse momentum $6.5 < p_{\mathrm{T}} < 10$, and $10 < p_{\mathrm{T}} < 30\,\mathrm{GeV}/c$ bins for the 1st run. Transvers energy in HF is $20 < E_T^{HF|\eta|>4} < 30\,\mathrm{GeV}$.

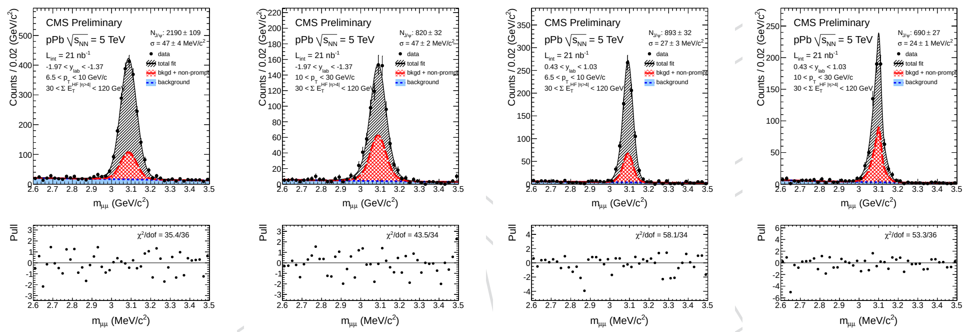

Figure 100: Mass fit for $-1.97 < y_{lab} < -1.37$ and $0.43 < y_{lab} < 1.03$, for the different transverse momentum $6.5 < p_{\mathrm{T}} < 10$, and $10 < p_{\mathrm{T}} < 30\,\mathrm{GeV}/c$ bins for the 1st run. Transvers energy in HF is $30 < E_T^{HF|\eta|>4} < 120\,\mathrm{GeV}$.

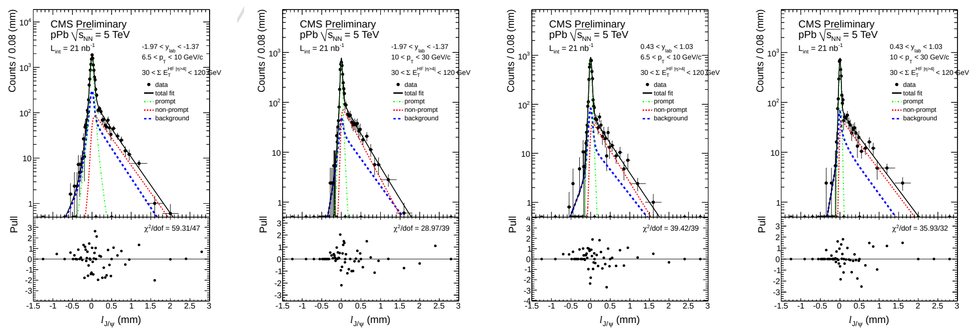

Figure 101: Lifetime fit for $-1.97 < y_{lab} < -1.37$ and $0.43 < y_{lab} < 1.03$, for the different transverse momentum $6.5 < p_{\mathrm{T}} < 10$, and $10 < p_{\mathrm{T}} < 30\,\mathrm{GeV}/c$ bins for the 1st run. Transvers energy in HF is $30 < E_T^{HF|\eta|>4} < 120\,\mathrm{GeV}$.

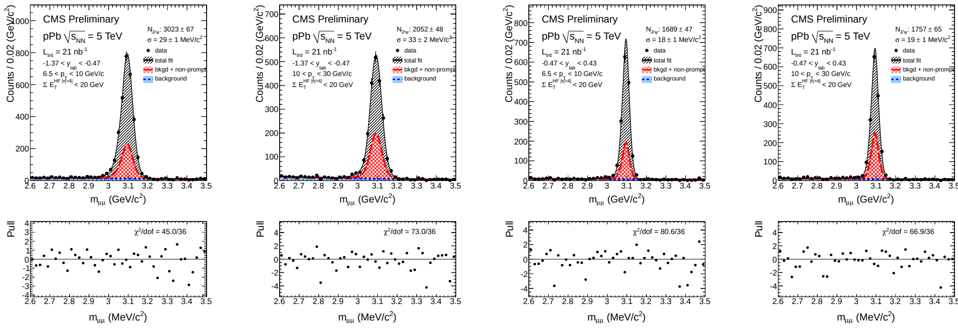

Figure 102: Mass fit for $-1.37 < y_{lab} < -0.47$ and $-0.47 < y_{lab} < 0.43$, for the different transverse momentum $6.5 < p_{\mathrm{T}} < 10$, and $10 < p_{\mathrm{T}} < 30\,\mathrm{GeV}/c$ bins for the 1st run. Transvers energy in HF is $0 < E_T^{HF|\eta|>4} < 20\,\mathrm{GeV}$.

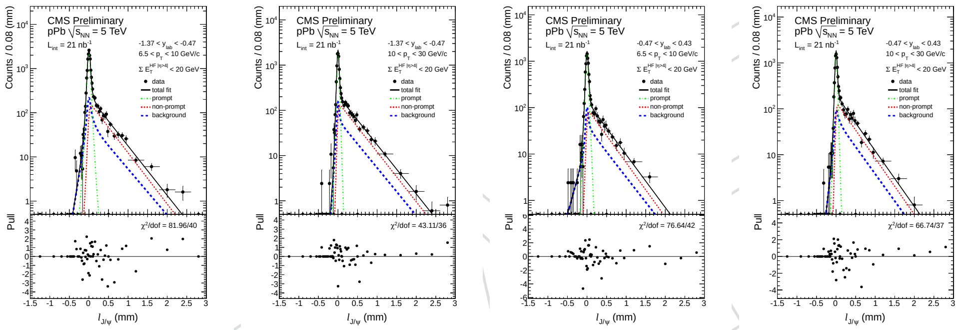

Figure 103: Lifetime fit for $-1.37 < y_{lab} < -0.47$ and $-0.47 < y_{lab} < 0.43$, for the different transverse momentum $6.5 < p_{\mathrm{T}} < 10$, and $10 < p_{\mathrm{T}} < 30\,\mathrm{GeV}/c$ bins for the 1st run. Transvers energy in HF is $0 < E_T^{HF|\eta|>4} < 20\,\mathrm{GeV}$.

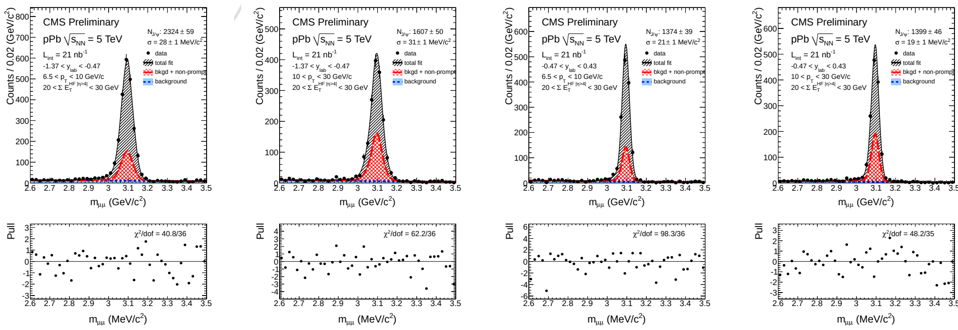

Figure 104: Mass fit for $-1.37 < y_{lab} < -0.47$ and $-0.47 < y_{lab} < 0.43$, for the different transverse momentum $6.5 < p_{\mathrm{T}} < 10$, and $10 < p_{\mathrm{T}} < 30\,\mathrm{GeV}/c$ bins for the 1st run. Transvers energy in HF is $20 < E_T^{HF|\eta|>4} < 30\,\mathrm{GeV}$.

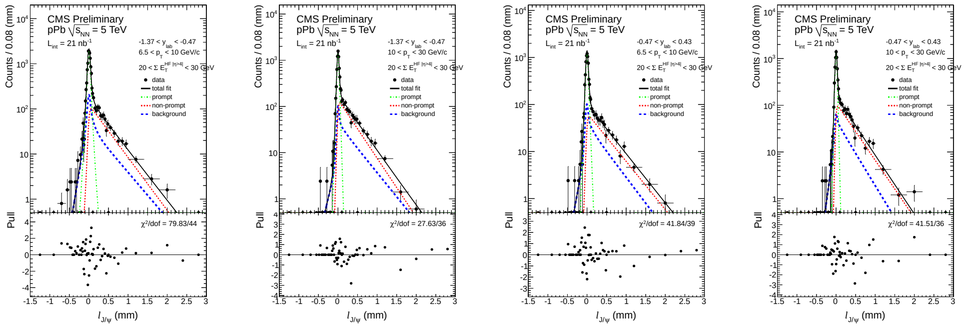

Figure 105: Lifetime fit for $-1.37 < y_{lab} < -0.47$ and $-0.47 < y_{lab} < 0.43$, for the different transverse momentum $6.5 < p_{\mathrm{T}} < 10$, and $10 < p_{\mathrm{T}} < 30\,\mathrm{GeV}/c$ bins for the 1st run. Transvers energy in HF is $20 < E_T^{HF|\eta|>4} < 30\,\mathrm{GeV}$.

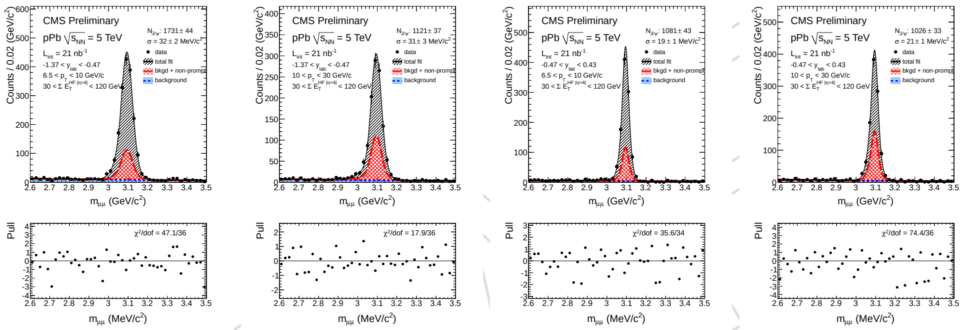

Figure 106: Mass fit for $-1.37 < y_{lab} < -0.47$ and $-0.47 < y_{lab} < 0.43$, for the different transverse momentum $6.5 < p_{\mathrm{T}} < 10$, and $10 < p_{\mathrm{T}} < 30\,\mathrm{GeV}/c$ bins for the 1st run. Transvers energy in HF is $30 < E_T^{HF|\eta|>4} < 120\,\mathrm{GeV}$.

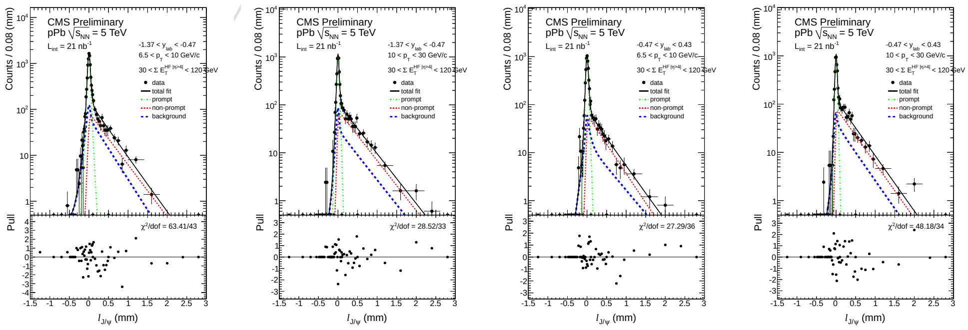

Figure 107: Lifetime fit for $-1.37 < y_{lab} < -0.47$ and $-0.47 < y_{lab} < 0.43$, for the different transverse momentum $6.5 < p_{\mathrm{T}} < 10$, and $10 < p_{\mathrm{T}} < 30\,\mathrm{GeV}/c$ bins for the 1st run. Transvers energy in HF is $30 < E_T^{HF|\eta|>4} < 120\,\mathrm{GeV}$.

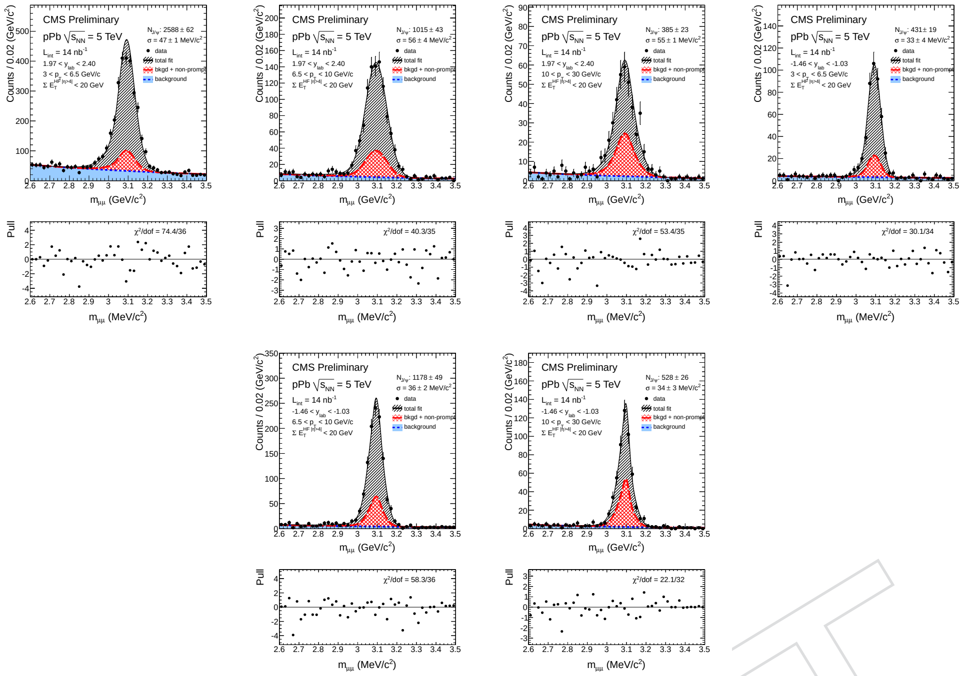

Figure 108: Mass fit for $1.97 < y_{lab} < 2.4$ and $-1.46 < y_{lab} < -1.03$, for the different transverse momentum $3.0 < p_T < 6.5$, $6.5 < p_T < 10$, and $10 < p_T < 30\,\text{GeV}/c$ bins for the 2nd run. Transvers energy in HF is $0 < E_T^{HF|\eta|>4} < 20\,\text{GeV}$.

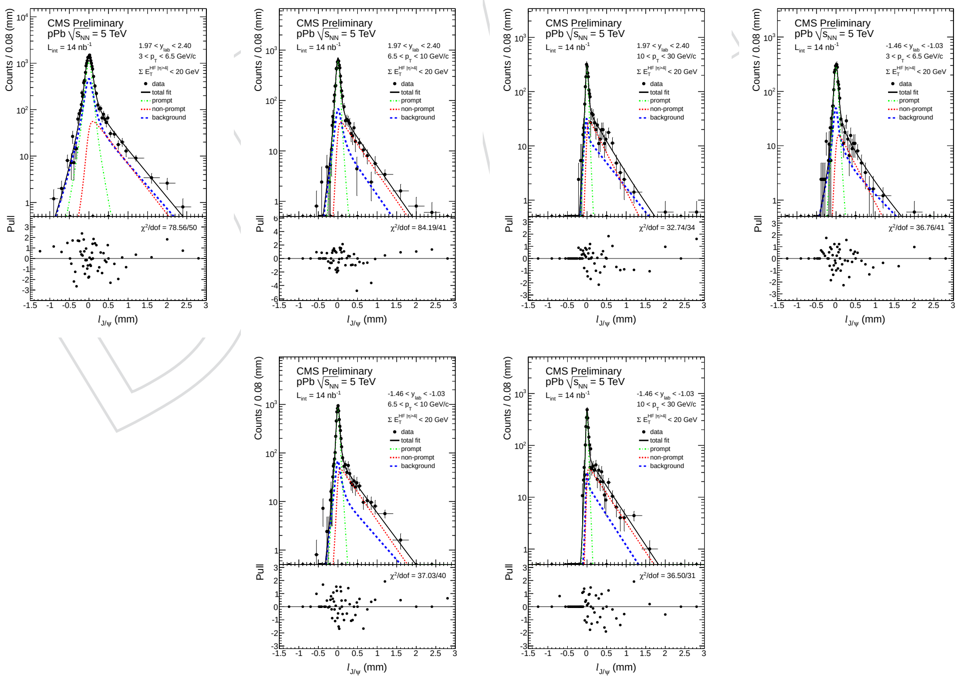

Figure 109: Lifetime fit for $1.97 < y_{lab} < 2.4$ and $-1.46 < y_{lab} < -1.03$, for the different transverse momentum $3.0 < p_T < 6.5$, $6.5 < p_T < 10$, and $10 < p_T < 30\,\text{GeV}/c$ bins for the 2nd run. Transvers energy in HF is $0 < E_T^{HF|\eta|>4} < 20\,\text{GeV}$.

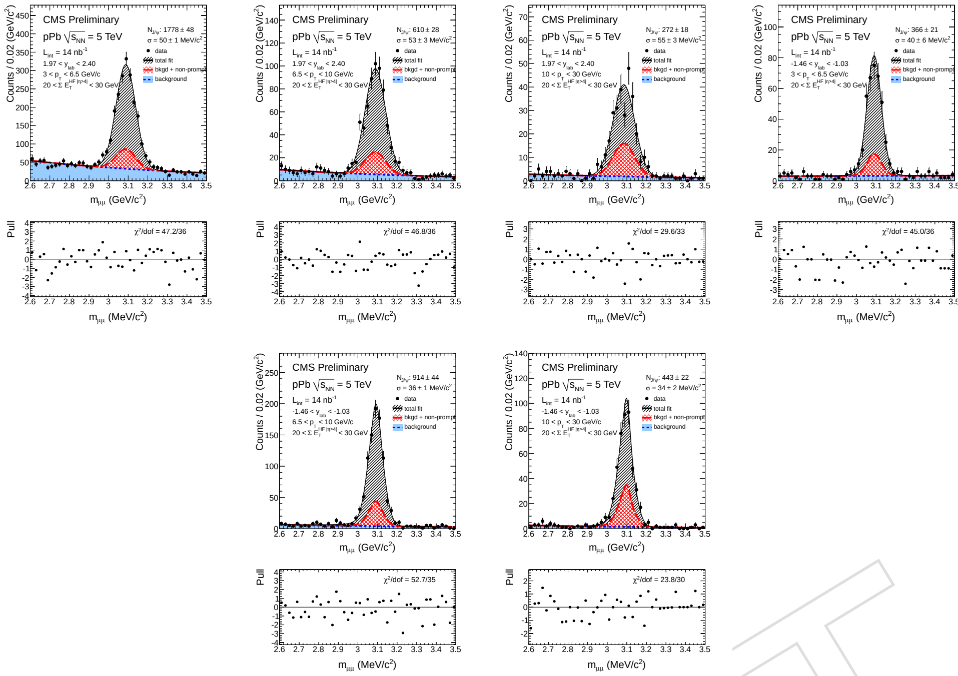

Figure 110: Mass fit for $1.97 < y_{lab} < 2.4$ and $-1.46 < y_{lab} < -1.03$, for the different transverse momentum $3.0 < p_T < 6.5$, $6.5 < p_T < 10$, and $10 < p_T < 30\,\mathrm{GeV}/c$ bins for the 2nd run. Transvers energy in HF is $20 < E_T^{HF|\eta|>4} < 30\,\mathrm{GeV}$.

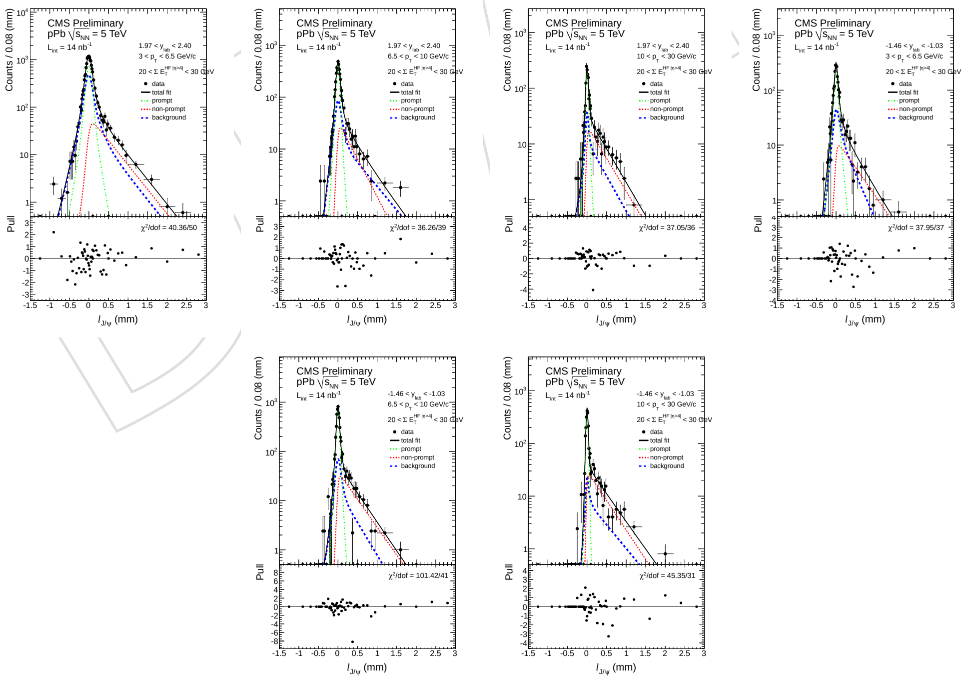

Figure 111: Lifetime fit for $1.97 < y_{lab} < 2.4$ and $-1.46 < y_{lab} < -1.03$, for the different transverse momentum $3.0 < p_T < 6.5$, $6.5 < p_T < 10$, and $10 < p_T < 30\,\mathrm{GeV}/c$ bins for the 2nd run. Transvers energy in HF is $20 < E_T^{HF|\eta|>4} < 30\,\mathrm{GeV}$.

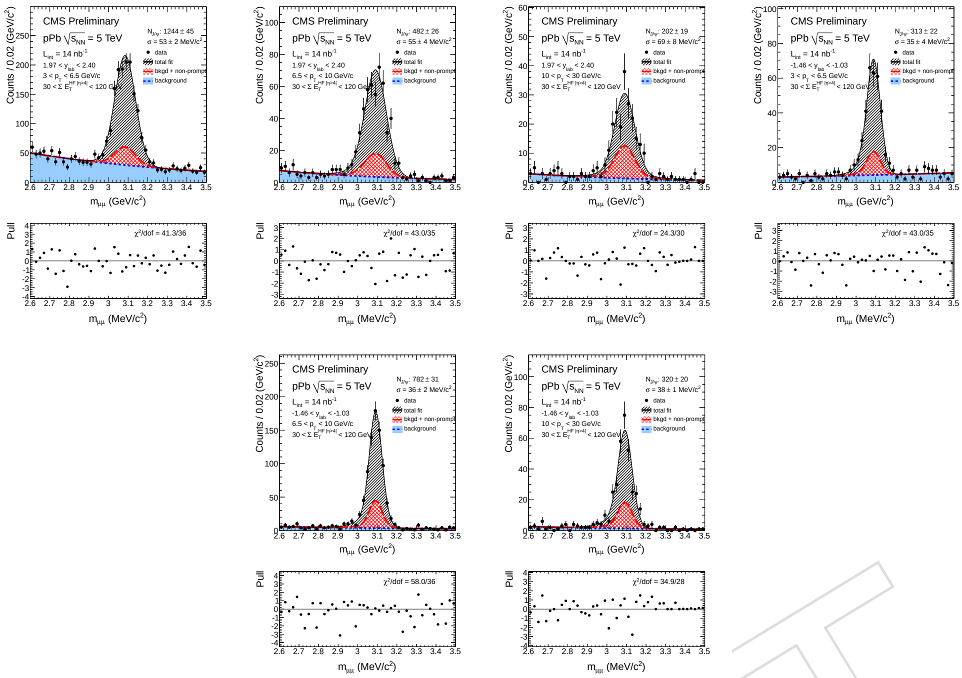

Figure 112: Mass fit for $1.97 < y_{lab} < 2.4$ and $-1.46 < y_{lab} < -1.03$, for the different transverse momentum $3.0 < p_T < 6.5$, $6.5 < p_T < 10$, and $10 < p_T < 30\,\text{GeV}/c$ bins for the 2nd run. Transvers energy in HF is $30 < E_T^{HF|\eta|>4} < 120\,\text{GeV}$.

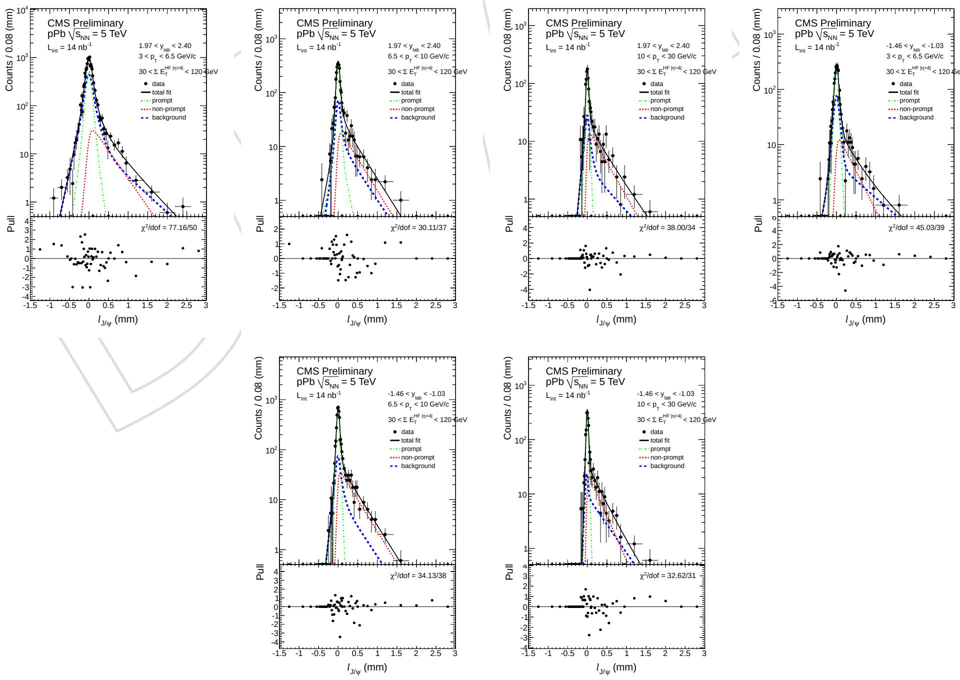

Figure 113: Lifetime fit for $1.97 < y_{lab} < 2.4$ and $-1.46 < y_{lab} < -1.03$, for the different transverse momentum $3.0 < p_T < 6.5$, $6.5 < p_T < 10$, and $10 < p_T < 30\,\text{GeV}/c$ bins for the 2nd run. Transvers energy in HF is $30 < E_T^{HF|\eta|>4} < 120\,\text{GeV}$.

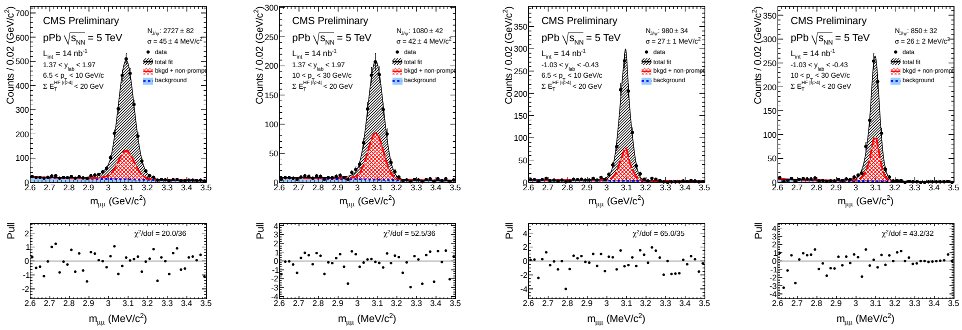

Figure 114: Mass fit for $1.37 < y_{lab} < 1.97$ and $-1.03 < y_{lab} < -0.43$, for the different transverse momentum $6.5 < p_{\mathrm{T}} < 10$, and $10 < p_{\mathrm{T}} < 30\,\mathrm{GeV}/c$ bins for the 2nd run. Transvers energy in HF is $0 < E_T^{HF|\eta|>4} < 20\,\mathrm{GeV}$.

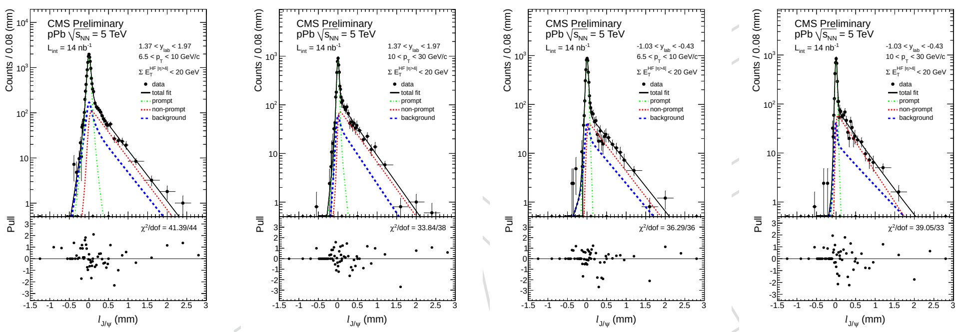

Figure 115: Lifetime fit for $1.37 < y_{lab} < 1.97$ and $-1.03 < y_{lab} < -0.43$, for the different transverse momentum $6.5 < p_{\mathrm{T}} < 10$, and $10 < p_{\mathrm{T}} < 30\,\mathrm{GeV}/c$ bins for the 2nd run. Transvers energy in HF is $0 < E_T^{HF|\eta|>4} < 20\,\mathrm{GeV}$.

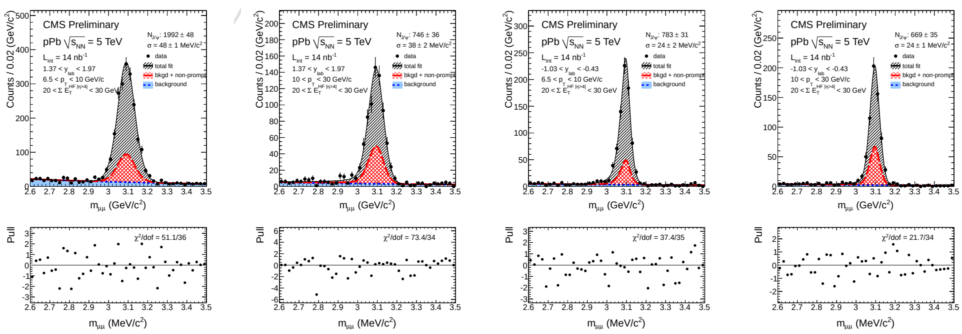

Figure 116: Mass fit for $1.37 < y_{lab} < 1.97$ and $-1.03 < y_{lab} < -0.43$, for the different transverse momentum $6.5 < p_{\mathrm{T}} < 10$, and $10 < p_{\mathrm{T}} < 30\,\mathrm{GeV}/c$ bins for the 2nd run. Transvers energy in HF is $20 < E_T^{HF|\eta|>4} < 30\,\mathrm{GeV}$.

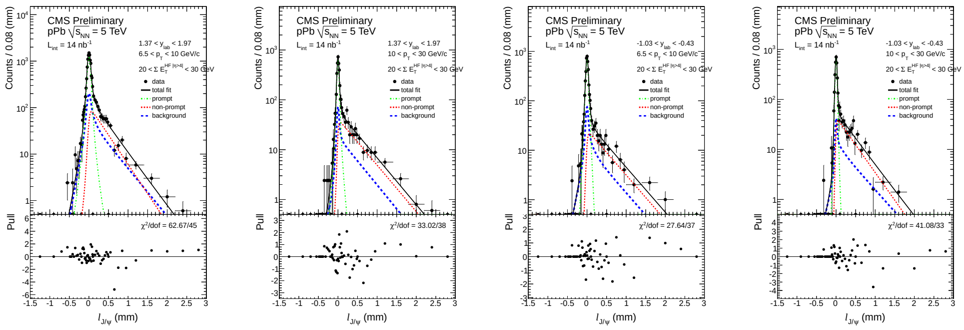

Figure 117: Lifetime fit for $1.37 < y_{lab} < 1.97$ and $-1.03 < y_{lab} < -0.43$, for the different transverse momentum $6.5 < p_{\mathrm{T}} < 10$, and $10 < p_{\mathrm{T}} < 30\,\mathrm{GeV}/c$ bins for the 2nd run. Transvers energy in HF is $20 < E_T^{HF|\eta|>4} < 30\,\mathrm{GeV}$.

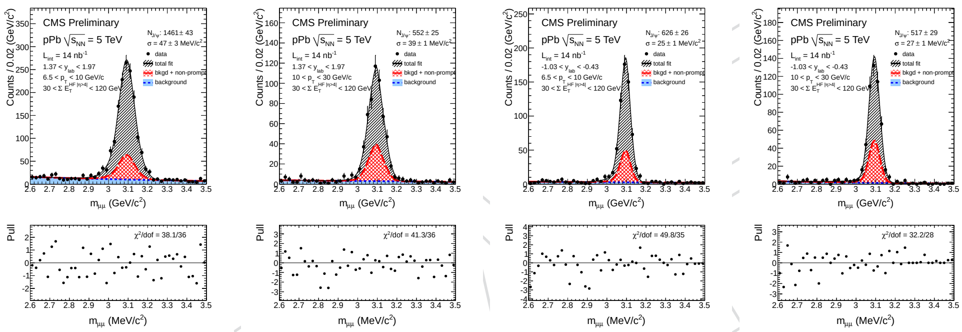

Figure 118: Mass fit for $1.37 < y_{lab} < 1.97$ and $-1.03 < y_{lab} < -0.43$, for the different transverse momentum $6.5 < p_{\mathrm{T}} < 10$, and $10 < p_{\mathrm{T}} < 30\,\mathrm{GeV}/c$ bins for the 2nd run. Transvers energy in HF is $30 < E_T^{HF|\eta|>4} < 120\,\mathrm{GeV}$.

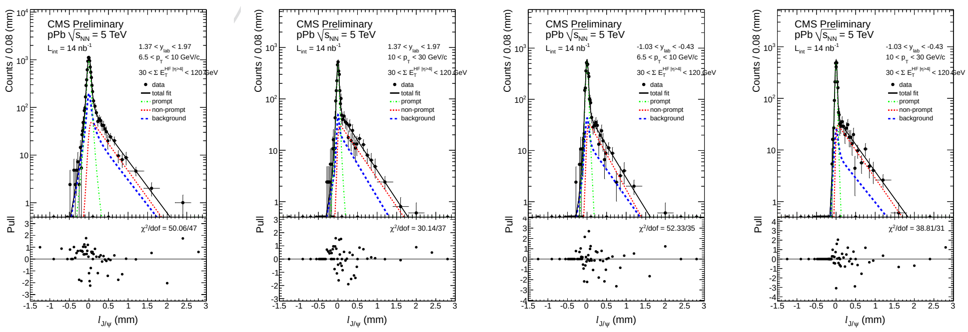

Figure 119: Lifetime fit for $1.37 < y_{lab} < 1.97$ and $-1.03 < y_{lab} < -0.43$, for the different transverse momentum $6.5 < p_{\mathrm{T}} < 10$, and $10 < p_{\mathrm{T}} < 30\,\mathrm{GeV}/c$ bins for the 2nd run. Transvers energy in HF is $30 < E_T^{HF|\eta|>4} < 120\,\mathrm{GeV}$.

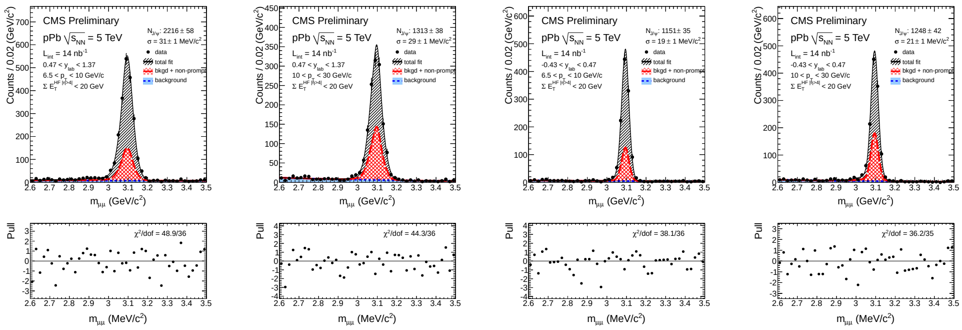

Figure 120: Mass fit for $0.47 < y_{lab} < 1.37$ and $-0.43 < y_{lab} < 0.47$, for the different transverse momentum $6.5 < p_T < 10$, and $10 < p_T < 30\,\mathrm{GeV}/c$ bins for the 2nd run. Transvers energy in HF is $0 < E_T^{HF|\eta|>4} < 20\,\mathrm{GeV}$.

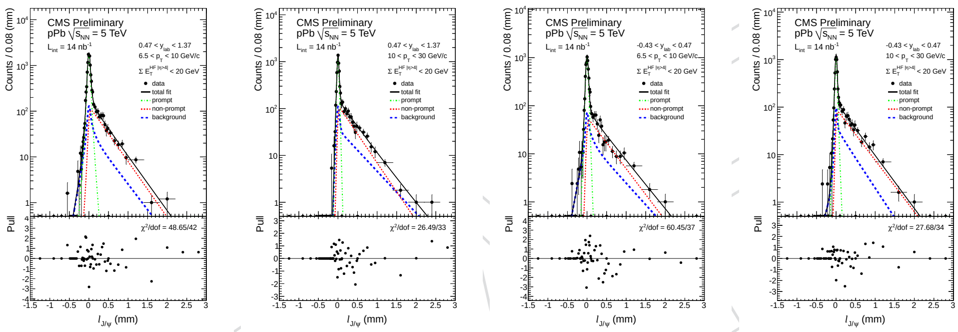

Figure 121: Lifetime fit for $0.47 < y_{lab} < 1.37$ and $-0.43 < y_{lab} < 0.47$, for the different transverse momentum $6.5 < p_T < 10$, and $10 < p_T < 30\,\mathrm{GeV}/c$ bins for the 2nd run. Transvers energy in HF is $0 < E_T^{HF|\eta|>4} < 20\,\mathrm{GeV}$.

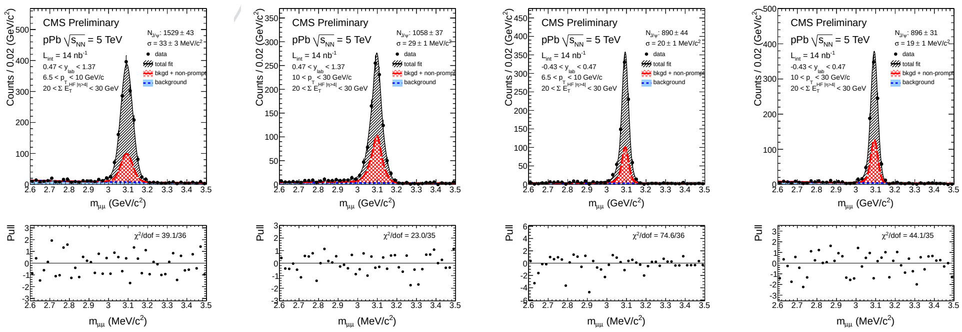

Figure 122: Mass fit for $0.47 < y_{lab} < 1.37$ and $-0.43 < y_{lab} < 0.47$, for the different transverse momentum $6.5 < p_T < 10$, and $10 < p_T < 30\,\mathrm{GeV}/c$ bins for the 2nd run. Transvers energy in HF is $20 < E_T^{HF|\eta|>4} < 30\,\mathrm{GeV}$.

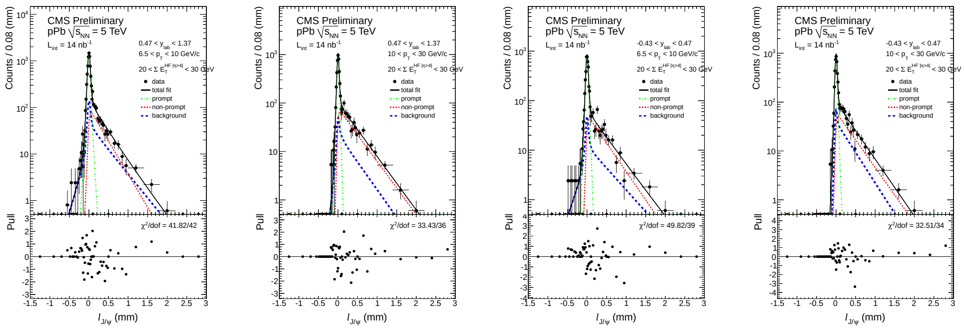

Figure 123: Lifetime fit for $0.47 < y_{lab} < 1.37$ and $-0.43 < y_{lab} < 0.47$, for the different transverse momentum $6.5 < p_{\mathrm{T}} < 10$, and $10 < p_{\mathrm{T}} < 30\,\mathrm{GeV}/c$ bins for the 2nd run. Transvers energy in HF is $20 < E_T^{HF|\eta|>4} < 30\,\mathrm{GeV}$.

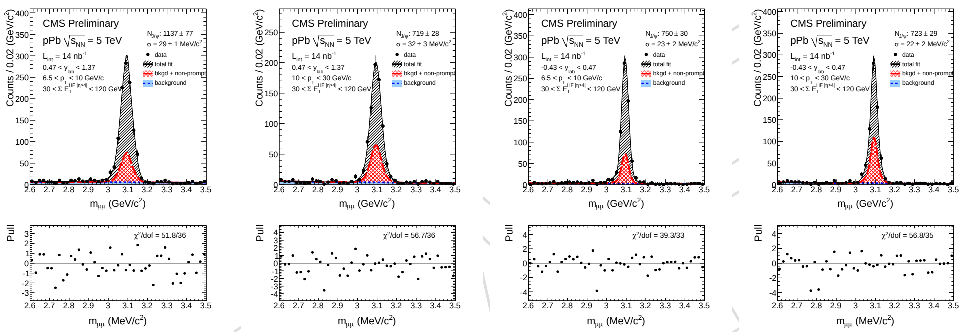

Figure 124: Mass fit for $0.47 < y_{lab} < 1.37$ and $-0.43 < y_{lab} < 0.47$, for the different transverse momentum $6.5 < p_{\mathrm{T}} < 10$, and $10 < p_{\mathrm{T}} < 30\,\mathrm{GeV}/c$ bins for the 2nd run. Transvers energy in HF is $30 < E_T^{HF|\eta|>4} < 120\,\mathrm{GeV}$.

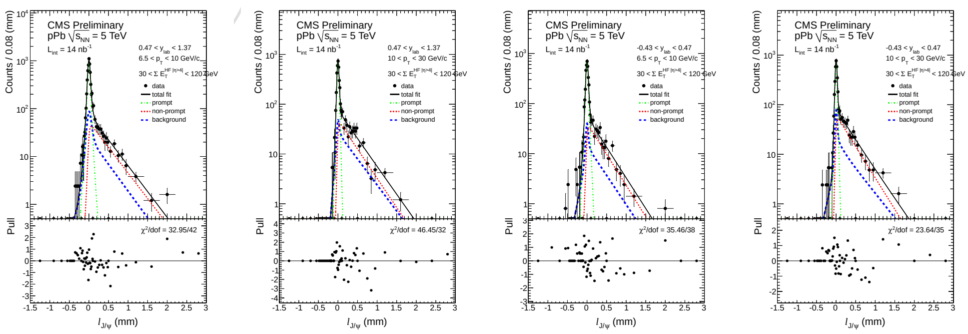

Figure 125: Lifetime fit for $0.47 < y_{lab} < 1.37$ and $-0.43 < y_{lab} < 0.47$, for the different transverse momentum $6.5 < p_{\mathrm{T}} < 10$, and $10 < p_{\mathrm{T}} < 30\,\mathrm{GeV}/c$ bins for the 2nd run. Transvers energy in HF is $30 < E_T^{HF|\eta|>4} < 120\,\mathrm{GeV}$.

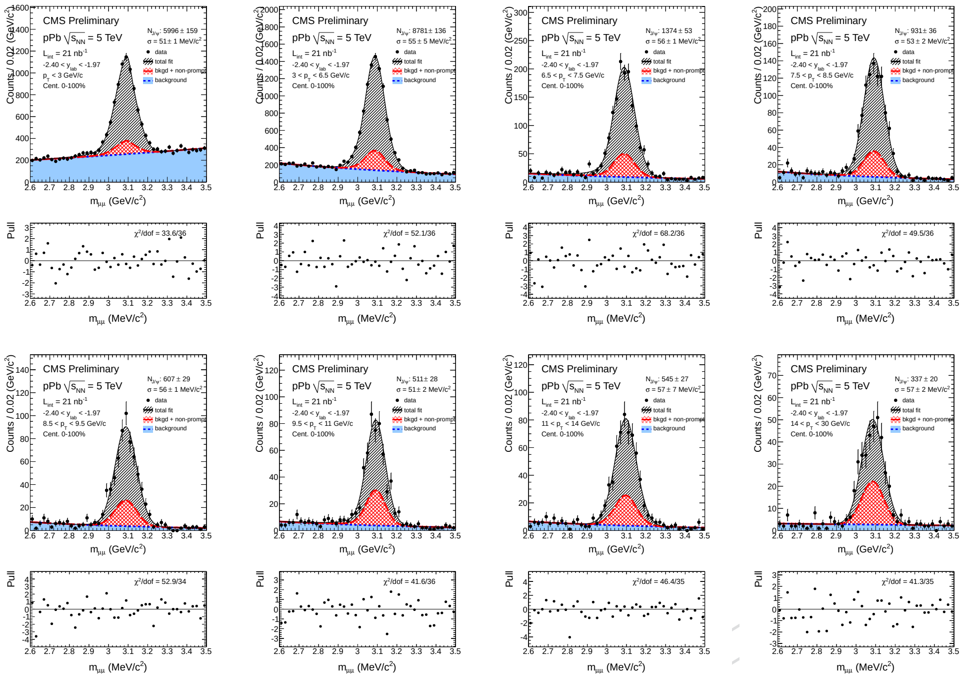

Figure 126: Mass fit for $-2.4 < y_{lab} < -1.97$ for the several transverse momentum ranges from the 1st run.

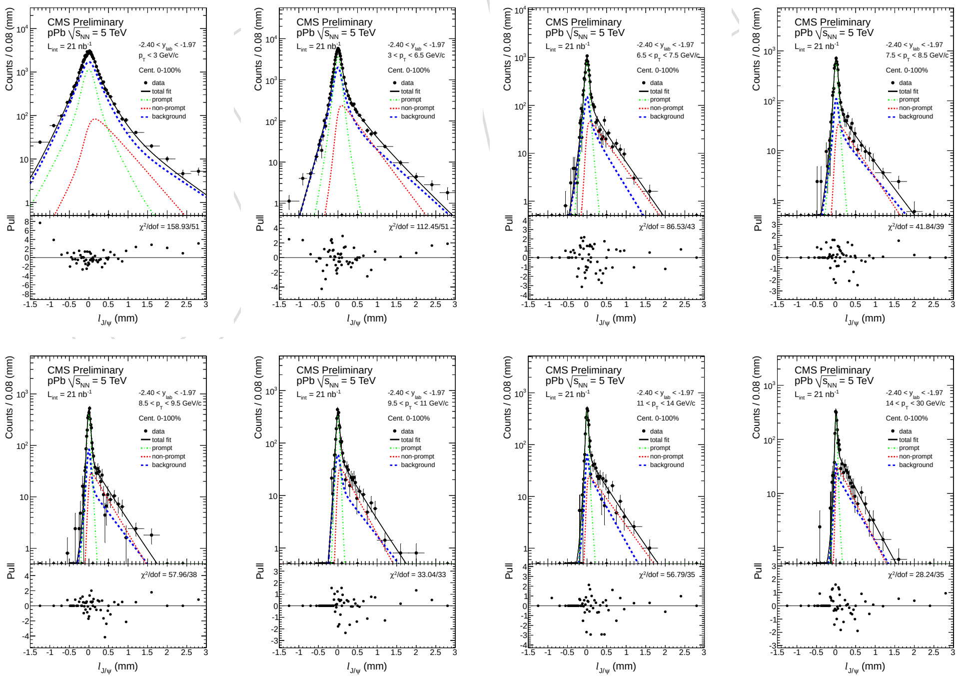

Figure 127: Lifetime fit for $-2.4 < y_{lab} < -1.97$ for the several transverse momentum ranges from the 1st run.

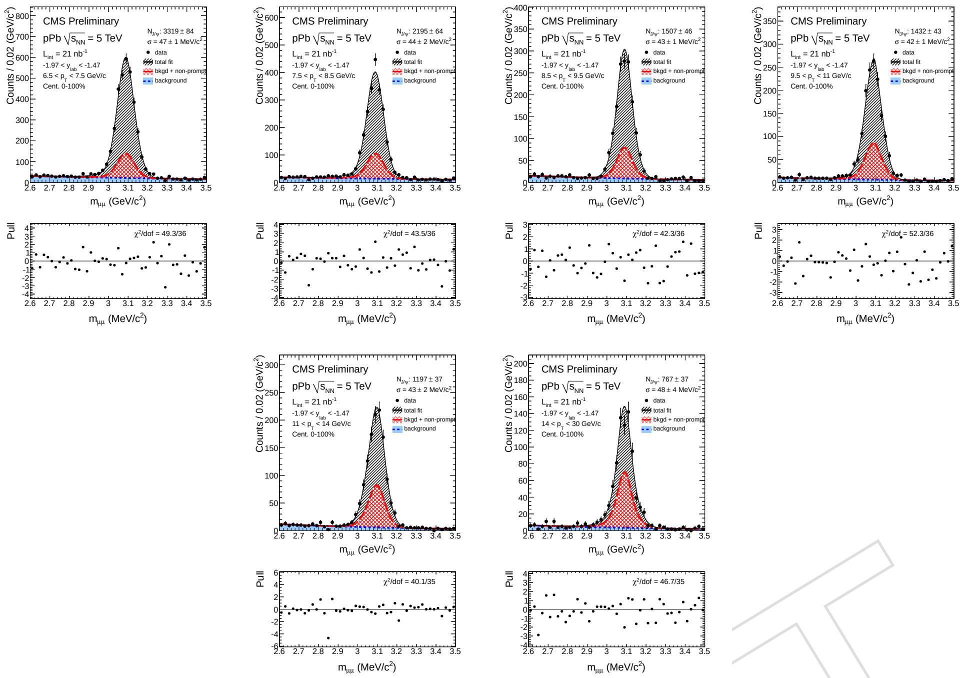

Figure 128: Mass fit for $-1.97 < y_{lab} < -1.47$ for the several transverse momentum ranges from the 1st run.

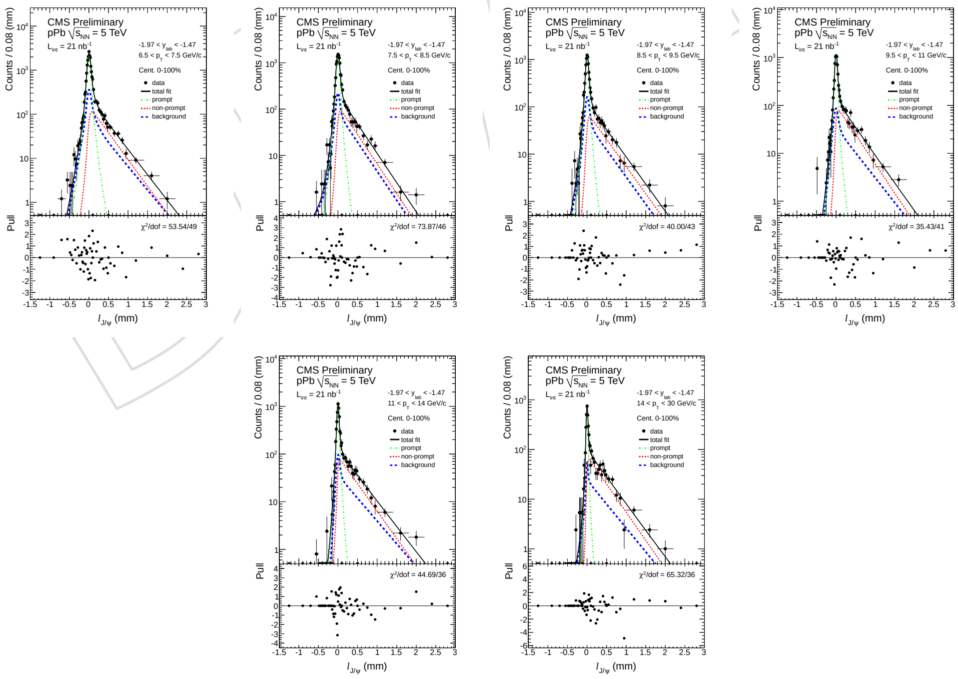

Figure 129: Lifetime fit for $-1.97 < y_{lab} < -1.47$ for the several transverse momentum ranges from the 1st run.

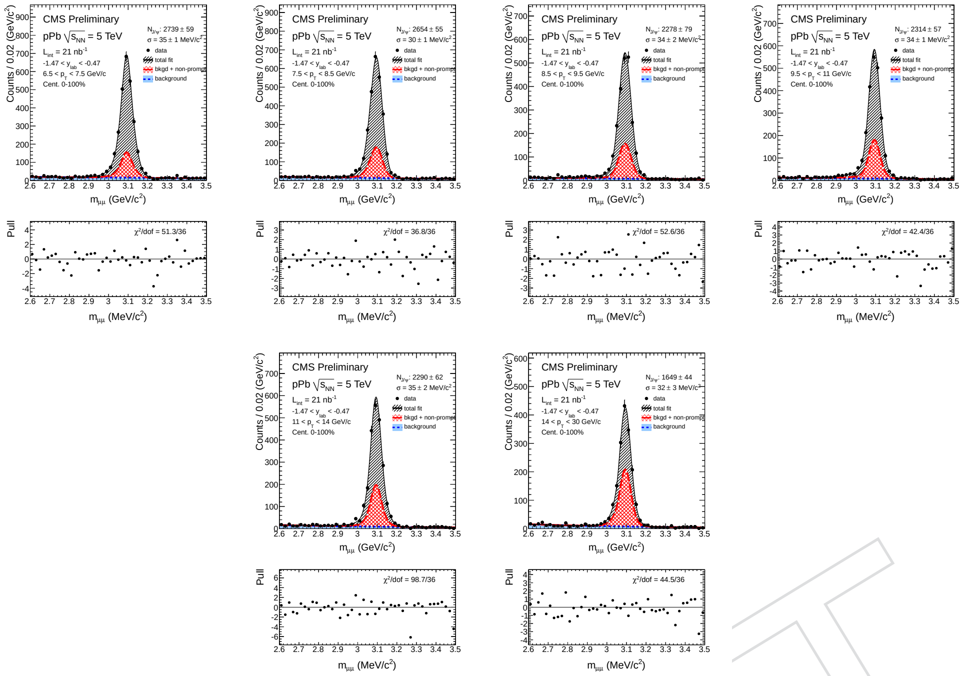

Figure 130: Mass fit for $-1.47 < y_{lab} < -0.47$ for the several transverse momentum ranges from the 1st run.

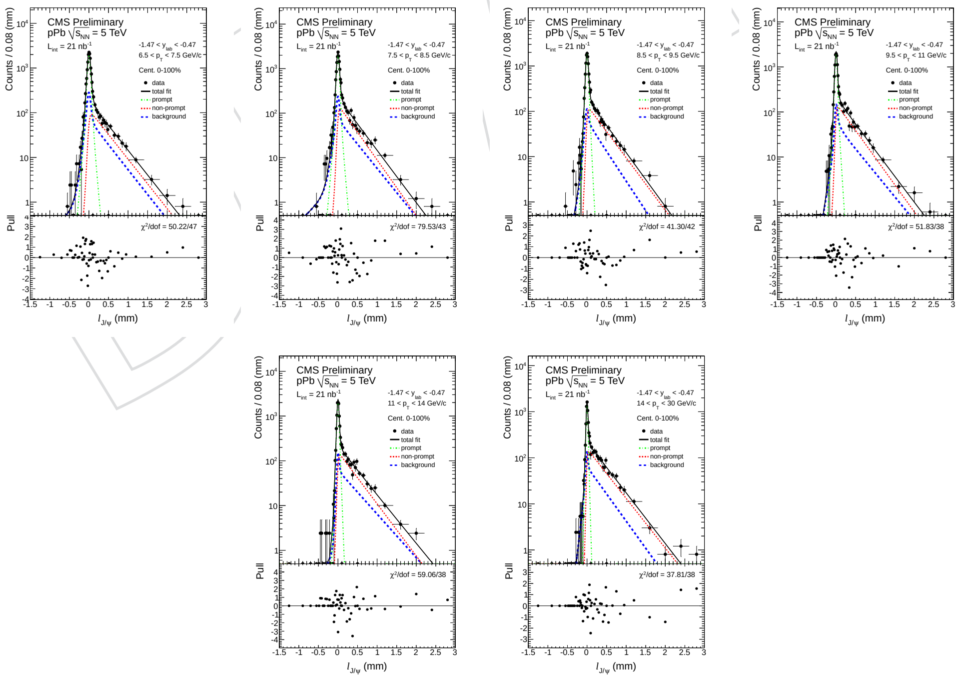

Figure 131: Lifetime fit for $-1.47 < y_{lab} < -0.47$ for the several transverse momentum ranges from the 1st run.

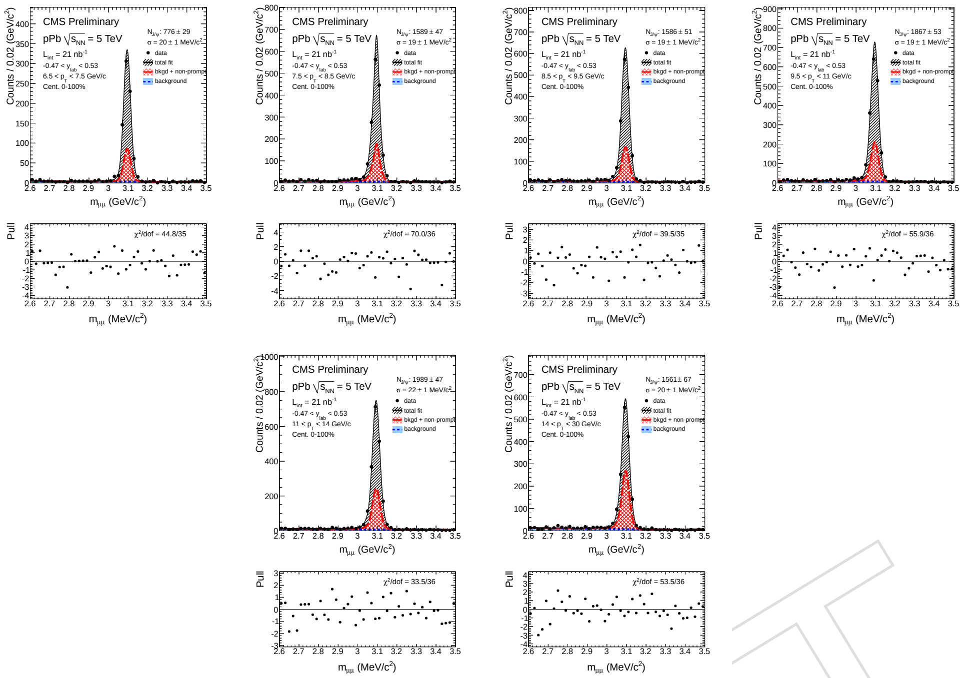

Figure 132: Mass fit for $-0.47 < y_{lab} < 0.53$ for the several transverse momentum ranges from the 1st run.

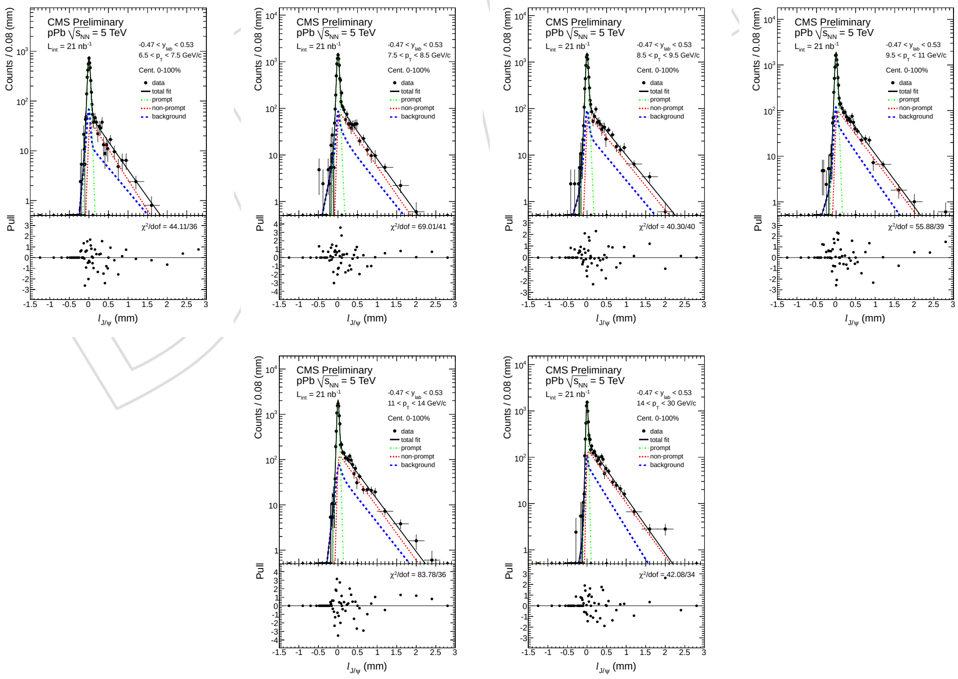

Figure 133: Lifetime fit for $-0.47 < y_{lab} < 0.53$ for the several transverse momentum ranges from the 1st run.

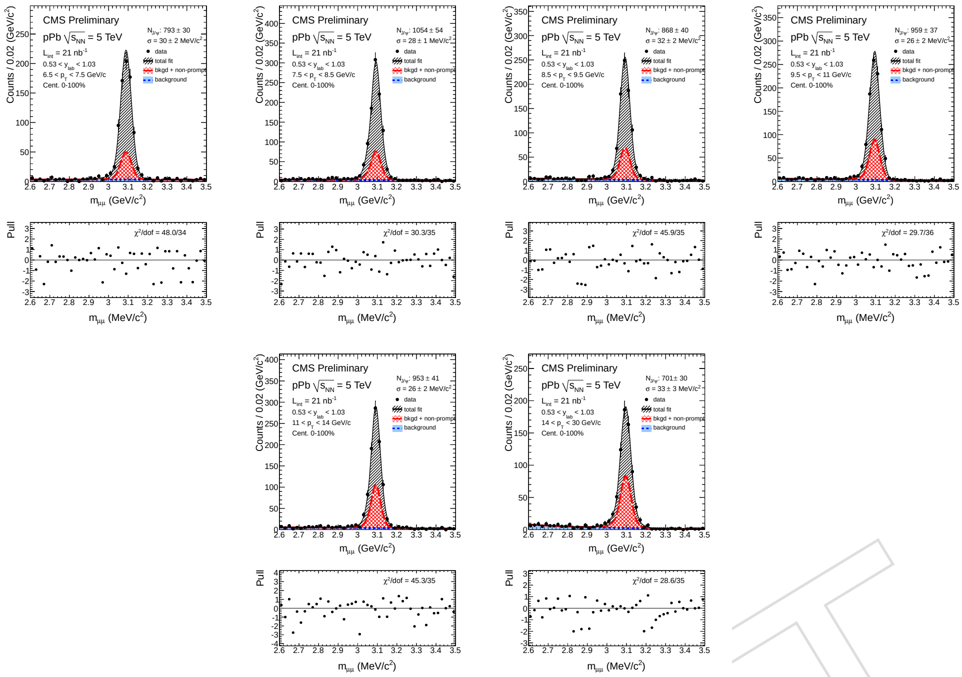

Figure 134: Mass fit for $0.53 < y_{lab} < 1.03$ for the several transverse momentum ranges from the 1st run.

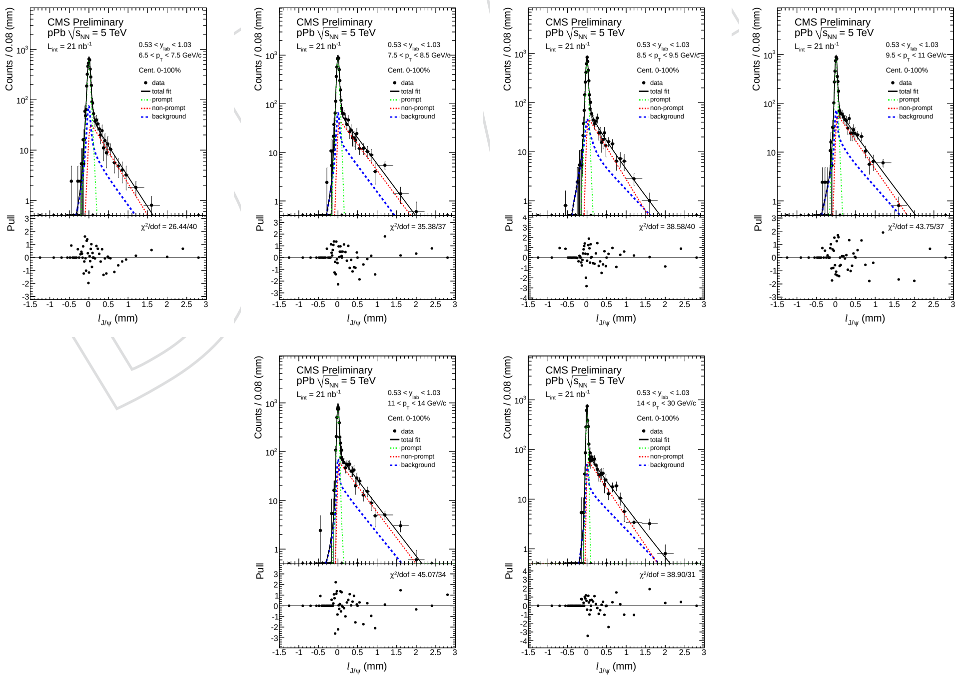

Figure 135: Lifetime fit for $0.53 < y_{lab} < 1.03$ for the several transverse momentum ranges from the 1st run.

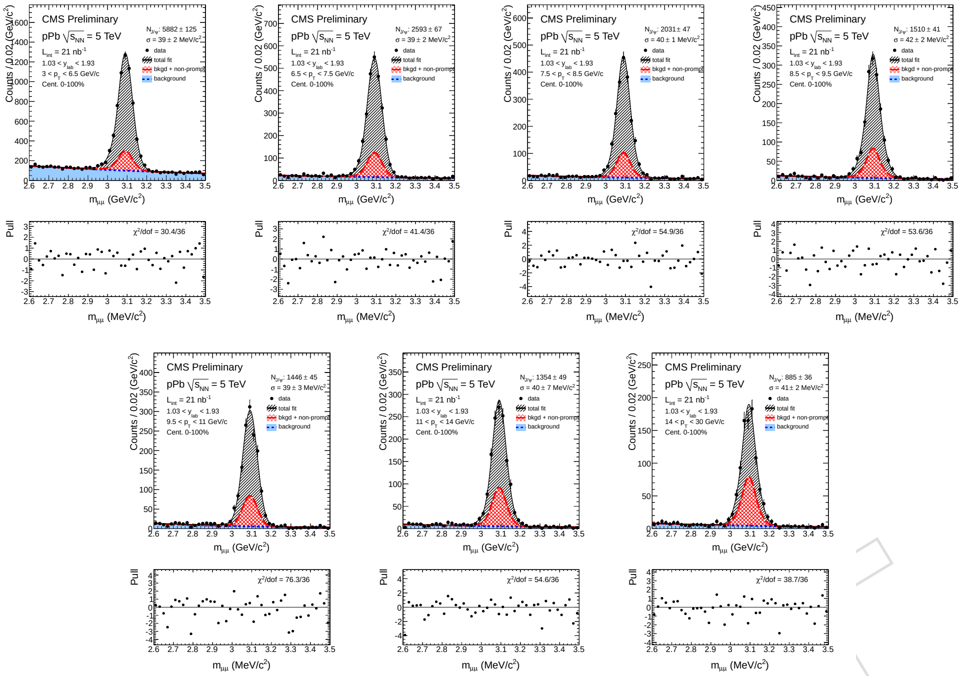

Figure 136: Mass fit for $1.03 < y_{lab} < 1.93$ for the several transverse momentum ranges from the 1st run.

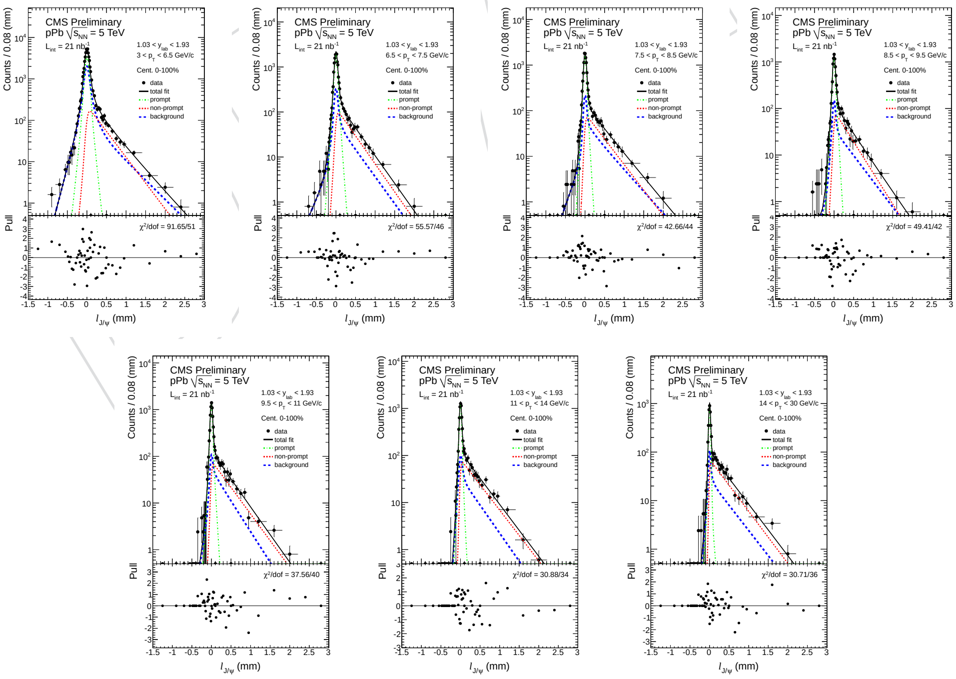

Figure 137: Lifetime fit for $1.03 < y_{lab} < 1.93$ for the several transverse momentum ranges from the 1st run.

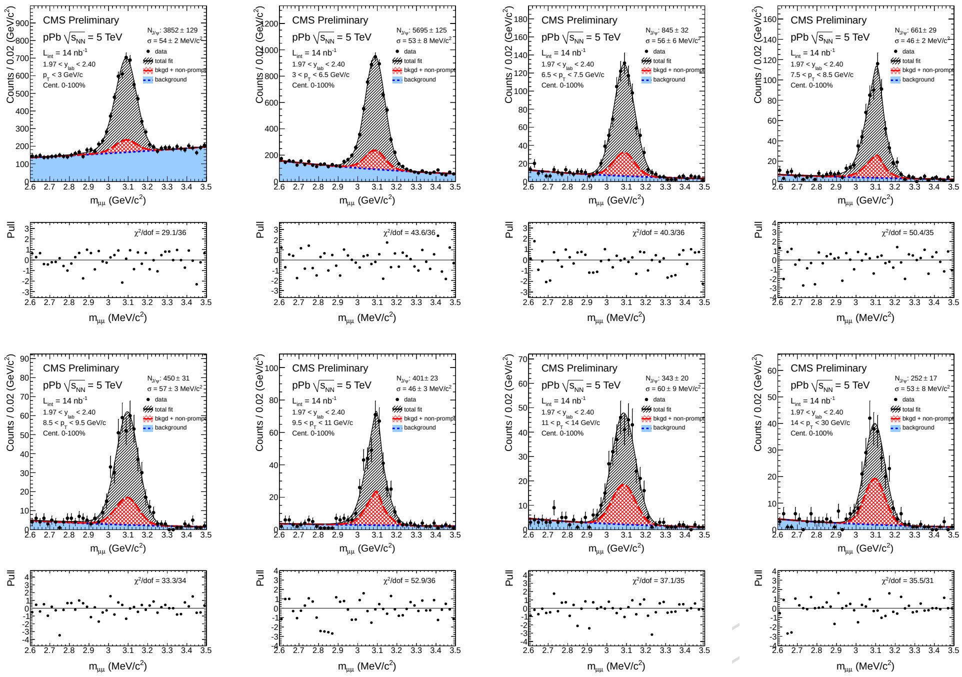

Figure 138: Mass fit for $1.97 < y_{lab} < 2.4$ for the several transverse momentum ranges from the 2nd run.

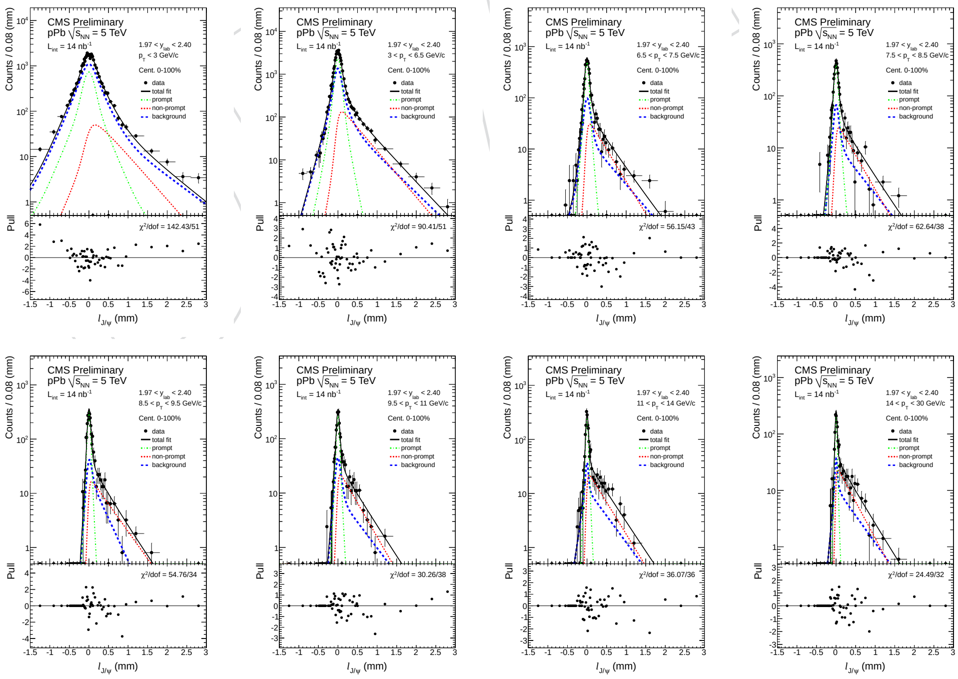

Figure 139: Lifetime fit for $1.97 < y_{lab} < 2.4$ for the several transverse momentum ranges from the 2nd run.

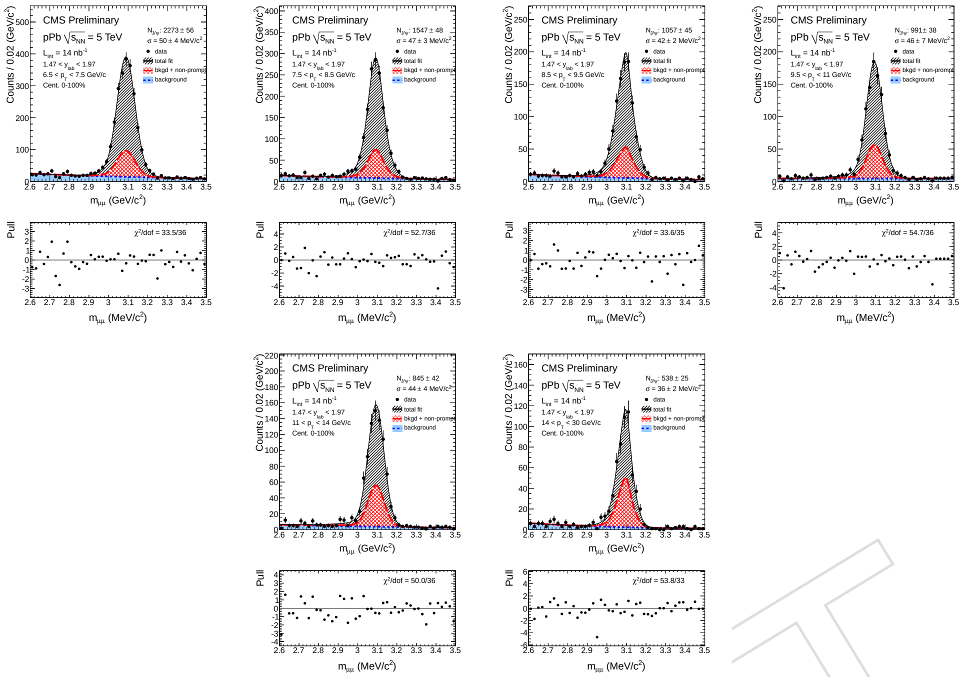

Figure 140: Mass fit for $1.47 < y_{lab} < 1.97$ for the several transverse momentum ranges from the 2nd run.

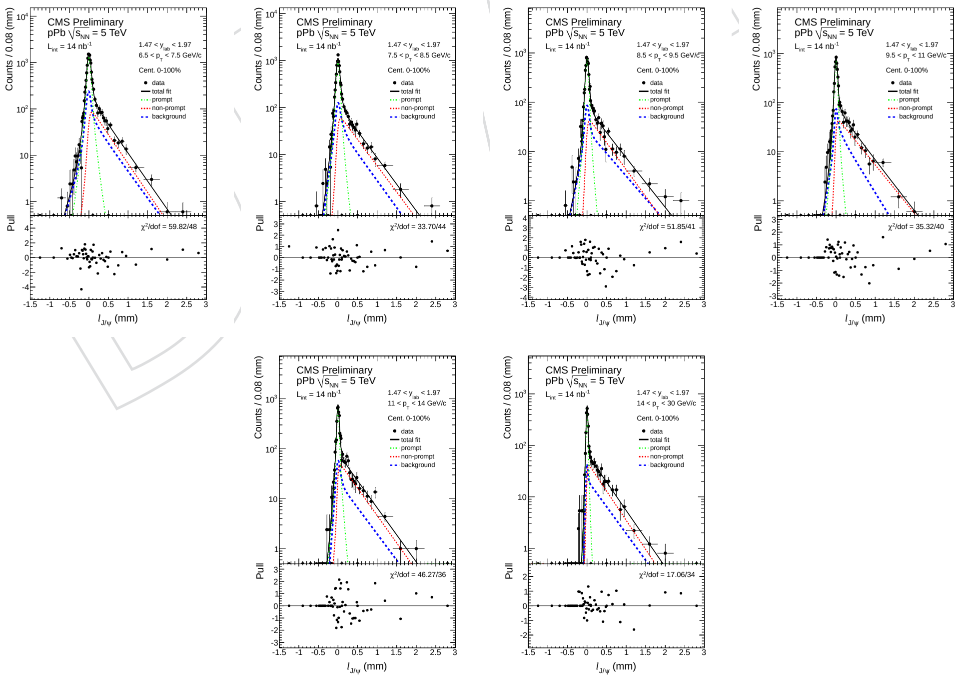

Figure 141: Lifetime fit for $1.47 < y_{lab} < 1.97$ for the several transverse momentum ranges from the 2nd run.

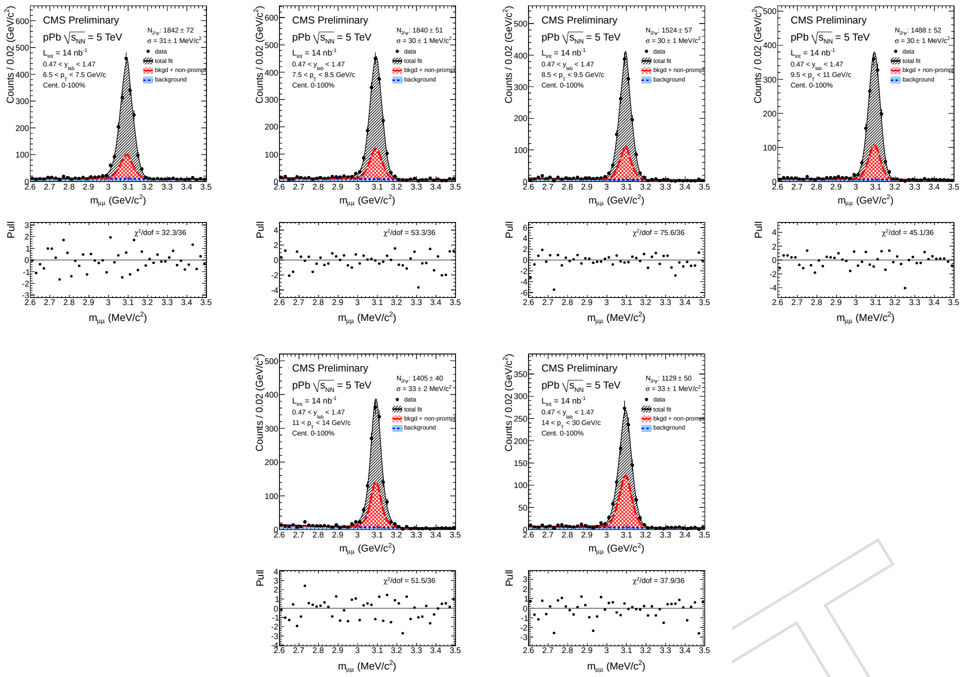

Figure 142: Mass fit for $0.47 < y_{lab} < 1.47$ for the several transverse momentum ranges from the 2nd run.

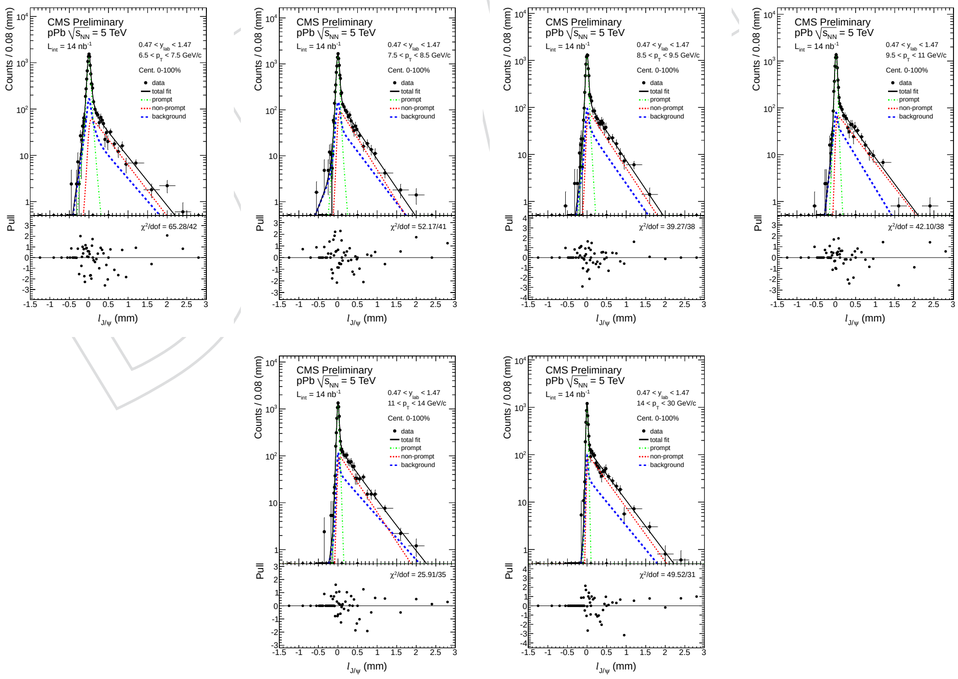

Figure 143: Lifetime fit for $0.47 < y_{lab} < 1.47$ for the several transverse momentum ranges from the 2nd run.

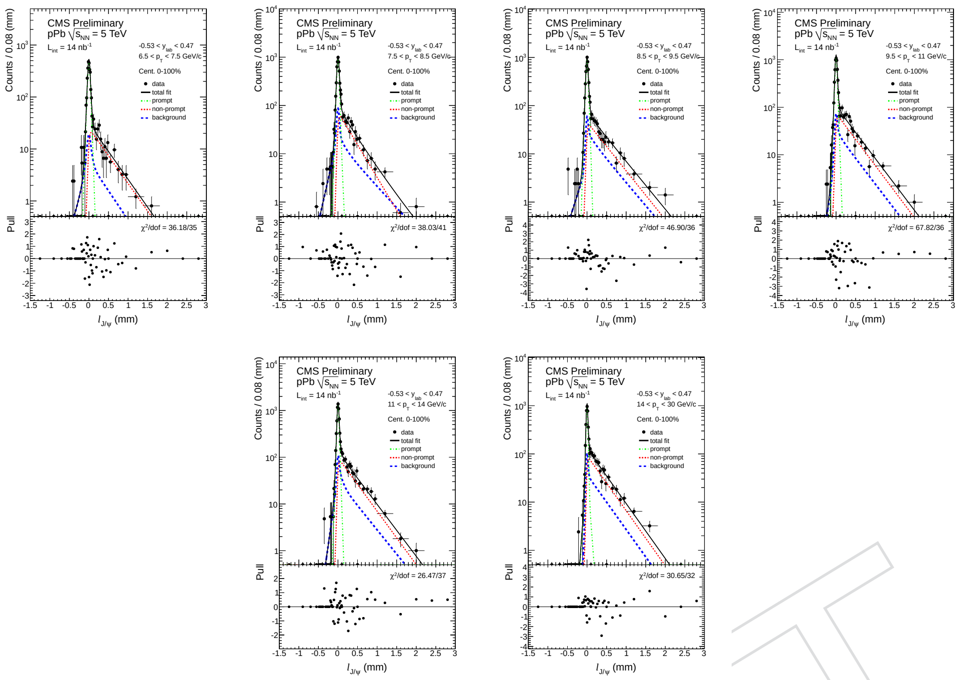

Figure 145: Lifetime fit for $-0.53 < y_{lab} < 0.47$ for the several transverse momentum ranges from the 2nd run.

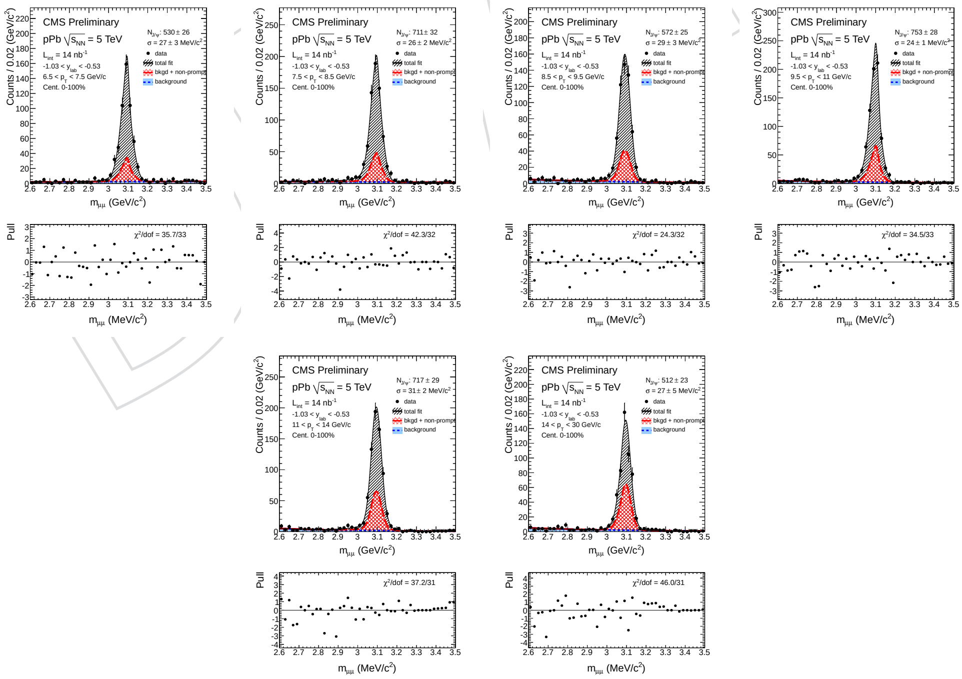

Figure 146: Mass fit for $-1.03 < y_{lab} < -0.53$ for the several transverse momentum ranges from the 2nd run.

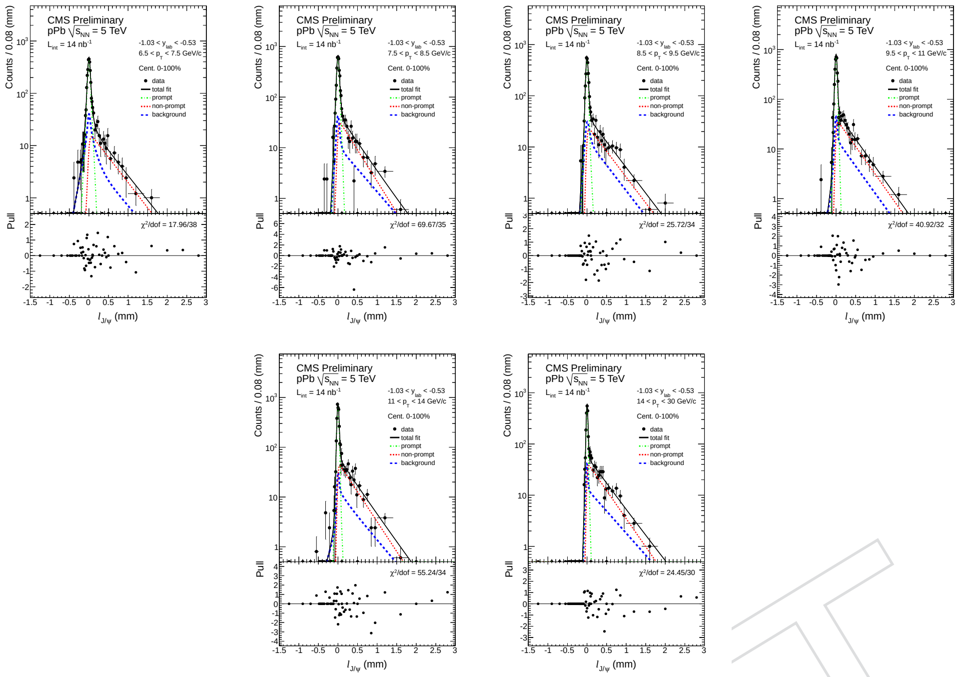

Figure 147: Lifetime fit for $-1.03 < y_{lab} < -0.53$ for the several transverse momentum ranges from the 2nd run.

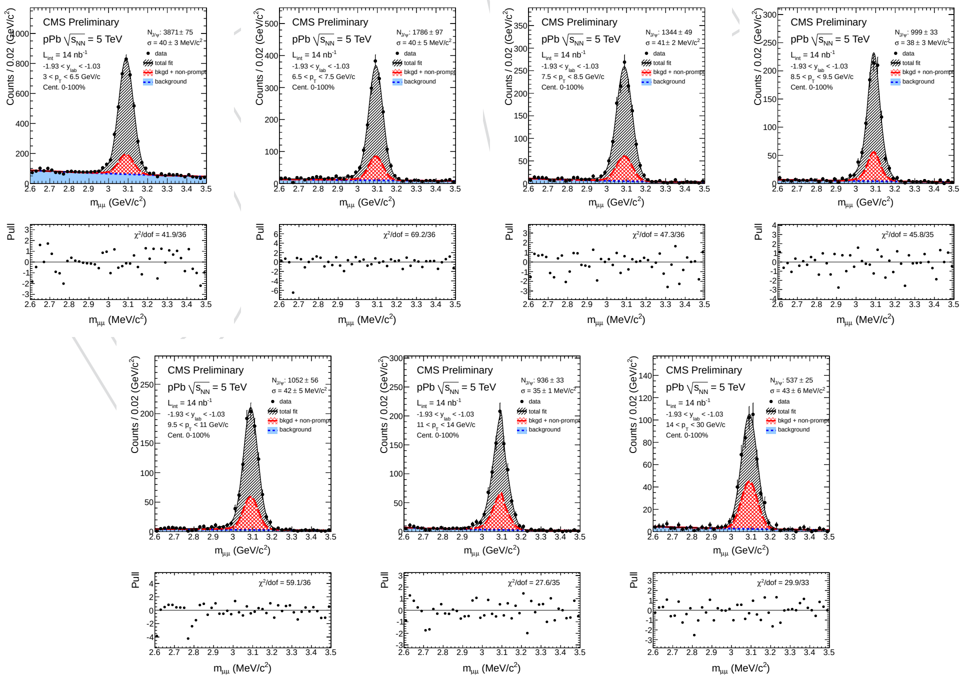

Figure 148: Mass fit for $-1.93 < y_{lab} < -1.03$ for the several transverse momentum ranges from the 2nd run.

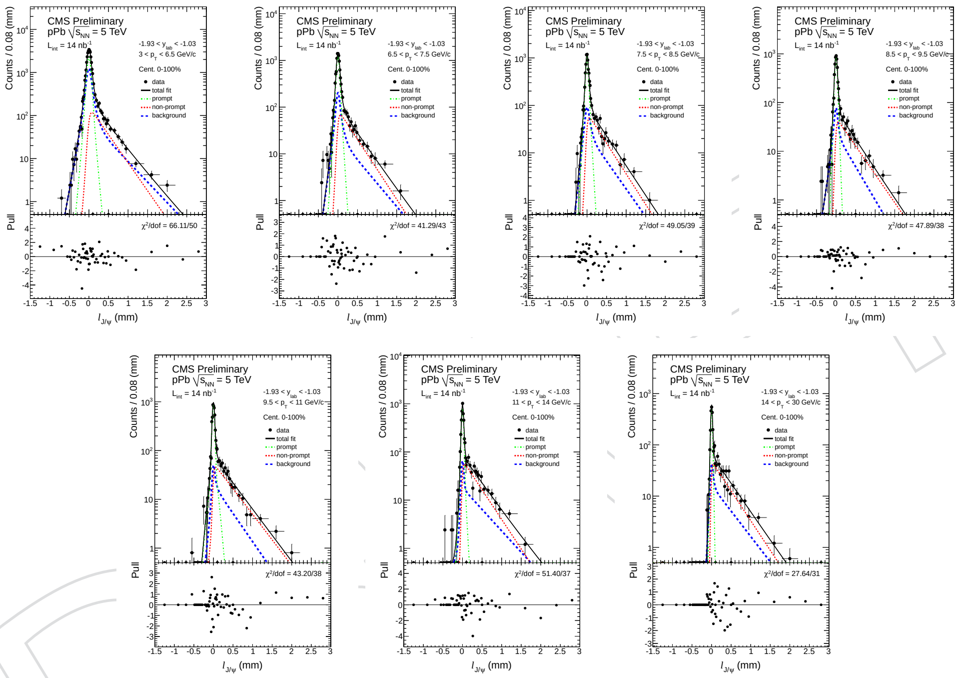

Figure 149: Lifetime fit for $-1.93 < y_{lab} < 1.03$ for the several transverse momentum ranges from the 2nd run.

B Unfolding study

When we investigate the efficiency by Monte Carlo sample, numerator is filled with the reconstructed p_T and denominator is filled with the generated p_T. Therefore, the effect of the bin migration (a J/ψ being reconstructed at a slightly different p_T due to finite resolution) is studied.

Figure 150 and figure 151 show the generated vs. reconstructed p_T distributions before binning. For the right plots, the first p_T bin region (6.5-7.5 GeV/c) is zoomed in and pointed by the red dashed regions.

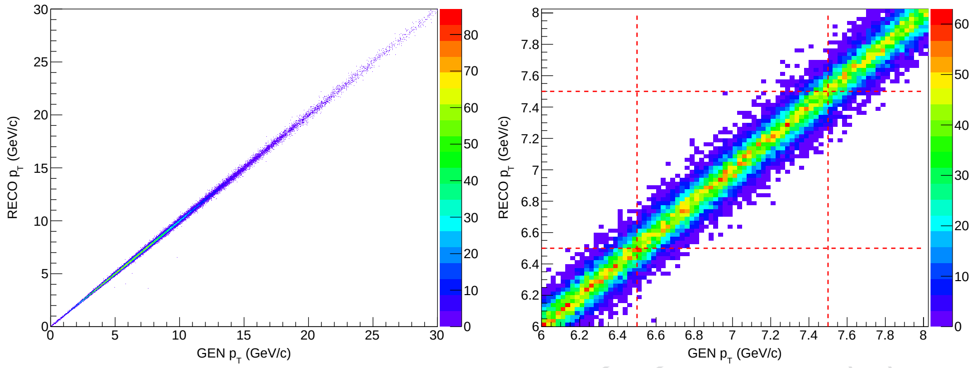

Figure 150: reco p_T vs gen p_T form prompt J/ψ.

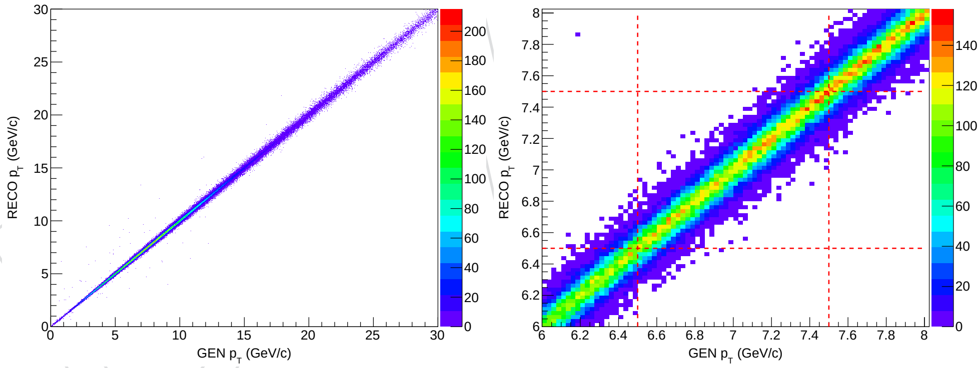

Figure 151: reco p_T vs gen p_T form non-prompt J/ψ.

Figure 152 shows the matrix of the generated vs. reconstructed p_T distributions.

The following plots show the distribution of p_T of reconstructed particles subtracted by p_T of the generated particles and then divided by p_T of the generated particles.

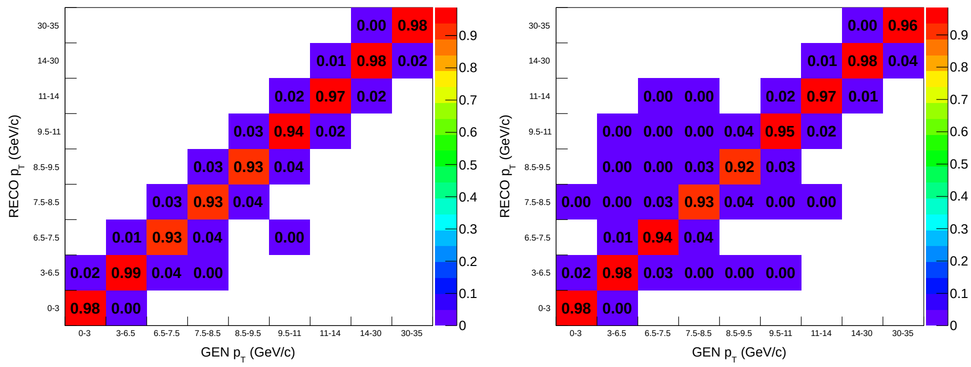

Figure 152: Matrix of generated versus reconstructed p_{T} for the prompt J/ψ (Left) and non-prompt J/ψ (Right) in the MC used in this analysis. The axis labels display the p_{T} range of the bin.

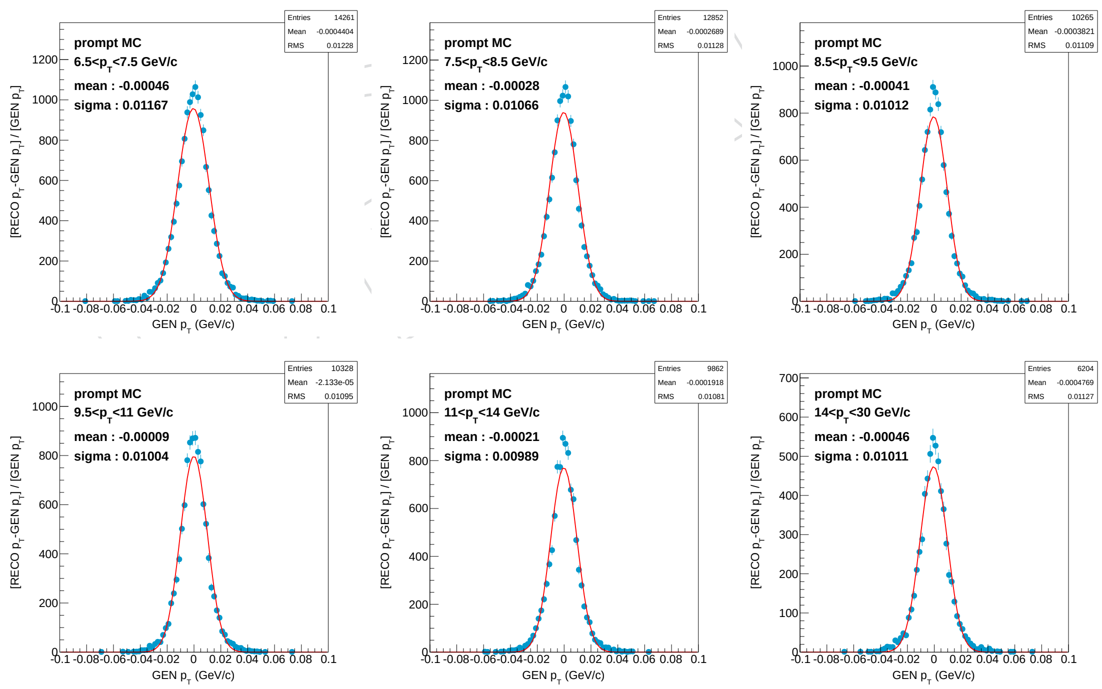

Figure 153: $[Reco p_{\mathrm{T}} - GEN p_{\mathrm{T}}]/GEN p_{\mathrm{T}}$ distributions of each p_{T} bins for prompt J/ψ official MC sample.

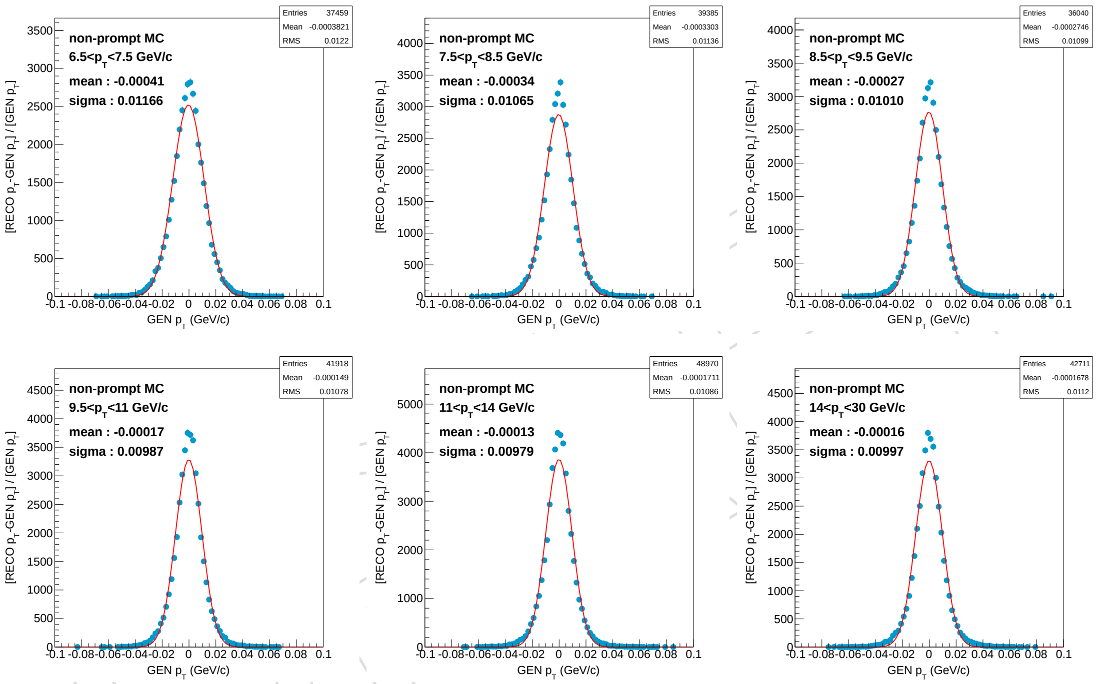

Figure 154: $[Reco\, p_{\mathrm{T}} - GEN\, p_{\mathrm{T}}]/GEN\, p_{\mathrm{T}}$ distributions of each p_{T} bins for non-prompt J/ψ official MC sample.

C Tag and Probe plots

In this appendix section, the invariant mass fittings used for Tag and Probe anlaysis are collected. For each figure, top left plot is passing probe pair, top right plot is failing probe pair, bottom left plot is total pair and the bottom right box is fitting parameters. Each figure is used for one bin of efficiency distribution.

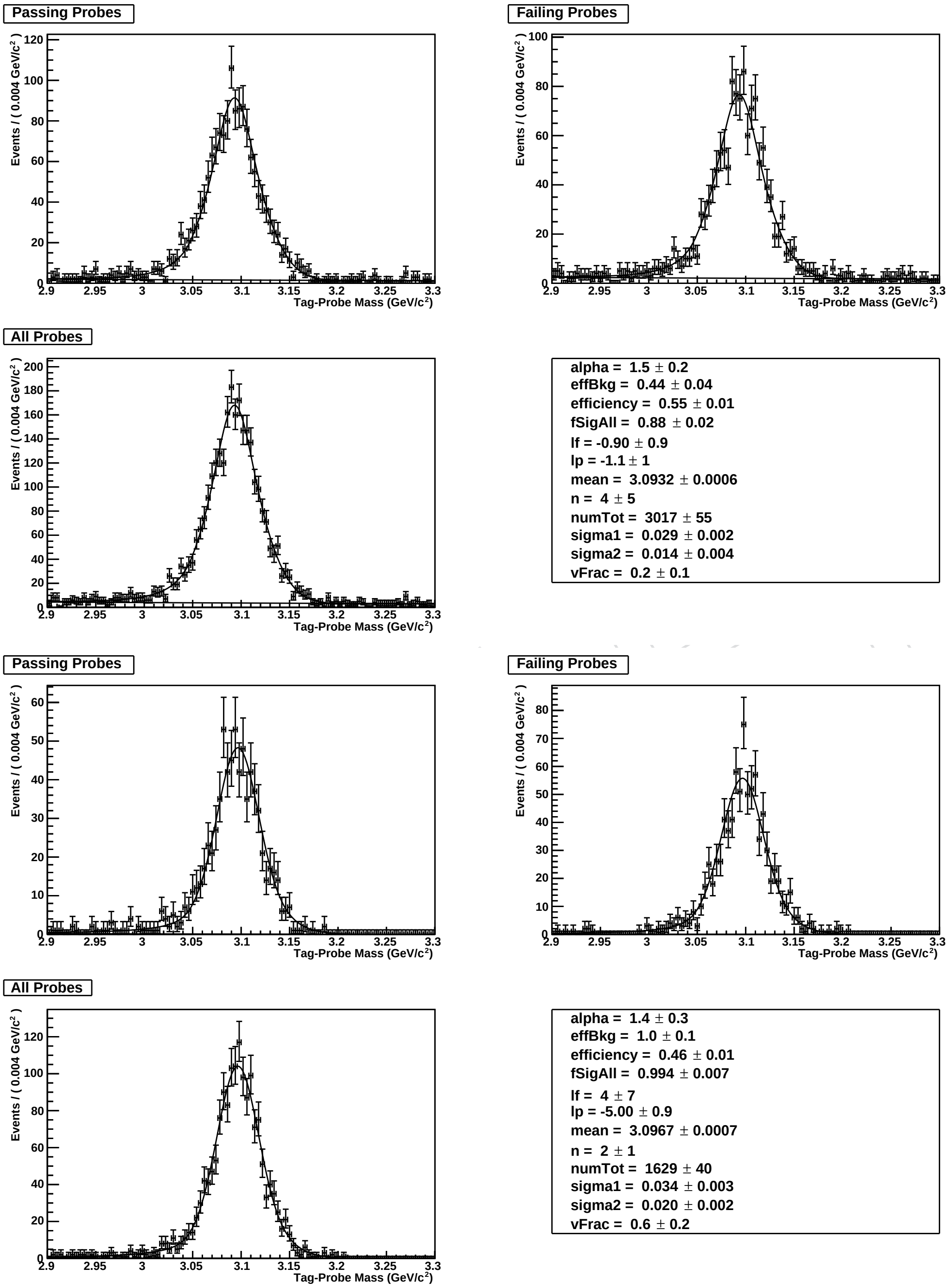

Figure 155: Mass distribution of tag-probe pair for Muon ID and trigger cuts in Data (Top) and MC (Bottom), in $|\eta| < 1.2$ and the lowest p_{T} bin.

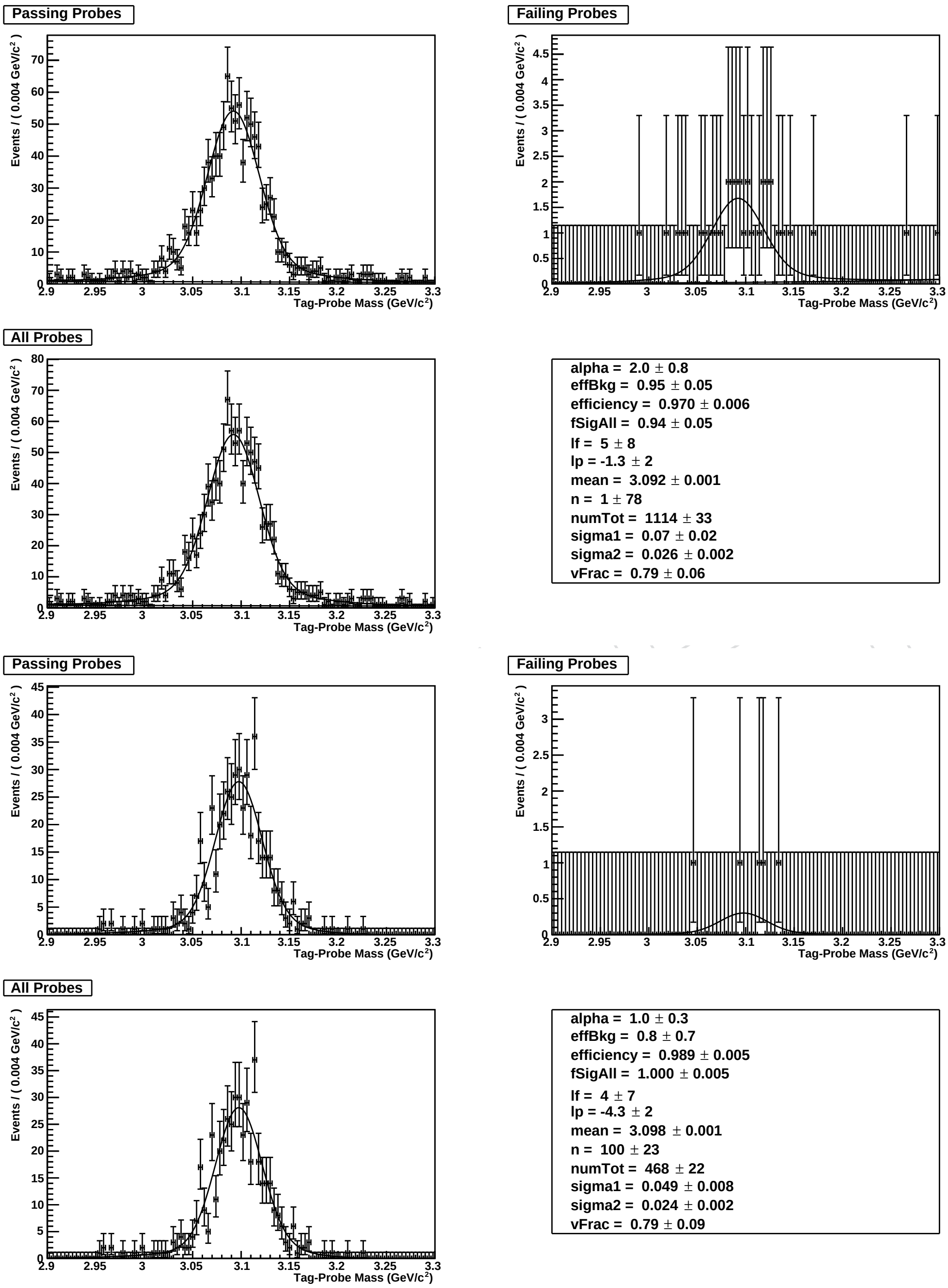

Figure 156: Mass distribution of tag-probe pair for Muon ID and trigger cuts in Data (Top) and MC (Bottom), in $|\eta| < 1.2$ and the highest p_T bin.

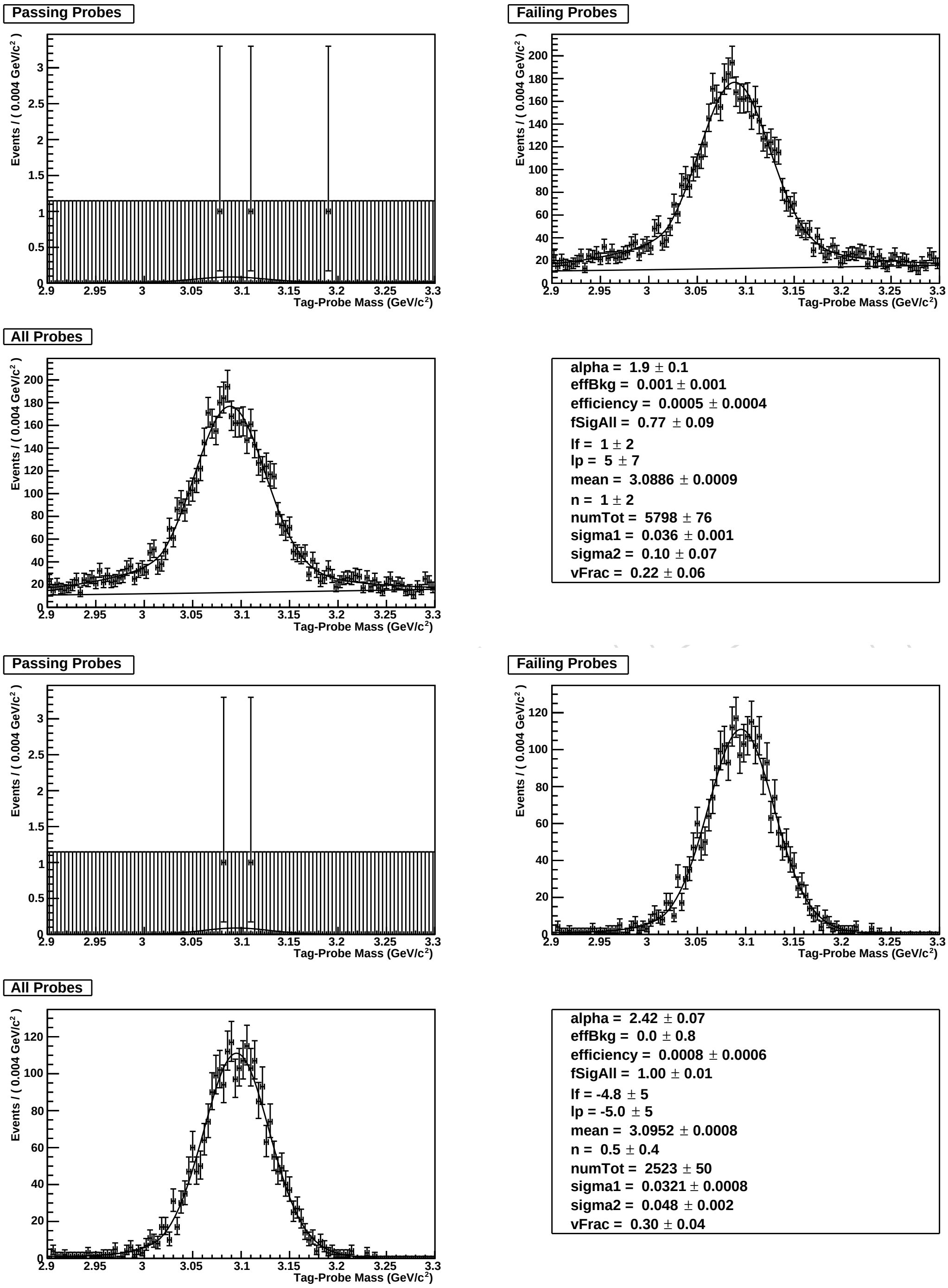

Figure 157: Mass distribution of tag-probe pair for Muon ID and trigger cuts in Data (Top) and MC (Bottom), in $1.2 < |\eta| < 1.6$ and the lowest p_T bin.

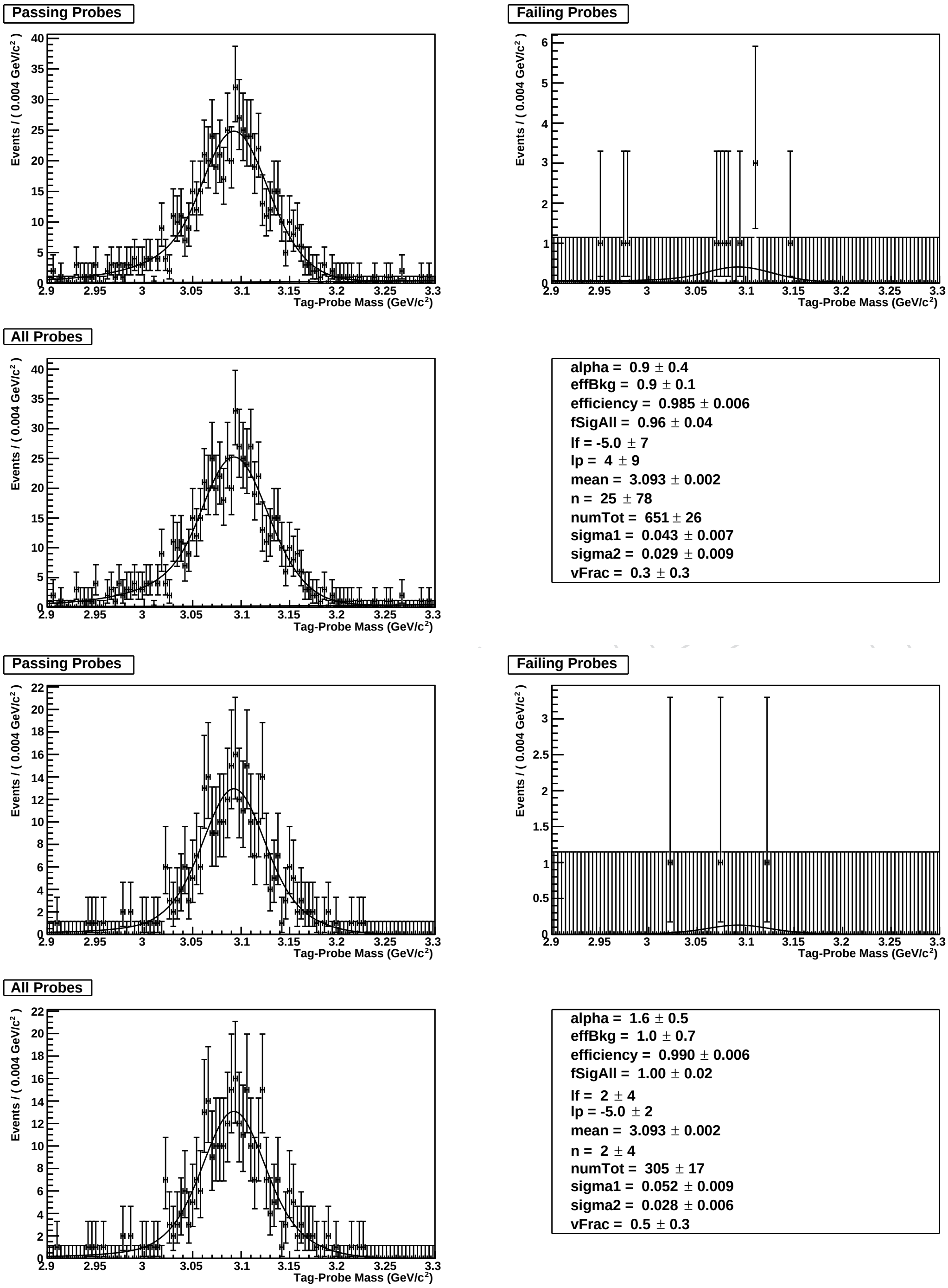

Figure 158: Mass distribution of tag-probe pair for Muon ID and trigger cuts in Data (Top) and MC (Bottom), in $1.2 < |\eta| < 1.6$ and the highest p_{T} bin.

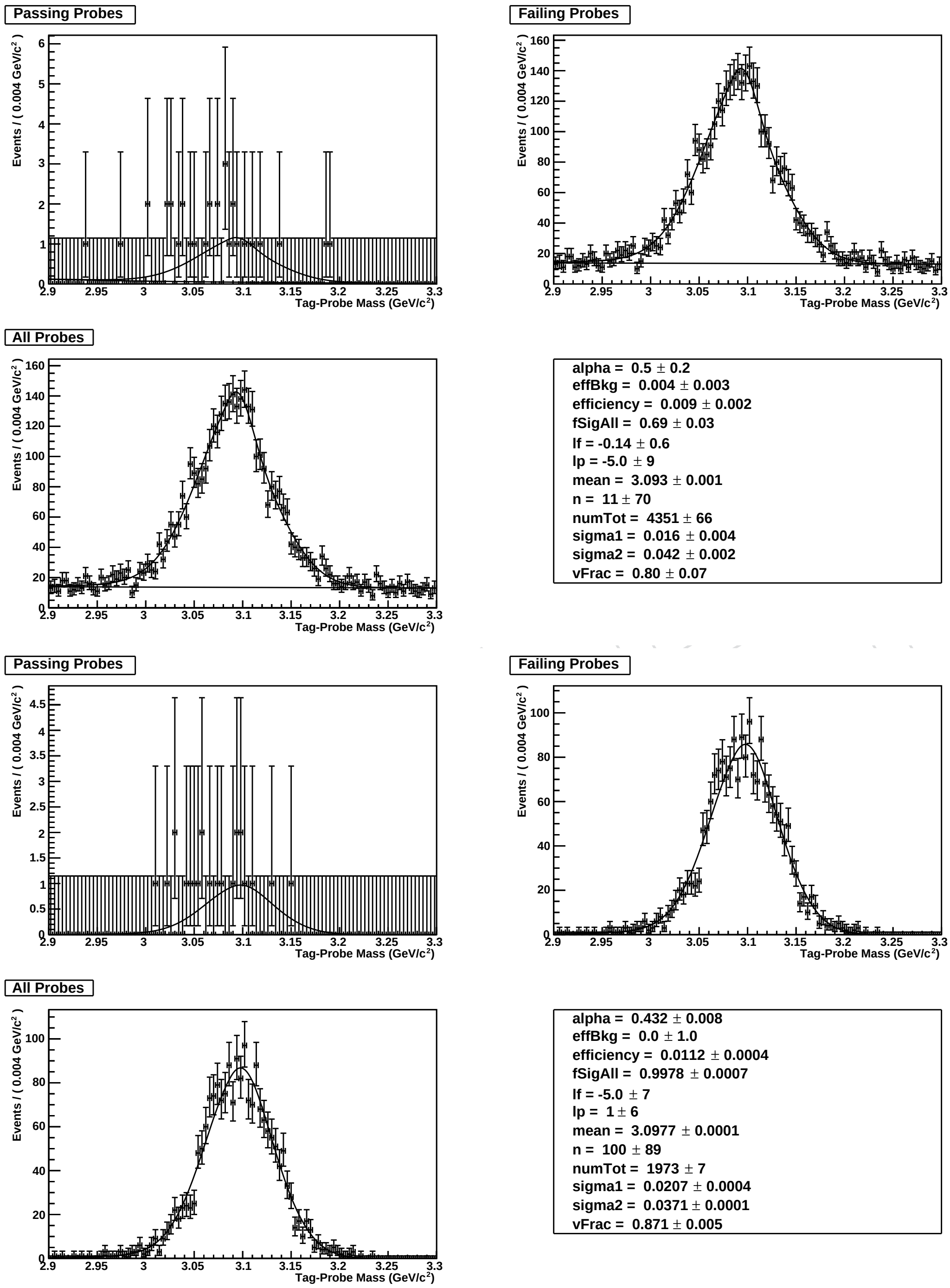

Figure 159: Mass distribution of tag-probe pair for Muon ID and trigger cuts in Data (Top) and MC (Bottom), in $|\eta| > 1.6$ and the lowest p_{T} bin.

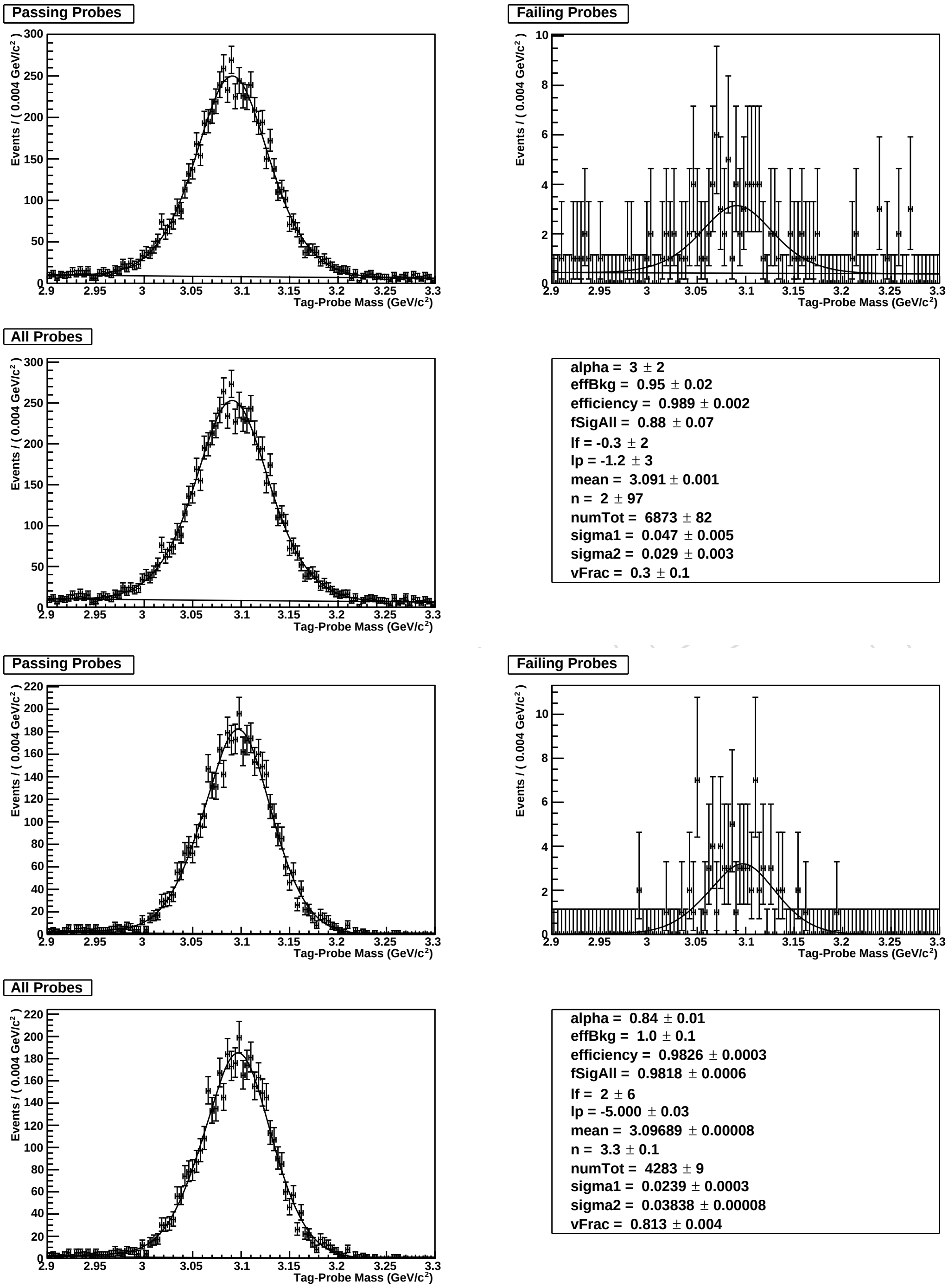

Figure 160: Mass distribution of tag-probe pair for Muon ID and trigger cuts in Data (Top) and MC (Bottom), in $|\eta| > 1.6$ and the highest p_T bin.

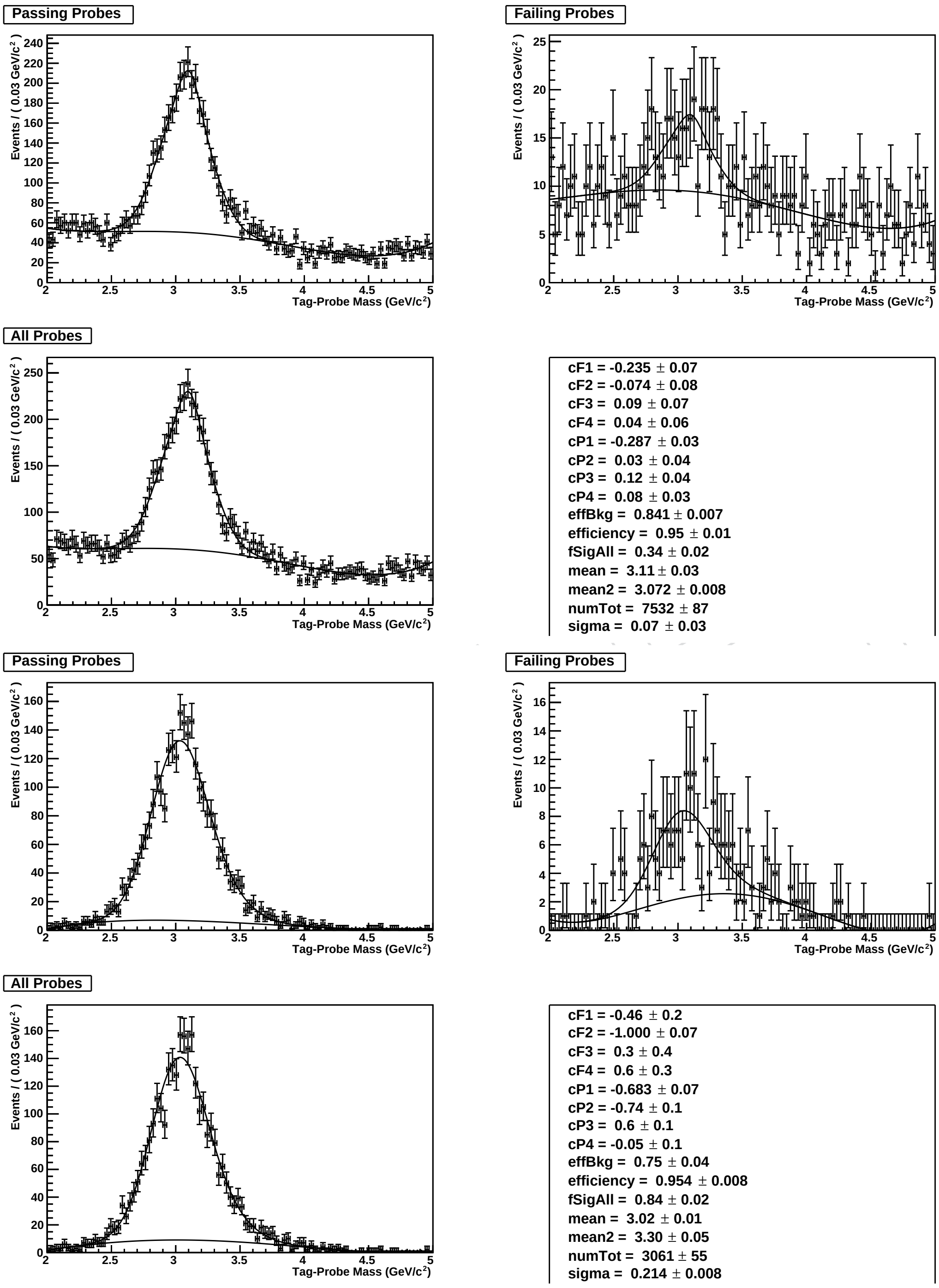

Figure 161: Mass distribution of tag-probe pair for tracking efficiency in Data (Top) and MC (Bottom), in $|\eta| < 1.2$ and the lowest p_T bin.

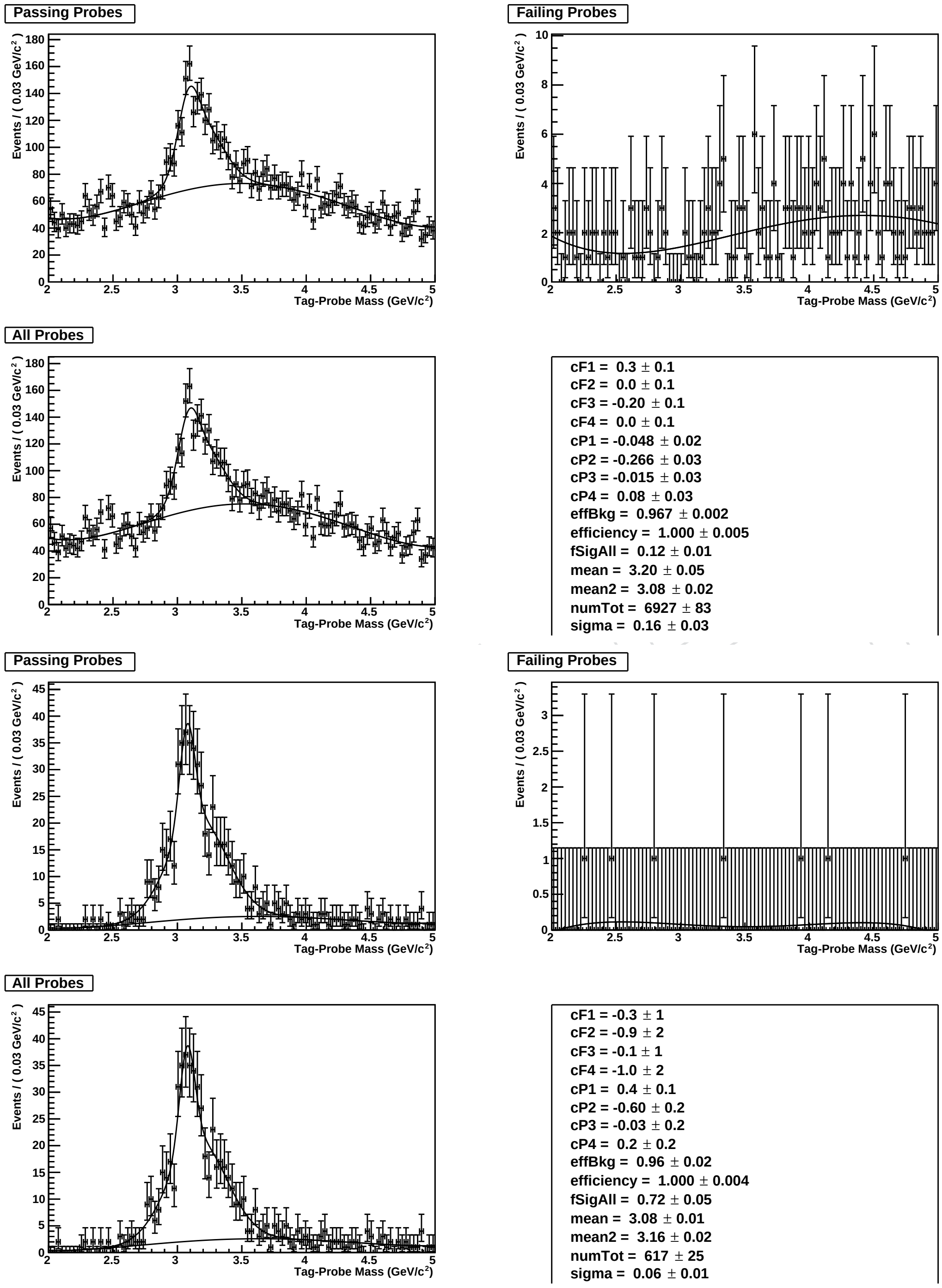

Figure 162: Mass distribution of tag-probe pair for tracking efficiency in Data (Top) and MC (Bottom), in $|\eta| < 1.2$ and the highest p_{T} bin.

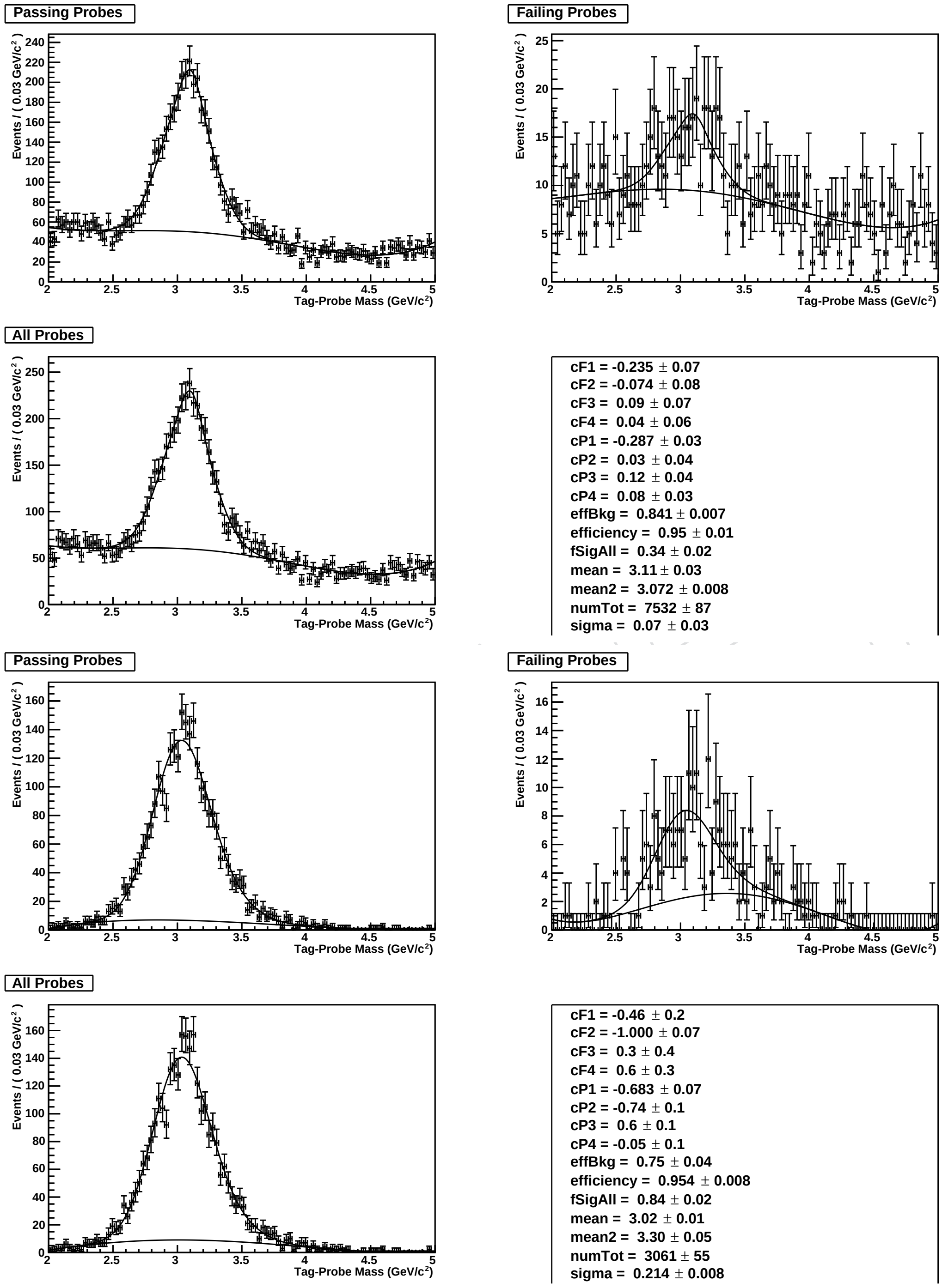

Figure 163: Mass distribution of tag-probe pair for tracking efficiency in Data (Top) and MC (Bottom), in $1.2 < |\eta| < 1.6$ and the lowest p_{T} bin.

TagAndProbe/M

TagAndProbe/M

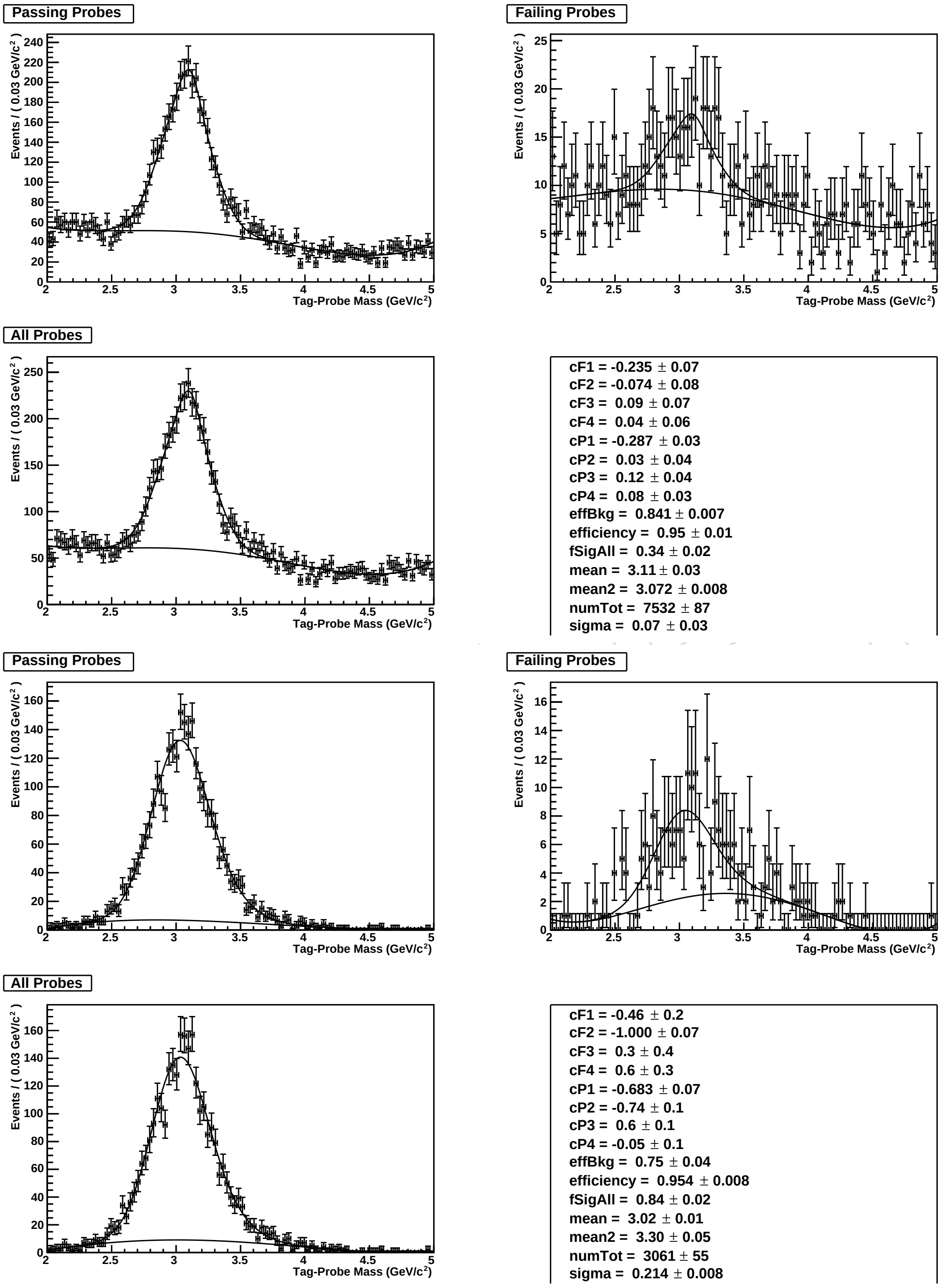

Figure 165: Mass distribution of tag-probe pair for tracking efficiency in Data (Top) and MC (Bottom), in $|\eta| > 1.6$ and the lowest p_{T} bin.

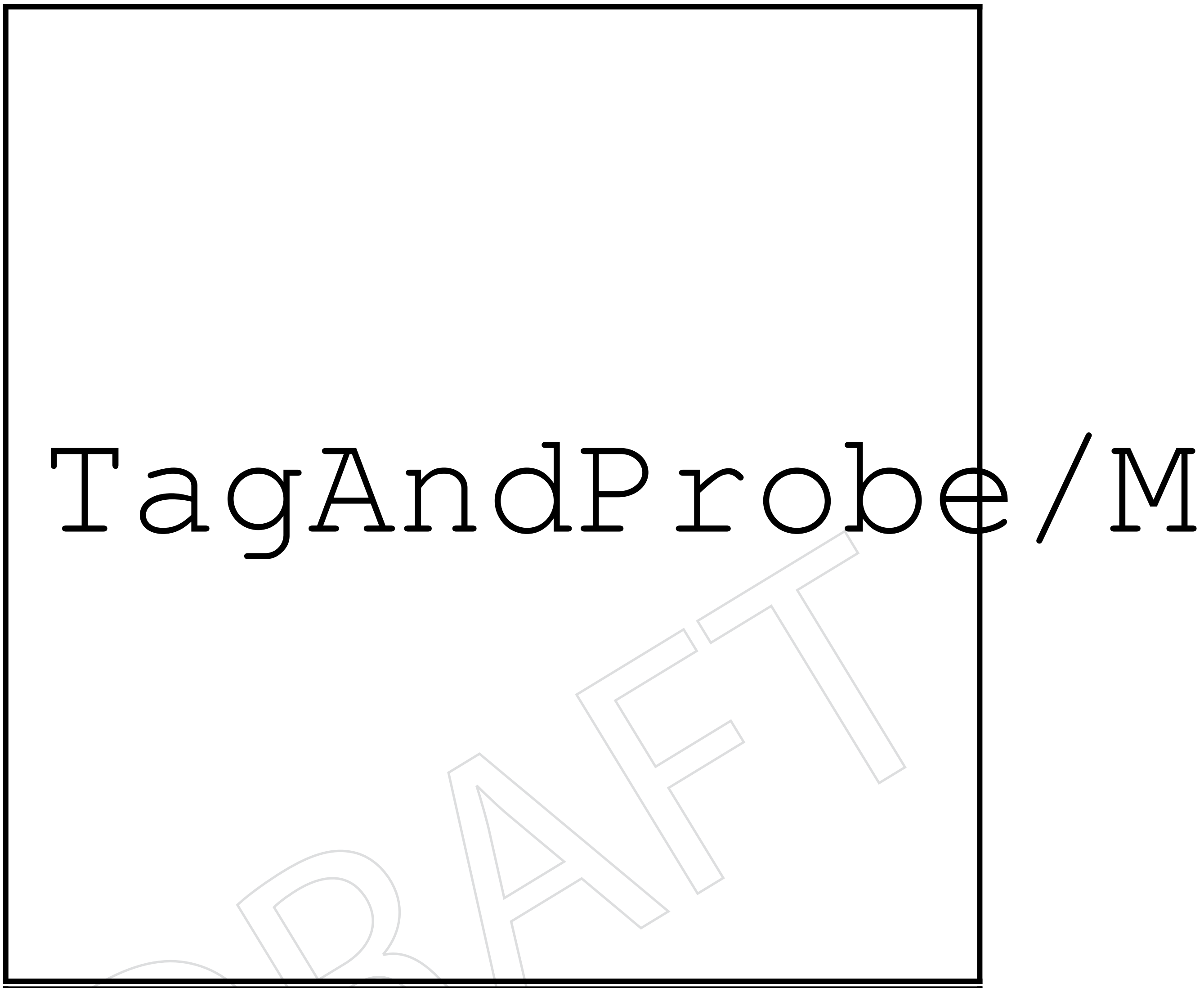
TagAndProbe/M

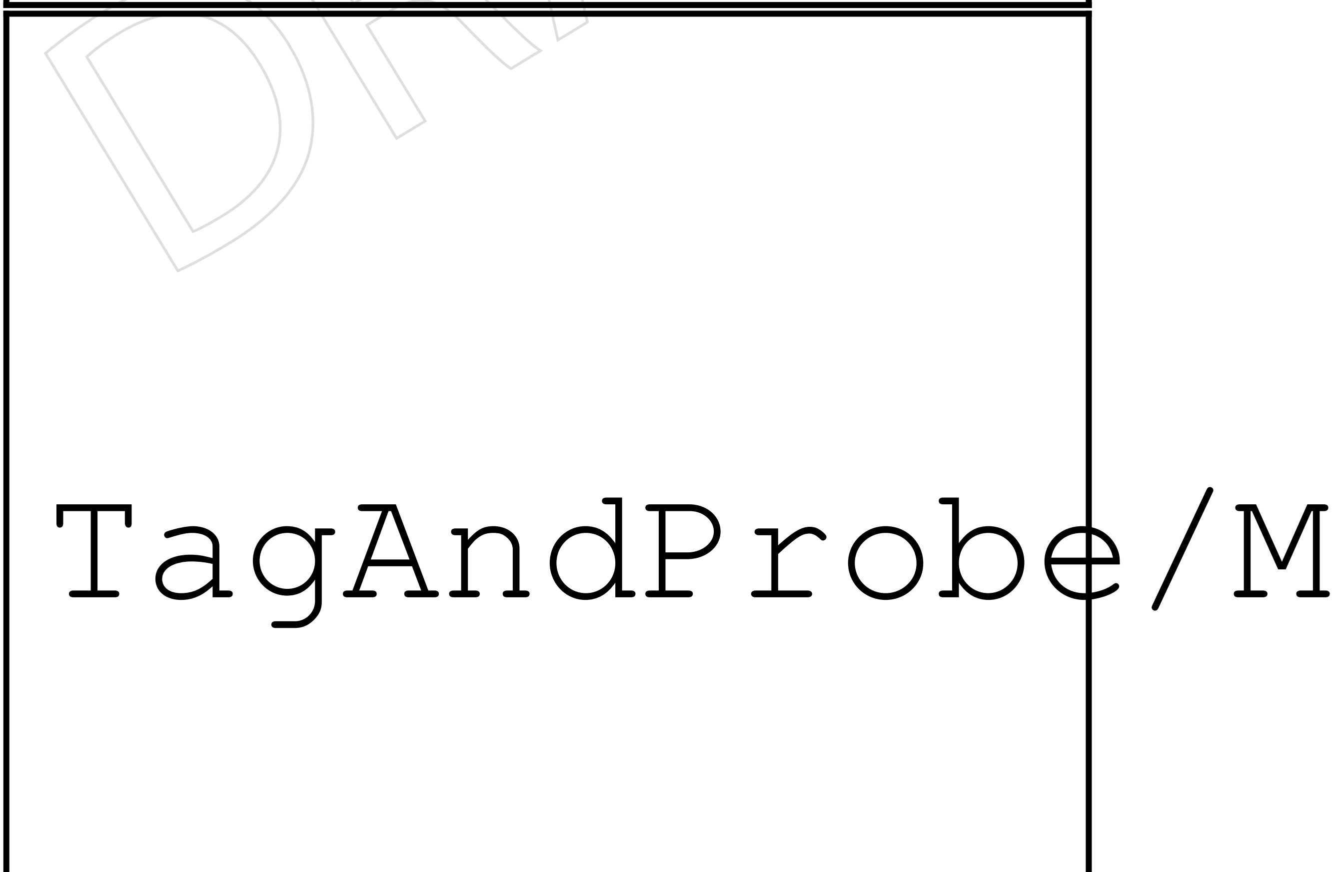
TagAndProbe/M

D Fitting parameters

This section gives an overview of the 2D fits to invariant mass and lifetime distributions. Results are shown as a function of J/ψ p_{T} in 8 rapidity bins considered in the analysis. Also, distributions of the 1st run and 2nd run are plotted separately, in order to check the consistency of two datasets.

Figure **??** shows the raw yields of the inclusive J/ψ extracted fromt the fits. The b-fraction increases strongly with p_{T} for all rapidity bins.

Figure 168 shows the b-fraction, the fraction of the non-prompt J/ψ production originating from b-hadron decays as a function of J/ψ p_{T} in several rapidity bins considered in the analysis. The b-fraction increases strongly with p_{T} for all rapidity bins.

Fig **??** and **??** show the yield of prompt and non-prompt J/ψ extracted from ithe 2D fits respectively.

Fig 171 shows the width of the signal functions in dimuon invariant mass distributuions that is the sum of the one Crystal Ball and one Gaussian, as functions of p_{T} in different rapidity ranges. The width becomes wider as it goes to forward or backward rapidity range while it shows no strong p_{T} dependence.

Fig 172 shows the slope of an exonential functions for backgrounds in mass distributions, as functions of p_{T} in several rapidity bins. Fig 173 shows the slope of an exonential functions describing lifetime distribution of non-prompt J/ψ, as functions of p_{T} in several rapidity bins. This parameter is first fitted to non-prompt J/ψ MC template, and then fitted value is given as a initial value when we actually fit to data.

Fig 174 shows the width of the resolution functions that is the combination of two Gaussian and corresponds to the lifetime distributions of prompt J/ψ. The width of one Gaussian is fixed to MC, and that of the other Gaussian is left free and fixed to data. This paramter is almost unity for the whole kinematic ranges, and this guarantee the fitting function describes the resolution shape well.

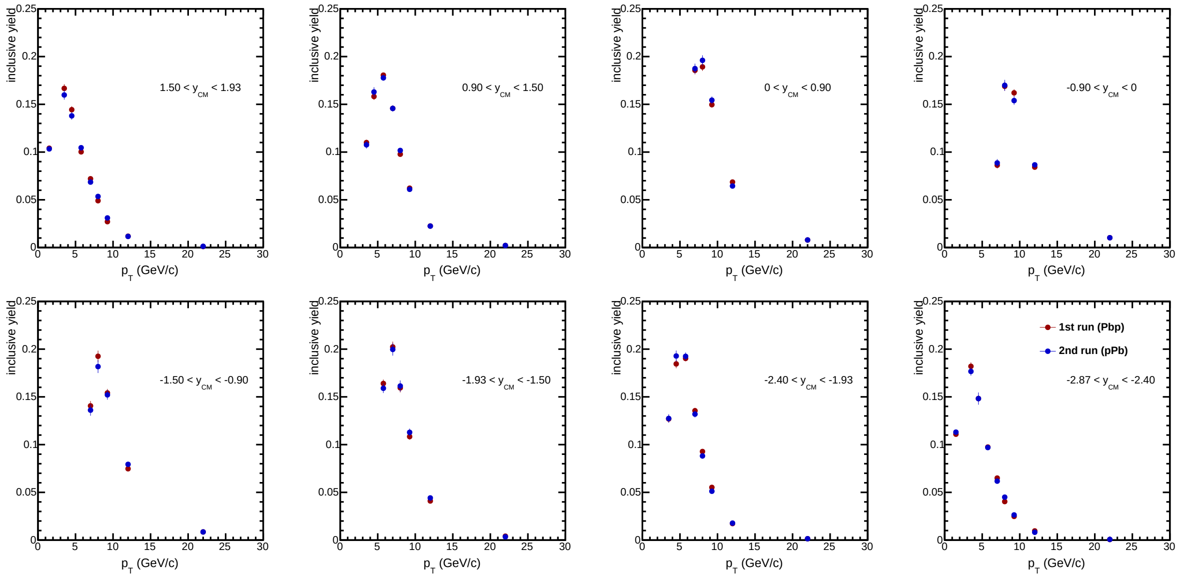

Figure 167: The raw yield of the inclusive J/ψ as a function of p_{T} in several rapidity bins for the 1st run(red) and the 2nd run(blue).

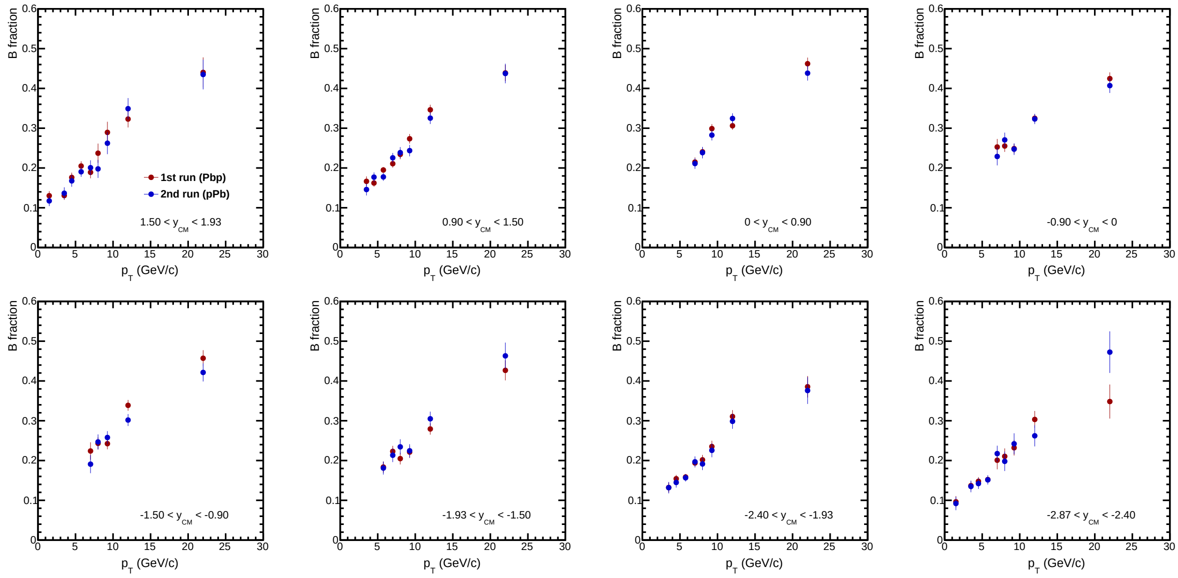

Figure 168: The b-fraction(fraction of non-prompt J/ψ production from b-hadron decays) as a function of p_{T} in 8 rapidity bins used in the analysis for the 1st run(red) and the 2nd run(blue).

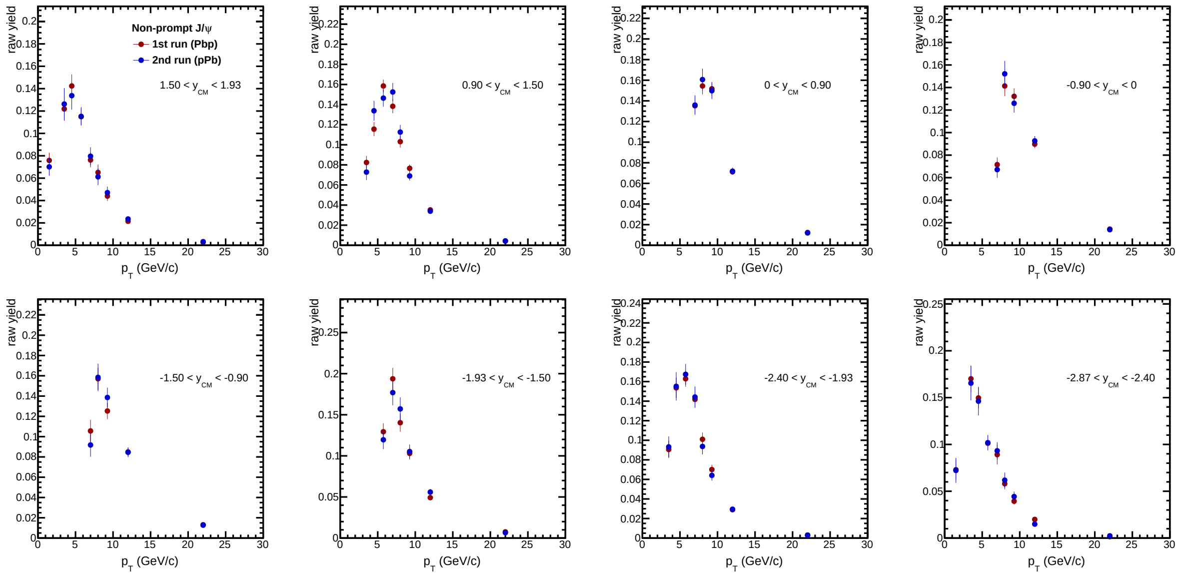

Figure 169: The prompt J/ψ yields as a function of p_{T} in 8 rapidity bins used in the analysis for the 1st run(red) and the 2nd run(blue).

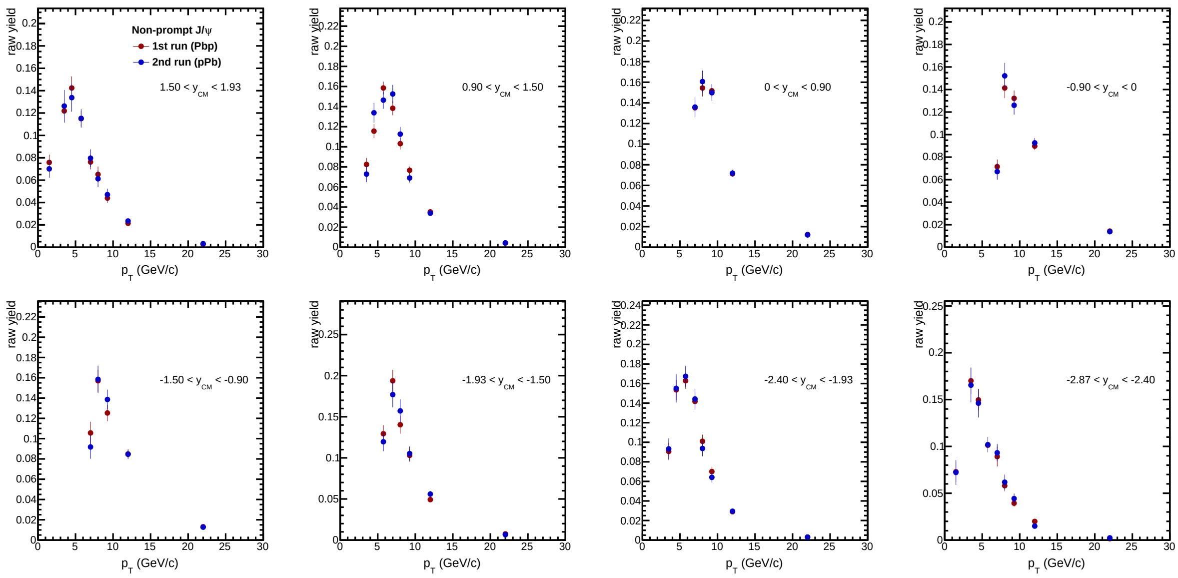

Figure 170: The non-prompt J/ψ yields as a function of p_{T} in 8 rapidity bins used in the analysis for the 1st run(red) and the 2nd run(blue).

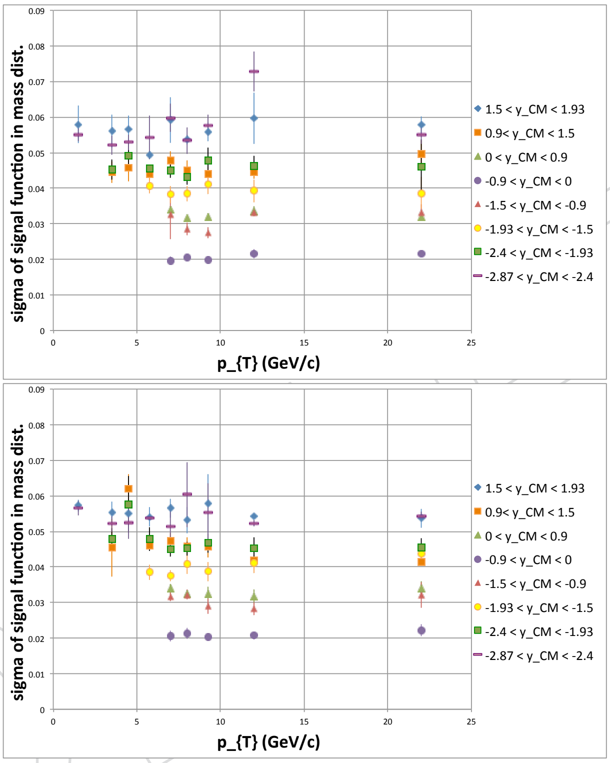

Figure 171: the width of the signal functions in dimuon invariant mass distributions as a function of p_T in 8 rapidity bins used in the analysis for the 1st run(left) and the 2nd run(right).

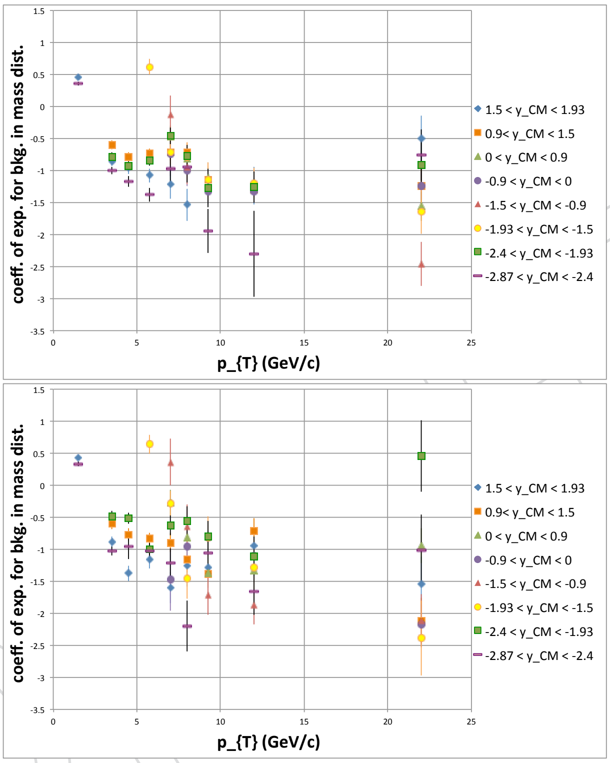

Figure 172: Slope of the exponential function for backgrounds in dimuon invariant mass distributions as a function of p_T in 8 rapidity bins used in the analysis for the 1st run(left) and the 2nd run(right).

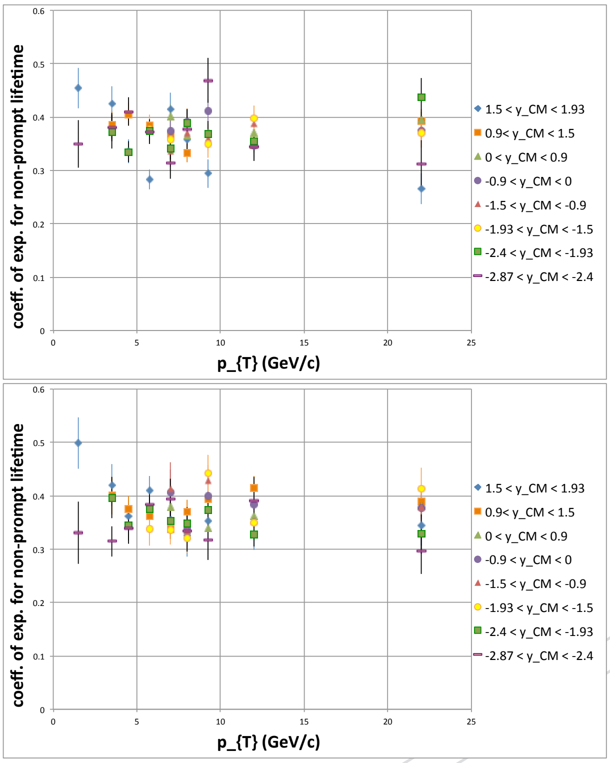

Figure 173: Slope of the exponential function for lifetime distributions of non-prompt J/ψ as a function of p_{T} in 8 rapidity bins used in the analysis for the 1st run(left) and the 2nd run(right).

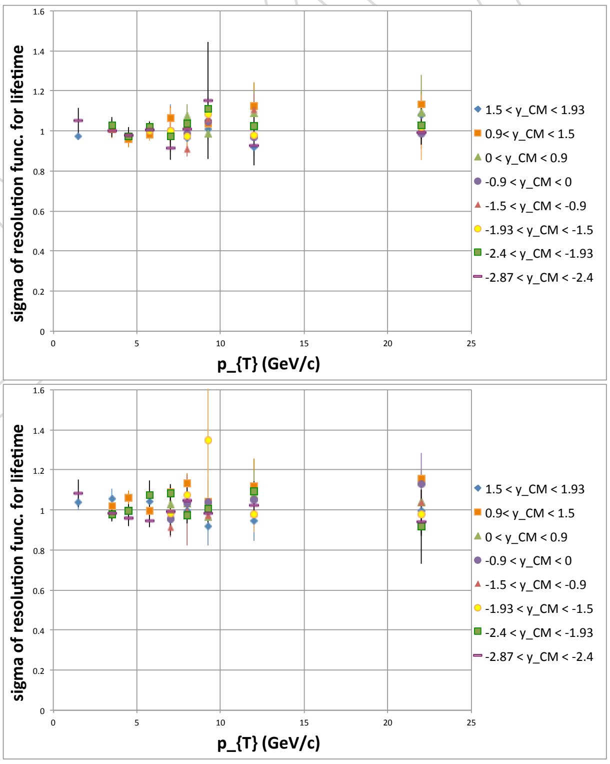

Figure 174: The width of the resolution function for lifetime distributions of prompt J/ψ as a function of p_{T} in 8 rapidity bins used in the analysis for the 1st run(left) and the 2nd run(right).

E Acceptance Systematics

Figure 175-182 represent the acceptance distributions for prompt J/ψ in each p_{T} and rapidity bins, and that of non-prompt J/ψ are illustrated in Figure 183-190.

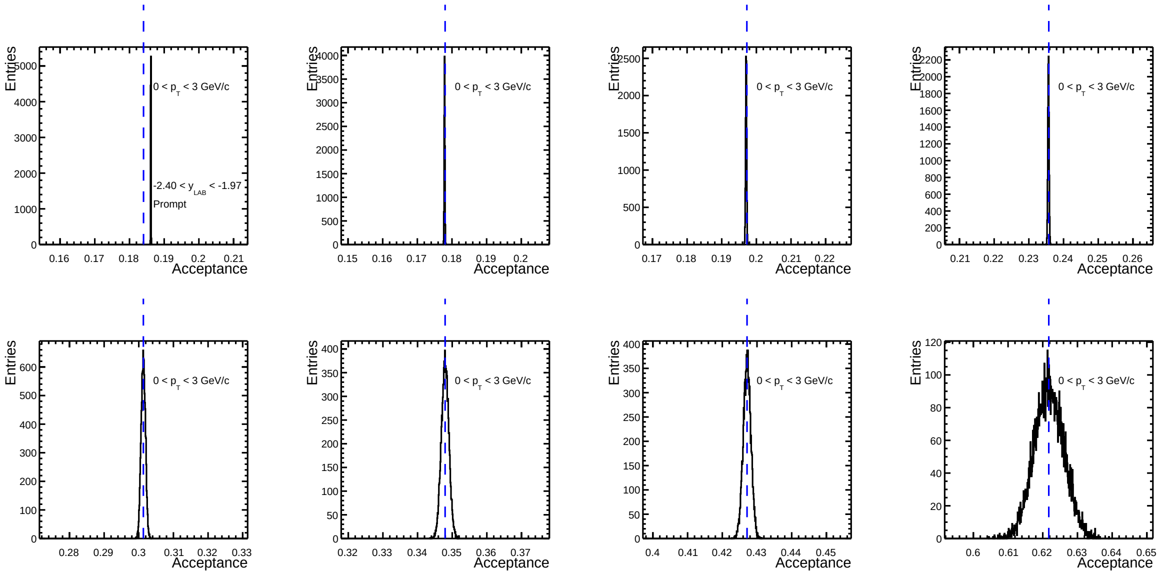

Figure 175: Acceptance distributions for prompt J/ψ of the 1st run period in bins of p_{T} over the range of $-2.40 < |y_{LAB}| < -1.97$.

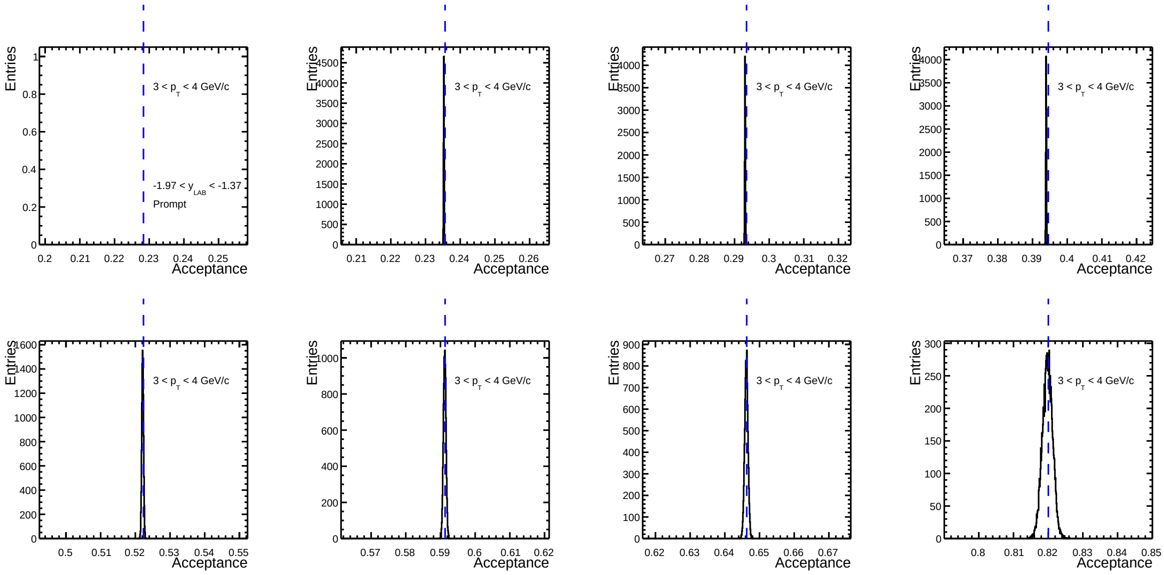

Figure 176: Acceptance distributions for prompt J/ψ of the 1st run period in bins of p_{T} over the range of $-1.97 < |y_{LAB}| < -1.37$. First panel should be ignored because it is out of the analysis kinematic range.

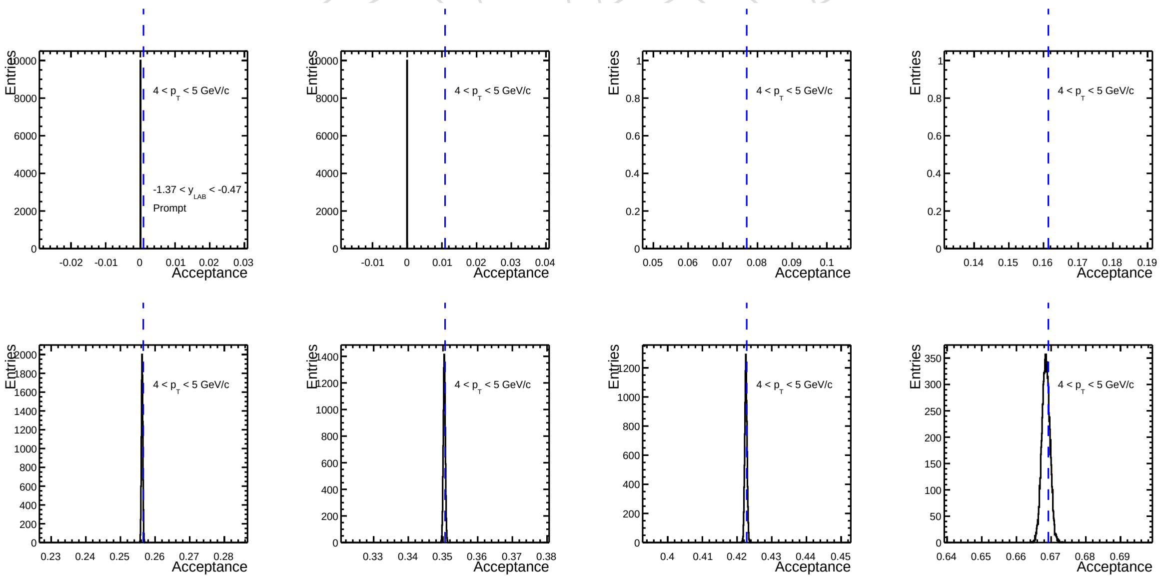

Figure 177: Acceptance distributions for prompt J/ψ of the 1st run period in bins of p_{T} over the range of $-1.37 < |y_{LAB}| < -0.47$. First four panels should be ignored because these are out of the analysis kinematic range.

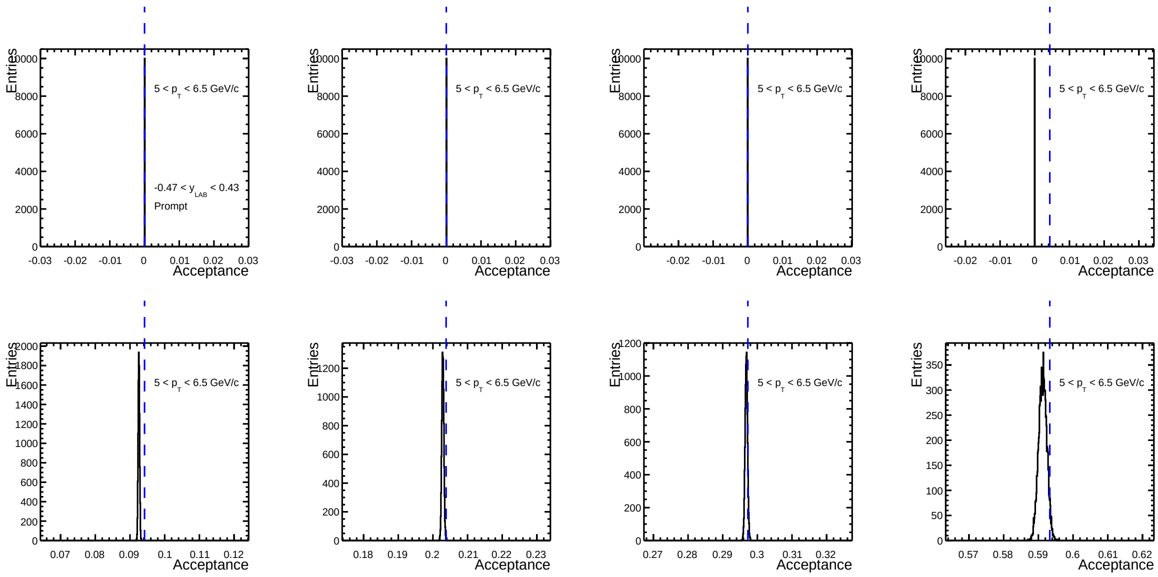

Figure 178: Acceptance distributions for prompt J/ψ of the 1st run period in bins of p_{T} over the range of $-0.47 < |y_{LAB}| < 0.43$. First four panels should be ignored because these are out of the analysis kinematic range.

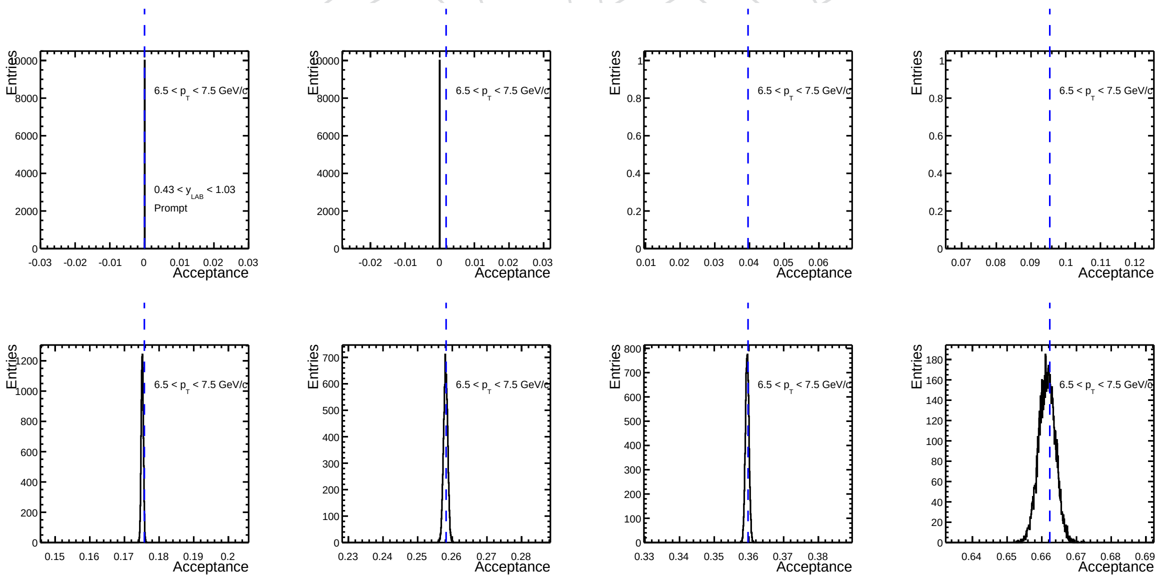

Figure 179: Acceptance distributions for prompt J/ψ of the 1st run period in bins of p_{T} over the range of $0.43 < |y_{LAB}| < 1.03$. First four panels should be ignored because these are out of the analysis kinematic range.

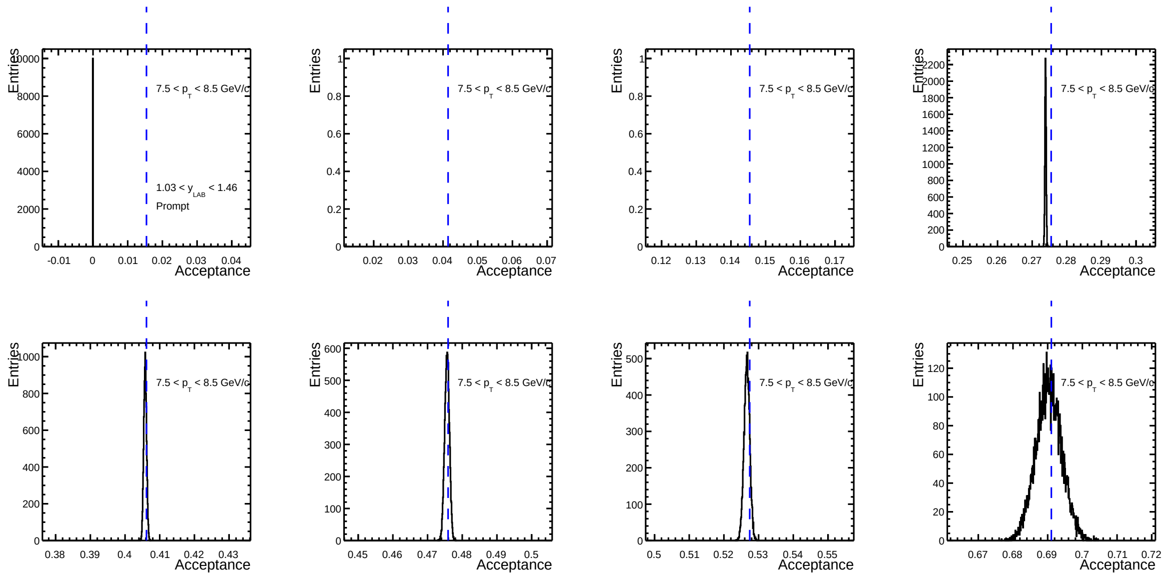

Figure 180: Acceptance distributions for prompt J/ψ of the 1st run period in bins of p_{T} over the range of $1.03 < |y_{LAB}| < 1.46$. First three panels should be ignored because these are out of the analysis kinematic range.

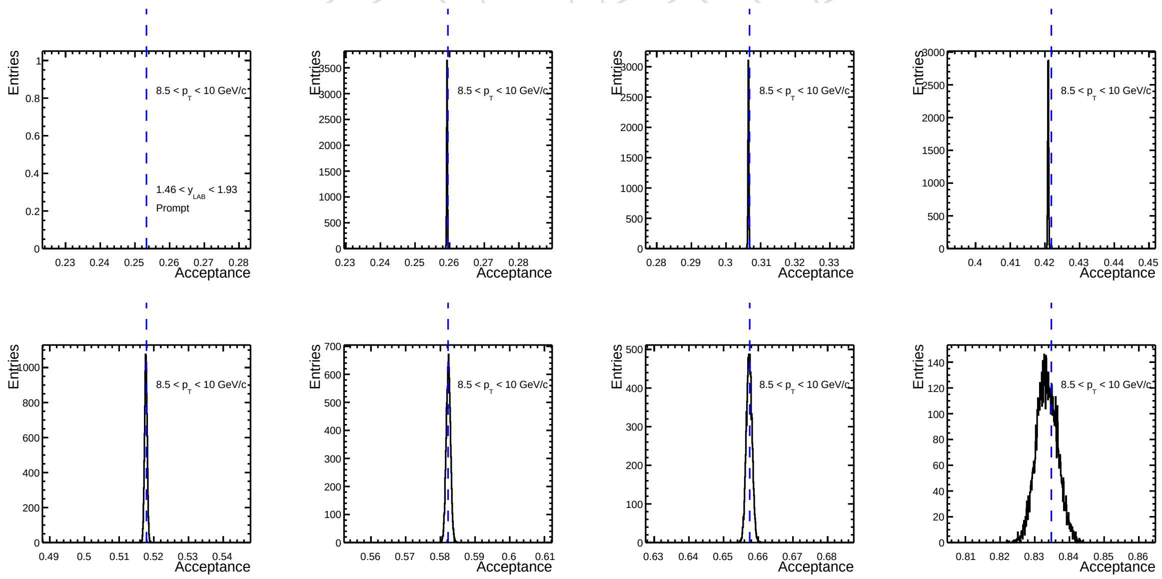

Figure 181: Acceptance distributions for prompt J/ψ of the 1st run period in bins of p_{T} over the range of $1.46 < |y_{LAB}| < 1.93$. First panel should be ignored because it is out of the analysis kinematic range.

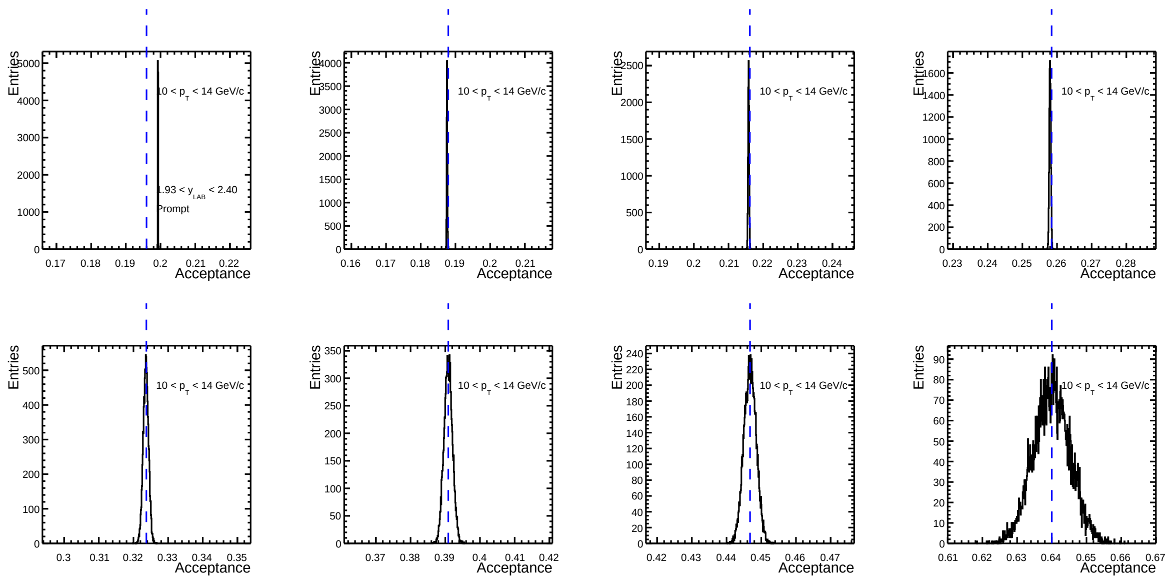

Figure 182: Acceptance distributions for prompt J/ψ of the 1st run period in bins of p_{T} over the range of $1.93 < |y_{LAB}| < 2.40$.

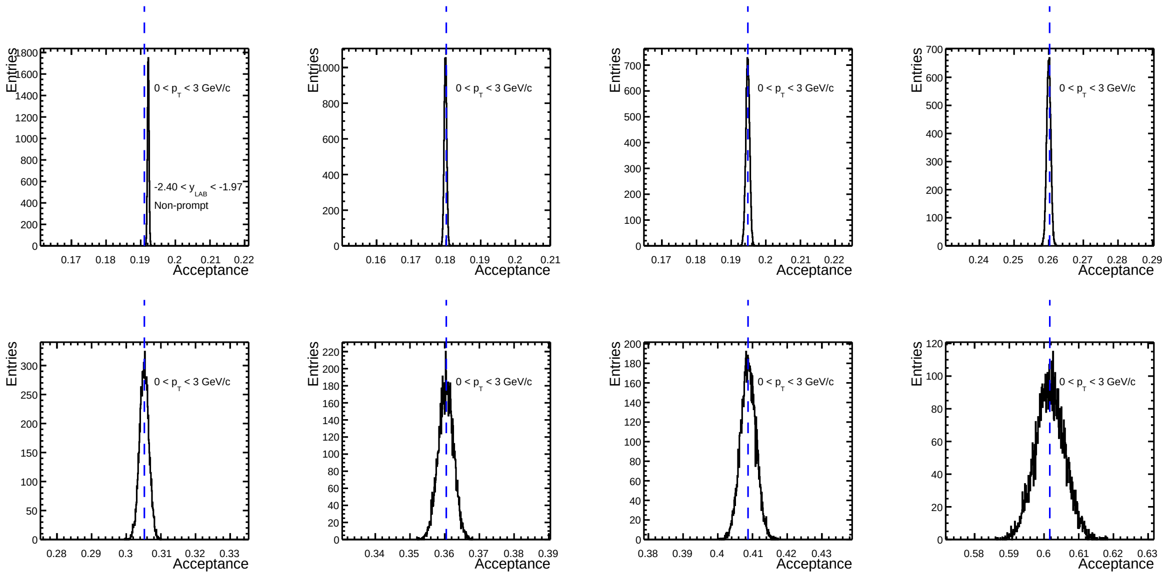

Figure 183: Acceptance distributions for non-prompt J/ψ of the 1st run period in bins of p_{T} over the range of $-2.40 < |y_{LAB}| < -1.97$.

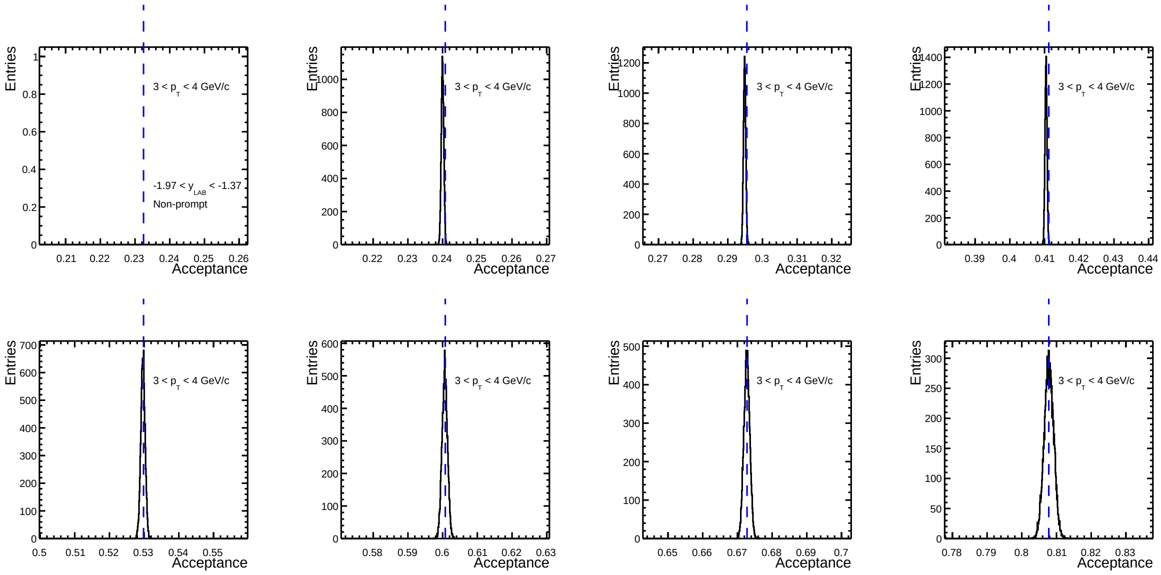

Figure 184: Acceptance distributions for non-prompt J/ψ of the 1st run period in bins of p_{T} over the range of $-1.97 < |y_{LAB}| < -1.37$. First panel should be ignored because it is out of the analysis kinematic range.

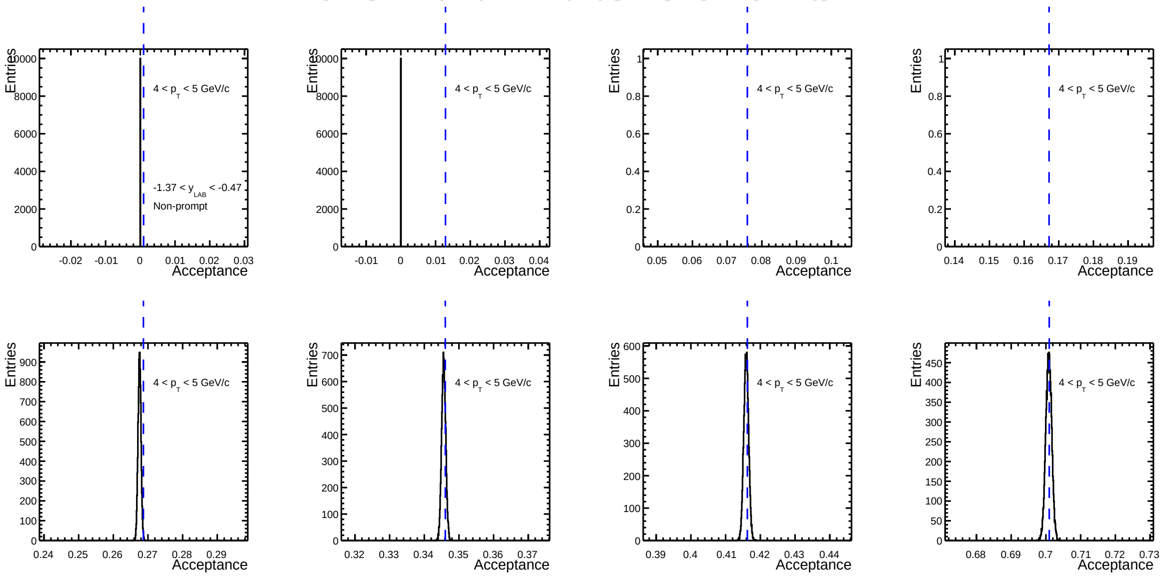

Figure 185: Acceptance distributions for non-prompt J/ψ of the 1st run period in bins of p_{T} over the range of $-1.37 < |y_{LAB}| < -0.47$. First four panels should be ignored because these are out of the analysis kinematic range.

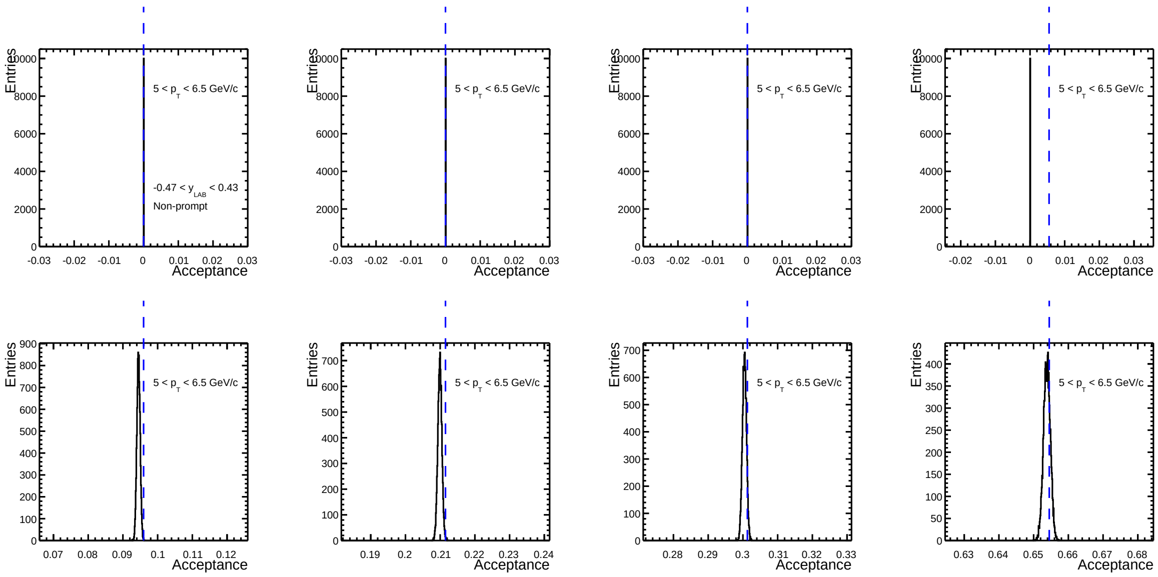

Figure 186: Acceptance distributions for non-prompt J/ψ of the 1st run period in bins of p_{T} over the range of $-0.47 < |y_{LAB}| < 0.43$. First four panels should be ignored because these are out of the analysis kinematic range.

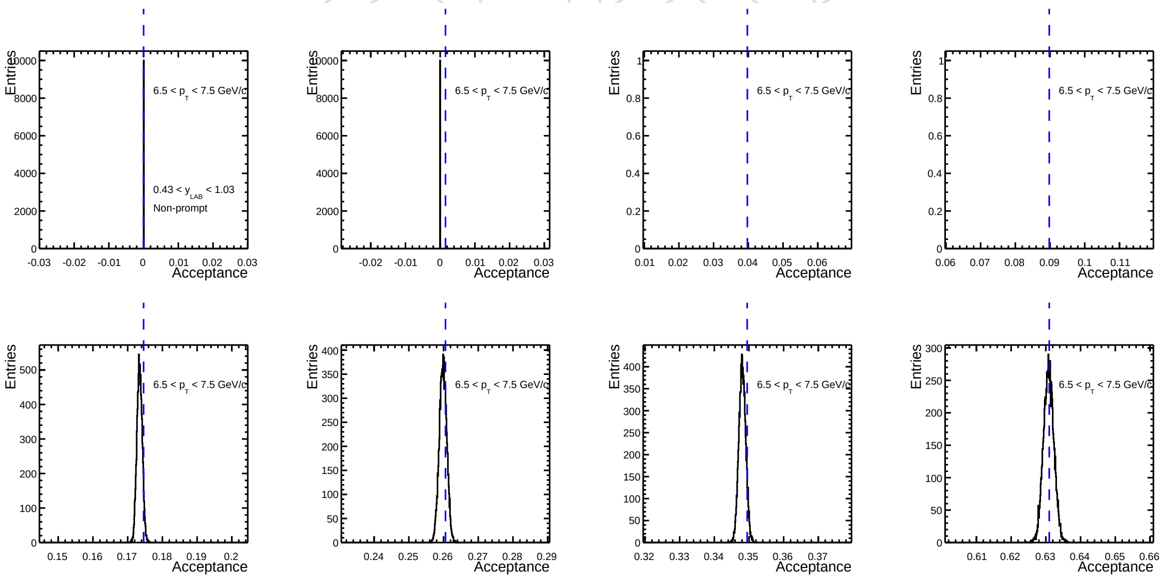

Figure 187: Acceptance distributions for non-prompt J/ψ of the 1st run period in bins of p_{T} over the range of $0.43 < |y_{LAB}| < 1.03$. First four panels should be ignored because these are out of the analysis kinematic range.

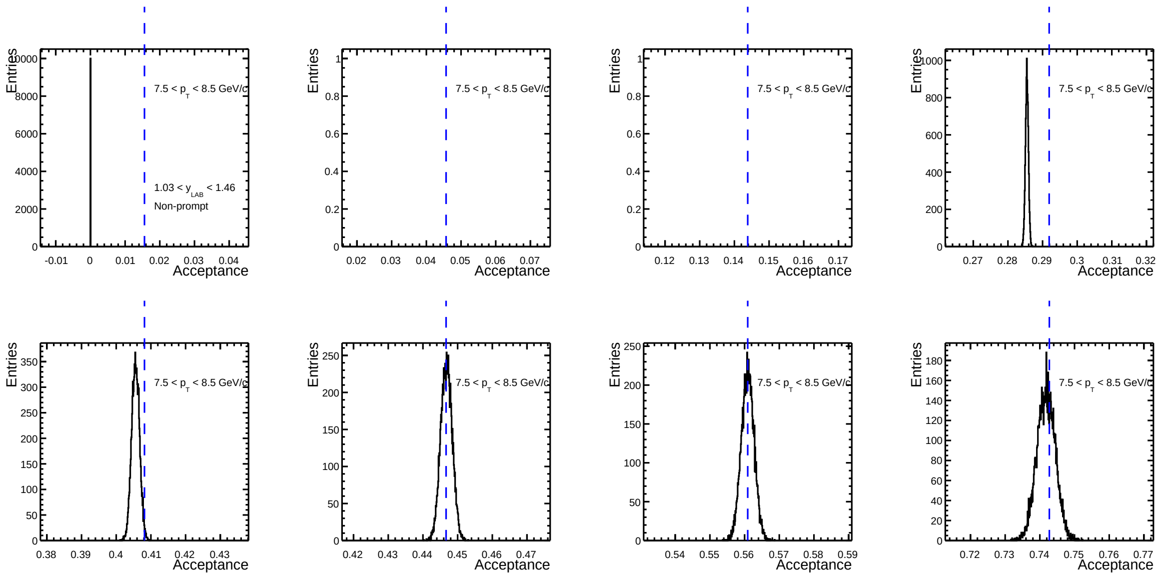

Figure 188: Acceptance distributions for non-prompt J/ψ of the 1st run period in bins of p_{T} over the range of $1.03 < |y_{LAB}| < 1.46$. First three panels should be ignored because these are out of the analysis kinematic range.

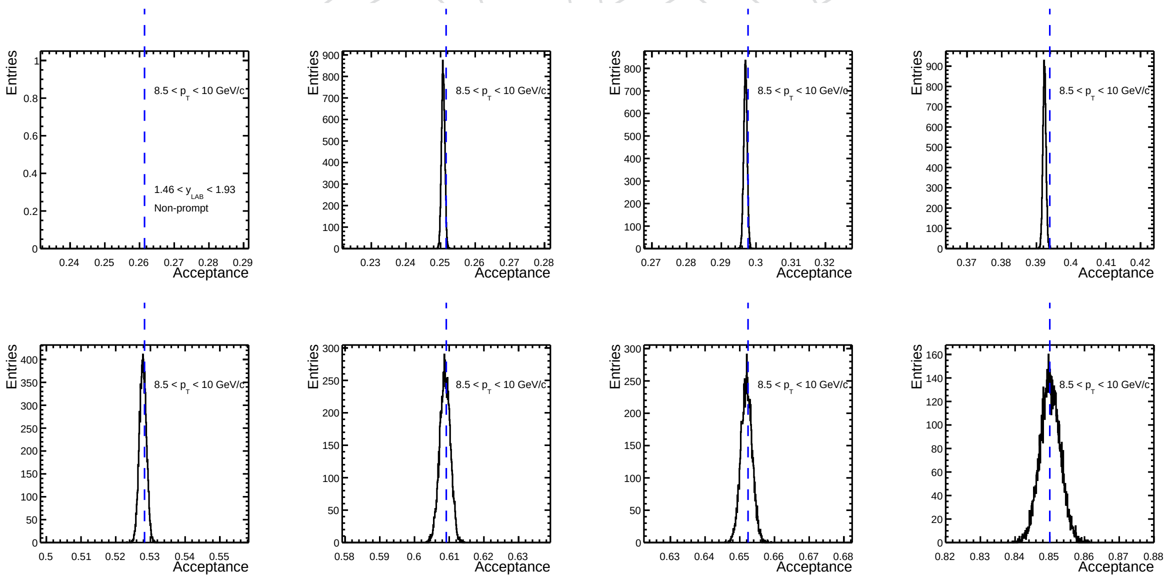

Figure 189: Acceptance distributions for non-prompt J/ψ of the 1st run period in bins of p_{T} over the range of $1.46 < |y_{LAB}| < 1.93$. First panel should be ignored because it is out of the analysis kinematic range.

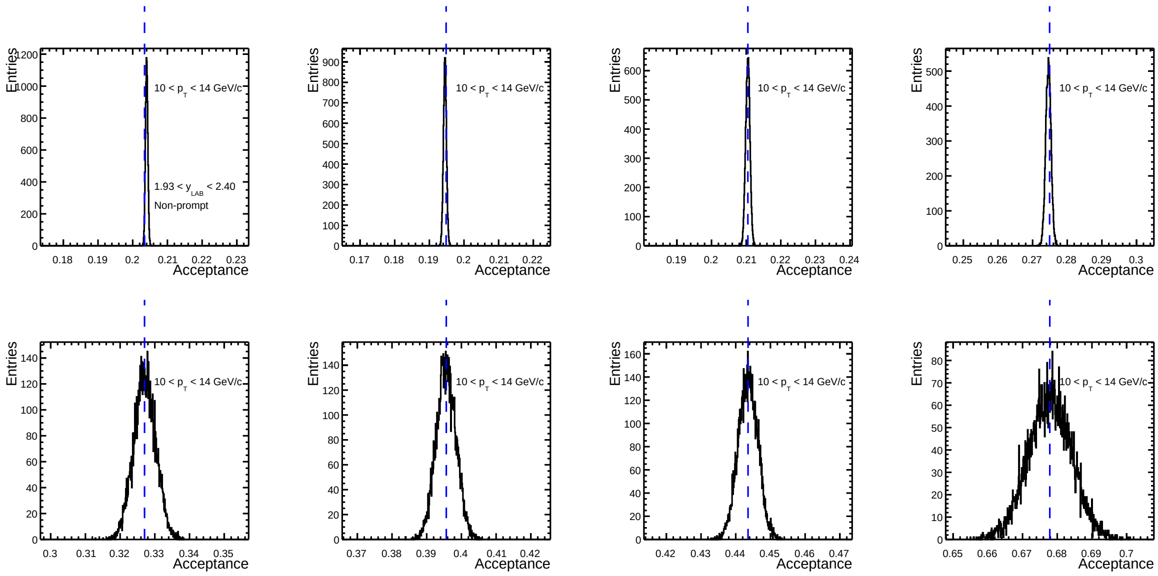

Figure 190: Acceptance distributions for non-prompt J/ψ of the 1st run period in bins of p_{T} over the range of $1.93 < |y_{LAB}| < 2.40$.